

# **Diffusion-based modelling of flood inundation over complex floodplains**

**Dapeng Yu**

Submitted in accordance with the requirements  
for the degree of Doctor of Philosophy

University of Leeds  
School of Geography  
September 2005

The candidate confirms that the work submitted is his  
own and that appropriate credit has been given where  
reference has been made to the work of others.

This copy has been supplied on the understanding that it is  
copyright material and that no quotation from the thesis may be  
published without proper acknowledgement.

# Acknowledgements

My deepest gratitude goes to my supervisor Professor Stuart Lane for his close and systematic supervisions and guidance as well as the constructive comments throughout the research study without which the completion of the thesis would have been impossible. He is a great supervisor. Although he is extremely busy most of the time, he has always been able to find time for me and his supervision has been really excellent. It has been an honour to work with him.

I would also like to thank Professor Adrian McDonald and Professor Pauline Kneale for their critical views and valuable suggestions on my work at the Research Group Meetings.

Thanks to my colleagues Richard Hardy, David Mould and Sim Reaney for the lots of fun they brought me when they pushed me through the final stage of my Ph.D.

Thanks also goes to my beloved wife Dongbin for her constant love and understanding during my study. She gave me the power and energy to reach where I am. Thank her for the most precious gift she gave me on the way to my PhD: the arrival of our lovely baby Zhenyuan Yu on the 28<sup>th</sup> of June, 2004. Great fun is that, when he smiles, he looks like his mother and when he does not, he looks like me.

I would also like to thank my parents. Although they don't know much about what I have been doing, they have been supportive all the time. They are really great parents.

# Abstract

High-resolution data obtained from airborne remote sensing are increasing opportunities for representation of small-scale structural elements (e.g. walls, buildings) in complex floodplain systems using two-dimensional (2D) models of flood inundation. At the same time, 2D inundation models have been developed and shown to provide good predictions of flood inundation extent, with respect to both full solution of the depth-averaged Navier-Stokes equations and simplified diffusion wave models. However, these models have yet to be applied extensively to urban areas. This study applies a 2D raster-based diffusion wave model, either loosely-coupled or tightly-coupled to a 1D river flow model, to determine patterns of fluvial flood inundation in urban areas using high-resolution topographic data.

The aim of this study is to explore the interaction between spatial resolution and small-scale flow routing process, through model validation and verification. The model assumes that the prime source of the flood is fluvial: pluvial floods and floods associated with urban drainage systems are not addressed. The topographic data are based upon airborne laser altimetry (LiDAR) obtained for the City of York, U.K. Validation data were available in the form of inundation patterns obtained using aerial photography at a point on the falling limb of the flood event. Inflow data is provided either by a loosely-coupled or a tightly-coupled 1D river flow model. The model was used to simulate a major flood event which occurred in the year 2000 in the City of York on the River Ouse at 4 different sites.

Applications of the basic model showed that even relatively small changes in model resolution have considerable effects on the predicted inundation extent and timing of flood inundation. Timing sensitivity would be expected given the relatively poor representation of inertial processes in a diffusion wave model. Compared with previous work, sensitivity to inundation extent is more surprising and is associated with three connected effects: (i) the smoothing effect of mesh coarsening upon input topographical data; (ii) poorer representation of both cell blockage and surface routing processes as the mesh is coarsened, where the flow routing is especially complex; and (iii) the effects of (i) and (ii) upon water levels and velocities which in turn determine which parts of the floodplain the flow can actually travel to. The combined effects of wetting and roughness parameters can compensate in part for a coarser mesh resolution. However, the coarser the resolution, the poorer the ability to control the inundation process as these parameters not only affect the speed but also the direction of wetting. Thus, high resolution data will need to be coupled to more sophisticated

representation of the inundation process in order to obtain effective predictions of flood inundation extent.

A sub grid scale wetting and drying correction approach was developed and tested for use with 2D diffusion wave models of urban flood inundation. The method recognises explicitly that representations of sub grid scale topography using roughness parameters will provide an inadequate representation of the effects of structural elements on the floodplain (e.g. buildings, walls) as such elements not only act as momentum sinks, but also have mass blockage effects. The latter may dominate, especially in structurally complex urban areas. The approach developed uses high resolution topographic data to develop explicit parameterization of sub grid scale topographic variability to represent both the volume of a grid cell that can be occupied by the flow and the effect of that variability upon the timing and direction of the lateral fluxes. This approach is found to give significantly better prediction of fluvial flood inundation in urban areas as compared with traditional calibration of sub grid-scale effects using Manning's  $n$ . In particular, it simultaneously reduces the need to use exceptionally high values of  $n$  to represent the effects of using coarser meshes, whilst simultaneously increasing the sensitivity of model predictions to variation in  $n$ .

Finally, the model was coupled (tightly) to a one-dimensional solution of the Navier-Stokes equations. This showed that significantly better representation of urban inundation could be achieved in a tightly-coupled formulation as a result of better representation of boundary condition effects.

# Table of Contents

<b>Acknowledgements .....</b>	<b>i</b>
<b>Abstract.....</b>	<b>ii</b>
<b>Table of Contents .....</b>	<b>iv</b>
<b>List of Tables .....</b>	<b>vii</b>
<b>List of Figures.....</b>	<b>viii</b>
<b>Chapter 1 .....</b>	<b>1</b>
<b>Introduction.....</b>	<b>1</b>
1.1 Research context .....	1
1.1.1 Specification of the problem.....	2
1.1.2 The approach: modelling effects of structural elements in flood inundation modelling .....	5
1.2 Research aims and objectives.....	7
1.2.1 Research aims.....	7
1.2.2 Research objectives .....	7
1.3 Thesis structure .....	8
<b>Chapter 2 .....</b>	<b>11</b>
<b>Literature Review .....</b>	<b>11</b>
2.1 Introduction.....	11
2.2 Chapter aims and objectives.....	11
2.3 Review of river flow and flood inundation modelling .....	12
2.3.1 General practice in river flow and flood inundation modelling.....	13
2.3.2 Raster-based flood inundation modelling.....	23
2.3.3 Urban flood inundation modelling .....	25
2.3.4 Implications for this research .....	30
2.4 The application of remotely sensed data in flood inundation modelling.....	31
2.4.1 Topographic data requirements for high-resolution flood inundation modelling.....	32
2.4.2 Remote sensed data for high-resolution flood inundation modelling .....	37
2.4.3 Airborne scanning laser altimetry (LiDAR) .....	38
2.4.4 Implications for this research .....	41
2.5 Data representation in hydraulic models in relation to Geographical Information System (GIS).....	41
2.5.1 Data representation for floodplain topography in relation to GIS .....	42
2.5.2 Implications for this research .....	44
2.6 Chapter Summary.....	45
<b>Chapter 3 .....</b>	<b>46</b>
<b>Case-study applications, data sources and methods .....</b>	<b>46</b>
3.1 Introduction .....	46
3.2 Loose coupling between channel and floodplain treatments.....	47
3.3 Case-study applications carried out.....	48
3.4 Summary of the data needs for the case-study applications using the loosely-coupled model .....	52

3.5 Model validation and approach .....	53
3.5.1 Validation/verification approach .....	54
3.5.2 Quantitative description of agreement .....	56
3.5.3 Validation data .....	60
3.6 Model geometry data (MG).....	66
3.6.1 Floodplain topography.....	66
3.6.2 Creation of the 4m, 8m, 16m and 32m meshes .....	72
3.7 Boundary condition Data (BC) for the loosely-coupled model.....	76
3.7.1 Inflow hydrograph along the river-floodplain boundary .....	76
3.7.2 Roughness parameterization.....	77
3.8 Chapter summary .....	78
<b>Chapter 4 .....</b>	<b>80</b>
<b>Model developments and testing 1: conventional 2D diffusion wave modelling of urban fluvial flooding .....</b>	<b>80</b>
4.1 Introduction.....	80
4.2 Chapter aims and objectives.....	81
4.3 Model description.....	81
4.3.1 Process representation .....	81
4.3.2 Discretization and solution .....	86
4.4 Model Graphic User Interface (GUI) description.....	87
4.4.1 Main model user interface .....	87
4.4.2 User interface of the loosely-coupled version .....	89
4.5 Model application 1: extensive analysis at Site 1 (Naburn Weir) .....	91
4.5.1 Results 1: 4 m simulations.....	92
4.5.2 Results 2: mesh resolution effects .....	93
4.5.3 Results 3: roughness parameterization .....	99
4.5.4 Discussion of Site 1 results.....	105
4.6 Model application 2: simplified analysis at Site 2 (A64 Trunk Road) and Site 3 (City Centre of York) .....	108
4.6.1 Results 1: Site 2 .....	109
4.6.2 Results 2: Site 3 .....	114
4.6.3 Discussion of Site 2 and 3 applications .....	117
4.7 Conclusion .....	120
<b>Chapter 5 .....</b>	<b>123</b>
<b>Model Developments and Testing 2: development and testing of a sub grid-scale treatment for urban fluvial flooding .....</b>	<b>123</b>
5.1 Introduction .....	123
5.2 Chapter aims and objectives.....	124
5.3 Theoretical derivation of a sub grid-scale topographic treatment .....	125
5.3.1 Cell blockage effects .....	125
5.3.2 Cell flux effects .....	129
5.3.3 Model validation using the sub grid-scale treatment .....	131
5.4 Model testing 1: extensive analysis in Site 1 – Naburn Weir.....	131
5.4.1 Results 1: Inundation patterns through time .....	133
5.4.2 Results 2: Model validation and verification.....	137
5.4.3 Results 3: Comparison of calibration using Manning’s n with sub grid-scale treatment... ..	140
5.4.4 Discussion of Site 1 application .....	145
5.5 Model testing 2: simplified analysis at Site 2 – A64 Trunk Road.....	148

5.5.1 Result 1: Inundation patterns through time .....	149
5.5.2 Result 2: Model validation .....	153
5.5.3 Computational performance of the sub grid wetting treatment .....	155
5.5.4 Discussion of the Site 2 application.....	157
5.6 Conclusion .....	158
<b>Chapter 6 .....</b>	<b>159</b>
<b>Coupling of a 1D solution of the St. Venant equations to the 2D diffusion wave model.....</b>	<b>159</b>
6.1 Introduction .....	159
6.2 Chapter aims and objectives.....	160
6.3 Model description.....	160
6.3.1 1D model process representation, discretization and solution.....	160
6.3.2 Model coupling.....	168
6.3.3 Model Graphic User Interface (GUI) .....	171
6.4 Model application: data processing .....	172
6.5 Model applications: results and discussion .....	181
6.5.1 Model calibration and validation .....	181
6.5.2 Discussion .....	191
6.6 Chapter summary .....	194
<b>Chapter 7 .....</b>	<b>196</b>
<b>Conclusions and future development .....</b>	<b>196</b>
7.1 Research achievements with respect to aims and objectives.....	196
7.1.1 Achievements with respect to the development of the flood inundation model .....	197
7.1.2 Achievements with respect to coupled modelling of river flow and floodplain flow .....	197
7.1.3 Achievements with respect to the development of sub grid wetting treatment .....	199
7.1.4 Achievements with respect to model applications.....	200
7.2 Critical assessment of methods and results .....	204
7.2.1 Limitations in model development .....	204
7.2.2 Limitations in model applications .....	205
7.3 Future research developments .....	208
7.3.1 Development of the 1D river flow model.....	209
7.3.2 Representation of momentum transfer at the river-floodplain boundary.....	209
7.3.3 Coupling the flood inundation model with other hydrological processes.....	210
7.3.4 Representation of small-scale wetting treatments .....	211
<b>Appendix A .....</b>	<b>212</b>
<b>Bibliography .....</b>	<b>214</b>

# List of Tables

Table 1.1 Summary of present-day flood risks and flood-management costs (Evans <i>et al.</i> , 2004).....	2
Table 2.1: Recent applications of raster-based flood inundation modelling (continued on next page). ....	27
Table 2.1: Recent applications of raster-based flood inundation modelling (continued from last page).....	28
Table 3.1: Summary of applications conducted and the associated coupling methods.....	51
Table 3.2: Summary of the data needs and availability for the loosely-coupled model.....	53
Table 3.3: Spectral profiles of the features in the validation imagery (minimum and maximum DN values).....	62
Table 3.4: Contingency matrix obtained using the signatures produced from the training samples. ....	63
Table 4.1: Accuracy statistics for model validation at a single point when the aerial imagery is used as the reference validation data (Site 1). ....	98
Table 4.2: Comparisons of conditional Kappa (wet cells) using the Z statistic. ....	99
Table 4.3: Accuracy statistics for model validation at a single point when the aerial imagery is used as the reference data (Site 2). ....	112
Table 4.4: Accuracy statistics for model validation at a single point when the aerial imagery is used as the reference data (Site 3) ....	116
Table 5.1: Illustration of the sub-grid effective calculation. ....	130
Table 5.2: Accuracy assessment based upon model predictions with different mesh resolutions and with and without the sub grid treatment. The validation data are based upon remotely-sensed imagery obtained at 300 hours into the flood event (Site 1).....	138
Table 5.3: Accuracy assessment based upon model predictions with different mesh resolutions and with and without the sub grid treatment. The validation data are based upon remotely-sensed imagery obtained at 300 hours into the flood event (Site 2).....	155
Table 5.4: The total computational time used to simulate the flood event for simulations with different mesh resolution and wetting treatment. ....	156
Table 6.1: Summary of the data needs and availability for the tightly-coupled model.....	174
Table 6.2: Boundary condition requirements for the 1D river model (Option 2 is used in this application).....	177

# List of Figures

Figure 1.1: An example showing the effect of structural elements on the floodplain upon flow routing and flood inundation. The picture was taken on the River Ouse during a major flood event occurred in the year 2000. ....	3
Figure 2.1: Hydraulic parameters in the river-floodplain system (after Knight and Shiono, 1996).....	14
Figure 2.2: Illustration of airborne LiDAR in operation (after Flood, and Gutelius, 1997).....	39
Figure 3.1: The location of the River Ouse. ....	49
Figure 3.2 Location of three case-study sites on the River Ouse, York, UK (Illustration map produced using Ordnance Survey digimap data downloaded from <a href="http://www.digimap.co.uk">www.digimap.co.uk</a> ) .....	50
Figure 3.3 Landline data of three case-study sites on the River Ouse, York, UK (Illustration map produced using Ordnance Survey digimap data downloaded from <a href="http://www.digimap.co.uk">www.digimap.co.uk</a> ) .....	51
Figure 3.4: Illustration of projecting a 2 m reference mesh into a mesh of model resolution (4 m) for model validation and verification: (a) original 2 m and projected 4 m reference data; and (b) wetting status of the projected reference data. ....	56
Figure 3.5: Error matrix for accuracy assessment (after Congalton and Green, 1999).....	56
Figure 3.6: Aerial imagery taken on the 9 <sup>th</sup> November, 2000 at Site 1 in the River Ouse: (a) Site 1: Naburn Weir; (b) Site 2: A64 Trunk Road; and (c) Site 3: City Centre of York. 61	61
Figure 3.7: Feature space images of the image shown in Figure 3.6a: (a) Red vs. Green; (b) Red vs. Blue; and (c) Green vs. Blue. ( <i>x</i> is the horizontal axis and <i>y</i> is the vertical axis). .....	63
Figure 3.8: Classification of the aerial imagery at Site 1 on the River Ouse, into four classes: trees, water bodies, grass, and building and roads.....	64
Figure 3.9: Tree locations derived from aerial images for LiDAR-derived DEM processing at Site 1 of the River Ouse: (a) tree layer; (b) tree layer superimposed on the aerial image. .....	65
Figure 3.10: Inundation extent derived from the aerial images for the River Ouse Site 1 application: (a) inundation extent layer; (b) inundation extent layer superimposed on the aerial images.....	66
Figure 3.11: LiDAR-derived DEM covering the River Ouse with a resolution of 2 meters....	67
Figure 3.12: Original LiDAR-derived 2 m DEMs for the three application sites in the River Ouse. (a) Naburn weir; (b) A64 Trunk Road; and (c) the city centre of York. ....	68

Figure 3.13: Extraction of the river channel at Site 1 on the River Ouse: (a) the water bodies in the simulation domain; (b) water bodies that need to be removed; and (c) extracted river channel with overlapping area with bridge; and (d) the extracted river channel. ...	69
Figure 3.14: 2 m LiDAR-derived DEM for the application Site 1 on the River Ouse. (a) DEM without elevations associated with tree canopies removed; (b) DEM with elevations associated with tree canopies removed.....	71
Figure 3.15: Processing of the along bank low cells (Site 1): (a) Along-bank cells that are lower than the initial stage (6.937 m) in the river channel; and (b) DEM with along-bank lower cells raised to the initial inflow stage in the river channel (6.937 m).....	72
Figure 3.16: DEMs of different resolutions for the application carried out at Site 1 (4m, 8m, 16 m and 32 m).....	74
Figure 3.17: DEMs of different resolutions for the application carried out at Site 2 (4m, 8m, 16 m and 32 m).....	75
Figure 3.18: 8 m DEM for the application carried out at Site 3.....	75
Figure 3.19: Inflow hydrographs obtained from a 1D river flow model (ISIS) in the River Ouse: (a) at Site 1; and (b): at Site 2 and 3. Arrow points to the time when validation data were acquired.....	76
Figure 4.1: Schematic view of the numerical solution of the 2D diffusion wave model in a raster environment.....	87
Figure 4.2: Model Graphical User Interface.....	88
Figure 4.3: Loosely-coupled flood inundation model main configuration frame.....	89
Figure 4.4: Hydrograph input and application type panel.....	90
Figure 4.5: Panel for model output.....	90
Figure 4.6: Panel for accuracy assessment.....	91
Figure 4. 7: Inundated areas over time for the first 100 hours with different wetting threshold values.....	92
Figure 4.8: Time series of inundation extent obtained from the 4 m simulation: inundation extents overlain with LiDAR images (dark areas are low-lying floodplains).....	93
Figure 4.9: Time series of estimated inundation extent (for the first 38 hours) obtained from simulations with different resolutions.....	94
Figure 4.10: Time series of total inundated area for the 8 m, 16 m and 32 m simulations.....	95
Figure 4.11: Maximum inundation extent obtained from the 4 m (4.11a), 8 m (4.11b), 16 m (4.11c) and 32 m (4.11d) mesh simulations.....	96
Figure 4.12: Predicted inundation extents obtained using different model resolutions at the time when the validation data was acquired (around 300 hrs into the flood event).....	97
Figure 4.13: Aerial imagery taken on the 9 <sup>th</sup> November, 2000 at Site 1 (Naburn Weir) on the River Ouse (reproduced from Figure 3.6a).....	98

Figure 4.14: Comparison of time series of overall accuracy (4.14a) and conditional Kappa (wet cells only) (4.14b) using the 4 m inundation patterns as reference data.....	100
Figure 4.15: Predictions of inundated area through time for the first 50 hours of simulations with different mesh resolutions and values of Manning's $n$ .....	102
Figure 4.16: The relationship between $n$ and the percentage over-estimation of inundated extent at 50 hours into the simulation. A negative over-estimation is equivalent to under-estimation. ....	103
Figure 4.17: Conditional Kappa (wet cells) during the first 50 hours of simulation with 8 m (4.17a), 16 m (4.17b) and 32 m (4.17c) mesh resolutions and spatially uniform roughness values between 0.4 and 10.0.....	104
Figure 4.18: Comparison of time series of conditional Kappa values for wet cells for model predications with different interpolation methods at each time step, with the inundation extents from 4 m resolution simulation used as the reference verification data (first 60 hours).....	106
Figure 4.19: Time series of estimated inundation extent (for the first 100 hours) obtained using an 8 m DEM.....	109
Figure 4.20: Time series of estimated inundation extent (for the first 100 hours) obtained using a 16 m DEM.....	110
Figure 4.21: Time series of estimated inundation extent (for the first 100 hours) obtained using a 32 m DEM.....	111
Figure 4.22: Predicted inundation extents obtained using different model resolutions at the time when the validation data was acquired (around 300 hrs into the flood event): 4.22a, validation data; 4.22b; 8 m; 4.22c; 16 m; and 4.22d; 32 m. ....	112
Figure 4.23: Estimated inundation areas through time obtained from simulations with different mesh resolutions. ....	113
Figure 4.24: Overestimation of the inundation area using the 32 m simulation compared with the 16 m simulation: (a) Site 1 application; and (b) Site 2 application. (A negative value is equivalent to underestimation).....	113
Figure 4.25: Time series of the estimated inundation extent during the first 185 hours of the flood event, obtained from an 8 m simulation in the city centre of York.....	115
Figure 4.26: Estimated inundation extent at the validation point (around 300 hours into the flood event).....	115
Figure 4.27: Validation aerial imagery taken at around 300 hours into the flood event. ....	115
Figure 4.28: Comparison of the stages at A64 Trunk Road and Skelton Gauging Station (stage at A64 Trunk Road is used at Site 3).....	117
Figure 4.29: Inundation extent predicted using the stage hydrograph (Figure 4.28) at Skelton Gauging Station as inflow data at the validation point (300 hrs into the flood event). .	117

Figure 4.30: Inflow hydrograph plotted against predicted time series of inundated areas obtained from different mesh resolutions: (a) application at Site 1; and (b) application at Site 2.....	119
Figure 5.1: A schematic illustration of the effects of averaging a high-resolution topographic dataset (a) to a lower resolution (b) in relation to a wave of water moving from the left (elevation shown in italic). Topographic data in (a) (non-italic) is averaged to (b) (non-italic) on a coarsening ratio of 2:1. Solid lines are the coarsened mesh cell boundaries. Dotted lines are the sub grid cell boundaries.....	124
Figure 5.2: Schematic view of the sub grid topography. (a) shows the model with its sub grid cells; $e_1$ , $e_2$ , $e_3$ and $e_4$ are sub grid cell bed elevations; $w$ is the resolution of the model grid. (b) shows the four elevations unwrapped onto a 1D plain; $H$ is the sub grid water surface elevation; $E$ is the bed elevation of the model cell which is equal to the average of its sub grid cell elevations. ....	125
Figure 5.3: Super-position of elevation-flux relationship (Equation 5.1) (dashed line) on sub grid elevation-flux relationship (Equation 5.2). ....	127
Figure 5.4: Complex sub grid features and their volume-water surface elevation relationship. ....	128
Figure 5.5: Comparison of the time series inundation extents in the first 40 hours for: (a) the original diffusion model; and (b) the sub grid treatment model; using an 8 m resolution DEM.....	134
Figure 5.6: Comparison of the time series inundation extents in the first 40 hours for: (a) the original diffusion model; and (b) the sub grid treatment model; using a 16 m resolution DEM. ....	135
Figure 5.7: Comparison of the time series inundation extents in the first 40 hours for: (a) the original diffusion model; and (b) the sub grid treatment model; using a 32 m resolution DEM. ....	136
Figure 5.8: Predictions of inundated area against time for the first 300 hours of model simulation for three mesh resolutions with both default treatments and sub grid-scale treatments. ....	137
Figure 5.9: Accuracy statistics (overall accuracy, Kappa and conditional Kappa for wet cells only) determined for model simulations at 32 m, 16 m and 8m, with and without a sub grid treatment. These are determined as a function of time, taking the 4 m solution without a sub grid treatment as ‘true’ for verification purposes.....	139
Figure 5.10: Plots of inundation area versus time for the first 50 hours of simulation, with different mesh resolutions and values of $n$ . ....	141
Figure 5.11: Overall accuracy (a, b, c), Kappa (d, e, f) and conditional Kappa (for wet cells only) (g, h, i) for the 8 m (a, d, g), 16 m (b, e, h) and 32 m (c, f, i) original (heavy	

weighted lines) and sub grid (light weighted lines) treatments, with varying values of $n$ . To aid plotting, the different $n$ simulations are not highlighted. In almost all cases, higher values of $n$ are given by the upper lines and lower values of $n$ by the lower lines. Where this is not the case, it is highlighted on the relevant plot. (continued on next page)	143
Figure 5.11: Overall accuracy (a, b, c), Kappa (d, e, f) and conditional Kappa (for wet cells only) (g, h, i) for the 8 m (a, d, g), 16 m (b, e, h) and 32 m (c, f, i) original (heavy weighted lines) and sub grid (light weighted lines) treatments, with varying values of $n$ . To aid plotting, the different $n$ simulations are not highlighted. In almost all cases, higher values of $n$ are given by the upper lines and lower values of $n$ by the lower lines. Where this is not the case, it is highlighted on the relevant plot. (continued from last page)	144
Figure 5.12: The peak inundated area estimated with the original and the sub grid treatments and $n = 0.06$ . (a) shows the 8 m default simulation; (b) shows the 16 m default simulation; (c) shows the 32 m default simulation; (d) shows the 8 m sub grid simulation; (e) shows the 16 m sub grid simulation; and (f) shows the 32 m sub grid simulation.	147
Figure 5.13: Comparison of the time series inundation extents in the first 100 hours for: (a) the original diffusion model; and (b) the sub grid treatment model; using an 8 m resolution DEM.	150
Figure 5.14: Comparison of the time series inundation extents in the first 100 hours for: (a) the original diffusion model; and (b) the sub grid treatment model; using a 16 m resolution DEM.	151
Figure 5.15: Comparison of the time series inundation extents in the first 100 hours for: (a) the original diffusion model; and (b) the sub grid treatment model; using a 32 m resolution DEM.	152
Figure 5.16: Aerial imagery used to validate the model performance of the Site 2 application (reproduced from Figure 4.22a).	153
Figure 5.17: Predicted inundation extents obtained with the sub grid-scale treatment using different model resolutions at the time when the validation data was acquired (around 300 hrs into the flood event): (a) validation data; (b) 8 m; (c) 16 m; and (d) 32 m.	154
Figure 5.18: Computational performance of the simulations using different mesh resolutions for both the sub grid-scale and normal wetting treatments.	156
Figure 6.1: A sample solution to the Preissman Scheme using Java.	168
Figure 6.2: Comparison of the solution sequence for the loosely- and tightly-coupled models.	170
Figure 6.3: Tightly coupled model main configuration frame	171

Figure 6.4: 1D river flow model main configuration frame.....	171
Figure 6.5: Frame for defining cross-section geometry. ....	172
Figure 6.6: Location of the application of the tightly-coupled model on the river Ouse. ....	173
Figure 6.7: DEM derived from LiDAR data for the long reach simulation using the tightly-coupled model.....	173
Figure 6.8: Cross-section locations at application Site on the River Ouse.....	175
Figure 6.9: Location and naming of the cross-sections.....	176
Figure 6.10: Ground elevation profiles of the river according to cross-section geometries...	176
Figure 6.11: Representation of the 1D river channel (coloured polygon) in the raster environment of the 2D floodplain model according to the cross-sections (red lines across the river). ....	176
Figure 6.12: Stage hydrograph recorded at Skelton Gauging Station. ....	177
Figure 6.13: Discharge hydrograph recorded at the Skelton Gauging Station. ....	177
Figure 6.14: Stage hydrograph calculated at the A64 Road Bridge (from the ISIS model)...	178
Figure 6.15: Cross-section geometry of the Skelton Gauging Station (after Environment Agency, 2004). ....	178
Figure 6.16: Velocity hydrograph calculated for the Skelton Gauging Station .....	179
Figure 6.17: Discharge hydrograph corrected at Skelton Gauging Station compared with that recorded. ....	180
Figure 6.18: Velocity hydrograph corrected at Skelton Gauging Station compared with the original velocity estimates.....	181
Figure 6.19: Calibration using Manning's $n$ , with space derivative fixed at 0.52.....	183
Figure 6.20: Optimum calibration results at the Skelton Gauging Station.....	183
Figure 6.21: Optimum calibration results at the Skelton Gauging Station, obtained from the ISIS model. ....	184
Figure 6.22: Time series of inundation extents obtained from the tightly-coupled model at the long reach for the wetting phase (first 182 hours).....	187
Figure 6.23: Time series of estimated inundation extents obtained from the loosely coupled model at Site 3 for the wetting phase (first 185 hours) (reproduced from Figure 4.25). ....	188
Figure 6.24: Estimated inundation extent at the validation point (around 300 hours into the flood event): (a) using the loosely coupled model (reproduced from Figure 4.26); (b) using the tightly-coupled model; and (c) aerial imagery at the validation point (reproduced from Figure 4.26). ....	189
Figure 6.25: Velocity vectors in x and y directions: (a) flow velocity in x (horizontal) direction; and (b) flow velocity in y (vertical) direction; during the wetting phase (around 94 hours).....	190

Figure 6.26: Velocity vectors in x and y directions: (a) flow velocity in x (horizontal) direction; and (b) flow velocity in y (vertical) direction; during the drying phase (around 200 hours).....190

Figure 6.27: Comparison of stage profiles along the river used in the loosely coupled and tightly-coupled models at 10 hrs and 300 hrs (Site 3 starts with cross-section code CS72 (upstream) and ends with cross-section code CS38 (downstream))......192

Figure 6.28: Comparison of the stage hydrograph at the upstream cross-section of Site 3 (CS70) obtained using the tightly-coupled model with that used in the loosely coupled model. ....192

Figure 6.29: Flow direction at 94 hours in x direction: flow directions of the red areas are pointing to the right and blue to the left. ....193

Figure 7.1: Discretization of the domain topography for the coupled modelling of river flow and hillslope runoff in a 2D environment. (after Michaelides and Wainwright, 2002).210

# Chapter 1

## Introduction

Recent developments in hydraulic modelling have been associated with fundamental changes in approach to flood inundation modelling, arising mainly from: (i) the increased availability of high-resolution topographic data; and (ii) improvements in computational resources. At least in research terms, the approach has shifted from one-dimensional finite-difference schemes which solve some simplified forms of the Saint-Venant equations to two-dimensional finite-difference and finite-element schemes. Despite these developments, there remain fundamental issues to be addressed in both the methodological approach and data provision aspects of flood inundation modelling. Fluvial flood modelling usually requires the prediction of flow over complex topography. Much of the current research into two-dimensional modelling of flood inundation has focused upon relatively rural areas (e.g. Bates *et al.*, 1992; Bates and Anderson, 1996; Horritt and Bates, 2001a, b; Bradbrook *et al.*, 2004). Modelling tools have been lacking in the area of urban flood modelling where structural elements such as building, roads and walls on the floodplain may play an important role in the flood inundation (Wheater, 2002). This is a significant omission as potential flood damage is proportionately greater than in rural areas and urban flood inundation is receiving a relatively high political profile. Thus, the aim of this thesis is development of a two-dimensional diffusion wave flood inundation model that is capable of explicit representation of the structural complexity of both urban and structurally complex rural floodplains. Based upon this model, both the methodological and data provision issues relating to fluvial flood modelling in complex floodplain environments will be investigated in this thesis. This chapter will present the research context, identify the research aims and objectives and outline the structure of the thesis.

### 1.1 Research context

Recent floods in the UK (1998, 2000, 2001 and 2002) have raised public, political and scientific awareness of both flood risk and flood protection issues. Flooding has been widely recognized as an issue of strategic importance, with significant economic and social implications (Wheater, 2002). Take a flooding risk assessment in Britain for example: it was found that nearly 2 million properties in floodplains along rivers, estuaries and coasts in the UK are potentially at risk of river or coastal flooding, including eighty thousand properties in

towns and cities (Evans *et al.*, 2004). It is predicted that over the next 100 years, if the current levels of expenditure and approaches to flood management remain unchanged in the UK that: (i) river and coastal flood risk could increase between two and 20 times; (ii) economic damage could increase from £1bn to between £1.5bn and £21bn by the 2080s, compared with growth of GDP of between two and 14 times over the same period; and (iii) damage caused by coastal flooding could increase from 1.6 million today, to between 2.3 and 3.6 million by the 2080s (Evans *et al.*, 2004).

Table 1.1 Summary of present-day flood risks and flood-management costs (Evans *et al.*, 2004)

	Properties at risk	Average annual damage (£ million)	Flood management costs 2003-04 (£ million)
<b>River and coastal flooding</b>			
England and Wales	1,740,000	1,040	439
Scotland	180,000	32(fluvial only)	14
Northern Ireland	45,000	16(fluvial only)	11
<b>Intra-urban flooding</b>			
All UK	80,000	270	320
<b>Total</b>	<b>2,045,000</b>	<b>1,400</b>	<b>800</b>

Thus, this thesis is conducted in the context of a need to develop tools that can assist policy-makers and engineers in mitigating against increasing flood risk in the future.

### 1.1.1 Specification of the problem

Though there has been extensive application of two-dimensional models to flood inundation studies in recent years (e.g. Bates *et al.*, 1992; Feldhaus *et al.*, 1992; Bates *et al.*, 1995), most of these have focused upon relatively rural areas. There has been less development of tools explicitly for determination of flood inundation over topographically complex floodplains, particularly in urban areas<sup>1</sup>. This is partly due to the historically poor availability of high-resolution data that are capable of representing complex urban topography in two-dimensional models and partly due to the limitations of current computational resources. This is a significant omission as the potential flood damage is generally greater than in rural areas and floods in urban areas generally receive a higher political profile. Given this, Wheater (2002)

<sup>1</sup> This thesis is using a simple discrimination of 'urban' and 'rural'. In flood inundation terms there is really a continuum from structurally simple floodplains (here labelled "rural") to structurally complex floodplain (here labelled "urban"). It should be emphasised that structural complexity can be found in rural areas and structural simplicity can be found in urban area. For example, typical rural floodplains are often characterised by dry stone walls, embankments and sometimes, old channels. Thus, the label "urban" and "urban" are labels of convenience rather than fundamentals.

identified improved flood representation in urban areas at both local and catchment scales as one of the key issues for current practice in fluvial flood modelling.

This raises issues of whether or not existing model schemes can be used to simulate flood inundation over topographically complex urban floodplains. Flow over floodplain with complex topography is clearly two-dimensional (Knight and Shino, 1996). The presence of linear and block-like structural elements on the floodplain such as buildings, roads and walls may have a major effect upon both flow routing and flood inundation extent (e.g. the wall in Figure 1.1). The need to model the effect of these features in flood inundation models requires the development of flood inundation modelling in two ways: (i) use of high-resolution data that are capable of representing significant structural elements on the floodplain; and (ii), given (i), associated approaches to describing small-scale flow routing processes in the model. Thus, there is a need to develop both the data provision aspects of and the methodological approaches to process representation in flood inundation modelling.



Figure 1.1: An example showing the effect of structural elements on the floodplain upon flow routing and flood inundation. The picture was taken on the River Ouse during a major flood event occurred in the year 2000.

First, with respect to the data provision issue, recent developments in new data capture techniques provide increasing availability of high-resolution and high-accuracy data (Bates *et al.*, 2003). Indeed, for most applications, topographic data availability is no longer a limiting factor to flood inundation modelling and recent developments have seen a rapid shift from a data-poor to a data-rich and spatially complex modelling environment with ready possibilities for model testing and development (Bates *et al.*, 2003). High resolution topographic data are able to deliver more detailed information about the topographic and topological characteristics of the features. This raises two important issues. First, we need to know which

elements matter for the routing of flood water over floodplains. Any element of significant areal extent, that also has a high volume and which is impermeable, is likely to represent a net loss of storage. If there are many of these elements, the net loss of storage may be significant, and this is likely to be the case in urban areas. Such features may also impact upon routing. If the elements are linear in nature (e.g. a solid wall, a row of terraced houses), but of lower areal extent, then they may have a particularly important impact upon routing, but less of an impact on storage. There has been almost no attempt to assess urbanised floodplains in relation to storage and routing impacts. In this thesis, it is assumed that both topography and topology are important due to potential storage and routing effects. Second, it is necessary to assume that such elements are sufficiently represented in available data. This may not be the case. In this thesis, it is assumed that the available data are sufficient to represent storage and routing effects, although further research in remote sensing would be valuable to assess the extent to which this is the case. However, two-dimensional models are generally computationally expensive (Bates and De Roo, 2000). Full use of high-resolution topographic data in 2D models (e.g. RMA-2, TELEMAC-2D, MIKE21) that solve the full form of the depth-averaged Navier-Stokes equations, including finite-element (e.g. Gee *et al.*, 1990; Bates *et al.*, 1992), finite-difference (e.g. Zeilke and Urban, 1981) and finite-volume (e.g. Lane *et al.*, 1994) methods, may not be feasible, particularly over large scales. Furthermore, these methods usually require the topographic data to be filtered to fit the mesh used in the model. For example, the finite-element method commonly involves a two-stage filtering of raw data into a digital elevation model and then into a numerical mesh consisting of finite elements. This coarsens the data used in the model (Bates and Anderson, 1996). More computationally efficient two-dimensional schemes, such as those based on storage cell (e.g. LISFLOOD-FP in Bates and De Roo, 2000) and diffusion wave approaches (e.g. LISFLOOD-FP in Horritt and Bates, 2001a) can make better use of high-resolution data, at the expense of simplified representation of momentum transfer process on the floodplain.

Second, with respect to the representation of small-scale flow routing processes associated with structural elements in flood inundation models, in both one- and two-dimensional models (both diffusion wave and depth-averaged), topographic variability is commonly represented through up-scaling of a roughness parameter, using calibration if necessary (e.g. Cobby *et al.*, 2003; Mason *et al.*, 2003). Traditionally, one-dimensional, finite-difference methods (e.g. HEC-RAS, MIKE11, FLUCOMP) discretize the floodplain and river channel into a series of cross-sections perpendicular to the flow direction and calculate the cross-section averaged velocity and water depth at each cross-section given appropriate inflow and outflow boundary conditions (Bates and De Roo, 2000). The water depth is then either overlain onto a DEM or linearly interpolated across the floodplain to get the inundation extent.

As the topography between cross-sections is not explicitly represented, one-dimensional schemes are incapable of modelling the complex effects of structural features on the floodplain. In two-dimensional finite-element schemes, parameterization of the roughness coefficient is based upon manipulation of a sink in the momentum equations through the bottom stress term that appears in the depth-averaged equations (e.g. Cobby *et al.*, 2003). However, structural features such as houses, walls etc. also have a blockage effect or mass balance effect. Research by Lane *et al.* (2004b) shows that traditional parameterization of high-resolution topographic variability in 3D hydraulic models using up-scaling of roughness heights does not necessarily represent mass blockage effects correctly. The same conclusion may hold for floodplain structures in 2D models. Second, up-scaling of Manning's  $n$  may reduce fluxes across the linear sets of model elements that represent these features, but this may not result in zero flux, even where structural features on the floodplain create continuous barriers to flow.

Thus, in relation to data provision, there is a need for flood inundation models that are capable of efficient use of the increasingly available high-resolution high-accuracy data. Recent developments have seen the application of computationally efficient raster-based models using high-resolution topographic data. This is considered to be a promising direction for flood inundation modelling over topographically complex floodplains. Similarly, in relation to process representation, there is a need for two-dimensional models to describe local wetting and drying processes more adequately in order to realize the full potential of the application of high-resolution topographic data in such models. Various algorithms have been developed to describe local wetting and drying processes in finite-element models (e.g. Defina *et al.*, 1994; Bates, 2000). However, methods for describing local wetting and drying processes have been lacking for both two-dimensional storage cell approach and diffusion wave approaches. This is significantly important for flood inundation modelling in urban areas using high-resolution topographic data.

### **1.1.2 The approach: modelling effects of structural elements in flood inundation modelling**

Given the above research context, the two-dimensional storage cell approach (e.g. Cunge *et al.*, 1976; Bechteler *et al.*, 1994; Estrela and Quintas, 1994; Bates and De Roo, 2000) and diffusion wave approach (Chow *et al.*, 1988; Fread, 1993; Singh, 1996) are considered to be the most promising ways of modelling flood inundation over complex topography given their computational efficiency and ease of fusion with high-resolution topographic data. Storage cell and diffusion wave approaches are subtly different in terms of the calculation of the flow

between cells. A storage cell approach determines the magnitude of the flow from one cell to the other based upon a function of the free surface height difference between these two cells, using a uniform flow equation such as the Manning equation and Darcy-Weisbach equation. The flow rates in the  $x$  and  $y$  directions are not linked and are calculated independently. For example, the volumetric flow rates between two cells in  $x$  and  $y$  directions can be calculated by (Horritt and Bates, 2001b):

$$Q_x^{i,j} = \frac{h_{flow}^{5/3}}{n} \left( \frac{h^{i-1,j} - h^{i,j}}{\Delta x} \right)^{1/2} \Delta y \quad (1.1a)$$

$$Q_y^{i,j} = \frac{h_{flow}^{5/3}}{n} \left( \frac{h^{i,j-1} - h^{i,j}}{\Delta y} \right)^{1/2} \Delta x \quad (1.1b)$$

where  $h_{flow}$  is the free surface difference between two cells,  $n$  is the Manning's friction coefficient for the floodplain,  $h_{i,j}$  is the water free surface height at the node  $(i,j)$ , and  $\Delta x$  and  $\Delta y$  are the cell dimensions. For the diffusion wave approach the flow rate to the  $x$  and  $y$  directions is linked and, for example, flow to the  $x$  direction can be given by equation (1.2) (Horritt and Bates 2001b):

$$Q_x^{i,j} = \frac{\frac{h_{flow}^{5/3}}{n} \left( \frac{h^{i-1,j} - h^{i,j}}{\Delta x} \right)^{1/2} \Delta y}{\left[ \left( \frac{h^{i-1,j} - h^{i,j}}{\Delta x} \right)^{1/2} + \left( \frac{h^{i,j-1} - h^{i,j+1}}{2\Delta y} \right)^{1/2} \right]^{1/4}} \quad (1.2)$$

In a storage cell approach, the floodplain can be discretized into either regular structured grids or unstructured grids using a variety of geometries. The diffusion wave approach commonly represents the floodplain using regular sized cells ( $\Delta x = \Delta y$ ) and thus, is often termed 'raster-based'. This makes the use of high-resolution topographic data obtained using new data capture techniques more straightforward and to a large degree eliminates the problems encountered in the two-stage filtering process in a finite-element approach (e.g. Marks and Bates, 2000). The optimum use of high-resolution data in a diffusion wave model may, to some extent, reduce the dependence of the model upon parameterization of roughness related to structural elements on the floodplain. However, due to the poorly represented momentum transfer effects on the floodplain, the full potential of high-resolution data can only be realized if the small-scale wetting and drying processes relating to variations in topography are represented. Thus, this thesis approaches representation of wetting and drying under the basic philosophy of the diffusion wave approach: effective representation of a complex

process using a simplified representation whilst allowing an explicit representation of floodplain topography using high-resolution topographic data.

## **1.2 Research aims and objectives**

Based on the above, this thesis investigates the extent to which a two-dimensional diffusion wave approach can be used to model fluvial flood inundation over topographically complex floodplains, with a particular emphasis on urban areas, using high-resolution topographic data.

### **1.2.1 Research aims**

The main aim of this research study is to develop a two-dimensional raster-based diffusion wave model to simulate fluvial flood inundation over topographically complex floodplains, coupled with a one-dimensional flow model in the river channel, using high-resolution topographic data. Based on this model, the methodological issues concerning model application in urban areas will be investigated, focusing upon the interaction between mesh resolution, roughness parameterization and small-scale flow routing processes.

### **1.2.2 Research objectives**

In order to achieve the aims, several research objectives have been identified. Major progress has been made in storage cell and diffusion based modelling in a raster-based environment over the last 5 years (Bates and De Roo, 2000; Horritt and Bates, 2001a, 2001b; Bradbrook *et al.*, 2004). Thus, a literature review is required to make the originality of the work presented in this thesis explicit. Similarly, as a key component of model development in fusion between the model and the topographic data required, review of literature in relation to: (i) new data capture techniques such as Remote Sensing; and (ii) data representation approaches such as those using Geographical Information System; (GIS) is required. This objective seeks to understand the current practice in fluvial flow modelling, with a particular emphasis on assessing the role of new data from remotely-sensed sources. This also evaluates the current and potential role of GIS in model development, particularly with respect to data representation.

The second set of objectives are related to model development. First, a fluvial flood inundation model with a two-dimensional diffusion wave treatment is developed for the simulation of flow routing on the floodplain, loosely-coupled with an existing 1D river flow model through the common boundary. This will use existing flow modelling approaches for the river flow. Second, a one-dimensional river flow model, based upon Preissmann's Scheme,

which solves the full Saint-Venant equations, is developed and tightly-coupled with the 2D floodplain model. Both coupling approaches establish the connectivity between the river flow and floodplain flow through the provision of inflow data along the common boundary for the 2D model. The tightly-coupled model accounts for the effect of return water flows back into the river as calculated in the 2D model. This is novel as existing diffusion wave models are either only loosely-coupled to fully hydrodynamic 1D flow models or tightly-coupled to a simplified 1D flow model based on kinematic routing (e.g. Bates and De Roo, 2000) or diffusion wave models (e.g. Horritt and Bates, 2001a, b), or a highly simplified flow approximation (e.g. Bradbrook *et al.*, 2004).

The third set of objectives relate to data processing and model applications. Given available data, this objective seeks to apply the model to 4 sites on the River Ouse in the City of York. This will seek: (i) to assess the data requirements and undertake relevant data processing for model application; (ii) to explore the effects of structural elements upon flow routing and inundation extent; (iii) to explore the effect of spatial resolution upon flow routing and inundation extent; (iv) to explore the role of roughness parameterization in a diffusion wave approach by sensitivity analysis; (v) to assess the methods for coupling 1D model in the river and 2D model on the floodplain and implement the coupling; (vi) to compare the 1D model with existing models; (vii) to compare the 1D model with uncoupled solution; and (viii) to validate the model using quantitative methods.

The final set of objectives is concerned with the development of new process representation methods that describe small-scale flow wetting and drying in 2D raster-based diffusion wave models. The thesis seeks to develop a method for sub grid-scale topographic representation with an explicit treatment of the effects of structural elements on the floodplain upon both cell blockage and flux. This is believed to be a major contribution to the improved representation of urban flooding noted as being required by Wheater (2002).

Upon achieving these objectives, a better understanding will be gained about the fluvial flood modelling over complex topography where structural elements play an important role in flow routing.

### **1.3 Thesis structure**

The introduction has described the broad context of modelling fluvial flood inundation over complex topography with respect to developments in both the methodological approaches used and new data capture techniques available, the issues that need to be addressed when

modelling flood inundation over topographically complex floodplains (§1.1), and the aims and objectives that the thesis seeks to address (§1.2). This section presents the thematic structure of the thesis in terms of chapter outlines.

Chapter Two will address objective set one, by reviewing recent developments and general practice in hydraulic modelling including flood inundation and river flow. The review includes: (i) methodological development in flood inundation and river flow modelling (§2.3); (ii) opportunities created by new data capture techniques and application of Remote Sensing in flood inundation modelling (§2.4); and (iii) data representation in river flow and flood inundation modelling in relation to Geographical Information Systems (GIS) (§2.5).

Chapter Three describes the case study applications in terms of the applications carried out, data requirements and availability. This will be structured according to the types of data: (i) model geometry data, including river and floodplain topography; (ii) boundary condition data, including inflow hydrograph in the river-floodplain boundary, river hydrometric data and roughness coefficients for the river and floodplain; and (iii) validation data including inundation extent. This will cover objective set two.

Chapter Four describes the development and testing of the two-dimensional diffusion wave model for the modelling of fluvial flood inundation over complex floodplain topographies. The model application will be described, focusing upon the effects of spatial resolution and model sensitivity to roughness parameterization. This will address part of objective set three.

Chapter Five develops and tests a sub grid-scale wetting treatment approach for fluvial flood modelling over complex topography. The effects of this approach upon both cell blockage and flux related to structural features on the floodplain are investigated. Testing is undertaken to look at the impacts of this method upon inundation-time patterns and interactions with roughness parameterization as compared with the results from Chapter Four. This will address objective set four.

Chapter Six focuses upon the development of the tightly-coupled version of the model where a one-dimensional river flow model is coupled tightly to the two-dimensional diffusion wave model described in Chapter Four and applied in Chapter Four and Five. The application of this tightly-coupled model to a longer reach on the River Ouse across the City of York will be described. This addresses the second part of objective set three.

Chapter Seven concludes by referring back to the research context, aims and objectives described in Chapter Two, including an assessment of the methods used and results obtained, and identification of future research needs.

# Chapter 2

## Literature Review

### 2.1 Introduction

The last few decades have witnessed fundamental changes in approach to hydraulic modelling, including both river flow and fluvial flood inundation, in terms of process representation, data provision and modelling environment. An increasing number of physically based hydraulic models have been developed, providing considerable insight and understanding into flow processes. These models either describe a single process or couple several processes together by including proper treatment of common boundary conditions. The approach to modelling flow processes can be quite different in terms of model dimensionality and the degree of numerical simplification of the governing physical laws. The choice of model dimensionality and degree of numerical simplification should depend upon the properties of the area of interest and modelling scale, and will be constrained by data availability and quality as well as computational cost and feasibility. Data availability and computational cost and feasibility have all changed dramatically over the last two decades. These developments, along with the methodological advances in hydraulic modelling, provide the broad context for this review.

### 2.2 Chapter aims and objectives

This chapter reviews recent developments in hydraulic modelling with the aim of understanding current practice in river flow and fluvial flood modelling in general and, with reference to the modelling of flood inundation over complex topography, using high-resolution topographic data in particular. Current practice in river flow and fluvial flood modelling (§2.3) is considered in terms of process representation, topographic parameterization, model calibration and validation for both 1D and 2D modelling approaches. The development of new topographic data capture techniques and its implications for model parameterization, calibration and validation are presented in Section 2.4. Section 2.5 discusses briefly the role of GIS in river flow and flood inundation modelling, focusing upon the data representation options provided by GIS. These establish the fundamentals of the approach that is used for model development as presented in this thesis.

## 2.3 Review of river flow and flood inundation modelling

This thesis only considers fluvial flood and other flood types such as those caused by pluvial sources and floods associated with urban drainage systems are not considered in the thesis. Fluvial floods are normally caused by an increase in discharge, which results in an increase in water level, and flow is no longer constrained within the channel. However, the form of relationship between stage and discharge does not just depend on flow properties. It also depends on channel geometry, boundary properties such as roughness, and slope of the energy line. These processes refer to conveyance: poor conveyance will result in a rapid rise in water surface elevation for a given rise in discharge. Similarly, floodplain conveyance also depends upon flow and floodplain properties. River flow and fluvial flood inundation are essentially two integral parts of the natural river-floodplain system, with the channel geometry and roughness simply becoming more complex for over-bank flows on the floodplain (Knight and Shiono, 1996).

Until relatively recently, the most popular approaches to hydraulic modelling at the catchment scale (5-50km) have been the one-dimensional (1D) finite-difference schemes which solve the full Saint-Venant equations (e.g. Fread, 1984; Samuels, 1990), such as MIKE11, ISIS, ONDA, FLUCOMP and HEC-RAS (Bates and De Roo, 2000). For flow below bank full depth, there is an increasing consensus that flow processes can be adequately described by a one-dimensional representation (Shino and Knight, 1991; Knight and Shiono, 1996). However, over-bank flow typically has two-dimensional (2D) and even three-dimensional (3D) characteristics. It has been found that, at the interface of the floodplain and the river channel, development of intense shear layers leads to a strongly turbulent and three-dimensional flow field (e.g. Knight, 1989). Out-of-bank flow in meandering compound channels is now known to be highly three-dimensional and involves the development of a strong shear layer between the river channel and the floodplain (Knight and Shiono, 1996).

Indeed, two-dimensional, depth-averaged models have been described extensively in the literature for some time and are increasingly being applied to natural river-floodplain systems (see the review of Lane, 1998). In line with developments in methodological approaches to high-dimensional hydraulic modelling, new data capture techniques are emerging, particularly in the field of airborne remote sensing and photogrammetry, including interferometric synthetic aperture radar (SAR) (e.g. Brackett *et al.*, 1995; Horritt and Bates, 2001a), aerial digital photogrammetry (e.g. Biggin and Blyth, 1996; Lane, 2000; Lane *et al.* 2003, Westaway *et al.*, 2001, 2003), and laser induced detection and ranging (LiDAR) (e.g. Krabill

*et al.*, 1994; Flood and Gutelius, 1997; Marks and Bates, 2000; Charlton *et al.*, 2003; Lane *et al.*, 2004).

Two-dimensional models are best employed in conjunction with a DEM that describes the floodplain and river channel at a resolution that is commensurate with the model and that, with appropriate inflow and outflow boundary conditions, allows water depth and depth-averaged flow velocity to be computed at each computational node or cell at each time step (Bates and De Roo, 2000). The increasing availability of new data sources allows two-dimensional models to be applied over a larger area with a higher resolution, than has been possible using the data obtained from traditional field survey methods. Most recently, 2D raster-based models have gained credence in the modelling of flood inundation (Horritt and Bates, 2001a). Raster-based models typically use a 1D flow model in the river channel linked to a 2D treatment of flow routing on the floodplain. As raster-based models discretize the floodplain into structured grids, the use of a DEM is relatively straight forward compared with approaches that involve unstructured cells such as finite-element and storage cell approaches.

This section reviews general practice in river flow and flood inundation modelling (§2.3.1), from one-dimensional to two-dimensional approaches, followed by a review of raster-based modelling (§2.3.2) and a discussion of flood modelling over structurally complex floodplains (§2.3.3). Section 2.3.4 points out the implications of these developments for this research explicitly.

### **2.3.1 General practice in river flow and flood inundation modelling**

Recent research in hydraulic modelling tends increasingly to treat river and floodplains as an integral system with coupled analysis of hydraulic processes. This arises on the one hand from the perception that methodological approaches are available for coupled modelling and on the other hand from the heightened political awareness of the linkage between legislation and physical processes on the floodplain. Thus, the associated model complexity has increased due to the need to represent interactions between the river flow and floodplain flow, notably at the interface of the systems.

Conceptually, the river-floodplain system is illustrated in Figure 2.1 (Knight and Shiono, 1996). This shows how the presence of vorticity and turbulence exerts a strong influence upon water velocity and boundary shear stress via momentum transfer, particularly at the interface of the river channel and floodplain. At low depths on the floodplain, a shear layer develops

between the faster moving flow in the river channel and the slower moving flow on the floodplain. Thus, this section discusses developments in modelling the river-floodplain system, beginning with the traditional one-dimensional approach followed by more recent developments using two-dimensional approaches.

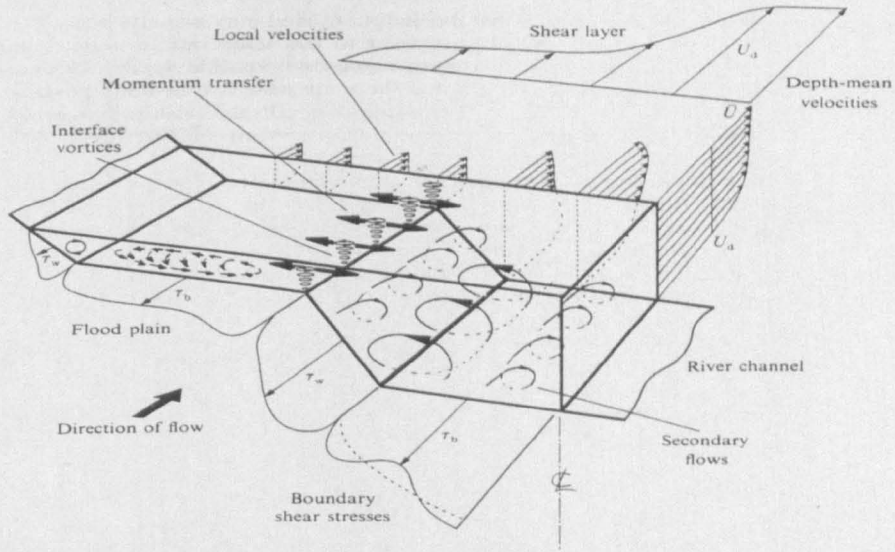


Figure 2.1: Hydraulic parameters in the river-floodplain system (after Knight and Shiono, 1996).

### One-dimensional river flow and flood inundation models

Traditional one-dimensional finite-difference schemes for hydraulic modelling, and thus implicitly flood inundation, normally solve the full or simplified form of the Saint-Venant equations developed by de Saint-Venant in 1871. The conservative form of the mass equation is

$$\frac{\partial Q}{\partial x} + \frac{\partial A}{\partial t} = 0 \quad (2.1)$$

and the momentum equation is

$$\frac{1}{A} \frac{\partial Q}{\partial t} + \frac{1}{A} \frac{\partial Q}{\partial x} \left( \frac{Q^2}{A} \right) + g \frac{\partial y}{\partial x} - g(S_0 - S_f) = 0 \quad (2.2)$$

where  $x$  is the increment over space,  $t$  is the increment over time,  $Q$  is the water volume,  $A$  is the cross-section area,  $g$  is the acceleration due to gravity,  $y$  is the water depth,  $S_0$  is the local bed slope and  $S_f$  is the slope of the energy grade line.

The derivation of the Saint-Venant equations is based on the following assumptions (Chow, 1988): (i) the flow is one-dimensional and depth and velocity vary only in the longitudinal

direction of the channel, with constant velocity and horizontal depth along each cross-section; (ii) the flow is assumed to vary gradually along the channel so hydrostatic pressure prevails and vertical accelerations can be ignored (Chow, 1959); (iii) the longitude of the channel is approximated as a straight line; (iv) the bottom slope of the channel is small and channel bed is fixed; (v) the flow is locally uniform so that relationships such as the Manning equation can be used to describe resistance effects; and (vi) the fluid has constant density and is incompressible.

Both the mass and momentum equations in the full Saint-Venant equations are essentially one-dimensional simplifications of the three-dimensional Navier-Stokes form. The momentum equation (Equation 2.2) can be further simplified by ignoring certain terms, leading to kinematic wave (Equation 2.3) and diffusion wave forms (Equation 2.4).

$$S_0 - S_f = 0 \quad (2.3)$$

$$\frac{\partial y}{\partial x} = S_0 - S_f \quad (2.4)$$

One-dimensional schemes using the full or simplified Saint-Venant equations, in their simplest form, treat the floodplain and river channel as an integral system and discretize the floodplain and river channel into a series of cross-sections perpendicular to the stream-wise flow direction (Bates and De Roo, 2000). Given appropriate boundary conditions and model parameters, numerical solutions can then be used to calculate cross-section-averaged water depth and velocity at each cross-section. If prediction of flood inundation extent is required, the water depth values at each cross-section are either overlain onto a DEM or interpolated between cross-sections to give the inundation extent (Bates and De Roo, 2000). The main problem in this is that flooding necessarily implies that the bank full depth has been reached. Whilst this approach is sufficient for channel flow (Knight and Shiono, 1996), once the bank full depth is reached, the situation will become much more complex. It has been found that flow on the floodplain is typically 2D and, at the interface of the floodplain and the river channel where development of intense shear layers leads to strong turbulent fields, even 3D (Knight and Shiono, 1996).

In the context of integrated fluvial flood modelling using 1D approaches this may give rise to a number of significant problems. Apart from the poorly represented topography between cross-sections, and consequently the increased chance of error when determining flood extent by interpolating water depths between cross-sections over complex topography, 1D models

may suffer from the increasing complexity in specifying the cross-sectional geometry and the related roughness coefficient arising from the discontinuity in the stage-discharge hydrograph resulting from over bank flow.

For 1D models, a major issue resulting from the discontinuity involves specification of the roughness parameter. In 1D models that solve the Saint-Venant equations, the roughness coefficient commonly appears through a friction-slope ( $S_f$  in Equation 2.2) relationship that not only represent bottom stress, but also turbulence effects (vertical and lateral shears) and dispersion processes upon the distribution of the mean flow properties, the latter resulting from depth- and width- integrating the full three-dimensional form of the Navier-Stokes equations (Lane and Hardy, 2002). Roughness is often used in 1D or 2D models to represent processes that are not explicitly represented in the model structure, e.g. secondary acceleration and turbulence effects (Lane and Hardy, 2002). Thus, strictly speaking, the roughness parameter in 1D models represents hydraulic roughness instead of bed roughness alone. One-dimensional models tend to have high sensitivity to roughness parameterization. This makes the roughness parameter a key calibration parameter in 1D models.

The friction slope in the Saint-Venant equations is commonly determined under the assumptions that: (i) the flow is locally uniform; and (ii) resistance laws derived for flow in circular pipes can be applied for open channel flow to calculate roughness coefficients. These allow uniform flow equations to be used. Since a roughness parameter is the property of both the river channel and the flow, specification of roughness coefficients is site-specific and depends upon the flow process being represented. In practice, this raises two issues in the specification of a roughness parameter. First, roughness in the governing equations is known to vary according to water depth or discharge in most river flows and the variation of the roughness coefficient with Reynolds number and relative roughness is normally defined by the Colebrook-White equation (1937, 1939, cited by Knight and Shiono, 1996). However, the Colebrook-White equation strictly speaking only applies to flow in circular pipes and is not suitable for flow in very complex cross-sections (Knight and Shiono, 1996). Second, in situations where there is a heterogeneous roughness distribution around the wetted parameter, ancillary equations need to be introduced since the Colebrook-White equation is only valid for uniform roughness values (Knight and Shiono, 1996).

Despite, and probably also due to, the complexity involved in determining roughness, various approaches exist for the specification of roughness parameters. In practice, approaches to determining the roughness parameter can be classified into four categories (Lane and Hardy, 2002). In the first category, the roughness parameter is determined from properties of the

channel and the flow using uniform flow equations. This may result in odd situations when water levels reach bank full depth and floodplain flow begins (Knight and Brown, 2001). At this point, there is a sudden increase in wetted perimeter, which results in an effective reduction in hydraulic radius, and hence roughness parameter. Here the shear layer developed at the interface of the floodplain and river channel and the high relative roughness of the floodplain features should result in a net increase in flow resistance. The second approach is based upon the concept that roughness is additive and recognizes that the effective roughness of a river depends upon the scale over which it is measured (e.g. Cowan, 1956, cited by Lane, 2003a; Knight and Shiono, 1996). Cowan (1956, cited by Lane, 2003a) argued that roughness can be specified by calculating the sum of roughness due to skin friction or individual grains ( $n_0$ ), due to bed geometry ( $n_1$ ), due to cross-section morphology ( $n_2$ ), and due to obstructions in the flow such as boulders or islands ( $n_3$ ) and vegetation ( $n_4$ ). Furthermore, this value may be scaled by  $m$  to represent the effect of channel curvature. Alternatively, the channel can be sub-divided into a series of sub-areas with similar hydraulic properties and a composite roughness value can be calculated from these of the sub-areas (Knight and Shiono, 1996). This is the method used in HEC-RAS. The third approach addresses this in part by specifying a relationship between channel bed material and the roughness parameter (e.g. Strickler, 1923, cited by Lane, 2003a; Mason *et al.*, 2003). The approach adopted by Mason *et al.* (2003) is an extension of Strickler approach but for the special case of vegetation. The final approach reflects all of these methods and is based upon photographs of river reaches of known roughness, often determined through uniform flow equations (e.g. Barnes, 1967; Hicks and Mason, 1991) (cited by Lane, 2003a).

There is one fundamental property in all of these roughness estimation approaches: roughness is being treated as an effective value, the one that is required to represent energy losses correctly for the given model being used. It is well accepted that the meaning of roughness changes with model process representation (e.g. Lane and Hardy, 2002). It is less reported that roughness is strictly a discretisation-dependent property: the required value of roughness may depend on cross-section spacing in a one-dimensional model; and mesh resolution in a two-dimensional model. This was illustrated for the two-dimensional case by Horritt and Bates (2001a) and Horritt and Bates (2002).

### **Two-dimensional flood inundation models**

Though traditional one-dimensional models have a long history in hydraulic modelling, and such models are still widely used, often at quite small spatial scales (see the review by Lane, 1998), recent years have seen widespread use of two-dimensional models of floodplain flow (Beven, 2000), including TELEMAC-2D (e.g. Bates and Anderson, 1993; Galland, *et al.*,

1994; Bates *et al.*, 1998a, b), MIKE21 (Feldhaus *et al.*, 1992) and RMA2 (e.g. Bates *et al.*, 1992, 1995; Bates and Anderson, 1996). Such models solve some form of the Navier-Stokes equations, in conjunction with a number of approximations, including representation of processes such as turbulence and boundary friction. Such approaches discretize domain geometry and topography into grids and define a network of computational nodes where the equations can be solved numerically. Following Lane (1998), 2D models begin by depth-averaging two key equations derived from Newton's law of motion, assuming hydrostatic pressure distribution and constant water density with depth: (i) the law of conservation of mass for an incompressible fluid in Eulerian form:

$$\frac{\partial u}{\partial x} + \frac{\partial v}{\partial y} + \frac{\partial w}{\partial z} = 0 \quad (2.5)$$

where  $u$ ,  $v$  and  $w$  are respectively the velocity in  $x$ ,  $y$  (horizontal) and  $z$  (vertical) direction; and (ii) the Navier-Stokes momentum equation for an incompressible fluid:

$$\begin{aligned} \frac{\partial}{\partial t}(u) + \frac{\partial}{\partial x}(u^2) + \frac{\partial}{\partial y}(uv) + \frac{\partial}{\partial z}(uw) - 2u\Omega \sin \Phi + g \frac{\partial h}{\partial x} + g \frac{\partial z_b}{\partial x} + \frac{1}{\rho} \frac{\partial \tau_{xx}}{\partial x} \\ - \frac{1}{\rho} \frac{\partial \tau_{xy}}{\partial y} - \frac{1}{\rho} \frac{\partial \tau_{xz}}{\partial z} = 0 \end{aligned} \quad (2.6)$$

$$\begin{aligned} \frac{\partial}{\partial t}(v) + \frac{\partial}{\partial x}(v^2) + \frac{\partial}{\partial y}(v^2) + \frac{\partial}{\partial z}(vw) - 2v\Omega \sin \Phi + g \frac{\partial h}{\partial y} + g \frac{\partial z_b}{\partial y} + \frac{1}{\rho} \frac{\partial \tau_{xy}}{\partial x} \\ - \frac{1}{\rho} \frac{\partial \tau_{yy}}{\partial y} - \frac{1}{\rho} \frac{\partial \tau_{yz}}{\partial z} = 0 \end{aligned} \quad (2.7)$$

where  $\rho$  is the density of the water,  $h$  is the water depth,  $z_b$  is the bottom elevation,  $\Phi$  is the latitude,  $\xi$  is the angular rotation of the earth,  $g$  is the acceleration due to gravity,

$$\frac{\tau_{ij}}{\rho} = \mu \left( \frac{\delta_j}{\delta i} + \frac{\delta_i}{\delta j} \right) \quad (2.8)$$

and  $\mu$  is the coefficient of viscosity of a Newtonian fluid.

Due to computational constraints, in practical applications at catchment scale, these equations are commonly simplified to their depth-averaged, Reynolds averaged form. These are defined by:

$$\bar{V}_i = \frac{1}{h - z_b} \int_{z_b}^h \bar{v}_i \partial z \quad (2.9)$$

This aims to calculate the horizontal distribution of the depth-averaged velocity components,  $\bar{U}$  and  $\bar{V}$  (Rodi *et al.*, 1981), where capital letters indicate depth-averaged quantities and over-bars indicate time-averaged quantities.

Combining this equation with Equation 2.5 for law of conservation of mass, the resulting mass equation is

$$\frac{\partial h}{\partial t} + \frac{\partial}{\partial x} [(h - z_b) \bar{U}] + \frac{\partial}{\partial y} [(h - z_b) \bar{V}] = 0 \quad (2.10)$$

Combining this equation with the momentum equations (Equations 2.6 and 2.7), ignoring the Coriolis terms, gives the  $x$  component and  $y$  component momentum equations

$$\begin{aligned} \frac{\partial}{\partial t} (\bar{U}) + \frac{\partial}{\partial x} (\bar{U}^2) + \frac{\partial}{\partial y} (\bar{U} \bar{V}) = & -g \frac{\partial h}{\partial x} - g \frac{\partial z_b}{\partial x} + \frac{1}{\rho} \frac{\partial}{\partial x} (\overline{\tau_{xx}}) + \frac{1}{\rho(h - z_b)} \frac{\partial}{\partial y} (\overline{\tau_{xy}}) - \frac{\tau_{hx}}{\rho(h - z_b)} \\ & + \frac{1}{\rho} \frac{\partial}{\partial x} \int_{z_b}^h \rho (\bar{u} - \bar{U})^2 \partial z + \frac{1}{\rho(h - z_b)} \frac{\partial}{\partial y} \int_{z_b}^h \rho (\bar{u} - \bar{U})(\bar{v} - \bar{V}) \partial z \end{aligned} \quad (2.11)$$

$$\begin{aligned} \frac{\partial}{\partial t} (\bar{V}) + \frac{\partial}{\partial y} (\bar{V}^2) + \frac{\partial}{\partial x} (\bar{U} \bar{V}) = & -g \frac{\partial h}{\partial y} - g \frac{\partial z_b}{\partial y} + \frac{1}{\rho} \frac{\partial}{\partial x} (\overline{\tau_{xy}}) + \frac{1}{\rho(h - z_b)} \frac{\partial}{\partial y} (\overline{\tau_{yy}}) - \frac{\tau_{hy}}{\rho(h - z_b)} \\ & + \frac{1}{\rho(h - z_b)} \frac{\partial}{\partial y} \int_{z_b}^h \rho (\bar{v} - \bar{V})^2 \partial z + \frac{1}{\rho(h - z_b)} \frac{\partial}{\partial x} \int_{z_b}^h \rho (\bar{u} - \bar{U})(\bar{v} - \bar{V}) \partial z \end{aligned} \quad (2.12)$$

This set of equations has been used in the last 20-30 years for modelling of free surface flows where the vertical distribution of velocity can be ignored. Models solving these equations are generally termed two-dimensional Shallow Water Wave Models (SWWM). Numerical methods for solving these equations include finite-difference (e.g. Holster, 1978; Rajar, 1978; Falconer and Chen, 1991); finite-element (e.g. Bates and Anderson, 1993; Holz and Leister, 1998); and finite volume approaches (e.g. Lane *et al.*, 1994; Tchamen and Kahawita, 1998;

Beffa and Connell, 2001; Nicholas and Mitchell, 2003; Lane *et al.*, 2004). The solution in space is then projected forward into time using a further numerical method. Given appropriate boundary conditions, the water depth and two depth-averaged components of the flow velocity at each computational node can be obtained at each time step.

The results of many two-dimensional models show reasonable correspondence to available field data and generally considered to be better than one-dimensional models as more known hydraulics are represented (Marks and Bates, 2000) (e.g. Tayefi, 2005; Tayefi *et al.*, in review). Indeed Tayefi *et al.* (in review) showed severe limits in terms of both numerical stability and model predictions when a 1D model was applied to a complex rural floodplain. However, it was shown by Horritt and Bates (2002) that, calibrated against discharge and inundation areas, 1D HEC-RAS outperforms 2D LISFLOOD-FP. LISFLOOD-FP produced relatively poor results if calibrated using discharge data. Thus, for 2D flood inundation models to be fully used, a number of problems still need to be addressed. These can be broadly divided into two categories: (i) those concerning the methodological approach inherent in the modelling procedure (such as representation of wetting and drying processes, turbulence representation, friction representation and the numerical solver used); and (ii) those that result from inadequate data provision (particularly topographic data). Two-dimensional models require distributed topographic data for calibration and validation and possibly for friction parameterization (Horritt and Bates, 2001b). With respect to methodological approaches, turbulence modelling has by far received the most attention while friction laws have generally been ignored in terms of physical development (Bates, 2000). For practically applicable numerical schemes, wetting and drying processes have not been given adequate treatment (Bates, 2000). For flood inundation over topographically complex floodplains, wetting and drying processes will have significant effects upon flow routing and flood extent. The next section will review the developments in wetting and drying treatment in shallow water flow modelling related to moving boundary problems.

### **Wetting and drying treatment in two-dimensional flood inundation models**

A major issue in current research into two-dimensional representation of flood inundation is representation of local wetting and drying processes, particularly those associated with a moving boundary within the calculation domain. Most of the current schemes suffer from some kind of numerical instability, usually in the form of an unphysical negative depth. The causes of the instability are diverse and can be broadly divided into three groups: (i) improper schemes which are unable to accommodate the complex flow conditions; (ii) inappropriate treatment of the friction source term and the large local curvature in topography; (iii) mishandling of the boundary cells that are partially wet/dry (Tchamen and Kahawita, 1998).

Much effort has been made to address these problems and a number of methods have been developed for representing wetting and drying in 2D flood inundation models (e.g. Lynch and Gray, 1980; Laura and Wang, 1984; Kawahara and Umetsu, 1986; Benkhaldoun and Monthe, 1994; Tchamen and Kahawita, 1998; Bates, 2000). These methods can be broadly divided into four broad groups (Lane, 1998): (i) fixed spatial elements, excluding partially wet elements; (ii) fixed spatial elements, but including partially wet elements with some special treatment; (iii) deforming boundary; and (iv) boundary dividing.

In the first approach, an element is removed or added into a simulation domain according to a pre-defined criterion which determines the status of the element, with some correction for the partially wet or dry elements through some form of boundary treatment (Lane, 1998). The status of the element is commonly determined by some small positive depth,  $\lambda$  (King and Roig, 1988; Leclerc *et al.*, 1990), to define the wet-dry threshold (Bates, 2000). The main problem with this approach is that it is not mass and momentum conservative (Holz and Nitsche, 1982) and it assumes an artificial wall at the interface of the partially wet cell and the fully wet cell (Bates, 2000). This approach is also likely to be computationally unstable, as large changes in the lateral extent of the free surface may result in spurious velocities on partially wet areas, where gravity terms in the momentum equation dominate the solution (Bates *et al.*, 1995; Lane, 1998). Though it is computationally efficient for simple changes in inundation extent (France, 1981), for applications involving complex inundation patterns and large inundation extents, additional computational nodes need to be calculated at each time step (Akanbi and Katopodes, 1988) and this can be computationally demanding (Lynch and Gray, 1980; Gopalakrishnan and Tung, 1983).

The second approach keeps the partially wet/dry cells in the calculation with a special treatment for the flow either in the mass equation or momentum equation. Holz and Nitsche (1982) developed a method which involves an iterative procedure whereby the velocity of a partially wet element is extrapolated to neighbouring and completely wetted elements to describe the mass transfer between the elements. The calculated water level on the element boundary is then compared with the water volume in the element to check whether convergence criteria are met. Though this approach achieves mass conservation, momentum is not conserved during the calculation and it is computationally demanding (Lane, 1998). Related to this, an assumption is made that some of the terms such as the above-water slope term, friction term, Coriolis force or wind stress in the momentum equations for the partially wet/dry elements can be cancelled (e.g. Leclerc *et al.*, 1990) or replaced to prevent the development of unrealistic velocities resulting from the spurious non-zero free surface gradient across the element (Bates, 2000). Although this approach has the advantages of

simple implementation, it is robust for model application and has improved momentum conservation, the mass within the domain is still not correct (Bates, 2000). The most realistic fixed-grid approaches involve reformulating the mass equations using a domain scaling coefficient  $\eta$  varying from 0 (fully dry) to 1 (fully wet) (Bates, 2000) to represent the proportion of actual water volume within an element at each time step that is available for outflow based upon the sub grid topography (e.g. RMA-2 (Bates *et al.*, 1992); Defina *et al.*, 1994; Bates and Anderson, 1993). Such methods improve mass conservation and have the most theoretical rigour. They provide an ideal basis for fixed-grid wetting and drying schemes. However, they still suffer from a number of problems (Bates, 2000): (i) mixed discretization whereby the scaling coefficient is defined per element and unknown variables are defined per node; and (ii) difficult parameterization of the scaling coefficient if the sub grid topography is unknown. Bates (2000) attempted to address the above limitations using a sub grid approach. In this approach, the Defina algorithm was explicitly implemented in the model. Instead of using a small depth criterion to identify the partially wet elements, a simple free surface slope analysis was undertaken at each time step to identify the partially wet elements by comparing the bed elevation at a given node with the free surface elevation at any of the other nodes in the same element. Based upon the sub grid topography, the mass equation is then implicitly scaled using the scaling coefficient  $\eta$  for the calculation of unknown variables. In this approach, the above-water slope terms in the momentum equation that may cause spurious water surface gradients are also cancelled. This approach improves both mass and momentum conservation and has been found to give significant improvement over standard finite-element techniques based on a simple test case (Bates, 2000).

The third approach involves node migration and mesh deformation for elements along the wetting/drying boundary (e.g. Katopodes and Strelkoff, 1978; Lynch and Gray, 1980; Gopalakrishnan and Tung, 1983; Akanbi and Katopodes, 1988). However, the velocity and direction of node migration may be difficult to determine and additional computation requirements involved in node migration and re-meshing may be prohibitively high (Bates, 2000). The fact that most shallow water problems involve complex bathymetry and the construction of a computational mesh needs to be coupled closely to the boundary characteristics make the implementation of grid deformation unfeasible in practical applications (Lane, 1998; Bates, 2000). Lane (1998) suggested that there might remain some potential for mesh deformation that is closely coupled with spatial variation in boundary conditions.

The final set of approaches describes the wetting and drying processes by tentatively assuming a position for the flow boundary at each time step, dividing the partially wet

elements in the boundary of the spatial domain into a number of sub-elements and deforming the sub-element boundary to accommodate the corrected position of the free surface using an iterative procedure, either implicitly (e.g. King and Roig, 1988) or explicitly (e.g. Holz and Nitsche, 1982).

### 2.3.2 Raster-based flood inundation modelling

Raster-based models have recently been developed and tested for modelling of floodplain flow inundation (e.g. Bates and De Roo, 2000; Horritt and Bates, 2001a, b; Bradbrook, *et al.*, 2004). The concept of raster-based modelling was first proposed by Cunge *et al.* (1976). Similar methods have been used by Bechteler *et al.* (1994) and Estrela and Quintas (1994). This typically uses a one-dimensional representation of channel flow linked to a simple 2D treatment of flow between adjacent cells on the floodplain. The 1D model in the river channel solves the Saint-Venant equation either through a kinematic wave approximation (Bates and De Roo, 2000; Horritt and Bates, 2001b) or a diffusion wave approximation (Horritt and Bates, 2001b). Floodplain flow routing is commonly treated using a storage cell or diffusion wave approach. This determines the magnitude of flow between any two adjacent cells on the floodplain in response to the water surface elevation difference estimated from mass conservation and the diffusive components of the depth-averaged momentum equations only. This leads to a change in the water depth in a cell.

Bates and De Roo (2000) developed a raster-based model (LISFLOOD-FP) based upon this concept and compared it (25-100 m) with a relatively coarse resolution (50-250 m) 2D finite-element scheme (TELEMAC-2D) and a planar surface model. Unlike other models, this model was specifically designed to predict flood inundation and ignored or minimized the representation of processes that were not considered central to the aim (Bates and De Roo, 2000). Tentatively, these results indicated that topography is more important than process representation for effective prediction of inundation extent. However, several issues such as model calibration, friction parameter representation and the differing resolutions of the two models needed to be addressed before conclusions could be substantiated (Horritt and Bates, 2001b). The effect of mesh resolution upon flow routing in the raster-based model was investigated by Horritt and Bates (2001a). LISFLOOD-FP was applied to a 60 km reach of the river Severn, UK to simulate a flood event that occurred in 1998, using a resolution ranging from 10 m to 100 m. In this study, it was found that resolutions better than 100 m give similar performance. The optimal roughness value was found to be constant with change in mesh resolution when calibrated against inundation extent. It was also noted that the storage area in low lying areas on the floodplain near the river channel was an important mechanism

affecting flood-wave travelling velocity. Horritt and Bates (2001b) compared LISFLOOD-FP with a two-dimensional finite-element model (TELEMAC-2D). Though the raster-based and the two-dimensional finite-element models showed similar performance, insufficiently accurate validation data and the lack of friction parameterization data made it difficult to distinguish between the two kinds of model formulations. More recently, the ability of the LISFLOOD-FP model to predict flood extent and flood-wave travel time has been compared with a 1D (HEC-RAS) and a 2D model (TELEMAC-2D) using independent calibration data from hydrometric and satellite sources (Horritt and Bates, 2002). Results revealed that the LISFLOOD-FP model required independent inundated area data for calibration in order to achieve good predictions of inundation extents. Recent research on raster-based modelling is summarised in Table 2.1 in terms of the application, discretization, processing representation, model calibration, validation and verification.

In terms of the coupling of river flow and floodplain flow, raster-based modelling has been using a relatively simple treatment (e.g. Bates and De Roo, 2000; Horritt and Bates, 2001a, b), which only accounts for the mass transfer between the river cells and floodplain cells while neglecting effects such as channel-floodplain momentum transfer and the effect of advection and secondary circulation on mass transfer. It should be noted that the poor representation of momentum transfer will become more of a problem as flow depth increases and inertial terms begin to dominate over terms associated with topographic forcing.

In terms of validation of the floodplain flow routing, the inundation extents have been the dominant data sources (e.g. Bates and De Roo, 2000; Horritt and Bates, 2001a, b). Validation of river flow using hydrometric data has also been addressed (e.g. Bates and De Roo, 2000). However, validation of flood prediction in terms of water depth and velocity on the floodplain has largely been ignored.

The wetting and drying representation at the sub grid-scale has not been addressed in raster-based 2D diffusion wave models (e.g. Bates and De Roo, 2000; Horritt and Bates, 2001a, b). If these processes are not represented correctly, it may cause the water to diffuse across the floodplain too quickly. In the model developed in this thesis, the wetting and drying processes within a cell are controlled by a wetting parameter (§4.3.1) that describes the percentage of the cell that is wet at each time step and out flow is not allowed if the cell is not fully wet as indicated by the wetting parameter (Following Bradbrook *et al.*, 2004). However, this does not address the direction of wetting and drying. Thus, a wetting and drying representation based on sub grid topography is developed and tested in this thesis (§5). In this approach, both the

direction and volume of the flux in and out a grid cell are controlled by the sub grid topography explicitly, by first order approximation.

The above research suggests that, compared to numerical solutions including finite-element (e.g. Giammarco *et al.*, 1996), finite-difference (e.g. Gee *et al.*, 1990) and finite volume (Lane *et al.*, 1994) forms, the advantages of raster-based models are their ease of formulation, computational efficiency and simplified calibration. Compared with finite-element approaches, the initialisation of raster-based models does not involve the construction of finite-element mesh. Instead, raster-based models allow direct use of a DEM. This eliminates the problem associated with two-stage filtering (§1.1.1) (Bates *et al.*, 1996) which coarsens the data used in finite-element models. It has been found that raster-based models have considerable computational advantages over the finite-element scheme (Horritt and Bates, 2001a). The relative disadvantage of the raster-based models is their simple representation of flow processes, due partially to the poor representation of momentum transfer on the floodplain, and between the river and floodplain. Thus, new issues such as the coupling of river flow and floodplain flow, and the representation of wetting and drying processes within a cell still need to be addressed in raster-based modelling, along with other fundamental issues such as model calibration, topographic parameterization and model validation and verification.

### 2.3.3 Urban flood inundation modelling

The presence of significant structural features (houses, walls, levees, abandoned channels, etc.) on a river floodplain is important in relation to both the volume of the floodplain that can be occupied by the flow and the direction and velocity that the flow takes across the floodplain. Field investigations have shown that these structural features can have significant control upon floodplain inundation patterns (Lewin and Hughes, 1980, Simm, 1993; Nicholas and Walling, 1997) and flow velocities (Nicholas and McLelland, 1999). For example, Connell *et al.* (2001), in their application of the Hydro2de model (Beffa, 1996) to the Waihao River, New Zealand, reported that fences on the floodplain were observed to gather debits during floodplain flow and increase water level on their upstream side by 0.1-0.3 m. Connell *et al.* (2001) conclude that if above-ground structural features such as building, fences and hedges, and in-water hydraulic features could be represented in the model, model performance might be improved considerably.

Hydraulic modelling in the river channel and on the floodplain using both 1D and 2D approaches involves the specification of a roughness related term which represents the

internal (flow related) and external (topography related) resistance to the flow. Whilst the meaning of roughness parameters in river channels might be clear, it becomes more challenging to define them in relation to flood inundation modelling. Traditionally, this has been due to the great heterogeneity of land cover and the lack of availability of detailed information about the topography of the floodplain. Lane and Richards (1998) found that even using a uniform channel roughness coefficient was problematic in that it neglected the great variety of bed forms present in reality and introduced significant errors into the prediction of velocity. In both 1D and 2D (both diffusion wave and depth-averaged) models, topographic structure is commonly represented through up-scaling of a roughness parameter (e.g. Cobby *et al.*, 2003; Mason *et al.*, 2003), with calibration where necessary. Up-scaling of roughness is well established for representing the effects of individual grains and grain organizations in models of flow in gravel-bed rivers where the roughness length is multiplied upwards (e.g. Lane & Richards, 1998, Lane *et al.*, 1999) and for representing the effects of vegetative roughness in floodplain flow models, where Manning's  $n$  is scaled upwards (e.g. Mason *et al.*, 2003). One-dimensional models tend to have a high sensitivity to roughness and this makes roughness a key focus of parameterization in 1D models. Raster-based flood inundation models have commonly used a uniform roughness coefficient for the floodplain but have treated it as the key calibration parameter (Bates and De Roo, 2000; Horritt and Bates, 2001a, b; Horritt and Bates, 2002). In relation to sensitivity, it has been found that LISFLOOD-FP is relatively insensitive to roughness specification on the floodplain (Horritt and Bates, 2002) when inundation area is considered.

Authors	Application/ Discretization	Main focuses	Process Representation in the raster-based model	Calibration/Roughness parameterization in the raster-based model	Validation/Verification of the raster-based model
Bates and De Roo (2000)	Applied to a 35 km reach of the River Meuse in the Netherlands to simulate a flood event occurred in January 1995.	Examine the general performance of the raster-based model (LISFLOOD-FP).	One-dimensional kinematic wave approximation solved using explicit finite-difference method for flow representation in the river channel.  Two-dimensional diffusion wave approach representation of floodplain flows.  Outflow is allowed in 4 directions.	Calibration was not undertaken.  Uniform Manning's $n_c = 0.02$ and $N_{fp} = 0.06$ were used in the model.	Flood inundation extent was validated against shorelines observed from air photography and SAR (12.5 m) imagery. 1D model results were validated against downstream observed discharge and stage.  Model performance (25 m model) was compared with inundated area predictions obtained using two other methods: a planar approximation to the free water surface based on a linear interpolation of maximum water surface elevations and a relatively coarser (50-250 m) 2D finite-element model.
Horritt and Bates (2001a)	The number of maximum cells used in the raster-based model is 108000.  Applied to a 60 km reach of the River Severn, UK to simulate two flood events occurred in the year 1998 and 2000.	Investigate the effect of model resolution upon flood inundation and the role of small-scale flow routing in large scale flood inundation modelling.	One-dimensional diffusion wave approximation solved using explicit finite-difference method for flow representation in the river channel.  Two-dimensional diffusion wave approach representation of floodplain flows.  Outflow is allowed in 2 directions.	The model was calibrated at two scales (50 m and 250 m), with floodplain roughness value fixed at 0.06 and ranging from 0.02 to 0.05 in upstream and the downstream of the river channel.	Raster model was validated against the flood shoreline obtained from SAR data (12.5 m) using a statistical active contour technique.
Horritt and Bates (2001b)	Floodplain was represented using a 10-100 m resolution DEM derived from airborne laser altimetry (LiDAR).  Applied to a 4 km reach of the upper River Thames, UK.  Floodplain was represented using a 50 m resolution DEM in the raster-based model. 76*48 cells are used in the simulations.	Compare two floodplain inundation modelling approaches: an improved version of LISFLOOD-FP and a 2D finite-element model (TELEMAC-2D).  Calibration of the improved LISFLOOD-FP model using roughness coefficient.	One-dimensional diffusion wave approximation solved using explicit finite-difference method for flow representation in the river channel.  Two-dimensional diffusion wave approach representation of floodplain flows.  Outflow is allowed in 2 directions.	The model was calibrated using different roughness values for the river channel (0.01-0.05) and floodplain (0.02-0.1)  Premium calibration was found in the centre of the parameter space.	Raster model was validated against the flood shoreline obtained from SAR data (12.5 m) using a statistical active contour technique.  Model performance was compared to inundated area predictions obtained using two other methods: a planar approximation to the free water surface based on a linear interpolation of maximum water surface elevations recorded and a relatively coarser (<50-100 m) 2D finite-element model.

Table 2.1: Recent applications of raster-based flood inundation modelling (continued on next page).

Authors	Application/ Discretization	Main focuses	Process Representation in the raster-based model	Calibration/Roughness parameterization in the raster-based model	Validation/Verification of the raster-based model
Horritt and Bates(2002)	Applied to a 60 km reach of the River Severn, UK to simulate two flood events occurred in the year 1998.  Floodplain was represented using a 50 m resolution DEM derived from airborne laser altimetry.	Compare the relative performance of the 1D (HEC-RAS) and 2D (LISFLOOD and TELEMAC-2D) flood inundation models, and in particular, the performance of flood inundation prediction on one flood event when calibrated on another.	One-dimensional diffusion wave approximation solved using explicit finite-difference method for flow representation in the river channel.  Two-dimensional diffusion wave approach representation of floodplain flows.  Outflow is allowed in 2 directions.	The model was calibrated using different roughness values for the river channel (0.01-0.05) and floodplain (0.02-0.1)	The raster model was validated against the flood shoreline obtained from two SAR images (12.5 m), one (for the 1998 event) using a statistical active contour technique and the other (for the 2000 event) using a simple classification approach.  Model performance (50 m model) was compared with inundated area predictions obtained using two other methods: a 1D model (HEC-RAS) and a relatively coarser ~30 m 2D finite-element model. Benchmark comparison between the JFlow and normal depth (for steady flows) and 1D hydrodynamic solutions (for unsteady flows).
Bradbrook <i>et al.</i> (2004)	Applied to a flood event on the River Thames at Buscot, UK. Floodplain was represented using a 50 m resolution DEM.	Assess the effects of channel parameterization.  Assess the treatment of wetting process.	One-dimensional kinematic wave approximation solved using explicit finite-difference method for flow representation in the river channel.  Two-dimensional diffusion wave approach representation of floodplain flows.  Outflow is allowed in 2 directions.	Sensitivity analysis was carried out with different floodplain roughness values.	Flood outline derived from derived from SAR images (the ERS-1) was used to validation the predicted inundation extent.

Table 2.1: Recent applications of raster-based flood inundation modelling (continued from last page).

In relation to flood inundation, roughness parameterization could become more complex if the required roughness values were allowed to vary spatially as a function of local structural complexity. Horritt (2000) used a simple distributed roughness calibration scheme in fluvial flood modelling and obtained a minor improvement over the uniform parameterization. LiDAR data have been successfully used to upscale Manning's  $n$  in a distributed way for floodplain vegetation (e.g. Cobby *et al.*, 2003 and Mason *et al.*, 2003) although this assumes that: (i) vegetative roughness relationships developed from flume experiments can be applied to two-dimensional mapping of  $n$  from vegetation height; (ii) the prime control on  $n$  is vegetative roughness and there is no need to calibrate roughness to take into account the effects of other processes (e.g. turbulence and secondary circulation); and (iii) the required value of  $n$  is determined by the surface and not the discretization of the model. However, the extent to which this approach can be extended to urban areas is questionable. First, parameterization of  $n$  is based upon manipulation of a sink in the momentum equations, either through the bottom stress term that appears in the full solution of the depth-averaged equations (which may in turn be expressed as a function of  $n$  within an appropriate resistance law), or through specification of  $n$  in the simpler momentum representation in a 2D diffusion model. Structural features such as houses, walls etc also have a blockage effect which reduces the volume of storage that is possible on the floodplain and which can have a major effect upon routing. Research by Lane *et al.* (2004) shows that traditional parameterization of high-resolution topographic variability in 3D hydraulic models using up-scaling of roughness heights does not necessarily represent mass blockage effects correctly. The same conclusion may hold for floodplain structural elements in 2D models. Second, many structural elements have topographical properties that create continuous barriers to flow (e.g. walls) and which can have a very major effect upon flow routing process. Upscaling of  $n$  may reduce fluxes across linear sets of grid cells, but will not necessarily recognize the full topological nature of a structure by eliminating those fluxes altogether.

Harnessing high-resolution data has its advantage in that it may reduce uncertainty over how we parameterize roughness in relation to structural features. Use of uniform flow equations in high-resolution raster-based models provides a way to recognize the mass blockage effect of these structural features as uniform flow equations determine the flow based upon ground elevation difference between cells. If the small-scale variation in topography between complex features is fully recognised, the direction of the flow can be determined relatively accurately.

Another major issue for flood inundation modelling over topographically complex floodplains; including urban areas is the complexity involved in model validation. First, validation data are often difficult to obtain for accurate representation of flood inundation patterns over complex terrain. Traditional field survey methods are able to provide hydrometric data for validation. But if the inundation extent prediction is the main concern, traditional field survey methods may not be able to provide detailed flood inundation patterns for strict validation purposes over the whole simulation area, even for topographically simple floodplains (further covered in §2.4.1). Even with emerging new data capture techniques, calibration in terms of inundation extent can still be a problem, particularly if complex topography is involved. For example, Bates and De Roo (2000) compared the inundation extents obtained from three data sources: (i) aerial imagery; (ii) SAR-derived inundation extents calculated using the standard thresholding technique (e.g. Tholey, 1995; Imhoff, 1997); and (iii) SAR-derived inundation extents calculated using the ‘snake’ technique (Cohen, 1991; Williams and Shah, 1992). It was found that, if the aerial imagery was assumed to be the ground truth, the relative accuracy of (ii) and (iii) was only 83.3 and 81.0%, respectively. Notably, two urban areas on the floodplain, which were treated in method (i) and (ii) as flooded were treated as dry in method (iii). Second, flood inundation is dynamic and validation using at-a-point in time data may not show the whole picture of the model performance with respect to flood inundation over time. For example, if the floodplain is laterally confined and the validation data is obtained long after the floodplain is fully flooded and before the drying phase of the flood event, the validation may produce good accuracy statistics. However, it does not show model performance on the falling and rising limb of the flood event, which may have very different performance. Thus, when complex urban topography is involved, model validation needs to be carefully interpreted.

### **2.3.4 Implications for this research**

The above sections (§2.3.1 – §2.3.3) have reviewed general practice in 1D and 2D river flow and flood inundation modelling (§2.3.1), including raster-based modelling approaches (§2.3.2), and the complexity of flood modelling over topographically complex floodplains (§2.3.3), particularly in urban areas. In terms of river flow modelling, there is increasing consensus that a 1D representation is adequate for most applications (Knight and Shiono, 1996). However, floodplain flow is much more complex and a 2D representation is normally required. This becomes more relevant if flood inundation over topographically complex floodplains is considered. The main difficulties in flood modelling over topographically complex floodplains, including urban areas, are related to representation of structural elements on the floodplain and the associated small-scale flow routing processes. Traditional

methods of representing small-scale topographic variability through up-scaling of roughness heights may not represent mass blockage effects correctly (Lane *et al.*, 2004). Furthermore, if spatially distributed roughness parameterization is required, the situation will be more complex and a number of assumptions have to be made. These provide the broad context for the aims that this thesis identified in Chapter One.

Recent research into raster-based modelling shows that this approach has a better capability for using higher-resolution topographic data than is possible with other computationally extensive approaches such as 2D finite-element methods, in particular over large areas. Flood inundation modelling using raster-based models, when integrated with high-resolution data, may reduce the uncertainty into how we parameterize the topographic surface, and hence reduce the dependence upon roughness parameterization in flood inundation modelling. These developments, along with developments in new data capture techniques (discussed in §2.4), provide opportunities for the research aims and objectives identified in section 1.2 to be addressed.

In line with the development of approaches to hydraulic modelling, new data capture techniques are emerging, which are providing increasing opportunities for high-resolution representation of small-scale topographies in 2D hydraulic models, including raster-based modelling. The next section reviews the topographic data requirements of hydraulic modelling and the opportunities created by new data capture techniques, in terms of topographic parameterization, calibration and validation.

## **2.4 The application of remotely sensed data in flood inundation modelling**

Remotely sensed data, obtained from airborne remote sensing and satellite imaging are increasingly becoming an important data source for hydraulic and hydrological studies. Recent developments in new data capture techniques have stimulated a significant potential for hydrodynamic application. Hydraulic models have developed significantly as the number of satellite and airborne platforms has multiplied and as their global coverage, spatial resolution and temporal resolution have improved (Pietroniro, 2002). Remotely sensed data are most often used to evaluate a watershed's physical characteristics and state variables. Three classes can be identified in the application of remotely sensed data in hydrology (Salomonson, 1983). The first involves simple delineation of readily identifiable, broad-scale surface features (e.g. Tholey *et al.*, 1997; Bates and Horritt, 2000). The second involves more detailed interpretation and classification of remotely sensed data to derive more detailed

information (e.g. Cobby *et al.*, 2003; Mason *et al.*, 2003). The third, involves the derivation of various hydraulic or hydrological state variables and parameters, either for model initialization or validation (e.g. Profeti and MacIntosh, 1997).

This section reviews these developments and their implications for hydraulic modelling, in particular for topographically complex floodplains. First, this section discusses the data requirements for high-resolution flood inundation modelling (§2.4.1) with respect to model parameterization, calibration and validation. This is followed by a review of the advantages of and recent developments in harnessing high-resolution remotely sensed data in river flow and flood inundation modelling (§2.4.2). Particular attention is given to the opportunities created by the emergence of airborne scanning laser altimetry (LiDAR) for high-resolution flood inundation modelling (§2.4.3).

#### **2.4.1 Topographic data requirements for high-resolution flood inundation modelling**

Recent advances in numerical modelling of river flow and flood inundation have raised a number of issues with respect to topographic data requirements. Traditionally, high-resolution flood inundation modelling has been hampered by the lack of accurate information about the characteristics of the river channel and floodplain for model parameterization/initialization, calibration and validation (Marks and Bates, 2000). The limited use of two-dimensional finite-element models in practical applications is partially due to the lack of distributed data they require (Horritt and Bates, 2001b). However, this situation has been gradually relieved in the past 5 years by the emergence of new data capture techniques and, in some cases, data availability is no longer a limiting factor for hydraulic modelling. This section reviews the data requirements for hydraulic modelling.

##### **Data for topographic parameterization/initialisation**

Parameterization can be thought as the qualification of physically based models with the actual conditions happening in the real world. In term of topographic parameterization, Bates and Anderson (1996) demonstrated the significant and complex effect that a small change in topography ( $\pm 10$  cm) might have on a two-dimensional finite-element model. For coupled analysis of river and floodplain flows, high-resolution topographic data on river bathymetry are also required.

In terms of river geometrical data for flow modelling, cross-section survey is normally required to provide parameters such as cross-section geometry and bed slope (e.g. Horritt and

Bates, 2001a, b). Combined with inflow and outflow boundary conditions, numerical solutions can then be used to solve the full or simplified governing equations.

In terms of floodplain topographic representation, before the routine collection of remotely sensed data, the only national topographic data available to parameterize a two-dimensional finite-element model was a 10 m DEM, produced from contours or spot height data provided by the UK Ordnance Survey (Marks and Bates, 2000). Ordnance Survey benchmark data are typically reliable to better than  $\pm 1$  cm (Bates and Anderson, 1996) if well maintained. However, contour data, particularly those in extensive low-lying floodplains, are considerably less reliable (Bates and Anderson, 1996) due to their sparse coverage (Marks and Bates, 2000). Ordnance Survey contour data are only recorded at 5 m spacing and are quoted to have a vertical accuracy of up to  $\pm 1.25$  m (Marks and Bates, 2000; Bates, 2004).

DEM data derived from contour data or spot heights are typically of a vertical accuracy of no better than 50 cm (Marks and Bates, 2000). For the DEM to be used in finite-element models, it has to be sampled further, on a node-by-node basis, to a different resolution. Thus, for data to be of practical use, they have to undergo a two-stage filtering process which will inevitably coarsen the data, resulting in less detailed representation of the land surface. For raster-based modelling, if contours and spot height data are used as raw data, the second filter stage is slightly different from that used in finite-element models in that the DEM is sampled on a cell-by-cell basis instead. Another major parameterization variable is surface roughness, which is usually determined through calibration.

### **Data for model calibration**

In addition to topographic parameterization, high-resolution flood inundation models require sufficiently accurate data for model calibration, which also involves some kind of parameterization. The aim of model calibration is to optimize model predictions by adjusting one or more parameters to replicate observed or validation data. One-dimensional flow models may be easier to calibrate, both because there are fewer parameters, and because sensitivity to those parameters is greater (Lane and Richards, 2001). Two-dimensional flood inundation models commonly contain one or more calibration parameters for each computational node, which must be specified by traditional field measurements or determined during model calibration based upon prior knowledge.

Calibration parameters are model dependent and inherent to the particular model structure selected. Two-dimensional finite-element models typically use boundary friction and turbulence closure model related coefficients for model calibration. For raster-based models,

as with almost all hydraulic models, roughness coefficients are commonly used as free parameters for calibration. Both 2D finite-element and raster-based models have commonly used a spatially and temporally uniform roughness value for the river channel and floodplain respectively (e.g. Bates *et al.*, 1996, Bates and De Roo, 2000). However, the effects of spatially varying (e.g. Horritt, 2002; Cobby *et al.*, 2003) and temporally varying (e.g. Kouwen and Unny, 1973; Kouwen and Li, 1980; Fathi-Moghadam and Kouwen, 1997; Wu *et al.*, 1999; Kouwen and Fathi-Moghadam, 2000) roughness values have also been investigated. Indeed, roughness coefficients have been dominantly used as calibration parameters in raster-based models. It has been found that raster-based models are relatively insensitive to roughness parameter values on the floodplain (Horritt and Bates, 2001a). Apart from the roughness parameter, another calibration parameter in finite-element models is the turbulent eddy viscosity ( $\nu t$ ), the importance of which increases as grid size decreases. Bates *et al.* (1998) found that TELEMAC-2D was relatively insensitive to  $\nu t$ .

As environmental systems are always indeterminate and the number of parameters is always greater than the number of equations describing the system, potentially different sets of parameters can lead to the same model predictions. This means that a model may get the right results for the wrong reasons. For example, Bates *et al.* (1996) show that a range of combinations of friction and turbulent viscosity values can predict the downstream hydrograph equally well in a 2D finite-element model, while giving 13% variation in the total inundation area. This is the concept of equifinality, which involves the same results being attained from different model structures or combinations of different calibration parameters (Beven, 1996). In 2D depth-averaged modelling of flood inundation, evaluation using the catchment outflow hydrograph is more likely to produce problems of equifinality than evaluation of model predictions using distributed patterns of floodplain inundation (Lane and Richards, 2001). Furthermore, as model application invariably involves assumptions and simplifications that require representation of their otherwise important effects using semi-empirical treatments (Lane, 2003a) and the interactions between calibration parameters are often unknown, the uncertainty surrounding parameterization could be paramount. Indeed, the fact that many numerical models are heavily dependent upon parameterization has led some (e.g. Beven, 1989) to question the physical basis of environmental models (Lane, 2003a).

However, given our current understanding of environmental systems and the limitation of computational resources, calibration has been seen as both a necessary and useful practice in hydraulic modelling. In terms of calibration using roughness coefficients, detailed field measurement of surface roughness over the reach scale is not only unrealistic, but may yield estimates that are only partially related to surface resistance. It has also been suggested that

roughness can be used to compensate for model inadequacies such as poorly represented momentum effects and topographic representation (Bates *et al.*, 1997). Though the advances in new data capture techniques are gradually relieving model dependence upon friction parameterization, the semi-empirical nature of the friction parameter is still the driving force of roughness calibration.

### **Data for model validation**

Model validation can be defined as the process of demonstrating that a given model is capable of making sufficiently accurate predictions for conditions different to those under which the model was calibrated (Refsgaard, 1997). By this definition, validation will be a formidable task as most model predictions are site-specific and there seems to be no easy way of proving the universal applicability of the model, if it has one at all. Beven (1996) defined the strictest validation of a numerical model as the comparison of internal quantities (flow property and process representation) to real world observations, although acknowledged that observation data are often unavailable or incomplete. Indeed, this definition is often used in high-resolution flood inundation modelling together with some accuracy analysis techniques to evaluate the accuracy of the model prediction.

Lane and Richards (2001) noted that two terms are often used interchangeably in numerical modelling studies: 'validation' and 'verification'. Conventional approaches validate a model by comparing model output with observed data. However, validation using these approaches only gives us a general test of the validity of the model. It doesn't help us to understand why the model is valid or invalid (Lane and Richards, 2001). Some discussion has suggested that validation is not an appropriate term to use since all models are approximations of a complex reality (Beven, 2001). Model evaluation or assessment (Sargent, 1982) has been suggested as a more structured and continuous set of procedures than simple empirical validation against observed data. Lane and Richards (2001) suggest several aspects of these alternative assessment strategies, including: (i) conceptual model assessment; (ii) assessment through computational tests and analytical solutions; (iii) assessment using sensitivity analysis; (iv) assessment based on visualization; and (v) evaluation against professional standards.

In the context of flood inundation modelling, validation data can include inundation extent or hydrometric data such as water depth, velocity and hence flood wave travel time. One-dimensional river flow models can be adequately validated against hydrometric data obtained from traditional field survey methods. However, data obtained from traditional field measurements are generally either unavailable or not accurate and complete enough for validation purposes in two-dimensional flood models. This is particularly true if hydrometric

data are used, as such measurements are usually only available from point gauging stations, which are usually far apart and often submerged during a flood event (Bates *et al.*, 1997). Even when such data are available and accurate, due to the different scales of model predictions and field measurements, it can be problematic to relate field data to model predictions. For example, to relate small-area measured velocity with depth to the large-area depth-averaged velocity predicted by two-dimensional models, a number of theoretical assumptions have to be made (Lane and Richards, 2001). In addition, problems of equifinality arising from model calibration may invalidate the model validation in some way. In such situations, it is often difficult to discriminate between different parameter combinations.

With the increasing availability of high-resolution topographic data, validation against inundation extent data has been the dominant approach for 2D (both depth-averaged and diffusion wave) flood inundation models (e.g. Bates *et al.*, 1995; Bates and Anderson, 1996; Bates and De Roo, 2000; Horritt and Bates, 2001a, b; Horritt and Bates, 2002). Bates *et al.* (1997) highlighted the practical importance of validation with inundation extent and noted that the importance is due to its great sensitivity to small changes in water depth (up until the point where the floodplain is laterally confined). The main advantage of using inundation extent as validation data is that it allows a series of accuracy statistics to be derived (§4.4), which can be used either to evaluate the performance of a single model simulation or to compare statistically different model simulations through verification. However, using inundation extent as validation data has its limitations, particularly if the validation data are single at-a-point in time data. If the floodplain is laterally confined or the inundation extent is obtained long after the peak extent has been reached and before the floodplain has dried out, validation using a single at-a-point inundation extent may suggest the model performs well. The real concern is peak inundation extent, which may or may not be well predicted in such cases. If the floodplain is laterally confined, and the concern is with inundation with a flow peak that is sufficient to fill the floodplain and the timing of the inundation process is not considered important, using single at-a-point data may be enough for validation purposes in some situations. However, if the floodplain is not laterally confined, given that the inundation is strongly sensitive to water depth, getting the timing of inundation right might be the only means of getting the peak inundation extent right. Thus there is a need for detailed distributed hydrometric data for the validation of high-resolution flood inundation models. Bates and Anderson (2001) suggested that surface velocity measurement might be the only data that could distinguish between different higher order model predictions.

### 2.4.2 Remote sensed data for high-resolution flood inundation modelling

Recent developments in topographic data capture techniques using interferometric synthetic aperture radar (SAR) (e.g. Brackett *et al.*, 1995; Bates and De Roo, 2000; Marks and Bates, 2000; Horritt *et al.*, 2001), airborne remote sensing (e.g. LiDAR) (e.g. Mason *et al.*, 2003; Cobby *et al.*, 2003) and digital aerial photogrammetry (e.g. Westaway *et al.*, 2000) have allowed a number of significant model parameterization, calibration and validation issues to be addressed.

In terms of topographic parameterization, remotely sensed data have been used to generate DEMs (e.g. Marks and Bates, 2000; Bates and De Roo, 2000), the quality of which has been known to have a significant effect upon flood inundation extent. More recently, spatially varying roughness values in relation to vegetation have been obtained from remotely sensed data and used in two-dimensional flood inundation models (Cobby *et al.*, 2003; Mason *et al.*, 2003). For example, Cobby *et al.* (2003) and Mason *et al.* (2003) demonstrated an approach to mesh generation in finite-element models based upon the vegetation height map derived from LiDAR data for model roughness parameterization.

Remotely sensed data have also been used to validate hydraulic models, either in the form of hydrometric data or flood inundation extent data. Remotely sensed data have recently been widely used to delineate flood inundation extent for model validation (e.g. Imhoff, 1987; Biggin, 1996; Townsend, 2002; Horritt *et al.*, 2001; Pearson, 2001). Similarly, radar altimeters show great promise for directly measuring stage variation in large rivers, for obtaining estimates of river discharge from space, and for using ground measurements and satellite data to construct empirical curves that relate water surface area to discharge (e.g. Smith, 1997).

Both Bates *et al.* (1997) and Smith (1997) identify the all weather capability of Synthetic Aperture Radar (SAR) imagery as a considerable advantage over other sensors operating at visible or infrared wavelengths of the electromagnetic spectrum which cannot penetrate the cloud cover often associated with flood events. SAR data can be used for both topographic data derivation (e.g. InSAR data) and model validation. SAR derived topographic data can give a high ground resolution (12.5 m pixel size for ERS-1 PRI data) (Bates *et al.*, 1997) and are able to generate DEMs of a vertical accuracy of more than 1 m (e.g. Wimmer *et al.*, 2000), which are sufficient for flood modelling at watershed-scales. Airborne SAR data can have a spatial resolution of 0.5 m (Bates, 2004). Indeed, SAR data are being adopted for watershed-scale DEM generation. However, the resolution of SAR data may still not be enough for flood

modelling over topographically complex floodplains as most structural features have a dimension much less than the resolution (c. 12.5 m) of some forms of satellite SAR data. Also, the vertical precision of SAR derived data is +0.8 m to +1.0 m, which is too degraded for flood modelling purposes. In terms of flood modelling over topographically complex floodplains where structural elements strongly affect local flow routing, harnessing high-resolution topographic data has appeal as it may reduce uncertainty over how to parameterize the effects of structural ‘topography’ upon inundation. Compared with satellite SAR data, airborne scanning laser altimetry such as LiDAR (Light Detection and Ranging or Laser Induced Direction and Ranging) derived topographic data can give a much higher spatial resolution (e.g. 2 m) which allows a much better representation of structural features in the model. The next section (§2.4.3) discusses the application of airborne scanning laser altimetry (LiDAR) in river flow and flood inundation modelling.

### **2.4.3 Airborne scanning laser altimetry (LiDAR)**

Airborne scanning laser altimetry is an important new data source for environmental applications. LiDAR has been termed in the literature either as ‘Light Detection And Ranging (Priestnall, 2000)’ or ‘Laser-induced Direction And Ranging’ (e.g. Marks and Bates, 2000). In river flow and flood inundation studies, it is used principally in the production of digital elevation models (Marks and Bates, 2000). LiDAR is based on sequential laser range measurements from an airborne sensor to points on the ground surface. Based upon the precise position and orientation of the airborne platform obtained from differential Global Positioning Systems (GPS) and Inertial Navigation Systems (INS), the laser beam is reflected off the ground surface to enable the three-dimensional position and elevation of surface points to be determined with decimetre accuracy (Figure 2.2).

The main advantages of LiDAR data, compared with other remotely sensed data, are its high-resolution and high accuracy. Given its digital nature and dense coverage (64600 points per km<sup>2</sup> reported by Marks and Bates, 2000), LiDAR data can be used to create high-resolution (1 m) and low RMSE (in theory  $\pm 0.10$  m to  $\pm 0.25$  m in the vertical) DEMs. For example, the LiDAR-derived DEM used in this thesis has a resolution of 2 m (§3.5.2), much higher than those derived from other remote sources such as satellite SAR (c. 12.5 m) or UK Ordnance Survey contour lines and spots heights (§2.4.1). The latter two sources are normally used by UK Ordnance Survey to produce nationally available DEM (10 m \* 10 m) that can be used for topographic parameterization in 2D flood inundation models. In terms of data quality, practical LiDAR applications have obtained data quality results with high relative vertical accuracy ( $\pm 10$ -15 cm) and horizontal ( $\pm 5$  cm) accuracy over large areas (Marks and Bates,

2000). This is much improved than those derived from contour lines (§2.4.1). Other advantages of using LiDAR data include its rapid collection and ease of the possible requirement of resurvey of temporally changing floodplain topography (Marks and Bates, 2000). The resolution of the DEM that LiDAR can provide exceeds the requirements and capacity of current 1D and 2D models. Thus, it is normal practice to resample the LiDAR-derived DEM to a coarser resolution for use in 2D models. Indeed, the use of LiDAR data in 2D models may create a large degree of redundancy due to the high-resolution of the LiDAR data and the computational ability of 2D models. Marks and Bates (2000) found that: (i) using high-resolution LiDAR data to create finite-element mesh created a large degree of redundancy in the two-stage filtering process; and (ii) the redundancy was further compounded by the use of unsophisticated interpolation methods where only a small number of topographic points were used to assign the elevation value to a given nodal point. However, the redundant data have also been used to correct for the wetting and drying representation in 2D finite-element models (Bates, 2000) using sub grid topographic information.

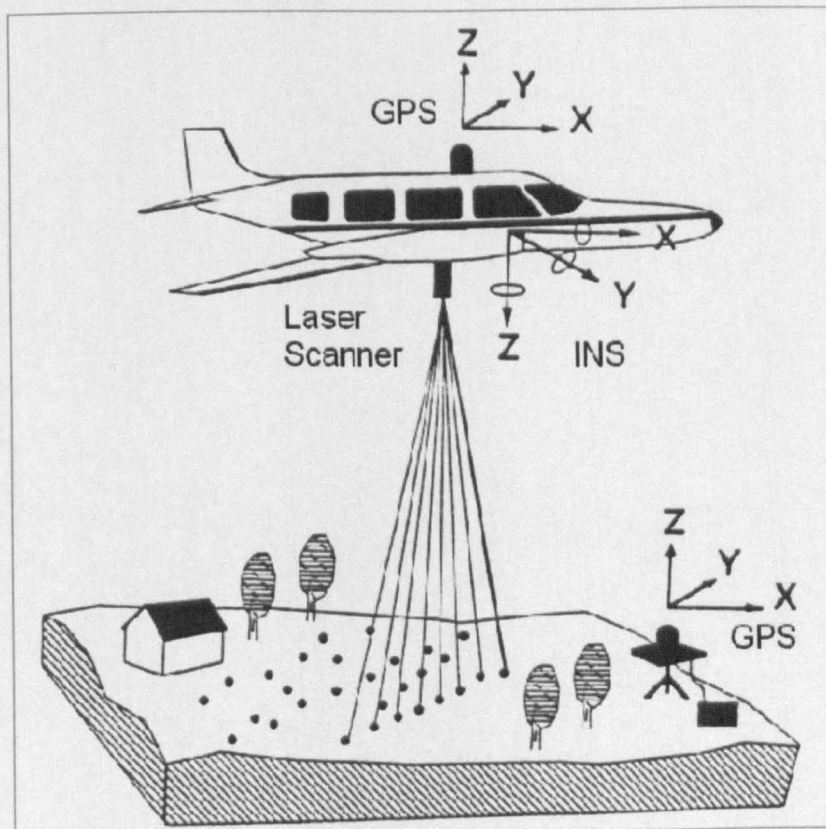


Figure 2.2: Illustration of airborne LiDAR in operation (after Flood, and Gutelius, 1997)

Recent developments have seen an increasing use of LiDAR for hydraulic modelling. The UK Environment Agency has commissioned regular LiDAR survey in a number of river and coastal environments (Charlton *et al.*, 2003). The major use of LiDAR data in hydraulic studies can be broadly categorised into two groups. First, LiDAR data have been used to produce structured (e.g. Horritt and Bates, 2001a) or unstructured DEMs (e.g. Marks and Bates (2000);

Cobby *et al.*, 2003; Mason *et al.*, 2003) for topographic parameterization in 2D models. For example, Marks and Bates (2000) investigated the effects of topographic representation on flood inundation extent prediction and presented the results of a flood simulation using a TIN-based computational mesh produced from airborne LiDAR data in a 2D finite-element model. In relation to raster-based models (e.g. Bates and De Roo, 2000; Horritt and Bates, 2001a, b), given their digital raster nature, LiDAR data require only minor processing, if necessary. This processing may include removal of elevations associated with local sinks and tree canopies. Horritt and Bates (2001a) examined the effect of spatial resolution upon flood inundation prediction in a raster-based model based upon a LiDAR-derived 10 m DEM.

Second, LiDAR data have been used as a source for spatially-distributed roughness parameterization in 2D models. In both finite-element and raster models, roughness coefficients are commonly used as free parameters to be adjusted to provide the best fit between model predictions and observations. The traditional method for roughness parameterization in 2D hydraulic models involves specifying a uniform roughness value for the floodplain and river channel respectively (e.g. Bates and De Roo, 2000; Horritt and Bates, 2001a, b). It has been noted in Section 2.3.3 that the uncertainty surrounding roughness parameterization is usually huge. Thus, there is a need for more sophisticated approaches for roughness specification. A spatially distributed roughness parameterization approach has been proposed and tested for a 2D finite-element model (TELEMAC-2D) based upon the vegetation height map derived from LiDAR data and shown to produce significant difference in predicted water levels compared with the uniform roughness parameterization (Mason *et al.*, 2003). However, apart from a number of assumptions and theoretical limitations of this approach noted in Section 2.3.3, there is no benchmark validation data to test and discriminate rigorously between these approaches (Bates *et al.*, 2000).

Another issue for the use of LiDAR data in hydraulic modelling is data quality. In the UK, although LiDAR data has been validated against ground truth data by Environment Agency (1997) and can be post-processed to provide a DEM with a relative vertical accuracy of  $\pm 10 - 15$  cm (Marks and Bates, 2000), it is still not clear whether such errors lead to differences in inundation extent prediction that can be conclusively discriminated on the basis of available validation data (Bates *et al.*, 2000). The increasing availability of remotely sensed data facilitates a move to a wider usage of two-dimensional models though new problems arise with these new techniques.

#### **2.4.4 Implications for this research**

The sections above (§2.4.1-2.4.3) have reviewed the data requirements of hydraulic modelling, the recent developments in remote sensing and the increasing opportunities created by these developments for high-resolution hydraulic modelling, with a focus on LiDAR data. This has significant implications for modelling flood inundation over topographically complex floodplains using raster-based approaches which is the primary aim of this research. In terms of topographic parameterization, LiDAR data can be used with minor processing and thus reduces the limitations associated with two-stage filtering which is the standard data processing procedure in 2D finite-element approaches. In terms of calibration, as noted in section 2.3.3, using high-resolution topographic data in 2D hydraulic models may reduce the dependence upon and the uncertainty in roughness parameterization for 2D hydraulic models. With respect to model validation, remotely sensed data can provide inundation extents which are normally difficult to obtain using traditional field survey techniques. Inundation extent has been the dominant approach to model validation in 2D flood inundation modelling over the past 5 years and is the validation data source used in this thesis.

One issue that has not been addressed in raster-based modelling is sub grid-scale process representation. High-resolution topographic data allow novel representation of small-scale wetting and drying processes based upon sub grid topography (e.g. Bates, 2000) in finite-element models. These issues are addressed in this thesis using a raster-based diffusion wave model integrated with high-resolution LiDAR data.

#### **2.5 Data representation in hydraulic models in relation to Geographical Information System (GIS)**

Geographical Information Systems (GIS) provide for spatial representation of landscape features. River flow and flood inundation models attempt to describe how water and other materials move within the river channel and over the floodplain and hence through space. Thus, there seems to be a natural connection between GIS and flood inundation modelling. There is no doubt that the one main advantage provided by current GIS is its capacity to store large amounts of data, whether spatially referenced or simply of a statistical nature. This is manifest in the widely accepted classification of the approaches to modelling within a GIS environment. Briefly speaking, there are three integration levels for modelling with GIS: loose coupling; tight coupling; and embedded coupling (Wessling et al., 1996). In loose coupling, the GIS is used to pre-process the input data into the desired model input file format and post-process the output data for illustration or further analysis. In tight coupling, the

model input and output can be addressed directly by the GIS. In embedded modelling, the model is written directly in a programming language within a GIS environment. This classification is based upon the treatment of data at the interface between GIS and hydrodynamic models.

For flow modelling over the floodplain and in the river channel, any one of these three coupling methods could be sufficient, although embedded modelling is a more robust way of modelling in that both the data processing and process representation can be addressed internally in the GIS. According to Burrough and McDonnell (1998), several difficulties arise when linking dynamic models to a standard GIS. First, there may be important conceptual differences between the ways modellers, data collectors and GIS programmers perceive the world and how their view of reality should be structured and organized in the computer. Second, the data in the GIS may not be recorded or stored in the most suitable format for the model and may need to be converted. Third, the procedures and algorithms provided by GIS can't be modified by modellers should these be inadequate or inefficient. Fourth, unless one is skilled in computer programming, it is difficult and time consuming to write dynamic models of spatial processes quickly and efficiently.

### **2.5.1 Data representation for floodplain topography in relation to GIS**

GIS has been used for more than 15 years for pre-and post-processing of spatially distributed hydrodynamic model data. Traditionally, most of the integration of GIS with river or flood inundation models has been carried out at a low level through loose coupling. Considering the spatially distributed nature of river flow and floodplain flow and the advantages that the GIS can provide besides the pre- and post-processing of spatially distributed data, there are yet more issues GIS should be able to deal with. Those issues include at least the assessment of spatial variability of the input data and its effect on the outcome, the effects of model resolution and parameter uncertainties and, at a high level, model construction within a GIS environment. Discussion of flood modelling over topographically complex floodplains in Section 2.3.3 has highlighted the need to model the effect of structural elements upon the flow.

To date, there are mainly two ways in which spatial features on the landscape can be encoded into the computer: using: (i) a vector data structure; and (ii) a raster data structure. Vector data structures use points, lines and polygons to describe geographical phenomena. Vector units are identified by the fact that their physical location can be precisely defined, as can their topological relationships (Burrough and McDonnell, 1998). For river flow and flood inundation studies, locations of topographically and hydrologically important features on the

floodplain can be represented using vector data. For example, river banks can be represented using lines, river stations on the cross-sections can be represented by points and land units on the floodplain can be represented using polygons. Spatial phenomena can also be represented by sets of regularly or irregularly shaped units. The simplest form is the square cell and the tessellated regular grid known as a raster data structure. In terms of raster representation, structural features can be represented in two-dimensional flood inundation models through their topographic input, typically in a digital elevation model (DEM). One approach to representation of significant features on the floodplain using raster-based data is to interpret the vector objects as a set of linked cells with similar topographic properties. For example, a linear feature (e.g. a wall) can be extended to the size of a set of connected grid cells. This may work well if the width of the linear feature is nearly equivalent to the width of one or more grid cells. In this case, the raster-based approach can provide a realistic representation of these features. However, as two-dimensional models are normally computationally demanding, these features may be averaged out in the re-sampling process to a lower resolution that can be used in the model, even if the original DEM is of high-resolution. This may present significant problems when the topographic complexity on the floodplain is such that coarsening mesh resolution may not preserve those important topographic features such as walls and buildings in the DEM and the associated flow processes are altered in some way.

The increasing availability of high-resolution data obtained from various sources provides the opportunity for structural features to be represented in two- and three-dimensional flood models. This refers not only to those data that are of raster format and obtained from remote sources (§2.5.2), but also those that are of vector format, which have been largely ignored in current flood inundation modelling. This is a significant omission, and potentially important for flood modelling over complex topographies. Modelling floodplain flows with the effects of structural features incorporated needs GIS to address the spatial relationship between spatial features more intelligently and precisely. Different structural features can have different boundary attributes that affect the flow in both spatial and temporal dimensions. The spatial relationship between spatial features is termed as topology in a GIS. It refers to the continuity of space and spatial properties, such as connectivity, that are unaffected by continuous distortion (Burrough and McDonnell, 1998). Topology is a defining characteristic of the GIS and topological relationships between spatial features can now be addressed in most commercial GIS. For example, in ArcView GIS, those features that 'are completely within', 'completely contain', 'intersect', 'are within distance of', 'contain the centre of' and 'have their centre in' can be identified very easily. However, this is far from enough for hydrodynamic modelling. Whereas in a vector data structure, the topology between different spatial units is explicitly recorded through a database pointer, in a raster data structure,

topology is only implicitly coded in the attribute values in the cell. The GIS functions for identifying the spatial relationship between spatial features are limited and in most cases are static. Therefore, they are not suitable when considering the dynamic nature of hydrodynamic modelling. Hydrodynamic modelling with topological features needs a GIS to interpret the topology simultaneously with the routing of flood flow.

With structural features in mind, the topology of spatial features and their relation to the processes that are modelled becomes important. Topology needs to be addressed intelligently in a GIS. For instance, topological relationships between adjacent land units on the floodplain need to be defined before water routing is carried out over them. In order to model flood flow over landline features, in relation to land units, topological relationships between landline features composing the land units and the land units themselves also need to be addressed. This should be an internal function of the model instead of external intervention of the users. For example, when water is approaching a landline feature in a land unit, it needs to find out the attributes of the feature to decide on how to behave. When the water level is about to exceed the height of a landline feature, the model should then possess information about topology so as to decide where the flow is expected to go.

With respect to hydraulic modelling within a GIS, although it is possible to build flood inundation models in some GIS packages that take into account structural features, programming issues are paramount. Vector-based representation of floodplain topography alone is not enough for flood inundation modelling. Point and linear features can be represented using vector data structure. However, raster-based representation is required for polygon features to account for the variation in topography within land units.

## **2.5.2 Implications for this research**

In GIS terms, and given the advantages of using a GIS, in particular the handling of vector-based data, and the need to represent structural elements for flood modelling over complex topography, a tight coupling is preferred. However, this is not attempted in the thesis. The linkage of the model developed in this thesis and GIS is at a low level through loose coupling and GIS is only used for the data processing for topographic input. The main reasons for taking this approach are that: (i) a loose coupling approach is thought to be enough for the modelling task attempted in this study, given the quality of topographic data available; and (ii) a tight coupling approach requires considerable programming efforts. Diffusion wave based flood inundation modelling requires that floodplain be discretized into grid cells. If the resolution of the topographic data used in the model is high enough, significant features on

the landscape can be represented reasonably well and their effects upon flow routing can be represented through topographic control. In this study, high-resolution topographic data are available. Thus, the loose coupling approach is chosen. Vector-based representation of significant structural features coupled with raster-based representation of other features is an issue for future model development.

## 2.6 Chapter Summary

This chapter has reviewed recent developments in river flow and flood inundation modelling (§2.3), focusing upon the limitations of using traditional one-dimensional treatments of the floodplain flow caused by the discontinuity in stage-discharge hydrographs, particularly at the interface of the floodplain and the river (§2.3.1) channel. The emergence of raster-based modelling approaches (§2.3.2) was then reviewed, with a focus upon its potential implications for modelling flood inundation over structurally complex floodplains, notably urban floodplains (§2.3.3). Particular attention was given to the wetting and drying treatment in two-dimensional models, with discussion of the general issues facing the moving-boundary hydrodynamic problems in shallow water and the approaches that have attempted to solve these problems.

The opportunities created by the emergence of new data capture techniques for flood inundation modelling over topographically complex floodplains were reviewed with respect to the data requirements (§2.4.1) for high-resolution flood inundation modelling in terms of model parameterization, calibration and validation. The applications and advantages of recent developments in remotely sensed data capture techniques were reviewed in Section 2.4.2, with focus upon the airborne laser scanning altimetry (LiDAR) data (§2.4.3) which are the topographic input for the model applications carried out in this study. The current status of the integration of GIS and hydrodynamic modelling (§2.5) was reviewed in terms of the coupling approaches between GIS and hydrodynamic modelling and the data representation methods provided by GIS.

The next chapter (Chapter 3) proceeds with the description of the case study application in terms of the flood event modelled, data requirements, availability and related validation approaches.

# Chapter 3

## Case-study applications, data sources and methods

### 3.1 Introduction

Prior to the description of model development and associated applications, this chapter describes the case-studies in terms of the flood events simulated, data requirements, data availability and data processing, with respect to model parameterization, calibration and validation. Three case-study applications are described, all for the River Ouse, York (Figure 3.1), in connection with a major flood event in the year 2000. Thus, the primary aim of this chapter is to describe the case-study applications in terms of the application carried out (§3.3), data requirements (§3.4), data availability and data processing (§3.5, §3.6 and §3.7) for model topographic parameterization, calibration and validation. The focus is on LiDAR data processing (§3.6.2 and §3.6.3) for model topographic input and processing of aerial imagery (§3.5.1) for both model parameterization and validation. The approach to accuracy assessment which allows quantitative assessment of model performance is presented in the context of flood inundation modelling for both model validation and model verification (§3.5.3).

The model developed in this study consists of a 1D river flow sub-model and a 2D floodplain flow sub-model. Two approaches to coupling the river flow and floodplain flow were developed in this study. First, a loosely-coupled version of the model was developed whereby river flow is calculated separately from the floodplain flow in an existing 1D river flow model. Second, a 1D river flow model was coupled tightly with a 2D floodplain flow model through explicit representation of the efflux onto the floodplain from the river and the return of water from the floodplain to the river at each time step. Thus, the associated data requirements are different for these two approaches. This chapter restricts the discussion to the loosely-coupled version of the model, which is the basis for the applications described in Chapter 4 and 5. Chapter 6 presents the tightly-coupled version of the model, including the associated data issues and application to a longer reach through the city centre of York.

The model can be further classified according to the approach to the wetting treatment. Two wetting treatment approaches were used in this study: (i) a normal wetting treatment where a wetting parameter calculated based upon flow velocity, cell size and time step (adopted Bradbrook *et al.* 2004) (Chapter 3 and 4); and (ii) a sub grid wetting treatment where the sub grid topography is used to control the wetting process (Chapter 5). The data requirements are similar for both approaches and the validation and verification procedures are slightly different. In this chapter, the descriptions related to model validation and verification are restricted to the model using the normal wetting treatment.

### **3.2 Loose coupling between channel and floodplain treatments**

Two versions of the model are developed in this study: (i) a loosely-coupled 1D model in the river channel and 2D model on the floodplain; and (ii) a tightly-coupled 1D model in the river channel and 2D model on the floodplain. Both versions assume that the floodplain is protected by an embankment that essentially acts as a continuous, broad-crested weir, which may be identified from topographic data (e.g. LiDAR). This is appropriate for the majority of the case-studies considered here.

The loosely-coupled model treats the river flow as a separate process in an existing 1D river flow model prior to the initialisation of the floodplain flow routing and uses the hydrograph produced from this model as the inflow hydrograph for the 2D floodplain model. Return flow only occurs when the floodplain water elevation is higher than the levee but the effects of this return flow on the main river flow are not accounted for as the 1D flow model takes this into account already. The development of the tightly-coupled model addresses this issue explicitly and whilst comparison of the tightly and loosely coupled results contains other factors besides this, it helps to indicate whether or not this is a problem (§6.5.2).

The tightly-coupled model takes into account the effects of floodplain routing on the return of water from the floodplain to the river channel at each time step and the river flow and floodplain flow are calculated simultaneously. The latter is covered in Chapter 6 in full. These address the second set of objectives with respect to model development as identified in Section 1.2.

The loosely-coupled model establishes the connectivity between the river channel and floodplain flows using a stage hydrograph at the river-floodplain boundary. This can either be produced from a 1D river flow model (e.g. HEC-RAS) or be obtained from existing stage records. This provides boundary condition data for the 2D floodplain flow routing. The

hydrograph is used in the 2D floodplain model to calculate the flow from the river channel onto the floodplain and from the floodplain back into the river channel. The connectivity is established by comparing the water surface elevations between the river channel and the floodplain at each contacting cell at every time step. If there is a difference in the water surface elevation between a river cell and its adjacent floodplain cell, flow exchange will occur. The approach to calculating the volume of flow exchange between the river channel and the floodplain is described in Chapter 4 (§4.3). Flow from the river channel into the floodplain is calculated using a weir equation (Equation 4.14) and this flow is used in the 2D diffusion wave model to drive the routing of floodplain flow. Flow from the floodplain to the river is simply removed from the calculation domain as mass loss at the river-floodplain boundary for the 2D floodplain flow model. Thus, this is a two-step process and the calculation of the river flow is not related to the floodplain flow in the 2D model explicitly. The return flow from the floodplain to the river channel has no effect upon the 1D river flow as the inflow hydrograph has been calculated from the 1D model prior to running the 2D floodplain flow model. Either a uniform hydrograph for the whole river or non-uniform hydrographs for different reaches of the river can be used as inflow boundary condition data for the 2D floodplain flow model. This approach has its limitation in that it does not account for the way the floodplain flow returns to the river channel in the 1D river flow model. This is concerned with both the direction and the timing of the floodplain flow back into the river. Both the timing and direction of the return flow from the floodplain are strongly affected by the floodplain flow routing, particularly over topographically complex floodplains. This could significantly affect the calculation of the river flow. This is the rationale behind the model development described in Chapter 6.

### **3.3 Case-study applications carried out**

This section describes the case study applications carried out in this study in terms of the study locations and the flood event modelled. The model was applied to simulate a flood event that occurred in the year 2000 on the River Ouse, UK. The location of this river is shown in Figure 3.1.

The non-tidal reach of the River Ouse comprises a wide, sinuous, lowland channel that flows through the Vale of York. The reach receives the majority of its flows from three sub-catchments: the Swale; the Ure; and the Nidd (Figure 3.1). In these river catchments, there has been a tendency to higher magnitude and more frequent flood events since the 1940's, with the exception of a period of notably lower peak flows in the early 1970s (Lane, 2003b). The flood magnitude of the non-tidal Ouse is controlled by the magnitude and relative timings

of flood peaks in the three sub-catchments. The notable increase in flood frequency after 1944 was noted to be coincident with an expansion of arable activity, a reduction in grassland, and the commencement of widespread gripping in the Dales. The flood event simulated on the River Ouse began on the 27th of October, 2000 at 2200 hours and continued until 19th of November, 2000 at 0000 hours. Thus, this flood had a duration of more than 530 hours or 23 days. It was estimated to be the highest recorded in York since 1625 and to have a return period of greater than 100 years (Lane, 2003b). The River Ouse was chosen because of the availability of a one-dimensional hydraulic model (ISIS from the Environment Agency) for the river flow, high quality LiDAR data for the floodplain surface, the presence of structural features on the floodplain characteristic of urban areas and remotely sensed data on inundation extent and water levels for the flood event. The latter data have been used to determine inundation patterns and water levels using digital photogrammetry and image analysis (Lane *et al.*, 2003). This river includes a mixture of undeveloped and developed floodplain. The urbanized areas are mainly at the downstream end of the non-tidal reach of the River Ouse. Evidence (wrack lines) suggested that the developed floodplain had been extensively inundated during the peak flow of the 2000 flood event and, in some parts of the floodplain, the lateral confinement of the floodplain was marginally exceeded.

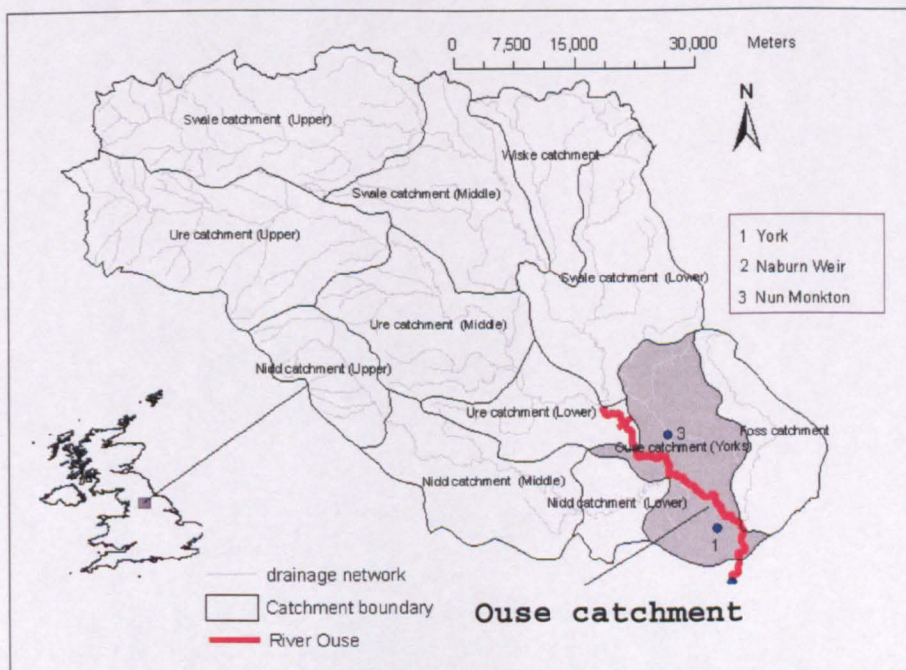


Figure 3.1: The location of the River Ouse.

Three reaches on the River Ouse were chosen: (i) a reach near Naburn Weir; (ii) a reach near the A64 Trunk Road; and (iii) a reach through the city centre of York. The locations of these sites on the River Ouse are illustrated in Figure 3.2. The purpose of the simulations carried out at Site 1 (Figure 3.2) is to examine the general performance of the model and to investigate the interaction between model spatial resolution and roughness parameterization

by means of model validation and verification (Chapter 4), and to test the sub grid-scale wetting treatment approach developed in the model (Chapter 5). This is carried out using the loosely-coupled version of the model (§3.2), with a stage hydrograph at the river-floodplain boundary as inflow data for the 2D floodplain model. Thus, this addresses objectives 2, 3, 4 and 8 in the second set of objectives as identified in Section 1.2. Similar applications were also carried out at Site 2 and Site 3 to test the repeatability of model performance, but with a focus upon model validation. This testing methodology has its limitations as it only assesses the performance of the model on one river and for one flood event. In terms of the dynamic performance, ideally, the model should be tested for different flood events. Thus, repeatability testing carried out here only accounts for the model performance at different locations for one flood event. The sub grid wetting treatment is tested at Site 1 and 2 with reference to the final set of objectives. Furthermore, the performance of the tightly-coupled (§6) 1D river flow and 2D floodplain model over a longer reach (over 10 km) was examined by the simulations conducted at Site 3 of the River Ouse, which is a reach through the city centre of the York. This addresses the objectives 5, 6 and 7 in the third set of objectives (§1.2). This is summarised in Table 3.1.

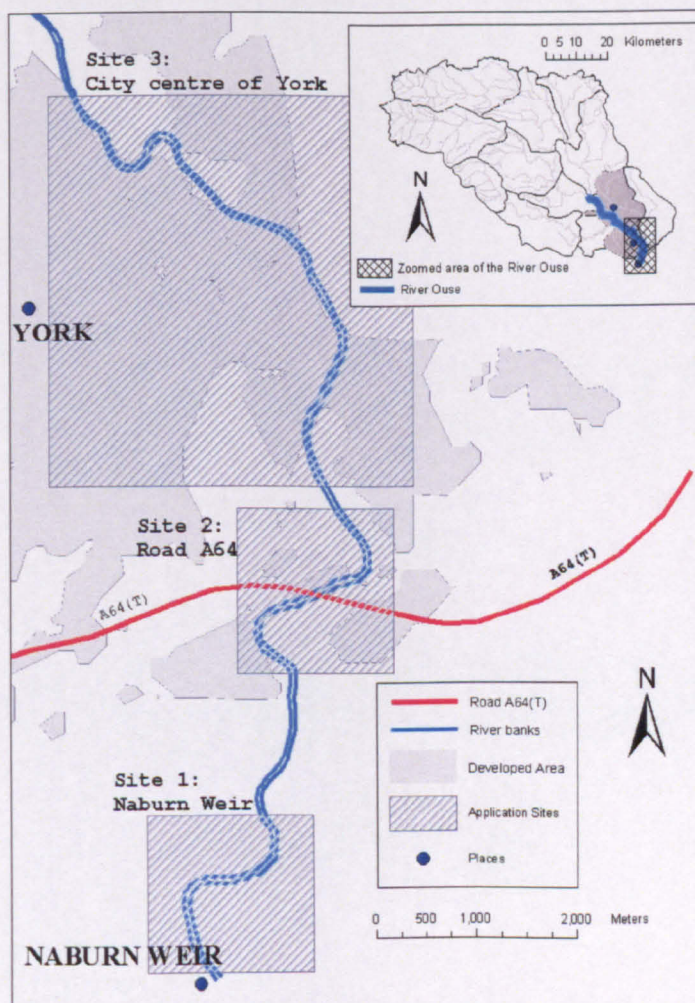


Figure 3.2 Location of three case-study sites on the River Ouse, York, UK (Illustration map produced using Ordnance Survey digimap data downloaded from [www.digimap.co.uk](http://www.digimap.co.uk))

Table 3.1: Summary of applications conducted and the associated coupling methods.

	Loosely-coupled version	Tightly-coupled version
Site 1 (Naburn Weir)	(Chapter 4, 5)	Not carried out
Site 2 (A64 Trunk Road)	(Chapter 4, 5)	Not carried out
Site 3 (City Centre)	(Chapter 4)	(Chapter 6)

These three sites show different degrees of urban characteristics, associated with different levels of topographic complexity. To analyze further the topographic characteristics of the floodplain and to justify the selection of the three sites for urban flood inundation modelling, Ordnance Survey landline data were obtained. Figure 3.3 shows the Ordnance Survey landline data covering the three case-study sites.

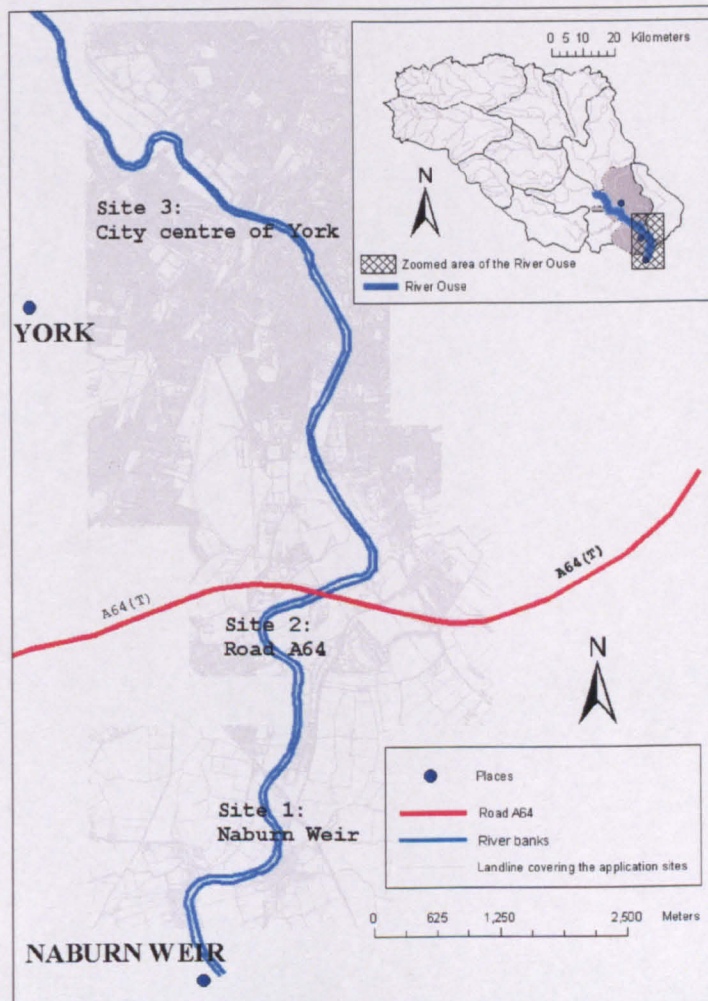


Figure 3.3 Landline data of three case-study sites on the River Ouse, York, UK (Illustration map produced using Ordnance Survey digimap data downloaded from [www.digimap.co.uk](http://www.digimap.co.uk))

For Site 1, in the proximity of the riverbank, there are two small residential sites in the bottom left and middle right. On the floodplain, there are quite a few linear features, which can be identified in the aerial image as hedges and roads. Site 2 also has some urban features that may exert significant effects upon flow routing. Strictly speaking, Sites 1 (Naburn Weir) and 2 (A64 Trunk Road) (Figure 3.3) are semi-urban areas. However, as has been emphasised in

Section 1.1, the labels of ‘urban’ and ‘rural’ used in this study are for the purpose of convenience and these two sites are considered to be characteristic of urban floodplains: both sites have structural features on the floodplain and these are the structural features that are of interest in relation to prediction of flow routing and flood inundation. By choosing two identical sites on the same river, it is possible to test the repeatability of model performance. Site 3 (City Centre of York) has clear urban characteristics (Figure 3.3) and is well suited to this study.

This testing methodology has its limitations as it only assesses the performance of the model on one river and for one flood event. However, three different reaches of the same river were tested. Also, the flood event was of long duration and contained multiple peaks. Indeed, this event was of significantly longer duration than is typical of flood inundation modelling strategies. Although these peaks were not independent, and validation data are only available for a single point, the complexity of the event and the exploration of three different reaches represents a major test of the model. Indeed, the regulatory agency (the Environment Agency) encountered severe problems in producing an effective 1D model of the River Ouse for the November 2000 event, and this justifies its focus. In terms of the dynamic performance, ideally, the model should be tested for different flood events. Thus, repeatability testing carried out here only accounts for the model performance at different locations for one flood event. In addition, in terms of model validation, if multiple validation images are available, model temporal dynamics can be tested more rigidly (see §3.5, §4.5.4 and §4.7). However, this is not available in this study and is noted as a limitation of the validation approached used in this thesis (§7.2.2).

### **3.4 Summary of the data needs for the case-study applications using the loosely-coupled model**

This section describes the data requirements for the loosely-coupled model developed in this study in terms of the model geometry (MG), boundary condition (BC) and validation (V). Table 3.2 lists data needs and availability for the loosely-coupled model.

Model geometry data for flood inundation modelling typically include surveyed river cross-section data and floodplain topography. The topographic dataset required by the loosely-coupled model is floodplain topography. For modelling of floodplain flows, topographic data might need to be processed to remove elevations associated with vegetation and trees, as well as to correct the elevations associated with low bank cells (see §3.6). Boundary condition data for flood inundation studies normally include the roughness coefficient for the river channel

and floodplain and hydrometric data in the river channel. As the loosely-coupled model uses hydrometric data calculated from an existing 1D river flow model, the boundary condition data required are roughness coefficients for the floodplain and stage hydrograph at the river-floodplain boundary. The validation data used in this study are the flood inundation extents.

**Table 3.2: Summary of the data needs and availability for the loosely-coupled model**

Data Types		Data requirement and availability
Model Geometry (MG)	Cross-section data	Not required in a loosely-coupled model
	Floodplain topography with vegetation and trees removed (§3.6)	Required/Available
Boundary Condition (BC)	Stage hydrographs along river-floodplain boundaries (§3.7.1)	Required/Available
	Flow data	Not required in a loosely-coupled model
	Stage data	Not required in a loosely-coupled model
	Floodplain roughness (§3.7.2)	Required
	River channel roughness	Not required in a loosely-coupled model
Validation (V)	Inundation area (§3.5.3)	Required/Available
	Hydrometric data	Required/unavailable

The next sections describe the availability of the required data and how these data were generated and their quality ascertained. This is structured according to the data types classified in Table 3.2 and is further illustrated according to application locations (§3.2). As generating the validation data required image processing that was also needed for the floodplain topography, the model validation data and approach are presented (§3.5) prior to the description of the model geometry data (§3.6) and boundary condition data (§3.7).

### 3.5 Model validation and approach

Due to the increasing availability of inundation data from remote sources, inundation extent has been used extensively as the validation data in 2D flood inundation models (§2.4.1). It was noted in Section 2.4.1 that the importance of using inundation extent data for validation is due to its sensitivity to small changes in water depth. However, it is also recognized that using at-a-point in time inundation extent data can be problematic due to the relationship between the configuration of the floodplain and the size of the flood event modelled. For example, if the inundation extent data is acquired long after the floodplain is fully inundated and before the drying phase starts, the validation may not be a good indicator of the model performance as far as the timing of the flood wave is concerned. Single extent images do not validate dynamics at all, irrespective of position in hydrograph. For this reason, hydrometric data such as surface velocity might distinguish between different higher order models (Bates and Anderson, 2001). However, due to the lack of such data, the validation data used in this study are exclusively inundation extent acquired during the simulated flood event.

Besides model validation using observed data, this study seeks to evaluate model performance by using model predictions obtained from the finest resolution simulation as the reference data and comparing predictions obtained from coarser resolution models with these data. As validation usually involves the comparison of model prediction with real world data, this is not a form of validation. Rather, it represents a form of sensitivity analysis, in this case with reference to mesh resolution. This is considered to be part of the model verification process. Model verification is defined as “The process of determining that a model implementation accurately represents the developer’s conceptual description of the model and the solution to the model (AIAA, 1998)”. Roache (1998) considers two aspects in the verification of numerical models: (i) verification of a code; and (ii) verification of a calculation. The advantage of the verification approach used here is that it allows model predictions to be evaluated at each time step and provides time series accuracy statistics, which can be used to assess model performance quantitatively over time. This is termed as time series verification in this study. Comparison of time series of model prediction is particularly valuable for the evaluation of effect of model resolution and roughness parameterization upon flow routing and inundation extent. The assumption being made here is that a finer mesh resolution will give a better representation of the effects of the small-scale topographic variation and hence a better description of local flow routing and, perhaps, peak inundation extent.

Quantitative accuracy statistics are required for both model validation and verification. This study uses an accuracy assessment approach adopted from remote sensing. This approach allows a series of accuracy statistics to be derived. These can not only allow individual simulation to be evaluated using accuracy statistics, but also allow comparisons of different simulations to see whether there is significant difference between simulations. Section 3.5.1 and 3.5.2 presents the validation approach and quantitative description of agreement between model prediction and validation data. Section 3.5.3 discusses the validation data and the associated processing.

### **3.5.1 Validation/verification approach**

The output of the model at each time step includes, amongst other outputs, the water depths, velocity vectors, flow directions in x and y directions and wetting parameter (defined in §4.3). The water depth and wetting parameter can be used to evaluate the wetting status of each cell at each time step, thus determining the inundation extent. During simulation, each cell in the simulation domain is predicted as being of one of three classes: wet areas, dry areas and wetting front areas as indicated by the wetting parameter (defined in §4.3) and water depth in a single cell. A wet cell is one with a wetting parameter equal to or greater than one and a water

depth greater than the minimum depth specified in the wetting process (0.05 m). A dry cell is one with a wetting parameter equal to zero or water depth smaller than the minimum depth (0.05 m). Other cells are classified as wetting front cells. This provides the model prediction data for the validation. The minimum depth specified here is arbitrary and sensitivity analysis needs to be carried out in relation to this.

The model was validated using both a validation and a verification approach (§3.5). Both validation and verification require a reference dataset. In this study, model validation requires observed data at the validation point and model verification compares time series of model predictions with the best possible model predictions. In this study, the flood inundation extents classified from the aerial images are used as the reference data for model validation. This was projected onto the 2 m DEM for comparison with model predictions. For verification, the time series of inundation extents obtained with the finest resolution simulation (4 m mesh size) and the standard roughness parameter ( $n = 0.06$ ) were used as the reference data and compared with model predictions using the other model resolutions (8 m, 16 m and 32 m) and roughness values ( $n$  ranging from 0.04-10) over time.

In both cases, the reference data were downscaled onto the corresponding model output. An alternative is to upscale the model predicted data to the reference data. The wetness of a grid cell in the projected validation data was then determined by calculating the number of sub grid wet cells in the original validation dataset in this cell. The cells in the projected reference data are treated as wet if all the sub grid cells in the original reference data are wet. If none of the sub grid cells in the original reference data in a projected reference data are wet, it is treated as a dry cell. Otherwise, the cell is a wetting front cell. This is illustrated in Figure 3.4 in which the 2 m original reference mesh is projected to a 4 m reference mesh for validation of a 4 m simulation. Thus, the projected reference data have the same resolution with the output of the model. Model prediction can then be compared with the projected reference data on a cell-by-cell basis. This forms the bases for the quantitative description of model predictions which is described in the next section.

It should be noted that the upscaling approach of the measured data (2 m to 4 m) can be contrasted with downscaling of the modelled data (4 m to 2 m). The main difference between these approaches should emerge at the wetting/drying front. Along this front it is likely that the 2 m resolution data will already involve some pixel averaging (i.e. sub-pixel effects). There has not been that much investigation of such effects in relation to inundation of urban areas in floods and this may cause some uncertainty in the pixel classification at the wetting front. For this reason, the upscaling approach was adopted, accepting that cells thought to be

wet or dry close to the wetting front are more likely to be misclassified because of sub pixel scale effects.

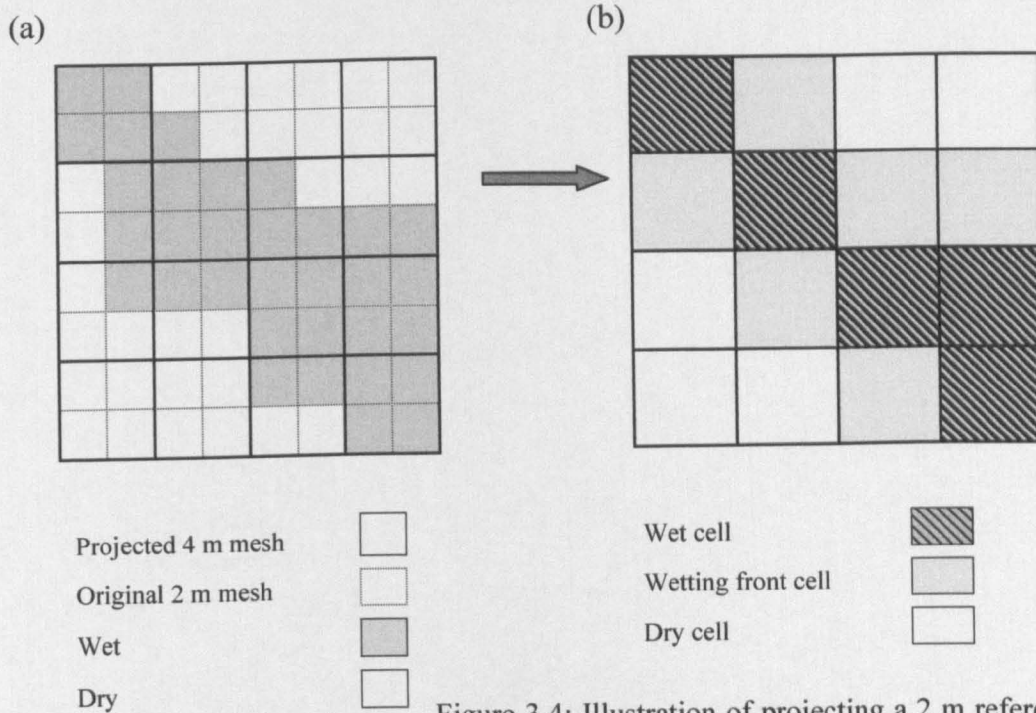


Figure 3.4: Illustration of projecting a 2 m reference mesh into a mesh of model resolution (4 m) for model validation and verification: (a) original 2 m and projected 4 m reference data; and (b) wetting status of the projected reference data.

### 3.5.2 Quantitative description of agreement

Based upon the validation and verification approaches, quantitative approaches can be used to describe the agreement between model prediction and reference data in order to assess the accuracy of model predictions. The foundation of all accuracy assessments is an error matrix (Figure 3.5).

		j=columns (Validation data)			row total	
		1	2	k	$n_{i+}$	
i=rows (Model prediction)	1	$n_{11}$	$n_{12}$	$n_{1k}$	$n_{1+}$	
	2	$n_{21}$	$n_{22}$	$n_{2k}$	$n_{2+}$	
	k	$n_{k1}$	$n_{k2}$	$n_{kk}$	$n_{k+}$	
column total		$n_{+j}$	$n_{+1}$	$n_{+2}$	$n_{+k}$	$n$

Figure 3.5: Error matrix for accuracy assessment (after Congalton and Green, 1999).

Here the error matrix is represented as having a 3 x 3 dimension, by considering not only wet areas and dry areas, but also those cells that are associated with the wetting (or drying) front (§3.5.1). This is especially important when considering mesh resolution changes (see below). The overall accuracy is computed from (3.1) as the sum of the correctly predicted cells divided by the total number of cells:

$$\text{Overall accuracy} = \frac{\sum_{i=1}^k n_{ii}}{n} \quad (3.1)$$

The main disadvantage with this statistic is that it is strongly dependent upon the number of mesh cells that are used in the computation in relation to the maximum inundated area: the statistic may appear to do very well if the number of dry cells, that are never wetted but are always both observed and predicted as dry, is large.

Besides the overall accuracy, a discrete multivariate technique called Kappa analysis was also used to allow statistical analysis of model performance and, in particular, if one error matrix is significantly different from another (Bishop *et al.*, 1975). The result of performing a Kappa analysis is a KHAT (or Kappa-Hat) statistic, which is often cited as a more reliable measure of accuracy or agreement than overall accuracy (Cohen, 1960). The Kappa statistic is based upon the difference between the actual agreement in the error matrix (i.e. the agreement between the predicted cell status and the reference data as indicated by the major diagonal) and the chance agreement as indicated by the row and column totals (i.e. marginal). A Kappa value can be calculated for each error matrix using equation (3.2) and is a measure of how well the predicted data agree with the reference data.

$$\hat{K} = \frac{n \sum_{i=1}^k n_{ii} - \sum_{i=1}^k (n_{i+} n_{+i})}{n^2 - \sum_{i=1}^k n_{i+} n_{+i}} \quad (3.2)$$

where:

$$n_{i+} = \sum_{j=1}^k n_{ij} \quad (3.3)$$

and

$$n_{+i} = \sum_{j=1}^k n_{ji} \quad (3.4)$$

(3.2) is essentially expressing the ratio of the observed excess over chance agreement to the maximum possible excess over chance agreement. Kappa has a value of 1.0 at perfect agreement and 0.0 when the observed agreement equals chance agreement (Everitt, 1998). This statistic still retains a dependence upon the number of dry cells used in the analysis. However: (i) it is well suited to a 3 x 3 matrix of the sort we have here; (ii) the non-diagonal terms are given greater weight in the derivation of the statistic; (iii) it corrects for bias in the level of agreement by correcting for chance agreements; and (iv), most importantly, it lends

itself to statistical assessment: the significance of Kappa for a single error matrix can be tested to determine if the agreement between the predicted data and the reference data is significantly different to no agreement by calculating the  $Z$  statistic using equation (3.5).

$$Z = \frac{\hat{K}}{\sqrt{\text{var}(\hat{K})}} \quad (3.5)$$

The denominator is the approximate large sample variance of Kappa. Note that the correction for bias gives the  $K$  statistic explicit meaning in relation to other parameters used to assess models in hydrology such as the Nash Sutcliffe index of model efficiency: if  $\hat{K} < 0$ , the model performs no better than randomly selected pixels from within the scene of interest; if  $\hat{K} > 0$ , the model is performing better than one based on random classification of cells as wet and dry.

Although the use of Kappa statistics has the advantage of allowing comparison of different error matrixes, Kappa still retains the bias in the overall accuracy measurement. In the context of flood inundation modelling, both the overall accuracy and Kappa will inevitably introduce bias into the results, especially in situations where a large proportion of both the simulation domain and the actual domain remain dry. Two main alternatives emerge. First, in most cases, we are interested in how the model-predicted wet areas agree with the validation dataset. Thus, model performance can be assessed using a measure of fit ( $F$ ) to compare the model predicted inundation extent with the validation dataset (e.g. Horritt and Bates, 2001a; Horritt and Bates, 2002). In terms of a contingency matrix,  $F$  is defined by:

$$F_i = \frac{n_{ii}}{n_{i+} + n_{+i} - n_{ii}} \quad (3.6)$$

In some situations, (3.6) needs to be corrected for bias, which may be introduced by the area occupied by the river (Horritt and Bates, 2001b). Second, a natural extension of this, and one that is important for statistical testing, is the conditional kappa statistic. This is based upon the maximum likelihood estimate of the Kappa coefficient for the conditional agreement of the  $i$ th category. The expected number of cells that would be wet ( $n_{ii}$ ) under a random simulation is  $(n_{i+}n_{+i}/n)$  and the maximum number of cells that are predicted as wet ( $n_{i+}$ ) is the maximum number of cells that could be classified correctly as wet. Thus,

$$\hat{K}_i = \frac{n_{ii} - \left(\frac{n_{i+}n_{+i}}{n}\right)}{n_{i+} - \left(\frac{n_{i+}n_{+i}}{n}\right)} = \frac{nn_{ii} - n_{i+}n_{+i}}{nn_{i+} - n_{i+}n_{+i}} \quad (3.7)$$

If  $\hat{K}_i$  is calculated for wet cells, use of (3.7) eliminates the effects on the numerator of a large number of cells that are always dry in both the model and the classification data. This eliminates the bias that comes from the number of cells that are always dry (and which will depend on the size of the domain). However, both the numerator and the denominator are affected by the total number of cells used in the computation. It also corrects for chance agreement, with the meaning of  $\hat{K}_i > 0$  and  $\hat{K}_i < 0$  being identified to that explained for  $\hat{K}$ . Correcting for chance agreement is important as when modelling, it is necessary to assess whether or not the model is performing any better than would be expected if, in this case floodplain cells were randomly labelled as ‘wet’ or ‘dry’. Thus, even though wet/dry pixels in both measurements and models are organized, we are still interested in how well the model does as compared with the random case.

In addition to being able to use the Kappa statistic to test for significant agreement, both the kappa and conditional kappa statistics can be used to compare different error matrices, through a measure that describes whether the two error matrices are significantly different from each other. Let  $\hat{K}_1$  denote Kappa (or conditional Kappa) obtained from error matrix 1 and  $\hat{K}_2$  denote Kappa (or conditional Kappa) obtained from error matrix 2. The Z test statistic is calculated from:

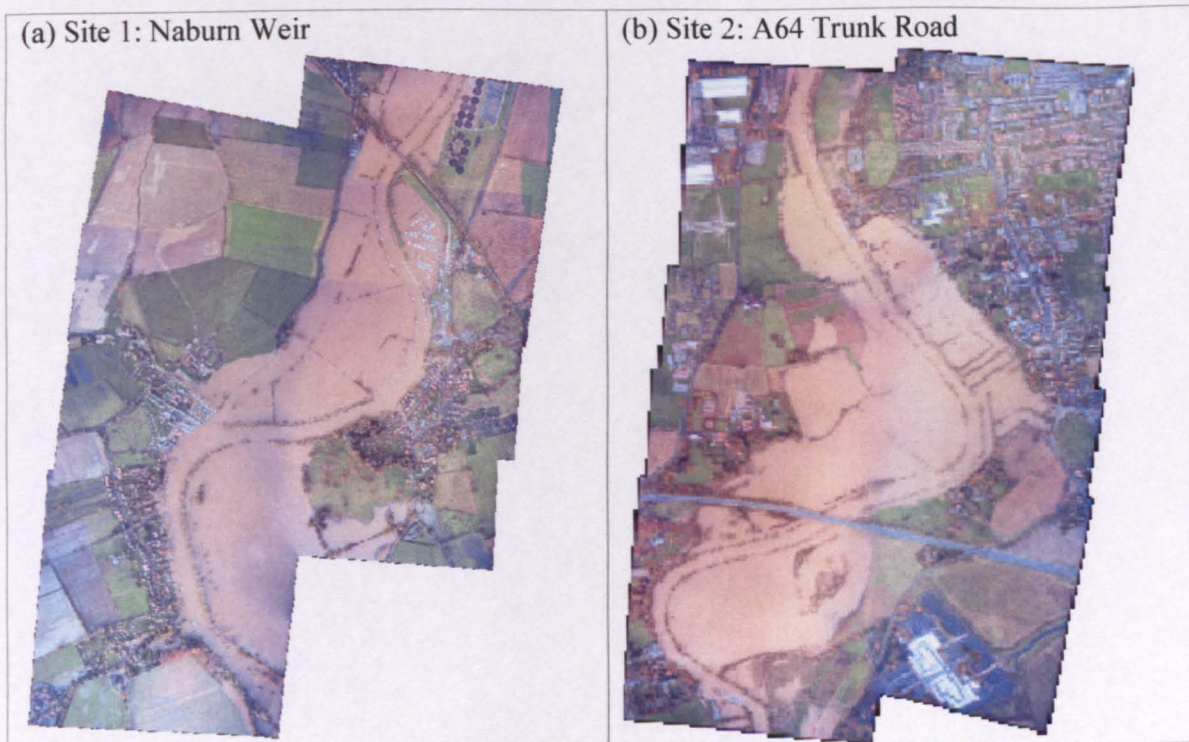
$$Z = \frac{\left| \hat{K}_1 - \hat{K}_2 \right|}{\sqrt{\hat{\text{var}}(\hat{K}_1) + \hat{\text{var}}(\hat{K}_2)}} \quad (3.8)$$

For flood inundation modelling, this allows us to compare the effects of different treatments (e.g. roughness calibration, mesh resolution) in relation to whether or not there is a significant difference in accuracy, given that there will always be some level of agreement due chance.

Given the relative merits of different accuracy statistics we report on all four described above, noting that  $F$  and conditional Kappa are likely to be the most reliable.

### 3.5.3 Validation data

For all the applications carried out, single-pass aerial imageries taken on the falling limb of the flood event were used to determine land cover types including inundation extent. These were obtained during the flooding using airborne remote sensing. The imageries were obtained on the 9th of November 2000. The images are in the form of rectangular tiles covering the flooded area. These have been merged to give images of flood extent that cover each application site and further rectified to British National Grid coordinate system based upon the topographic data (LiDAR) used in the model. The resulting aerial images covering the three application sites are shown in Figure 3.6. The image is 1:4500 in scale and consists of three spectral bands: red, green and blue. This was acquired during the falling limb of the flood event simulated on the River Ouse (§3.3). The images were scanned at  $21.2 \mu\text{m}$  resolution using a standard desktop scanner. Thus, the effective ground resolution of the images is 0.001m. Ordnance Survey benchmark data were used to rectify the imagery to a root mean square error of better than  $\pm 2.0 \text{ m}$ , using a polynomial transformation, which was judged to be sufficient for a relatively flat floodplain environment. As it is noted in Section 3.3, single-pass validation image is not able to judge model dynamic performance in terms of floodwave timing and might introduce bias into model assessment, particularly if complex floodplain configuration is involved (see §3.5, §4.5.4 and §4.7).



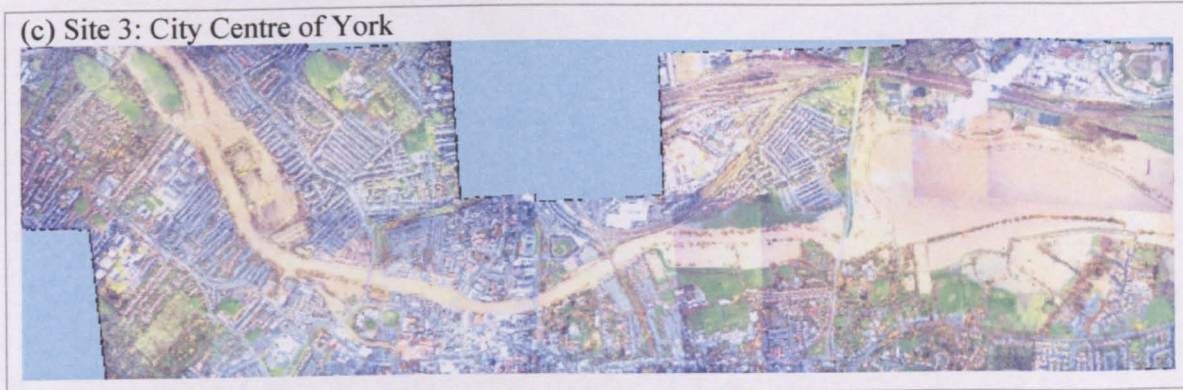


Figure 3.6: Aerial imagery taken on the 9<sup>th</sup> November, 2000 at Site 1 in the River Ouse: (a) Site 1: Naburn Weir; (b) Site 2: A64 Trunk Road; and (c) Site 3: City Centre of York.

The aerial imagery was used in both model topographic parameterization (§3.6) and validation. For topographic parameterization, the aerial imagery was used to obtain the location of the tree canopies for the removal of ground elevations associated with tree canopies in the LiDAR-derived DEM. The procedures involved are described in Section 3.6. For model validation, the aerial image was used to derive flood inundation extent, which is discussed in this section. These require that the imagery be classified into relevant land cover types including at least water bodies and trees. Image processing was carried out in ERDAS IMAGINE. The following section describes the procedures involved in the image processing for deriving the data for topographic parameterization (trees) and model validation (water bodies), using the aerial image covering Site 1 (Figure 3.6a) as an example.

Before image classification, the image was examined with respect to the spectral characteristics of different features, including water, trees, grass, buildings and roads, in order to decide on the classes to be classified. This was carried out using the profile tool in ERDAS IMAGINE and the maximum and minimum DN (digital number) values were taken for each individual class. Generally speaking, the available aerial imageries show a complex spatial and spectral structure. The complexity arises mainly from the urban areas where trees, building, roads and grasses are mixed at a very small scale. For flood modelling proposed in this study, the identification of inundation extent (water body) and trees will be sufficient. The examination of the spectral profiles of the classes, identified from the original photographs (Table 3.3), reveals that in all three bands (red, blue and green), the distinctions between the signatures of the classes are not obvious even when all sub classes are considered. If we narrow the signatures into three main classes (objective classes), the differences are even less obvious: the radiometric characteristic of flooding water in most of the bands is overlaid partly with those of the other classes. The spectral signatures of trees and grass also overlap quite a lot with each other in Band 2 and Band 3. Thus, the aim of the classification in

this study was to segment the image into four classes: (i) water; (ii) trees; and (iii) grass; and (iv) buildings and roads.

**Table 3.3: Spectral profiles of the features in the validation imagery (minimum and maximum DN values).**

Objective class	Water		Tree		Merged (Grass, building and roads)					
Sub Class	Water		Tree		Grass		Building and Road			
Detailed Class	Water		Tree		Grass		Building		Road	
	Min	Max	Min	Max	Min	Max	Min	Max	Min	Max
	DN	DN	DN	DN	DN	DN	DN	DN	DN	DN
Band 1 (Red)	125	215	54	107	72	95	94	207	160	192
Band 2 (Green)	105	145	85	170	120	150	103	216	150	175
Band 3 (Blue)	85	140	120	210	115	145	115	243	125	160

The image classification and the associated accuracy assessment were conducted using the supervised classification approach provided by ERDAS IMAGINE. First a supervised training was carried out. Training is the process of defining the criteria by which the spectral patterns are recognized (Hord, 1982). The aerial images used here are of a high-resolution and the features are easily discernable. So the training process is straightforward. Training samples were selected for the four desired classes. ERDAS IMAGINE provides several approaches for the identification of training samples, including Digitized Polygon, User-Defined Polygon, Seed Pixel and Thematic Raster Layer approaches. Since the desired classes in the aerial images used in this study can be easily identified, this study used the User-Defined Polygon approach with the AOL (area of interest) tool. Though it is recognized that the User-Defined Polygon approach may overestimate the variance of a class, it is considered to be the most suitable given the nature of the images to be classified. Pixels representing patterns of desired land cover types were identified in the training samples. Training can also be conducted in the feature space images, which are graphs of the data file values of one band of the data against the values of another band. Figure 3.7 shows three feature images created using different combinations of the three bands of the image in Figure 3.6a.

Feature space objects (polygons or rectangles) can be identified in the feature space image to create signatures for a specific class. Mapping a thematic layer into a feature space image can be useful for evaluating the validity of the parametric and non-parametric decision boundaries of a classification (Kloer, 1994). However, this is not used in the classification process, as again, it is recognized that the aerial images are of high-resolution, training in the images is considered to be a more objective way to create signatures for different classes.

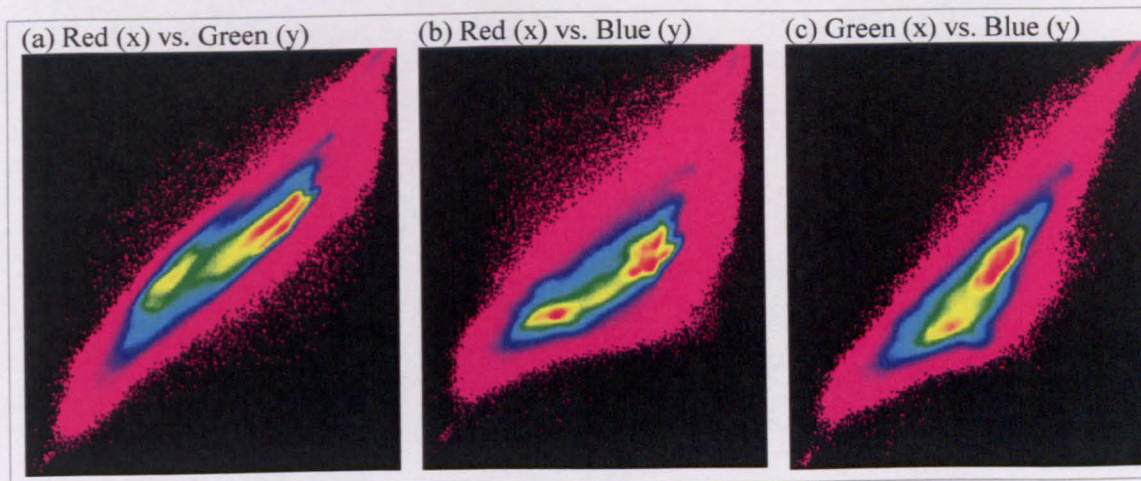


Figure 3.7: Feature space images of the image shown in Figure 3.6a: (a) Red vs. Green; (b) Red vs. Blue; and (c) Green vs. Blue. ( $x$  is the horizontal axis and  $y$  is the vertical axis).

The result of training for a specific class is a set of signatures that define a training sample, feature space object or cluster. This set of signatures can be merged to form a single signature that corresponds to a specific class. The signatures created using either supervised training or feature space objects defined in the feature space image can either be parametric or non-parametric. A parametric signature is based upon statistical parameters of the pixels in the training sites. A non-parametric signature is based upon discrete objects in a feature space image. As supervised training was used in this study, the signatures created here are parametric. Before the signatures can be used to classify the image, they need to be evaluated for accuracy. This is carried out using the contingency matrix in ERDAS IMAGINE. The contingency matrix gives the number of pixels classified into each class in the training samples that are used to create the signatures. It might be expected that the pixels of a training sample will always be classified into the desired class. However, the training samples only weight the statistics of the signatures. They are rarely so homogenous that every pixel actually assigned to the expected class. The contingency matrix created using the signatures produced from the training samples identified from Figure 3.6a is shown in Table 3.4.

Table 3.4: Contingency matrix obtained using the signatures produced from the training samples.

Classified Data \ Reference Data	Tree	Water	Grass	Building and Roads
Tree	83.48	0.31	15.08	11.07
Water	2.61	95.43	3.91	8.23
Grass	9.97	0.54	72.91	7.44
Building and Roads	3.95	3.72	8.10	73.25

The contingency matrix shows that water has a high percentage (95.43) of corrected classified pixels and this is followed by trees (83.48). However, it also suggests that there is a large percentage of trees and other features that are wrongly classified. It is interpreted from the image that this is largely associated with the misclassification of trees and grass. The accuracy

of these signatures is related to the spectral nature of the related features in the image, which has been shown to have significant overlapping areas in the spectral profiles (Table 3.3). Model validation and verification use an accuracy assessment approach adopted from remote sensing (§3.5.1). This approach was also used to evaluate the accuracy of the image classification through the assessment of spectral signatures (Table 3.4). The overall Kappa statistics and overall accuracy are calculated based on the contingency matrix.  $F$  statistics and conditional Kappa are calculated for water body and trees. These results are shown in Table 3.5.

Table 3.5: Quantitative assessment of image classification (before the correction of water bodies and trees).

	Tree	Water Body	Overall
$F$	0.660077	0.831634	N/A
Conditional Kappa	0.702335	0.821504	N/A
overall accuracy	N/A	N/A	0.812675
Overall Kappa	N/A	N/A	0.750233

Theoretically, the accuracy statistics obtained from the model could not be expected to exceed the accuracy statistics of the classification. However, as the classified image is further processed with respect to the water body (see below) using a mask layer, the accuracy might be improved. The classification was carried out using the signatures created during training process with a parametric decision rule (maximum likelihood). This results in the classification image shown in Figure 3.8.

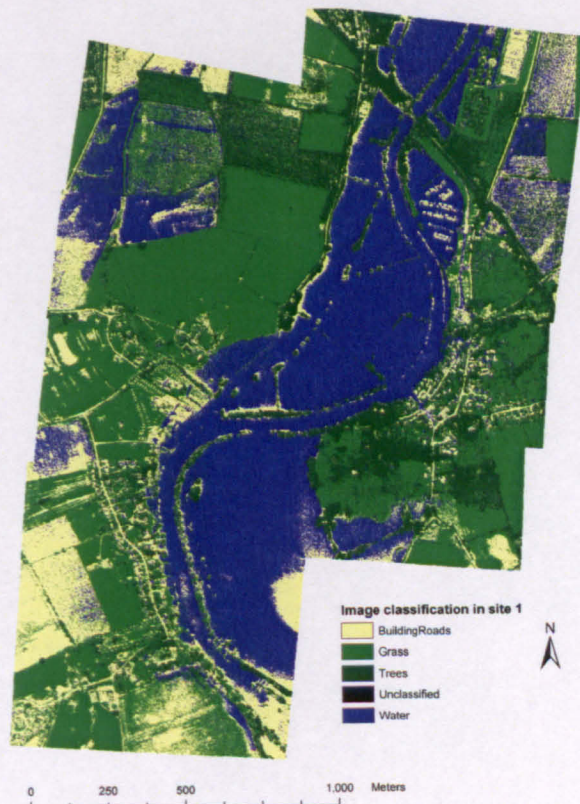


Figure 3.8: Classification of the aerial imagery at Site 1 on the River Ouse, into four classes: trees, water bodies, grass, and building and roads.

A close examination of the classified image (Figure 3.8) shows that most of the water and tree features within the flooding area have been identified correctly although quite large percentages of trees and other areas are misclassified as water outside of the flooding domain. Notably, at the interface of the water and urban features, the classification performs poorly. This study requires identification of trees for LiDAR processing, and this should not be affected by these errors. However, model validation and verification do require discrimination of flooded and dry areas in the vicinity of the urban features, and this may cause problems.

The classification was improved by a mask layer created based on visual observation of the image. The mask layer covers the areas that are observed to be flooded and the adjacent areas where the presence of trees might have an effect on flood inundation. Thus, the apparent errors in the classifications (e.g. the errors in the upper left corner of Figure 3.8) were corrected. Within the mask layer the trees are taken out as a separate layer for LiDAR processing in section (§3.6.4), resulting in a tree layer shown in Figure 3.9a. Figure 3.9b superposes the tree layer on the aerial image for comparison. This is expected to improve the accuracy of the classification.

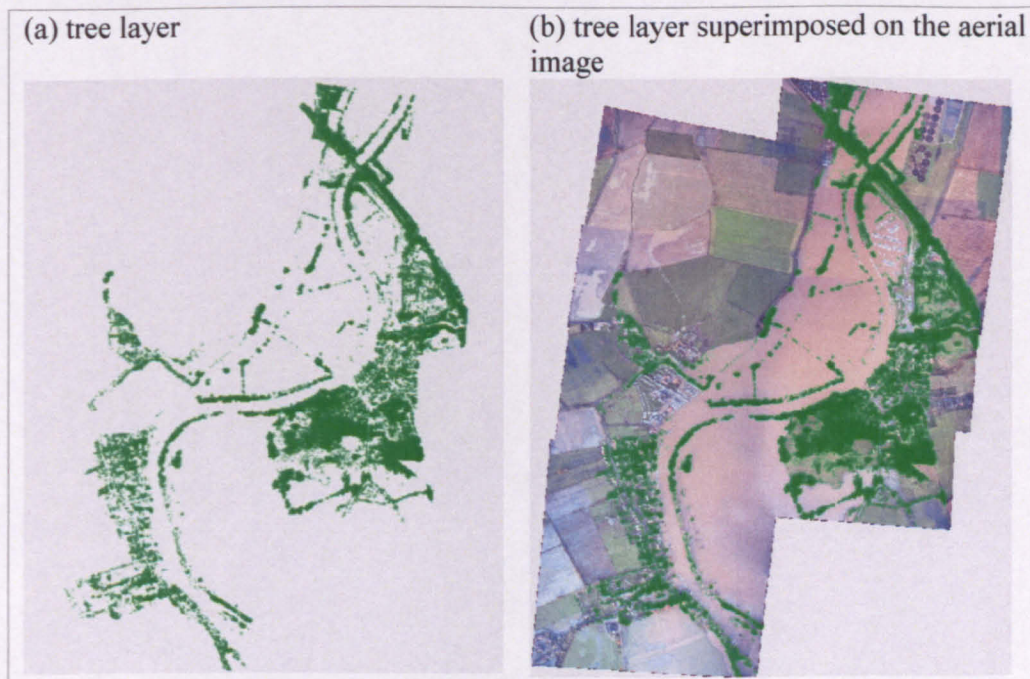


Figure 3.9: Tree locations derived from aerial images for LiDAR-derived DEM processing at Site 1 of the River Ouse: (a) tree layer; (b) tree layer superimposed on the aerial image.

Water bodies were also taken out as a separate layer to be used in model validation. This was also carried out using a mask layer based on known knowledge of the flooded areas (Figure 3.6a). This results in the inundation extent shown in Figure 3.10a. This is superposed on the aerial image and shown in Figure 3.10b. The results are fairly pixellated due to the processing of the originally high resolution data, which involved rectification and merging. The scene

should be naturally pixelated as a result of the presence of small dry buildings etc. within the scene, especially close to the wetting front.

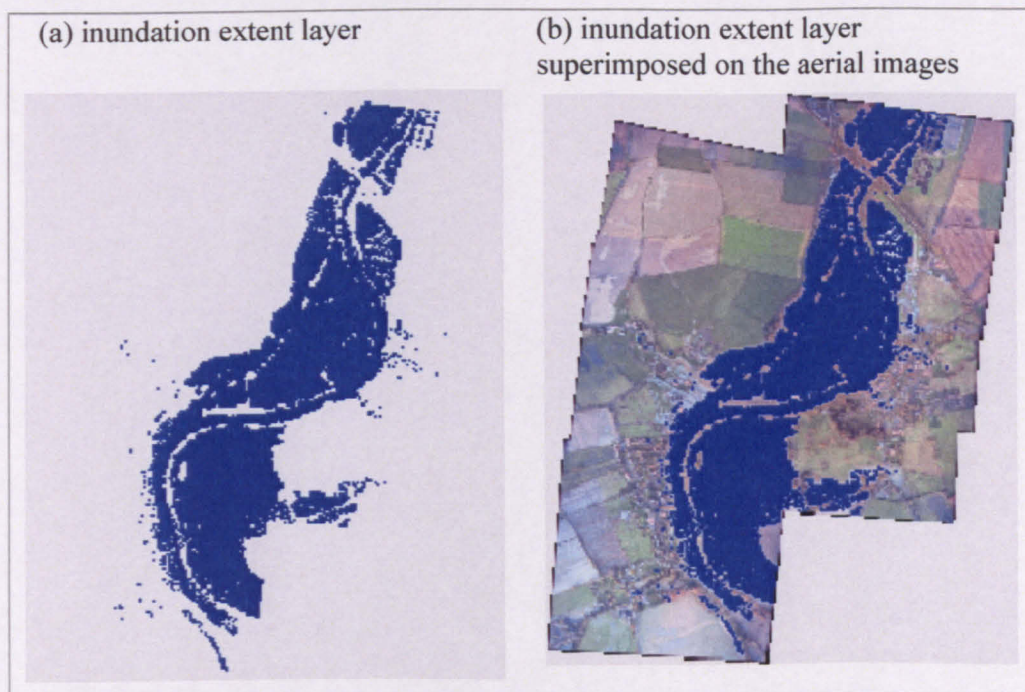


Figure 3.10: Inundation extent derived from the aerial images for the River Ouse Site 1 application: (a) inundation extent layer; (b) inundation extent layer superimposed on the aerial images.

Flood extent can also be digitised manually. However, for complex floodplain, this was proved to be rather complex as the presence of buildings, roads etc, makes this difficult in some situations. After testing (e.g. where the same operator digitised the flood boundary on different occasions), we did not feel manual digitisation was reliable.

### 3.6 Model geometry data (MG)

The geometry dataset required by the loosely-coupled model is floodplain topography. This section describes the availability of this dataset and the associated processing of this dataset for use in the models developed. As cross-section data that described river geometry are only required for the tightly-coupled model, these are addressed in Chapter 6 (§6.4).

#### 3.6.1 Floodplain topography

The topographic data available for the three case-study sites in the River Ouse include a raw LiDAR dataset in the form of point data containing the x and y coordinates and the ground elevation (z) of the point. This is the earlier first return LiDAR data and precludes doing a first return and last return analysis. This study used the unfiltered LiDAR data provided by Environment Agency. The original raw LiDAR data had been post-processed to standard data

quality requirements using methods set by the U.K. Environment Agency’s National Centre for Environmental Data Surveillance in Twerton, Bath. This included an assessment of data quality to guarantee a vertical precision of  $\pm 25$  cm throughout, improving to  $\pm 15$  cm in relatively flat areas with solid reflectance surfaces. The result is a raster-based DEM of 2-meter resolution (Figure 3.11).

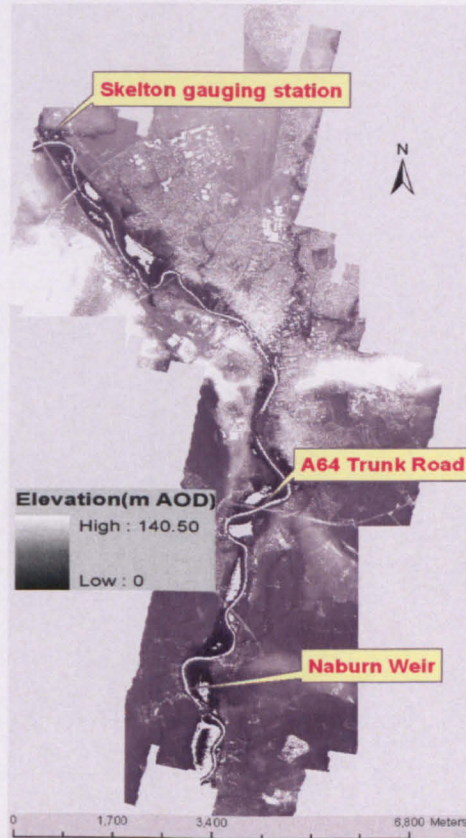
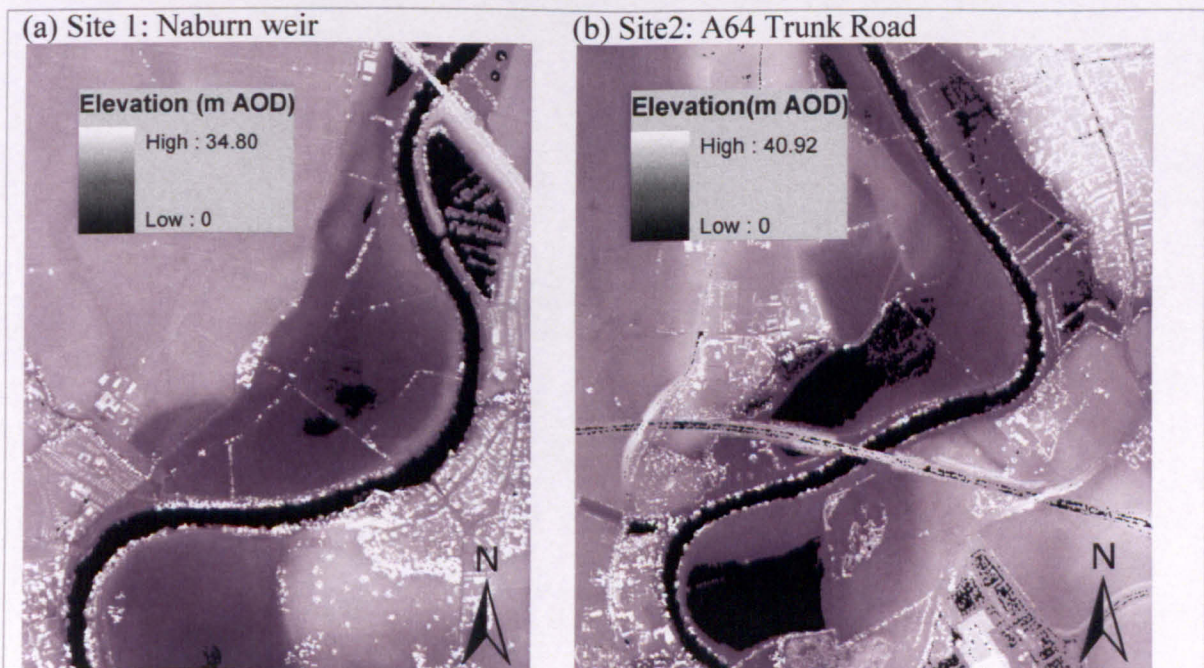


Figure 3.11: LiDAR-derived DEM covering the River Ouse with a resolution of 2 meters. The original LiDAR-derived 2 m DEMs for the three sites in the River Ouse are shown in Figure 3.12, with the orientation of the DEM in Site 3 changed for computational efficiency.



(c) Site 3: City Centre



Figure 3.12: Original LiDAR-derived 2 m DEMs for the three application sites in the River Ouse. (a) Naburn weir; (b) A64 Trunk Road; and (c) the city centre of York.

The actual quality of the original and processed (e.g. tree removal) topographical data at the application sites is not examined due to the lack of validation data. Although this can be obtained through field survey, this is not undertaken and is noted as a limitation of the thesis in Chapter 7. Bates and Anderson (1996) suggested that the target vertical point quality of a DEM used for flood modelling should be  $\pm 10$  cm. The vertical point quality for scanning systems given by all the major LiDAR system manufacturers is  $\pm 15$ -20 cm (Baltsavias, 1999b). The vertical point quality of the LiDAR-derived DEM used here ( $\pm 25$  cm) is therefore degraded as compared with the target precision. Of particular concern is where dense vegetation is present. It has been found that the quality of LiDAR-derived DEM may decrease as the density of tree canopy and understory vegetation increases (Cobby *et al.*, 2003), with overestimated ground elevations in vegetation covered areas. Cobby *et al.* (2003) attributed the error to two factors: (i) the decreased planimetric and vertical accuracy during detrending by interpolating the LiDAR minimum elevations in sloped terrains (Kraus and Pfeifer, 1998, Baltsavias, 1999a; Hyypä *et al.*, 2000); and (ii) misclassification between understory vegetation/tree trunks and the ground surface due to inadequate ground hits caused by low penetration in the presence of dense vegetation cover.

In the context of urban inundation modelling, some additional image processing needs to be undertaken for the LiDAR-derived DEMs to be used in this study. Depending on the specific reach, these may include: (i) the extraction of the river channel; (ii) the removal of elevations associated with tree canopies; (iii) the correction of riverbank elevations for model stability during model initialisation; and (iv) the correction of elevation associated with other features such as bridges and lakes, etc. This is illustrated using the 2 m LiDAR-derived DEM (Figure 3.12a) for Site 1.

First, for both the loosely- and tightly-coupled models, the common boundary between the river channel and the floodplain needs to be identified whereby the connectivity between the river flow and floodplain flow can be established. This requires the identification of the river channel location to which the boundary flow data can be applied. This can be done based on map data. However, it is recognized that this may not recognize the important features along the bank. Thus, this approach was not undertaken. Instead, river channel was identified using the LiDAR derived DEM. The separation of the river channel and the floodplain in the River Ouse was carried out based upon the observation that the LiDAR-derived DEMs have the same digital signature for water features including river channel and lakes which give no returns at all off-nadir scan angles. The water bodies on the floodplain including the river channel were identified and are shown in Figure 3.13a.

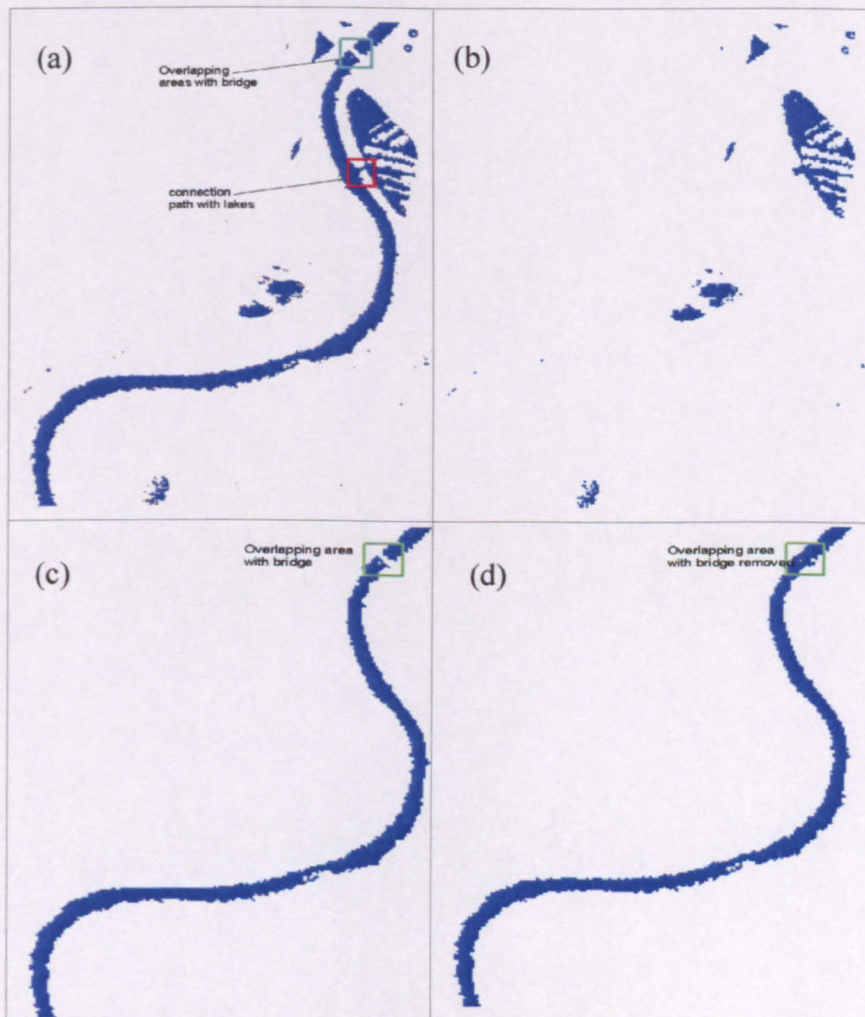


Figure 3.13: Extraction of the river channel at Site 1 on the River Ouse: (a) the water bodies in the simulation domain; (b) water bodies that need to be removed; and (c) extracted river channel with overlapping area with bridge; and (d) the extracted river channel.

The model assumes that only the river channel could pass water onto the floodplain based upon the stage hydrograph in the river channel. Thus, this requires that water bodies other

than the river channel are removed from this layer. As the river channel is not a single feature in this layer, some additional processing needs to be conducted before this can be carried out. First, the linkage between the river channel and the lake (labelled in Figure 3.13a) at the upper middle of the site was removed. Then the water bodies excluding the river channel on the floodplain were identified (Figure 3.13b) and removed from Figure 3.13a and this results in the river channel shown in Figure 3.13c. However, at the upper right of the simulation site, a bridge overlaps with the main river channel (labelled in Figure 3.13a and 3.13c) and divides the river channel into two parts. These two parts needs to be connected. This was conducted in ERDAS IMAGINE by assigning the elevation of the overlapping areas of the river channel and bridges the elevation value of the river cells, resulting in the extracted river channel shown in Figure 3.13d. Water bodies on the floodplain are mainly lakes. The lake areas are assigned the lowest bank points of the lakes. Thus, this assumes there is storage to this level in the lakes before the flood ever occurred. Secondly, as LiDAR data give no return in places where water is detected, in some situations, the processing of LiDAR-derived DEM involves the correction of elevations associated with water bodies other than river channels on the floodplain. This is relevant to all the three case studies sites presented here. Based upon the assumption that the elevation of the water body in the lake is the same as the elevation of lowest bank point of the lake, the water surface elevations associated with lakes are assigned the value of the lowest bank point of each individual lake.

Thirdly, for flood inundation modelling, whilst buildings need to be retained, it is necessary to remove elevations associated with tree canopies within the LiDAR-derived DEM under the assumption that only tree trunks would have a significant effect upon inundation. Elevations associated with tree canopies need to be removed from the original LiDAR-derived DEM. This requires the locations and heights of the trees to be identified. Tree locations were identified from the validation aerial images (Figure 3.6) during image classification (§3.5.3). However, information about tree height is not available. Though tree heights can be obtained through field survey and there are also methods for extracting vegetation (comparing tree heights with neighbouring ground elevations) (e.g. Cobby *et al.*, 2003) from LiDAR data, these are not adopted in this study. In this study, an estimated uniform tree height of 0.8 m was used. The value used here seems to be quite low. However, it was found that using a high tree height value may create artificial low ground points on the floodplain, particularly in the regions near the riverbank. This may cause the near bank storage capacity to increase dramatically and in some situations, may cause instability of the model during the initial wetting process. In addition, this study also compares the relative performance of the model and it is expected that the effect of tree removal will have similar effects for all mesh resolutions. Thus, this is considered to be a reasonable assumption. The estimated tree height

was subtracted from the original LiDAR-derived DEM, resulting in a DEM that is ready to be used in the model. The resulting DEM for Site 1 is shown in Figure 3.14b, compared with the original LiDAR-derived DEM (Figure 3.14a). This approach has its limitation in that “trees” in this study are both shrubs and large trees. Uniform tree depth may introduce significant errors into the topographic data. Ideally a more sophisticated analysis is needed as this will allow a more rigid evaluation of absolute ability of competing process representations.

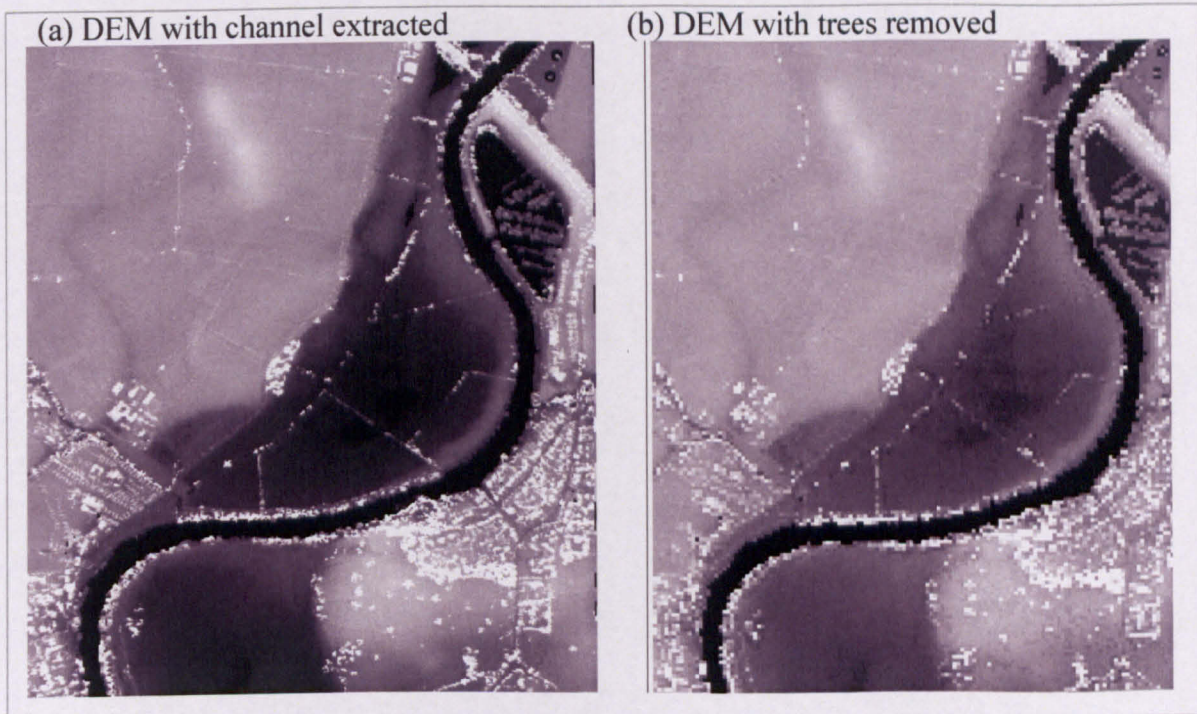


Figure 3.14: 2 m LiDAR-derived DEM for the application Site 1 on the River Ouse. (a) DEM without elevations associated with tree canopies removed; (b) DEM with elevations associated with tree canopies removed.

Fourthly, for the purpose of coupled modelling of river flow and floodplain flow (both loosely and tightly), the connectivity between river channel and floodplain at the initial stage of the simulation needs to be addressed carefully in that: (i) this will eventually determine the volume of water that can be transferred between the river channel and floodplain; and (ii) at the initial stage of the simulation, instability may occur if the water surface elevation in the river channel is too high compared with adjacent floodplain cells. Thus, in order to prevent model instability caused by unrealistic water transfer that may occur in situations where the water surface elevation in the river channel at the starting point of the simulation is higher than the adjacent river bank, these along-bank cells with a ground elevation lower than the starting inflow water surface elevation were set to the water surface elevation of the starting point in the river channel as provided by the 1D river flow model. This is only considered relevant for the loosely-coupled model used at sites 1 and 2 of the River Ouse. This was carried out by identifying the along-bank floodplain cells that are lower than the water surface

elevation of the river channel. The elevations of these cells were then raised to the water surface elevation of the starting point of the inflow hydrograph in the river channel. For Site 1, the cells that are lower than the initial inflow stage of the river (6.937 m) are shown in Figure 3.15a and the DEM with banks raised is shown in Figure 3.15b. Similar processing was carried out for Site 2 and 3 where necessary.

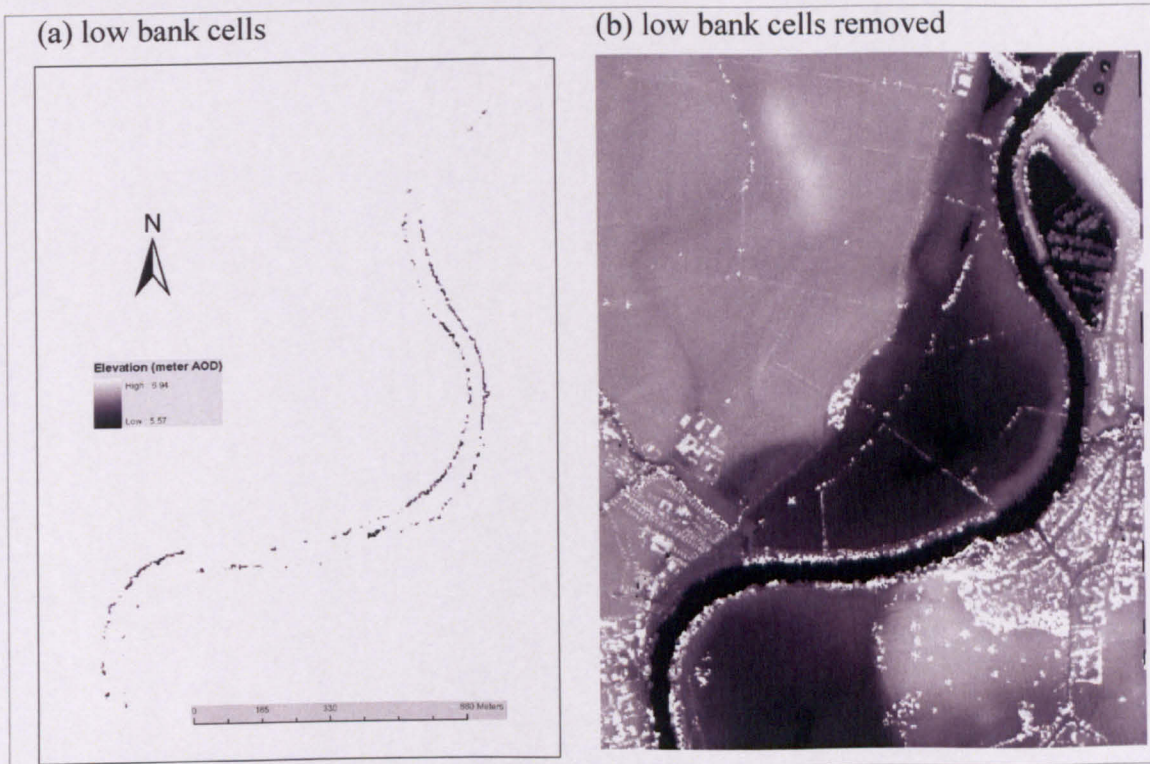


Figure 3.15: Processing of the along bank low cells (Site 1): (a) Along-bank cells that are lower than the initial stage (6.937 m) in the river channel; and (b) DEM with along-bank lower cells raised to the initial inflow stage in the river channel (6.937 m).

Ordnance Survey landline data showing the structural boundaries on the floodplain in vector form, are also available (Figure 3.3). However, only the LiDAR-derived DEM was used as the topographic input in the applications carried out in this study. Though it is recognized that vector data could be of enormous value for flood inundation modelling, this is not explored explicitly in this study.

### 3.6.2 Creation of the 4m, 8m, 16m and 32m meshes

In order to evaluate the effect of model spatial resolution (objectives defined in Section 1.2) upon flow routing and inundation extent over complex topography, the LiDAR-derived DEM was further processed to provide topographic data with different resolutions. The effect of mesh resolution upon flow routing and inundation extent was investigated at Site 1 and Site 2 on the River Ouse. 4m, 8m, 16m and 32m DEMs were created from the processed 2m DEM for these 2 sites. Compared with Site 1 and Site 2, Site 3 covers a larger area. Due to

computational performance, for Site 3, an 8 m DEM interpolated from the post-processed 2 m DEM was used throughout.

There is an interesting debate as to how to generate meshes at different resolution. Strictly speaking, you can not change a mesh resolution without changing the topographic content of the mesh in any situation where there is topographic variability at the scale of the finest mesh. In this case, at a scale of 2 m, this variability is present, due to the focus of urban areas. Thus, all mesh resolution tests in urban areas of this kind will also contain topographic variability effects. However, it is possible to change the topographic variability used in a simulation for a given mesh resolution. In this situation, the aim is to retain as much of the topographic variability as is possible and hence the focus is on changing mesh resolution, and exploring whether or not parameterisation can account for these effects. There are then two issues: (i) what elevation to assign to the coarsened mesh (see below); and (ii) how to deal with the sub-grid topographic detail that is no longer included. Point (ii) is dealt with using an effective roughness parameterisation approach in Chapter 4 and an explicit sub-grid topographic parameterisation approach in Chapter 5. In order to deal with (i) above, three commonly used re-sampling methods were considered: nearest-neighbour interpolation; bilinear interpolation; and cubic convolution interpolation; will each have some degree of smoothing effects on the input data. Bilinear interpolation determines the value of a cell based upon the weighed distance average of the four nearest input cell centres. Cubic convolution interpolation tends to smooth the data more than bilinear interpolation due to the smooth curve used and the large number of cells involved. The smoothing effects of nearest-neighbour interpolation are the least among these three methods. Thus, the primary interpolation method used in this study is nearest-neighbour interpolation, with test simulations undertaken to evaluate the effects of these three interpolation methods upon flow routing and inundation extent in the first case-study site (§4.5.3).

The DEMs with different resolution at Site 1 on the River Ouse are shown in Figure 3.16, with the original 2-meter resolution LiDAR-derived DEM re-sampled onto a 4-meter, 8-meter, 16-meter and 32-meter resolution DEM respectively. The smoothing effect of re-sampling of a DEM onto a coarser mesh is apparent, with the coarser the mesh, the smoother the land surface. This has a particular effect upon structural features. For example, the linear features in the middle of the 4-meter DEM gradually disappear in the DEMs of the 16 m and 32 m meshes. This is expected to have a significant impact upon flow routing process and the resultant inundation pattern over time.

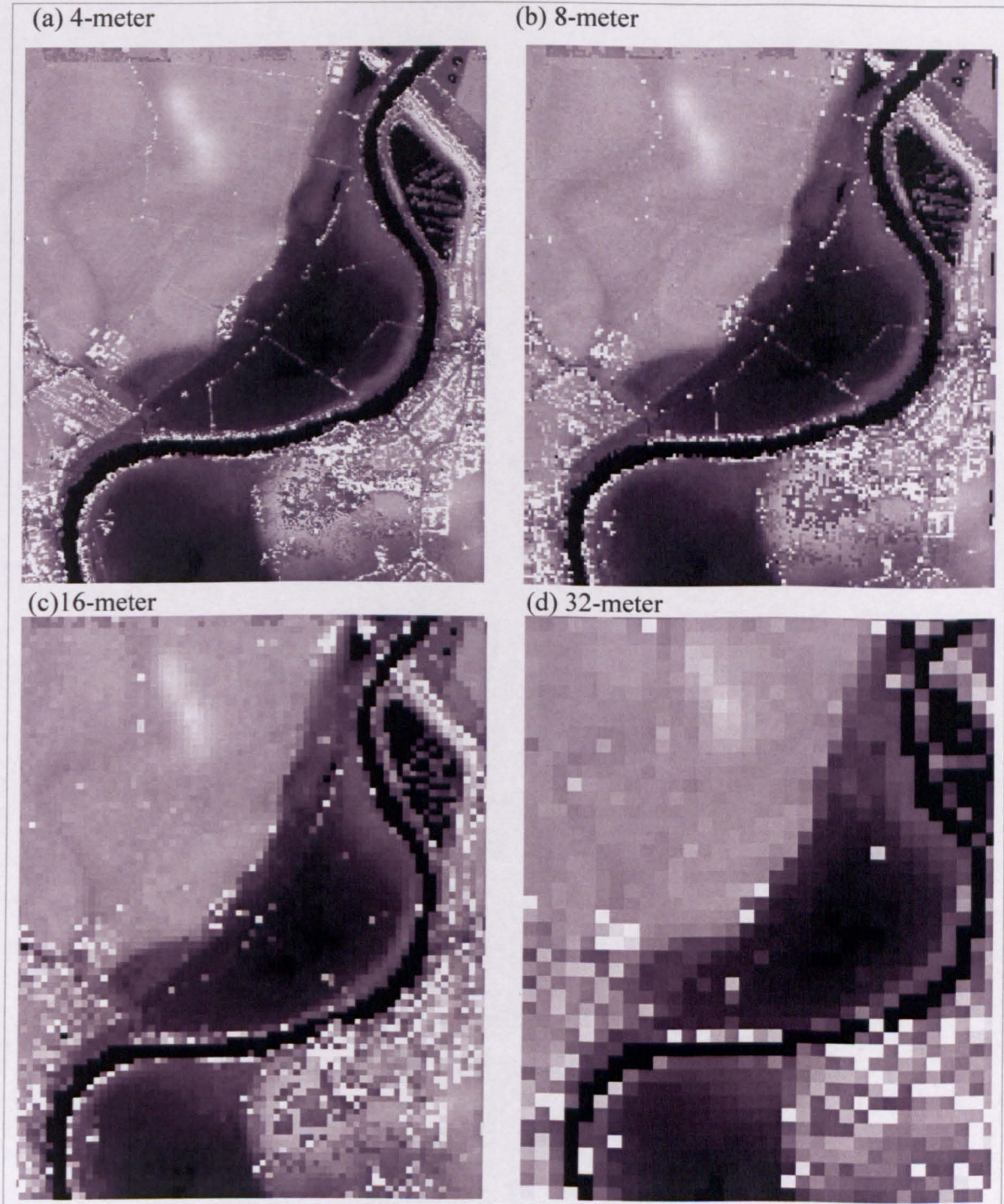


Figure 3.16: DEMs of different resolutions for the application carried out at Site 1 (4m, 8m, 16 m and 32 m).

Application to Site 2 was carried out using the 8 m, 16 m and 32 m DEMs and these are shown in Figure 3.17, together with the 4 m DEM. Similar observations regarding the smoothing effect of a coarser mesh resolution can be found in this site. The 8 m mesh used at Site 3 is shown in Figure 3.18. This is derived from the original 2 m DEM (Figure 3.12b) using the same procedure outlined above.

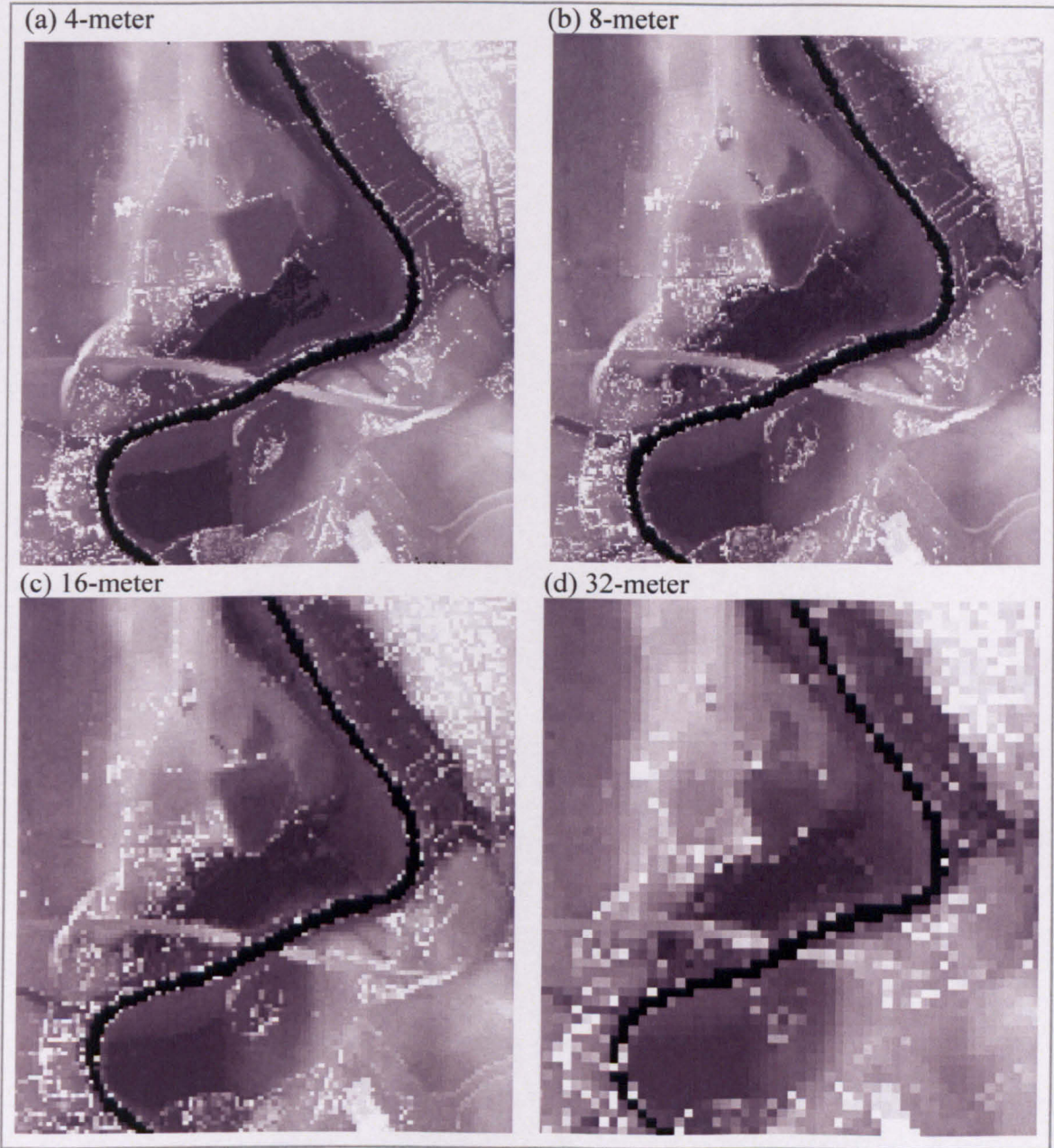


Figure 3.17: DEMs of different resolutions for the application carried out at Site 2 (4m, 8m, 16 m and 32 m).



Figure 3.18: 8 m DEM for the application carried out at Site 3.

### 3.7 Boundary condition Data (BC) for the loosely-coupled model

The boundary condition data for the loosely-coupled model include: (i) the inflow hydrograph at the river-floodplain boundary (§3.7.1); and (ii) the floodplain roughness coefficient (§3.7.2).

#### 3.7.1 Inflow hydrograph along the river-floodplain boundary

The loosely-coupled model was tested in all three application sites in the River Ouse. Thus, the inflow hydrograph in the river channel is required for these applications as the boundary condition for the floodplain flow. Inflow data at the river-floodplain boundary are obtained from an existing 1D model (ISIS) for sites 1 and 2 and from recorded sources for Site 3. These are shown in Figure 3.19.

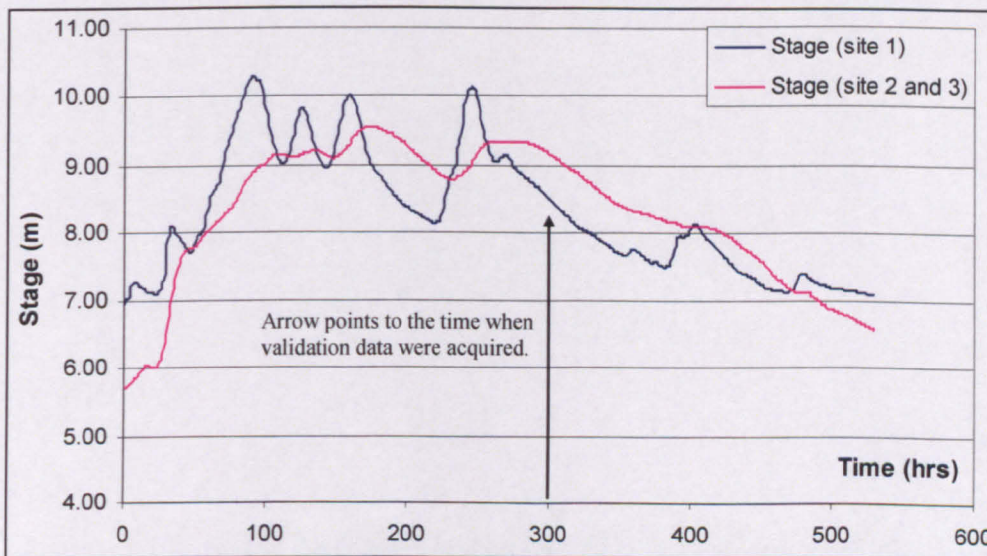


Figure 3.19: Inflow hydrographs obtained from a 1D river flow model (ISIS) in the River Ouse: (a) at Site 1; and (b): at Site 2 and 3. Arrow points to the time when validation data were acquired.

A one-dimensional hydraulic model of the River Ouse from Skelton (upstream of the city) through to Naburn Weir (downstream of the city) was used to provide estimates of flux from the river to the floodplain for all the applications. Time zero in the hydraulic model for this event was on the 27<sup>th</sup> of October at 22:00.

The inflow hydrograph shows that the flood event simulated is associated with several flow peaks and recessions, particularly for Site 1. This makes the simulation particularly interesting as it is likely to involve repeated wetting and drying, and hence provides an extreme model test. The aerial imagery showing the inundation extent was obtained at around 300 hours into the hydrograph (Arrow in the Figure 3.19).

As the loosely-coupled model uses a uniform inflow hydrograph for the three applications, this inevitably introduces some errors in relation to the inflow boundary data. Furthermore, due to the availability of inflow data, the location at which the representative stage hydrograph was obtained could further contribute to the errors associated with the inflow data. This can be further compounded by the shape of the river reach. In fact, high degrees of river channel curvature were found at all three sites. The inflow hydrograph at Site 1 was obtained at downstream of the river at Naburn Weir (Figure 3.2). Naburn Weir was constructed in the late eighteenth century and for navigation purposes upstream to York. The marked fluctuations at Site 1 arise from the operations of Naburn Weir (downstream of the site). The stage hydrograph at the intersection between A64 Trunk Road and the River Ouse was used at Site 2 as the inflow data.

As there is no available data within the river reach at Site 3, the downstream stage hydrograph at A64 Trunk Road was used for Site 3 application. Thus, for Site 3, the inflow hydrograph is more likely to underestimate inflow from the river channel to the floodplain in the 2D floodplain flow model.

### **3.7.2 Roughness parameterization**

In terms of roughness parameterization, 2D models have typically used a uniform roughness parameter (e.g. Bates and De Roo, 2000; Horritt and Bates, 2001a). Different surfaces (e.g. grass, road, garden etc.) might need to be allocated different roughness parameters and spatial distribution of roughness parameters has been explored in 2D models (e.g. Horritt, 2001; Cobby *et al.*, 2003). For example, Cobby *et al.* (2003) calculated the spatial distribution of roughness parameter based upon a vegetation map derived from LiDAR data to estimate friction values at each computational node in a finite-element model. Though this has been found to give better results than the traditional uniform roughness parameter, spatial distribution of roughness parameters is not addressed in this study. This is because of the philosophy implicit in Chapter 4 and 5: up-scaling of roughness parameters should be restricted to cases where topography can not be modelled explicitly. Instead, uniform roughness coefficients were used for different simulations in a roughness parameterization.

The effect of roughness parameterization upon flow routing was investigated in conjunction with the effect of mesh resolution at Site 1 on the River Ouse. Simulations were carried out using the 4 m, 8 m, 16 m and 32 m DEMs with different values of Manning's  $n$  values: 0.04, 0.06, 0.08, 0.10, 1.0, and 10.0 (Chapter 4 and 5). Some of these values clearly extend beyond the range of  $n$  values for which the Manning's relationship was originally formulated.

However, others (e.g. Mason *et al.*, 2003) have found that in order for roughness parameterization to have any significant effect upon model predictions, high values of roughness values have to be used. If it is recognised that  $n$  is being used as an effective calibration parameter, and if  $n$  can be shown to result in acceptable model predictions, then this may not be a problem. This is explored in Section 4.7 and Section 5.4.3.

For the applications carried out at Site 2 and Site 3, a uniform roughness value of 0.06 was used based on the typical values suggested by Chow *et al.* (1988) for a floodplain surface.

### **3.8 Chapter summary**

This chapter has described the three application sites on the River Ouse used in this research in terms of data requirements, options and processing procedures, with reference to model parameterization, coupling approach and validation. Two approaches for the coupling of the river flow and floodplain were developed in this study (§3.2). This chapter presents the loosely-coupled version of the model and the discussion with respect to the data requirements and availability is restricted to the loosely-coupled version of the model. In terms of the topographic data requirements, high-resolution topographic data are available in the form of a DEM of 2 m resolution (§3.6). This was produced from raw LiDAR data. Validation data are available in the form of aerial imagery during the falling limb of the flood event (§3.5.3). This is used to extract the inundation extent for model validation and to correct the height effect associated with tree canopies in the LiDAR-derived DEM. The inundation extents and tree canopy locations were obtained through image processing. Inundation extents were used in the model validation. The LiDAR-derived DEM was further processed to correct the elevations associated with the overlapping areas of bridges and river channels as well as low bank elevations (§3.6.2). The correction of tree canopy effects needs both the locations of trees and the heights of trees to be specified. The locations of trees were identified through image processing of validation data. Tree height information might be obtained in two ways: (1) through field survey; or (ii) through the processing of the double-return LiDAR data. However, none of these two approaches were adopted. Rather, the removal of tree canopies was undertaken under a crude assumption that trees heights are uniform in the simulation domain. This clearly has its limitations. However, in the absence of exact tree height information, this is considered to be a reasonable way forward, particularly in situations where the verification approach was used.

Given the validation data, the approaches to quantitative assessment of model performance were discussed using the concepts of model validation and verification (§3.5.1). Statistics

adopted from the remote sensing literature that allow quantitative analysis of model performance with respect to both the validation and verification, were presented (§3.5.2). These form the basis for the model applications described in Chapter 4, 5 and 6.

# Chapter 4

## Model developments and testing 1: conventional 2D diffusion wave modelling of urban fluvial flooding

### 4.1 Introduction

Chapter 3 discussed data requirements and data availability for three sites modelled in this study with reference to the loosely-coupled model. This chapter describes the 2D diffusion wave flood inundation model developed in this study, in terms of its governing equations and numerical solution in a raster-based environment. Based upon this model, the application to Site 1 is described and the results are presented, focusing upon exploring the interaction between model resolution and roughness parameterization in relation to inundation modelling of flow over topographically complex floodplains. Furthermore, applications to sites 2 and 3 are also presented to test the repeatability of the model performance, with the focus upon model validation. The diffusion wave model recognizes that significant structural elements on the floodplain can be averaged out in low-resolution models but that the effects of these features upon small-scale flow routing and large-scale inundation extent will thus be minimized and simplified. Traditional approaches to representation of these features usually involve up-scaling of the roughness parameter in the momentum equation. This has its limitations in that: (i) it does not recognize fully the mass blockage effects associated with some significant structural features; and (ii) it may reduce the mass transfer through these features, but it may not recognize that, in some situations, some of these features can act as complete barriers to the flow. Diffusion wave models use a simpler process representation than full 2D flow models but with an explicit representation of structural features on the floodplain. This allows its application over larger areas, at higher resolutions and for longer time periods.

Essentially there are two categories of solutions to the traditional representation of structural features in diffusion wave models. First, they can be represented explicitly using high-resolution topographic data. However, this can be unfeasible due to the computational

requirements of modelling over large areas or longer periods, even with 2D models. Second, the problem may be solved by explicit representation of small-scale flow routing processes associated with structural features, in either a raster or a vector treatment. The latter has been addressed in finite-element approaches of flood inundation modelling. However, approaches to small-scale flow process representation in 2D diffusion wave models have yet to be fully developed. Thus, as a starting point, this chapter addresses this problem through explicit representation of topographically significant structural features on the floodplain in a 2D diffusion wave model using high-resolution data. It undertakes a primary investigation, including model development and application, to explore the interactions between mesh resolution and roughness parameterization, with the aim of understanding the role of external data provision and internal process presentation in 2D diffusion wave models. This establishes the basis for the sub grid wetting representation treatment developed in Chapter 5.

## 4.2 Chapter aims and objectives

The overall aim of this chapter is to advance the understanding of the application of 2D diffusion wave approaches to modelling flood inundation over topographically complex floodplains. The specific objectives are: (i) to develop a 2D diffusion wave model for flood inundation modelling over complex topography; (ii) to explore the effect of mesh resolution upon flow routing and inundation extent; and (iii) to investigate the interaction between roughness parameterization and mesh resolution.

## 4.3 Model description

### 4.3.1 Process representation

The model used in this study takes the same structure as that of the JFLOW model developed by Bradbrook et al. (2004). The description here is taken from Bradbrook et al. (2004) but modified for the purpose of inundation over topographically complex floodplains.

The general form of the Manning's equation is:

$$Q = \frac{AR^{2/3}S^{0.5}}{n} \quad (4.1)$$

where  $Q$  is the flow ( $\text{m}^3\text{s}^{-1}$ ),  $A$  is cross-section area ( $\text{m}^2$ ),  $R$  is hydraulic radius (m),  $n$  is Manning's  $n$ , and  $S$  is energy slope. It is common practice in hydraulic analysis to split compound cross-sections into a series of panels and to calculate flow conveyance in them

separately (Bradbrook *et al.*, 2004). Bradbrook *et al.* (2004) note that if the floodplain is partitioned as a regular grid with a resolution  $w$ , the flow across the face of each cell can be treated as a separate panel. The flow area across the face of the cell is then calculated from:

$$A = w * d \quad (4.2)$$

where  $w$  is the width of the cell and  $d$  is the flow depth. The hydraulic radius is equal to the depth of the cell as:

$$R = \frac{A}{P} = \frac{w * d}{w} = d \quad (4.3)$$

where  $P$  is the wetted parameter (m). The Manning's equation then takes the form:

$$Q = \frac{wd^{5/3}S^{0.5}}{n} \quad (4.4)$$

Considering a regular grid cell and the four cells adjacent to it, the orthogonal directions of the grid cells are termed  $i$  and  $j$ . Two parameters need to be derived from the configuration: the energy slope  $S$ , and the effective depth  $d$  to solve Equation (4.4). The energy slope in each orthogonal direction is given by the difference in water levels between the cells divided by the distance between the cell centres (4.5a, 4.5b). Water is allowed to flow out of the cell only if the slope of the source cell to the other adjacent cells is positive.

$$S_i = \frac{h_{i,j} - h_{i\pm 1,j}}{w} \quad (4.5a)$$

$$S_j = \frac{h_{i,j} - h_{i,j\pm 1}}{w} \quad (4.5b)$$

The flow direction is determined by determining the vector sum of the energy slope in the  $i$  and  $j$  directions. Outflow is only allowed in two of the adjacent orthogonal directions defined by the vector sum of the slopes. This is similar to the approach described in Horritt and Bates (2001b). The vector sum of the slope values along  $i$  and  $j$  directions is given by:

$$S = \sqrt{S_i^2 + S_j^2} \quad (4.6)$$

The effective depth in each of the four directions is determined as the water level in the source above the higher of the two ground levels along either the  $i$  or  $j$  direction as given by (4.7).

$$d_i = h_{i,j} - \max[g_{i,j}, g_{i\pm 1,j}] \quad (4.7a)$$

$$d_j = h_{i,j} - \max[g_{i,j}, g_{i,j\pm 1}] \quad (4.7b)$$

where  $d$  is the effective depth,  $h$  is the water surface elevation and  $g$  is the ground elevation. The effective depth in the outflow direction is then calculated as the arithmetic mean of the two flow effective depths in the line of steepest slope:

$$d = \frac{d_i S_i^2 + d_j S_j^2}{S^2} \quad (4.8)$$

Substituting (4.6) and (4.8) into equation (4.4) solves the Manning's equation partitioned on a regular grid. The flow vector can then be solved in each of the two orthogonal directions of the grid, giving possible flow in up to 2 of the adjacent cells at each time step. For each time step, the fluxes into and out of each cell in the calculation domain are then given by (4.9a) and (4.9b).

$$Q_i = Q \frac{S_i}{S} = \frac{wd^{5/3} S_i}{nS^{0.5}} = \frac{wd^{5/3} \left( \frac{h_{i,j} - h_{i\pm 1,j}}{w} \right)}{n \left[ \left( \frac{h_{i,j} - h_{i\pm 1,j}}{w} \right)^2 + \left( \frac{h_{i,j} - h_{i,j\pm 1}}{w} \right)^2 \right]^{1/4}} \quad (4.9a)$$

$$Q_j = Q \frac{S_j}{S} = \frac{wd^{5/3} S_j}{nS^{0.5}} = \frac{wd^{5/3} \left( \frac{h_{i,j} - h_{i,j\pm 1}}{w} \right)}{n \left[ \left( \frac{h_{i,j} - h_{i\pm 1,j}}{w} \right)^2 + \left( \frac{h_{i,j} - h_{i,j\pm 1}}{w} \right)^2 \right]^{1/4}} \quad (4.9b)$$

The change of water depth in each of the cells is then calculated from equation (4.10) at the start of each time step.

$$\Delta d = \frac{\left( \sum_{d=1}^4 Q_{in,i,j}^d - \sum_{d=1}^4 Q_{out,i,j}^d - Q_{inf low} \right) \Delta t}{w} \quad (4.10)$$

where  $\Delta t$  is time step (in seconds). The water depth of a grid cell is calculated as the average depth over that whole cell. In this chapter, there is no consideration of the sub grid topography, which may increase the variance in water depth within the cell. When the cell first receives water, the wetting front edge lies within the cell. In most cases, only part of the cell will be wetted at that time step. If this problem is not dealt with, water will diffuse too quickly across the floodplain. When the flow volume leaving a cell is higher than that entering the cell, the cell is drying and there is the possibility that the water depth may be reduced to zero or a negative value based on the calculation from equations (4.9a) and (4.9b). This presents two separate problems in the model. Clearly, negative depths are impossible. However, more seriously, it is vital that partially wet cells are maintained accurately during drying to avoid the creation of isolated artificially wet patches. The model used here follows Bradbrook *et al.* (2004) and controls the wetting process by a wetting parameter and treats the drying process more realistically by specifying a minimum depth below which no outflow is allowed. This allows parts of the floodplain that were inundated at one point in a simulation to remain wet if, during drying, connectivity cannot be maintained with the river or other parts of the floodplain.

When the cell is wetting, the water should not be allowed to flow out of the cell until the wetting front has crossed the cell. Following Bradbrook *et al.* (2004), each cell has a property called *%wet*. When the cell is first wet, this is calculated from:

$$\%wet = \min\left(1, \frac{v\Delta t}{\Delta x}\right) \quad (4.11)$$

Water is not allowed to flow out of the cell until the wetting parameter reaches one (i.e. the cell is fully wet). The wetting parameter is updated each time step as water travels across a cell. Wetting parameter is accumulative, regardless of the direction of wetting. Thus, a cell can be wetted from two directions by its adjacent cells. This parameter is a necessary yet not sufficient condition for water to flow out of the cell. A minimum water depth is set. Before this depth is reached, no outflow is allowed. The direction of the wetting process within a cell is not addressed in this situation. For drying, a minimum water depth is also set, also

following Bradbrook *et al.* (2004). At each time step, the sum of the net inflow and outflow is calculated. If the water depth is reduced to the minimum depth, the outflow is scaled by a drying factor ( $d_f$ ):

$$d_f = \frac{w^2(d - d_{\min})}{\left( \sum_{d=1}^4 QIn_{i,j}^d - \sum_{d=1}^4 QOut_{i,j}^d - Q_{\text{inflow}} \right)} \quad (4.12)$$

The drying factor ensures mass conservation as the floodplain dries. The minimum value of water depth during wetting is set as 0.05m and during drying is set as 0.02m in this model. The choice of these values is arbitrary and sensitivity analysis on these values needs to be undertaken to explore their effects (§4.5.1).

As the above solution scheme is explicit, the Courant condition (Courant and Friedrichs, 1948, cited by Abbott and Basco, 1989) applies as a necessary but not sufficient condition for model stability and accuracy. The Courant condition requires that the time step be less than the time for the flow to travel the cell width. If the time step is so large that the Courant condition is not satisfied, there will be an accumulation of water without any change in hydrodynamic representation of the effects of that water. Thus the Courant condition must be determined at each time step during model solution using:

$$\Delta t \leq \frac{w}{v + \sqrt{gd}} \quad (4.13)$$

where  $d$  is the maximum water effective depth. The  $\sqrt{gd}$  term is not strictly necessary with the formulation used here, as result of the simplification of the momentum equations described above. Traditional methods for determining time steps involve finding the smallest  $t$  among those calculated for every grid point at a time line and using this value as the time step required for the next time step. Over complex topography, this value usually needs to be downscaled given that local low points may occur. Boundary conditions consist of an inflow hydrograph along each contact cell between the river channel and the floodplain. The approaches to coupling the 1D river flow to the 2D floodplain flow have been discussed in Section 3.2. The loosely-coupled version of the model uses a stage hydrograph as the inflow boundary for the floodplain flow. While the tightly-coupled model calculates the river stage at each time step as the inflow for the 2D floodplain flow at that time step in the river flow sub

model. Regardless of the coupling approach, the flux to the floodplain from the river channel is determined from predictions of water level in the river channel using a weir equation:

$$q = 1.704(H - \Delta z)^{3/2} \quad (4.14)$$

where  $H$  is the water surface elevation of the river channel and  $\Delta z$  is the ground elevation of the river embankment on the floodplain. Stage hydrographs are projected to each river cell and inflow from the river channel occurs once the water surface elevation of the river channel exceeds that of the adjacent floodplain cell.

For the outflow boundary, the model needs to decide when and how to allow water to flow out of the calculation domain. The solution adopted by Bradbrook *et al.* (2004) is used here. Once water reaches an outflow boundary, the depth in the cells on the other side of the boundary is set to be equal to the depth in the adjacent cell. Thus, the water surface slope is the bed slope across the boundary. If this results in a reverse water surface slope, the water depth on the other side of the boundary is reset such that the water surface level is the same as the adjacent cell. During the next time step, the outflow across the boundary is calculated depending on the water surface slope across the boundary. Mass conservation is checked at each time step to ensure that total outflow is equal to total inflow minus the increase in the floodplain storage during that time step if there is water flowing out of the outflow boundary.

### 4.3.2 Discretization and solution

For the scheme described above to be solved numerically, the floodplain domain is discretized into a mesh of grids with regular size. This is realized using the raster-based DEM derived from the LiDAR data (§3.6.2). This allows the term  $w$  in Equation (4.4) to be replaced by the DEM resolution and other terms such as  $d_i$ ,  $d_j$ ,  $S_i$  and  $S_j$ , etc, to be derived from  $w$  in combination with the ground elevation ( $g$ ) and water depth ( $d$ ) in every grid at each time step using appropriate equations.

The major steps involved in the numerical solution to the scheme are schematized in Figure 4.1.

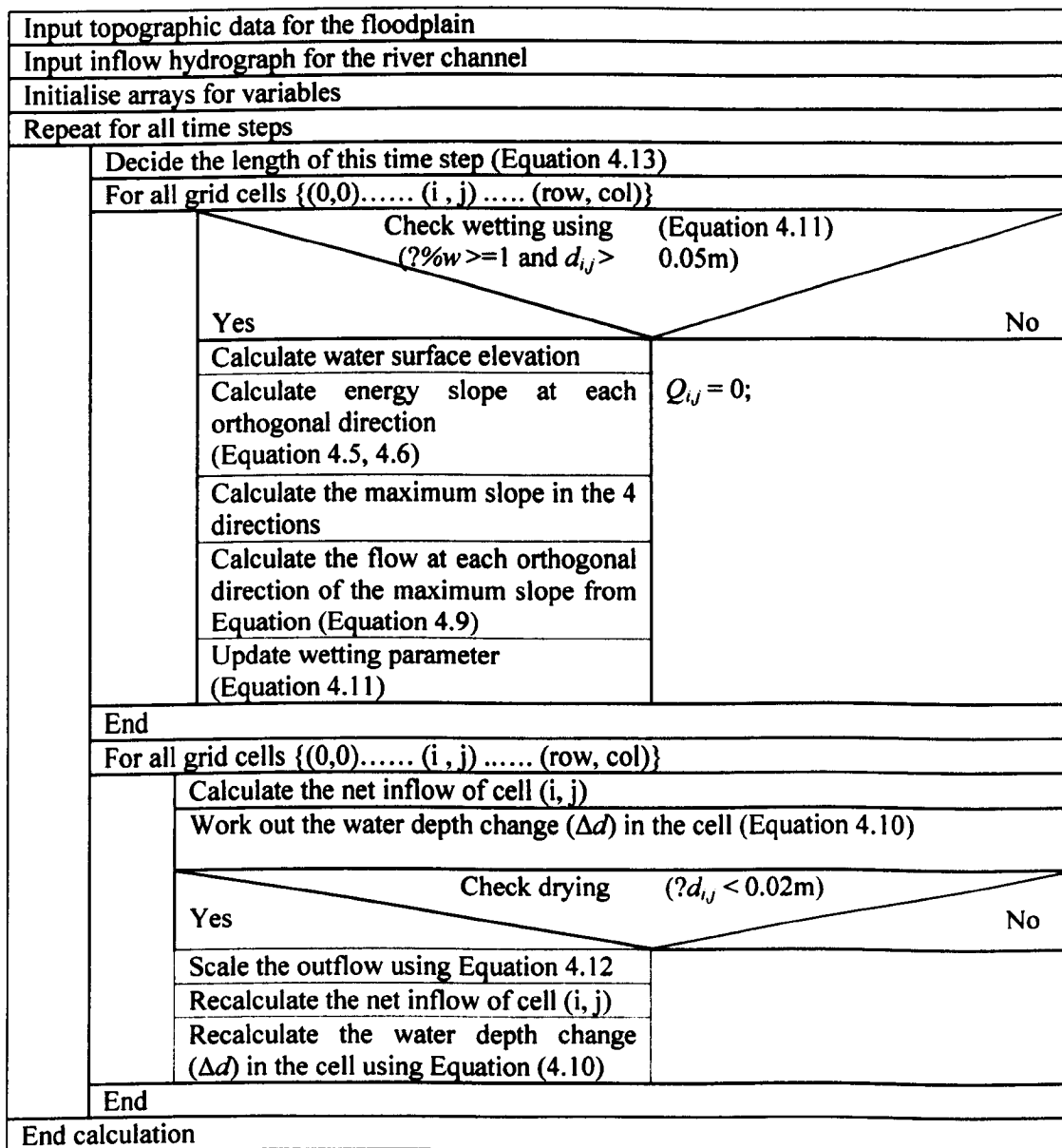


Figure 4.1: Schematic view of the numerical solution of the 2D diffusion wave model in a raster environment.

## 4.4 Model Graphic User Interface (GUI) description

### 4.4.1 Main model user interface

The model scheme was coded in an object-oriented programming language Java with a front end to Java for visualization purposes. Figure 4.2 illustrates the main model user interface, with labels of its components. This consists of a menu bar, a tool bar, a “*Model option*” panel, a “*Visualisation*” panel, a “*Runtime query*” panel and a “*Message viewer*” panel (as indicated in Figure 4.2).

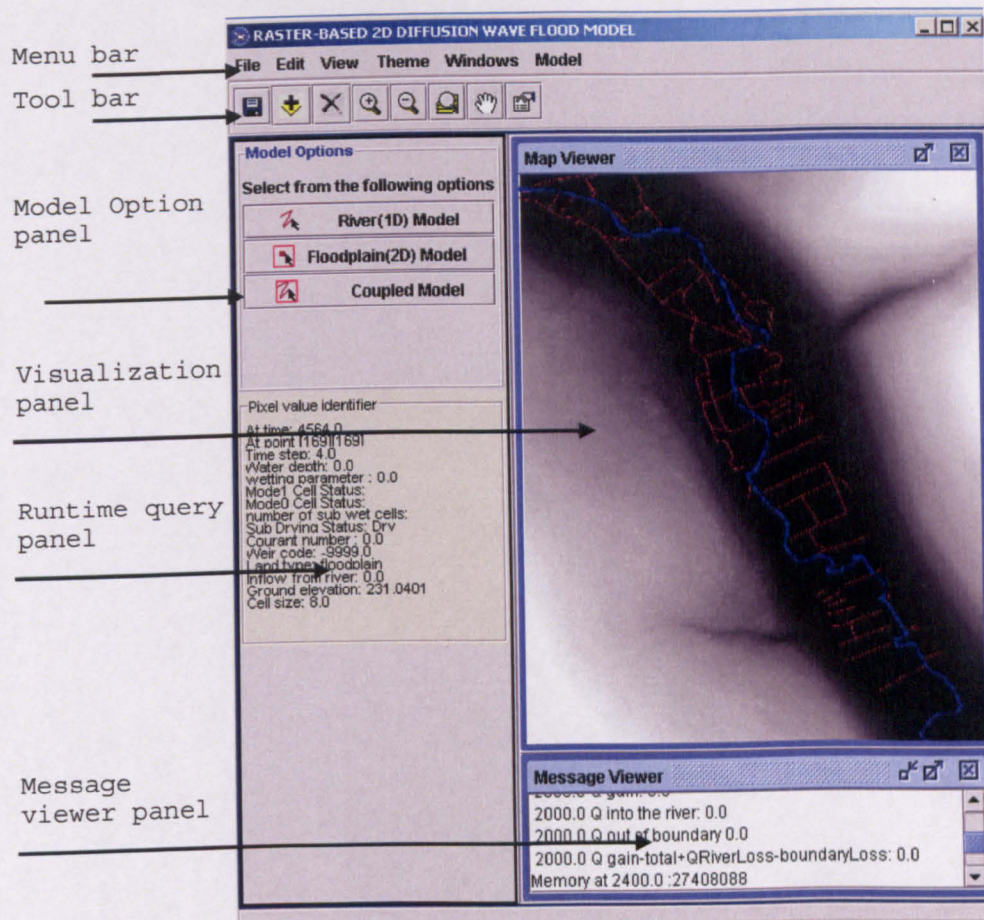


Figure 4.2: Model Graphical User Interface

The menu bar and tool bar provide basic functions such as zooming in, zooming out and adding data, etc. The “*Runtime visualisation*” panel shows the visualisation of the inundation process. The “*Runtime query*” panel shows the information about the cell on which the mouse resides in the “*Runtime visualisation*” panel at each time step during the simulation. Information shown in this panel includes the wetting parameter, water depth, ground features (river, floodplain and weir), Courant number and time-step, etc. The “*Message viewer*” panel gives the runtime information of the mass transfer between the river and the floodplain, mass error and the memory usage of the model.

As discussed in Section 3.2, two versions of the model are available: a loosely-coupled version and a tightly-coupled version. These are distinguished in the “*Model options*” panel (indicated in Figure 4.2). There are three options in the “*Model options*” panel: (i) “*River (1D) model*”; (ii) “*Floodplain (2D) model*”; and (iii) “*Coupled model*”. The “*Floodplain (2D) model*” button in the model option panel activates the loosely-coupled model and the “*Coupled model*” button activates the tightly-coupled version. The “*River (1D)*” button activates the one-dimensional river flow model.

#### 4.4.2 User interface of the loosely-coupled version

The loosely-coupled version of model has a main configuration frame as shown in Figure 4.3. This includes several sub panels, including: (i) the “*Define feature*” sub panel; (ii) the “*Define topography*” sub panel; (iii) the “*Define sub grid*” sub panel; (iv) the “*Input/output options*” sub panel; (v) the “*Accuracy analysis*” sub panel; the “*Define parameter*” sub panel; (vi) the “*Summary*” sub panel and (vii) a progress bar, indicating the progress of the model simulation in percentage.

**Floodplain Model 2D Configuration**

**Define Features**

Import River      Sub\_Grid River

Weirs      Sub\_Grid Elevation

**Define Topography**

Import DEM Data

**Define Sub-grid**

SubGrid\_Treatment

**Model Options**

Inflow Options

Output Options

Other Options

**Accuracy Analysis**

Import Validation Data

**Summaries**

Features	Status
River	Not Defined
DEM	Not Defined
Sub-Grid	False
Inflow	Not Defined
Inflow Type	Not Defined
Output ima...	False
Painting	False
Kappa M1	false

**Define Parameters**

Manning's n: 0.06

Run for (s): 1,908,000

Cell Size(m): 8

Time Step: 4  Implicit

Run the model

Figure 4.3: Loosely-coupled flood inundation model main configuration frame.

The location of the river is defined in the “*Define feature*” sub panel and the topographic input is defined in the “*Define topography*” sub panel. Both the river location and topographical input data need to be processed in ArcGIS into ASCII (.asc) format. The 2D model configuration frame (Figure 4.3) also defines whether the model will run with the sub grid-scale wetting treatment approach adopted (in the “*Define sub grid*” sub panel) and allows input of sub grid topographical data (in the “*Define feature*”, “*Define topography*” sub panels) accordingly. The sub grid wetting treatment approach is illustrated in Chapter 5.

The boundary inflow data is input into the model through the “*Input options*” button in the “*Input/output options*” sub panel in Figure 4.3. This brings out the “*Input panel*” shown in Figure 4.4.

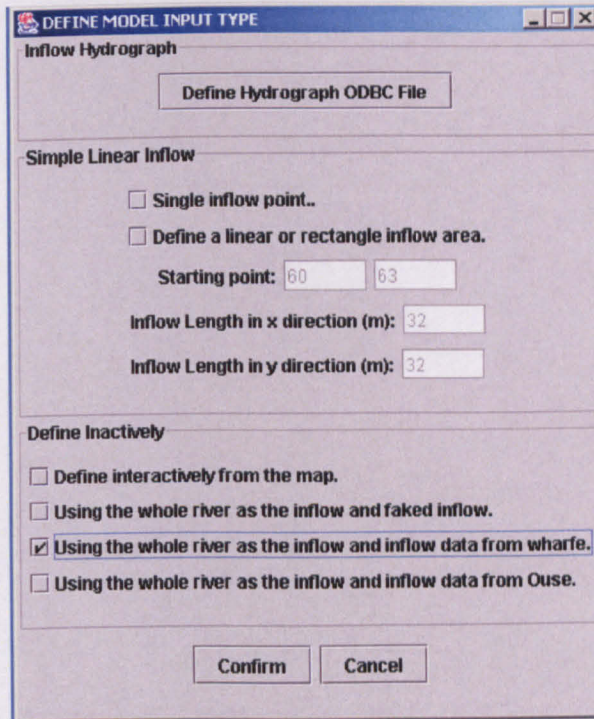


Figure 4.4: Hydrograph input and application type panel.

The inflow hydrograph is a uniform stage hydrograph for the whole river channel for the loosely-coupled model. The input hydrograph from the river channel is in Microsoft Excel Work Sheet (.xls) format. This panel also allows the selection of model applications. There are also other application options for general model testing purposes. These include simple artificial inflow patterns including single point inflow, linear or rectangle inflow areas, interactively defined inflow areas, and artificial inflow hydrograph. Output of the model is defined in the “*Model Output*” panel (Figure 4.5), which can be activated from the “*Output options*” button in the “*Input/output options*” sub panel in the main configuration frame of the loosely-coupled model (Figure 4.3).

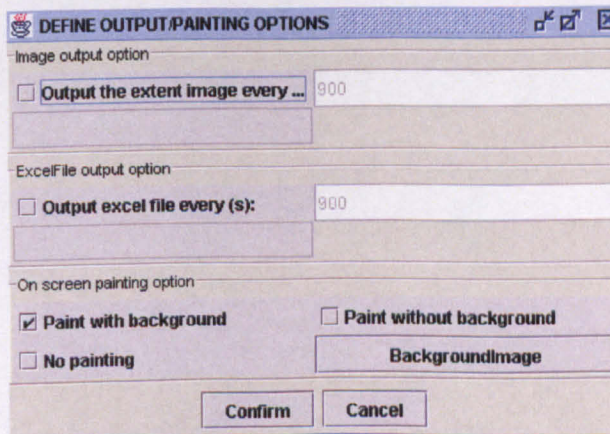


Figure 4.5: Panel for model output.

The outputs of the model are a time series of inundation extent (JPEG format) and the water depth at each cell (ASCII format), at pre-defined time intervals. This can be overlain with the DEM of the application domain to allow visual analysis of the inundation pattern over background features. The output image represents the inundation pattern using the relative depth of the inundated cells, with a darker colour representing a higher water depth. The output ASCII file contains the water depth at each cell. The “*Output options*” panel also defines the painting mode for the visualisation panel (in Figure 4.2), with options to paint the inundation pattern on the screen either with or without the background DEM, or no painting for computational efficiency. The input validation data and the output options for model accuracy assessment are defined from the “*Accuracy analysis*” panel (Figure 4.6) using the accuracy assessment approaches discussed in Section 3.5.1 and Section 3.5.2. It allows output of the related accuracy statistics at a regular time interval (e.g. for parameterization as part of model verification) or at a single point (e.g. for comparison with real data as part of model validation to Microsoft Excel Worksheet).

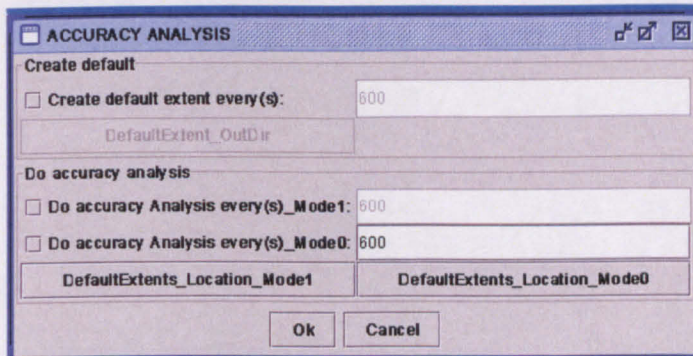


Figure 4.6: Panel for accuracy assessment

The “*Define parameter*” sub panel defines the value of Manning’s  $n$ , the mesh size and the length of the simulation. Another parameter defined here is the time step used in the model. This can either be explicit, where a uniform value is defined for the whole simulation, or implicit, where the model determines the most stable and efficient time step during run time. The “*Summary*” sub panel shows the status of the key input components of the model, including model geometry data, input and output options, painting mode and accuracy statistics.

#### 4.5 Model application 1: extensive analysis at Site 1 (Naburn Weir)

Sensitivity analysis was carried out at Site 2 to investigate the effects of the wetting threshold value (§4.3.1) (note that Site 1 or Site 3 could also have been used – the focus is on the wetting phase, which is modelled for all three sites). The effects of the drying threshold value are not tested as this is expected to have the same effect as that of the wetting threshold. The

tests were carried out for the most extreme case in relation to possible impacts: the 32 m DEM. Water depths lower than 0.05 m were thought to be too low to allow outflow. Four wetting threshold values were used: 0.05, 0.06 and 0.07. The predicted inundated areas over time for the first 150 hours are shown in Figure 4.7.

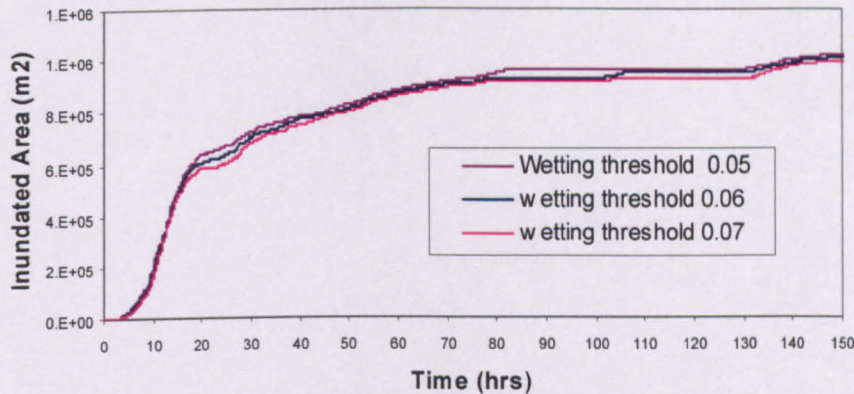


Figure 4. 7: Inundated areas over time for the first 100 hours with different wetting threshold values.

As expected, a higher wetting threshold has the effect of slowing down the wetting process, resulting in less inundated area. But the sensitivity to this value is low. The choice of 0.05 m seems to be reasonable and there is not much difference with small variations in this value.

#### 4.5.1 Results 1: 4 m simulations

The flood event was first simulated using the 4 m DEM at Site 1. Manning's  $n$  was set to be 0.06 in this simulation. Inflow data was described in Section 3.7.1. The time series of inundation extent for the first 38 hours are shown in Figure 4.8, overlain with the DEM (Figure 3.16a) of the simulation site.



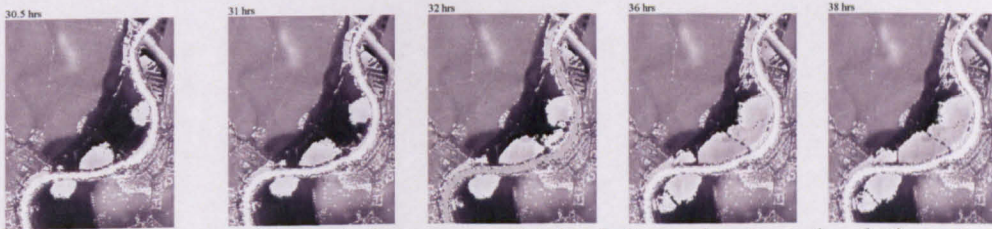


Figure 4.8: Time series of inundation extent obtained from the 4 m simulation: inundation extents overlain with LiDAR images (dark areas are low-lying floodplains).

Results suggest that the floodplain is inundated gradually within the first 30 hours and after that rapid inundation occurs. Two observations emerge from this simulation. First, the near-channel storage capacity of the floodplain controls the timing of the flood at the initial stage of inundation. The near-bank storage capacity is associated with the topographical complexity of the near bank regions. This will be mesh-dependent as the storage capacity of the near bank regions is strongly influenced by these topographically significant features near the bank and these features may be averaged out in a coarser mesh and result in a smoother land surface and thus, less storage capacity. It is expected that the storage capacity of the near bank regions in a coarser mesh will be less than that of a finer mesh and rapid inundation is more likely to occur before the case with a finer mesh (as noted by Horritt and Bates, 2001b). Once this capacity is exceeded, rapid inundation begins over the floodplain. Second, inundation is strongly controlled by the structural features on the floodplain, some of which can be identified as hedges and buildings from aerial images. Notably in the middle of the simulation site and at the vicinity of the residential areas (middle right and bottom left of the simulation site), these features apparently slow down the flood inundation process and at some point, in some cases, form complete barriers to the flow throughout the simulation. The results are compared to simulations using other mesh resolutions quantitatively in the next two sections (§4.5.2 and §4.5.3) for the quantitative assessment of model performance with respects to mesh resolution and roughness parameterization.

#### 4.5.2 Results 2: mesh resolution effects

The flood event was then simulated using different spatial resolutions: 8 m; 16 m; and 32 m. Floodplain topography, boundary condition data are set up the same as that used in the 4 m simulation. The time series of inundation extent for these simulations are shown in Figure 4.9 for the first 38 hours, together with those obtained from the 4 m simulation (Figure 4.8) for comparison. The model is mass conservative throughout the simulation length.



Figure 4.9: Time series of estimated inundation extent (for the first 38 hours) obtained from simulations with different resolutions.

Runtime simulation details such as time steps and simulation length are not reported here. Rather these are reported in Chapter 5 (§5.5.3) for comparison with the sub-grid treatment approach (§5.3). A time series of inundation area obtained using different mesh resolutions for the full flood event is shown in Figure 4.10.

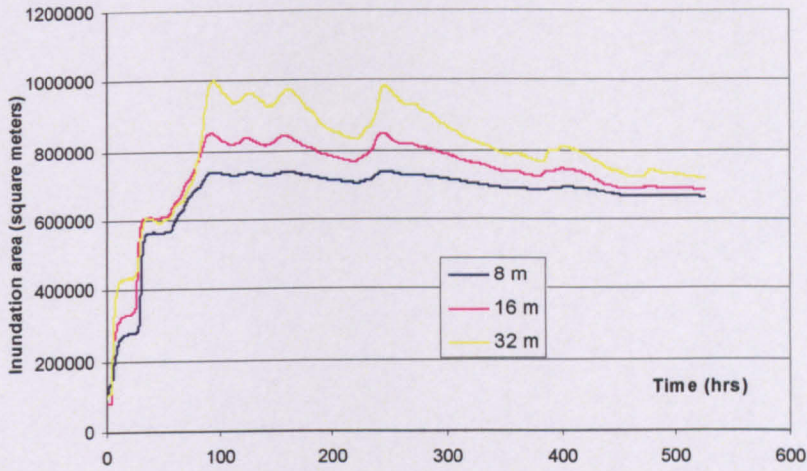
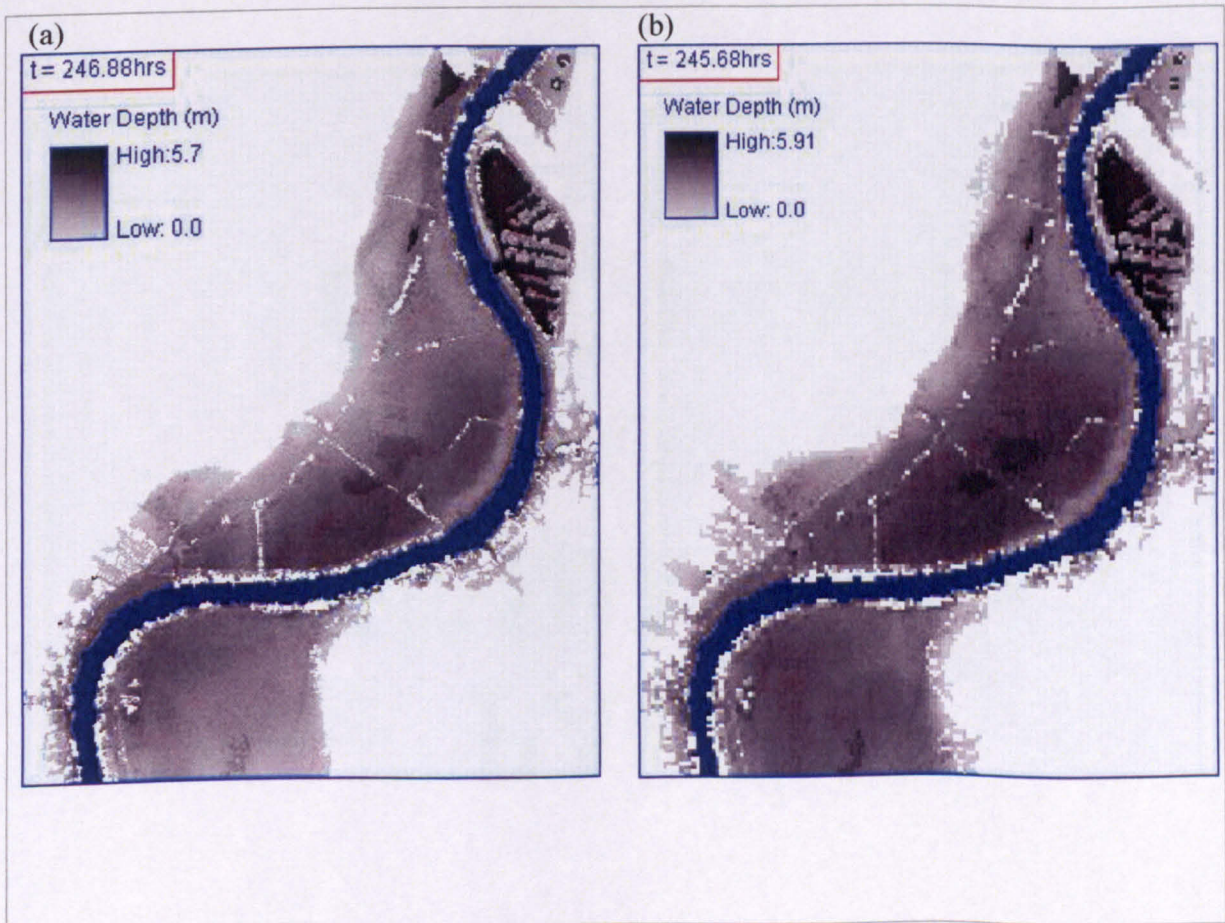


Figure 4.10: Time series of total inundated area for the 8 m, 16 m and 32 m simulations.

To examine the effect of mesh resolution upon the maximum inundation extent, Figure 4.11 shows the maximum inundation extent during the whole simulation for different mesh resolutions. The predicted inundation extents obtained using different model resolutions at the time when the validation data were acquired and at the last peak of the inflow hydrograph (around 249 hours into the main river channel inflow hydrograph) are shown in Figure 4.12 for comparison with the validation inundation extent shown in Figure 4.13, reproduced from Figure 3.6a.



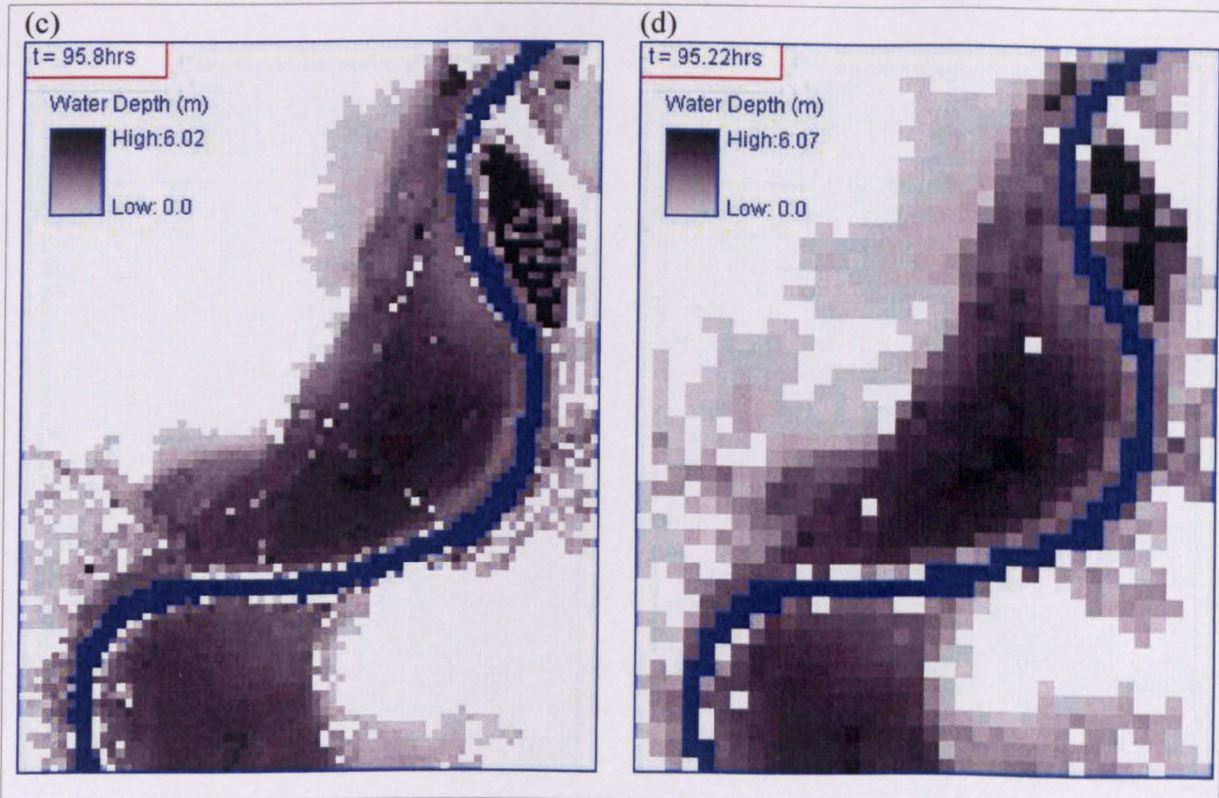


Figure 4.11: Maximum inundation extent obtained from the 4 m (4.11a), 8 m (4.11b), 16 m (4.11c) and 32 m (4.11d) mesh simulations.

Comparison of the time series inundation extents obtained using different model resolutions for the first 38 hours shows that model is quite sensitive to spatial resolution with respect to both the inundation extent and the flood wave travel time (Figure 4.9). Flood inundation is more rapid with a coarser resolution. For example, the model with a 32 m resolution has roughly the same inundation area at around 30.5 hours as that obtained with the 8 m resolution model at 38 hours. For the 16 m case, it took about 32 hours to get the same area. This is expected, considering the poorly represented inertial processes in a diffusion wave model. This is also confirmed when considering total inundated areas through time for the 8 m, 16 m and 32 m simulations (Figure 4.10). However, not only is the total inundated area greater as a function of time with coarser meshes but also the rate of change of inundated area is much more responsive to the event hydrograph (compare with Figure 4.9).

It appears that there is very strong sensitivity in terms of inundated area to mesh resolution with the diffusion wave treatment used here. Comparison of the maximum inundation extent predictions obtained from 4 m, 8 m, 16 m and 32 m simulations (Figure 4.11) suggests high model sensitivity to mesh resolution in relation to the predicted maximum inundation extent. Visual comparison of model predictions (Figure 4.12) with validation data (Figure 4.13) suggests that there is a rapid deterioration in model predictions with the 32 m simulations. The qualitative agreement with the 16 m simulation (compare Figures 4.11c and 4.12) is

better and appears to be best with the 4 m simulation (Figure 4.12b). The performance of the 8 m simulation lies between the 4 m and 16 m simulations.

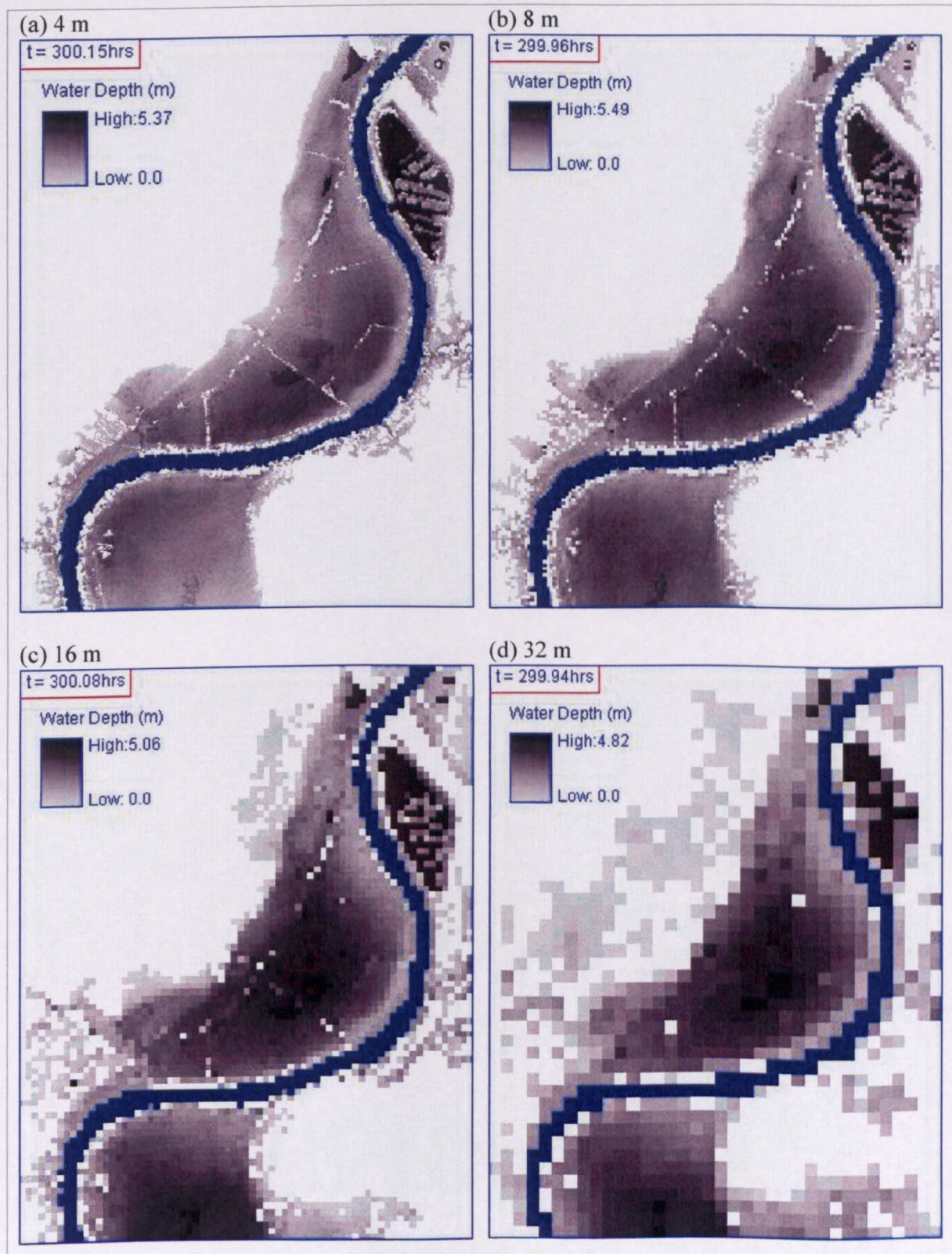


Figure 4.12: Predicted inundation extents obtained using different model resolutions at the time when the validation data was acquired (around 300 hrs into the flood event).

Accuracy assessment was carried out using the methods described in Section 3.5.3 and Table 4.1 shows the results. Table 4.1 shows that in terms of overall accuracy, there is no significant

difference between the 4 m, 8 m and 16 m simulations. This is not surprising in terms of overall accuracy, as this is biased strongly by the number of dry cells that are always dry in both the model and the validation data (i.e. the spatial extent of the area used for validation). On the basis of  $F$ , Kappa and conditional Kappa, which are more reliable statistics, the 4 m simulation performs better than the 8 m simulation and this confirms the qualitative inference from comparison of Figure 4.12 and Figure 4.13. Of most note in terms of both  $F$  and Kappa is the dramatic deterioration in model performance with the 32 m mesh. Of all of the statistics, the conditional Kappa values are most sensitive to mesh resolution, with very poor accuracies with the 32 m mesh, followed by the 16 m mesh, the 8 m mesh and the 4 m mesh. Both Figure 4.11 and Figure 4.12 show that some of the vegetation has not been removed from the LiDAR data. This is due to the uniform tree height assumption in image processing (§3.5.3). As the emergent vegetation has been classified as dry in validation data, errors should compensate.



Figure 4.13: Aerial imagery taken on the 9<sup>th</sup> November, 2000 at Site 1 (Naburn Weir) on the River Ouse (reproduced from Figure 3.6a).

Table 4.1: Accuracy statistics for model validation at a single point when the aerial imagery is used as the reference validation data (Site 1).

	4 m	8 m	16 m	32 m
Overall accuracy	90.7	88.8	83.7	71.4
$F$	82.0	78.3	70.1	51.0
Kappa	81.3	81.0	75.5	60.9
Conditional Kappa (Wet Cells)	89.5	80.3	64.8	40.3

The conditional Kappa values obtained using different cell sizes were compared with each other by calculating the  $Z$  statistics to check whether they are significantly different. At the 95% confidence level, with the sample size used here, the critical value of  $Z$  is approximately 1.96. All the pairwise comparisons give very high  $Z$  statistics, suggesting model predictions with different mesh resolutions are significantly different from each other at the 95% confidence level (Table 4.2). This confirms the early wetting results (Figure 4.9) and the full time series inundation results (Figure 4.10): mesh resolution has a major effect upon model predictions and this can be identified within the level of agreement between model predictions and point in time validation data.

Table 4.2: Comparisons of conditional Kappa (wet cells) using the  $Z$  statistic.

	4 m	8 m	16 m
8 m	83.1		
16 m	31.4	114.1	
32 m	278.6	368.7	243.4

### 4.5.3 Results 3: roughness parameterization

The roughness parameterization focuses on the first 50 hours of the simulation, when the floodplain is rapidly wetted, due to the computational constraints of running the model for the full 540 hours of the hydrograph. Prior to this, the model results for the 8 m, 16 m, and 32 m simulations were compared back to the 4 m simulation. This does not require us to assume that the 4 m data are the best. Indeed, the above section obtained the best results with the 4 m data. Focusing on the 4 m data as reference data allows us to assess the agreement between model predictions at different mesh resolutions as a function of time using the highest resolution simulated. Ideally, model predictions should be mesh independent. Therefore, which mesh is used as reference should not matter: all meshes should give the same conclusions.

The model was run using the same parameters as used in Section 4.5.1 and 4.5.2. Figure 4.14 shows the overall accuracy statistic (Figure 4.14a) and the conditional Kappa (wet cells) statistic (Figure 4.14b) as a function of time.

The agreement with the 4 m resolution, in terms of both overall accuracy (Figure 4.14a) and conditional Kappa (Figure 4.14b) decreases as mesh resolution is coarsened, demonstrating strong sensitivity to mesh resolution. The sensitivity is greatest in the first 35 hours of simulation, when the floodplain is rapidly wetting (Figure 4.9). As the rate of increase of inundated area falls from *c.* 35 hours (Figure 4.10), so the level of agreement with the 4 m resolution mesh improves. This reflects an element of lateral confinement in the floodplain,

which can be identified from Figure 4.13. The implication is that provided water levels are such that the inundated area remains laterally confined, the timing of inundation is relatively unimportant in relation to the maximum inundation extent reached. However, in a flood event of the size being simulated here, the water level required for flow to extend beyond the lateral confinement was exceeded. After *c.* 40 hours, Figure 4.14 shows that model agreement with respect to the 4 m data is degraded by an amount that increases as model resolution is coarsened. This results in much larger inundation extents as mesh resolution is coarsened.

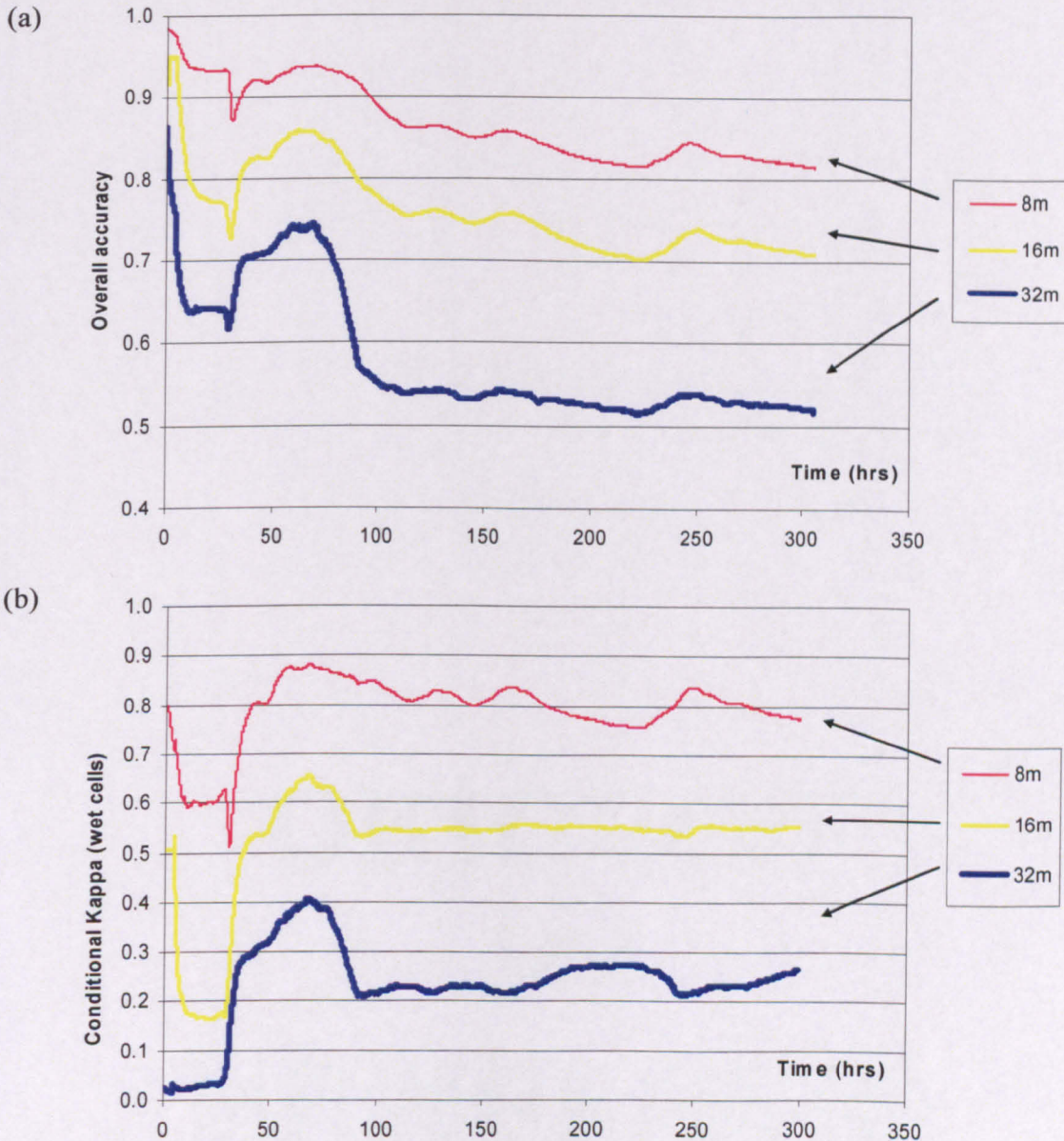
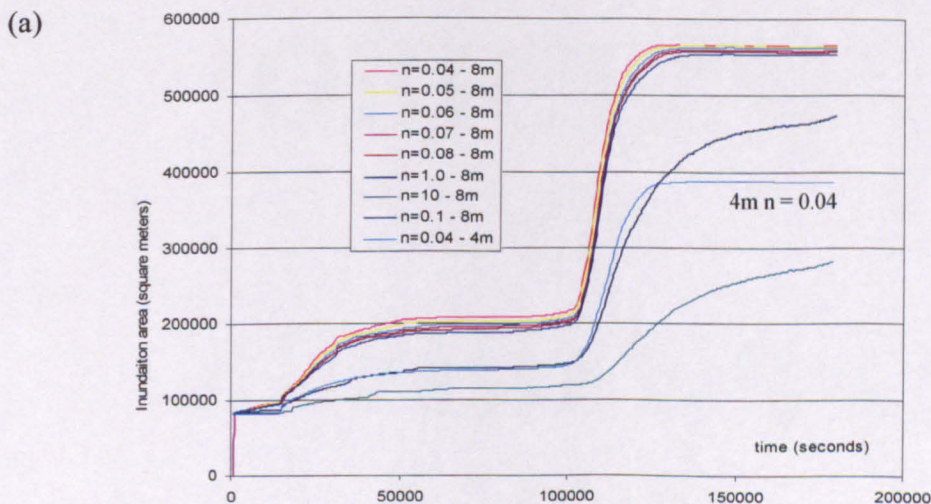


Figure 4.14: Comparison of time series of overall accuracy (4.14a) and conditional Kappa (wet cells only) (4.14b) using the 4 m inundation patterns as reference data.

Given the very strong sensitivity of model predictions to mesh resolution, the obvious question is whether or not this can be reconciled through adjustment of Manning's  $n$ . As noted above, only the first 50 hours of inundation was considered in order to be able to undertake a large number of simulations. Figure 4.15 compares the 4 m simulation, with the 8

m (Figure 4.15a), 16 m (Figure 4.15b) and 32 m (Figure 4.15c) simulations with different values of  $n$ : 0.04, 0.06, 0.08, 0.10, 1.0, and 10.0. The use of high values of Manning's  $n$  values is not theoretically based as some of the values clearly extend beyond those suggested in literature. Rather, it is based upon the understanding that the roughness parameter in a diffusion-based model represents not only bed roughness, but also energy losses associated with inertial terms, turbulence and secondary flows, which are not represented in the controlling equations. Thus, the roughness parameter, strictly speaking, represents hydraulic roughness rather than bed roughness alone. Others (e.g. Horritt and Bates, 2001b) have found that 2D raster-based models are relatively insensitive to roughness specification on the floodplain. Thus, here, very high values of roughness values are used to test model sensitivity to roughness parameterisation to test the limits of this approach. However, such high values of roughness parameter have not been reported previously in any other studies. Two explanations exist. First, this study is concerned with fairly complex floodplains whilst previous studies mainly deal with topographically-simple floodplains. One way of representing structural features on the floodplain is through the up-scaling of roughness values. Here, instead of assigning high values of roughness to structural elements alone, spatially uniform roughness is used, regardless of the relative magnitude of the value. Second, the aim of this set of sensitivity analysis is to look at the model performance with respect to the inundated areas through time during the initial wetting period of the flood event, thus, implicitly floodwave timing, which is known to be poorly predicted by raster-based models due to its relatively poor physical basis (Horritt and Bates, 2002). Thus, if high roughness parameters can produce reasonable flow patterns through time, this may not be a problem.



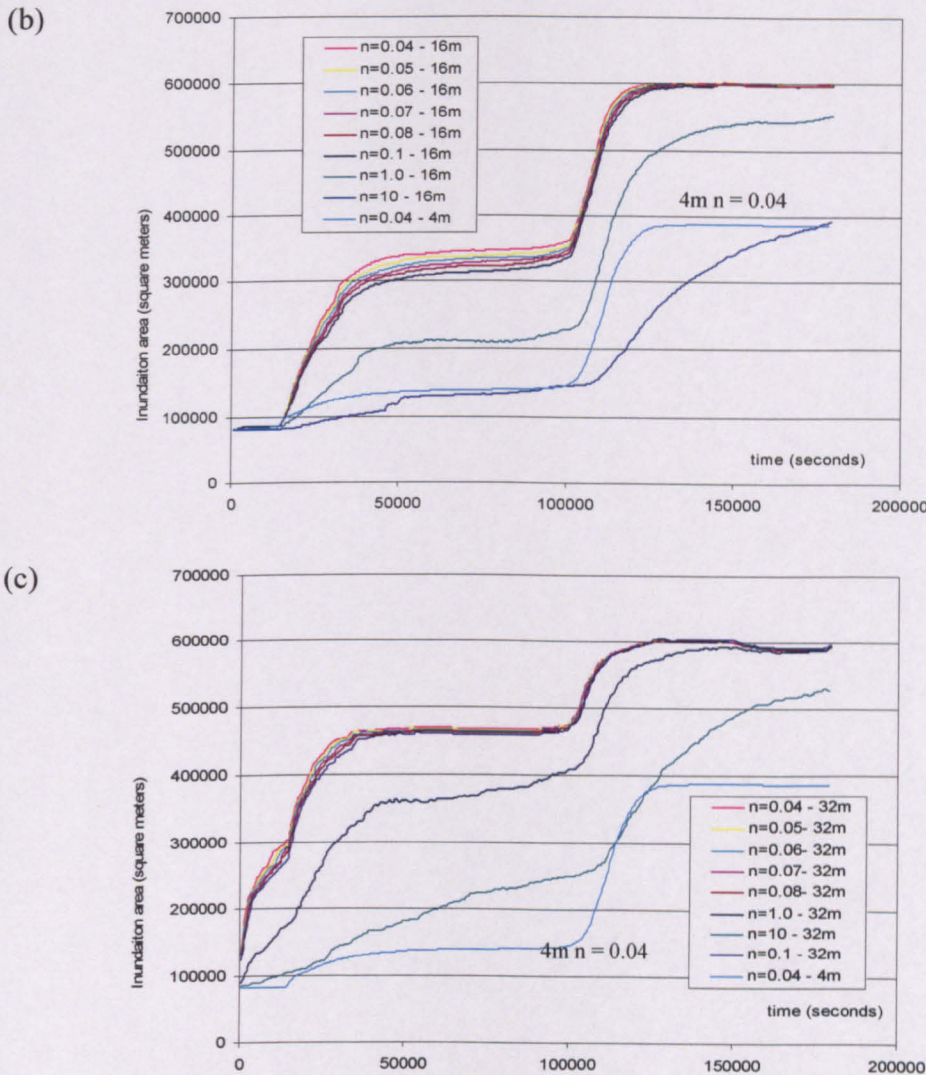


Figure 4.15: Predictions of inundated area through time for the first 50 hours of simulations with different mesh resolutions and values of Manning's  $n$ .

A number of observations arise. First, increasing  $n$  can be used to reduce the rate of increase of inundated area, but the size of the increase required is high, with  $n$  values of at least 1.0 required with all of the coarser mesh resolutions in order to reduce the inundated area to that of the 4.0 m simulation at *c.* 50 hours. Second, the magnitude of the increase in  $n$  required is positively correlated with mesh resolution: the 8 m mesh gives the 4.0 m mesh inundated area at *c.* 50 hours between  $n = 1.0$  and  $n = 10.0$ . It is clear that, for the 16 and 32 m meshes, higher values of  $n$  are required. Third, none of the coarsened mesh simulations reproduce the inundation area against time curve for the 4 m simulation. The 8 m simulation with  $n = 1.0$  gives the best results. The 16 m simulation with  $n = 10.0$  gives the correct inundation area at *c.* 50 hours, but it produces a highly inaccurate relationship between inundated area and time when compared with the 4 m simulation. These patterns are summarised in Figure 4.16, which shows the percentage over-estimation of inundated area extent with different mesh

resolutions and values of  $n$  at 50 hours into the simulation. It suggests that sensitivity to  $n$  is also reduced at coarser mesh resolutions.

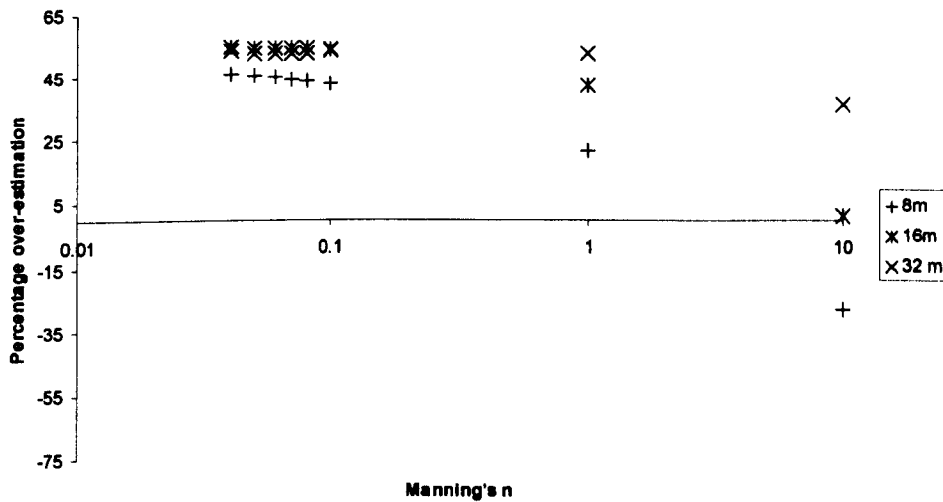


Figure 4.16: The relationship between  $n$  and the percentage over-estimation of inundated extent at 50 hours into the simulation. A negative over-estimation is equivalent to under-estimation.

Thus far, the results have explored sensitivity to Manning's  $n$  through a lumped assessment parameter, total inundation extent. Here consideration is extended to accuracy statistics. Following from Figure 4.16, simulations were run with higher values of  $n$ : 0.4, 0.6, 0.8, 1.0 and 10.0. Figure 4.17 shows the conditional Kappa for wet cells with these values of  $n$  with mesh resolutions of 8 m, 16 m and 32 m. For the 8 m simulation (Figure 4.17a), good levels of conditional Kappa are obtained with  $n = 10$ , throughout the first 50 hours. However, with the 16 m simulations (Figure 4.17b), even the high value  $n = 10$  simulation produces poor results and, aside from some improvement as the rate of inundation increase slows at *c.* 33 hours (Figure 4.9c), corresponding to the point where the flow is temporarily laterally confined, conditional Kappa declines through time. The 32 m simulation has very poor conditional Kappa values throughout the simulation. These results imply a limit to the extent to which  $n$  can be used as an effective calibration parameter to represent the effects of mesh coarsening, especially at coarser mesh resolutions.

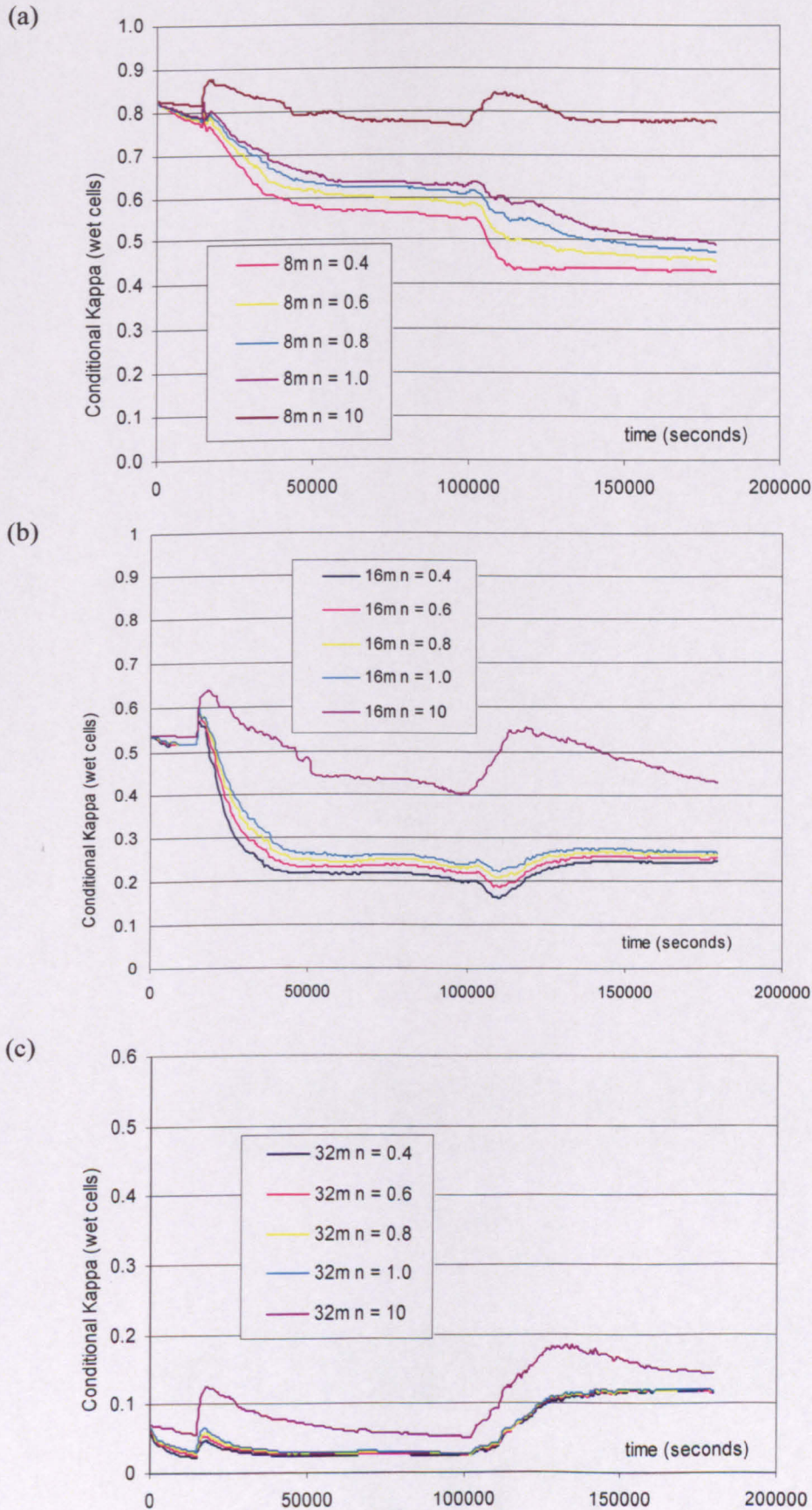


Figure 4.17: Conditional Kappa (wet cells) during the first 50 hours of simulation with 8 m (4.17a), 16 m (4.17b) and 32 m (4.17c) mesh resolutions and spatially uniform roughness values between 0.4 and 10.0.

#### 4.5.4 Discussion of Site 1 results

Both the validation data and the comparison with a higher resolution (4 m) mesh suggest that the model used here is highly sensitive to mesh resolution. This was evident in the inundation area plots (Figure 4.10), at the point when the validation data were acquired (Figure 4.12) and when inundated areas were compared through time to a 4 m simulation (Figure 4.15). Figure 4.11 confirms the extent to which this matters: were the model to be used to predict maximum flood inundation extent without calibration, the 4 m simulation (Figure 4.11a) would produce more confined predictions than the 8 m (Figure 4.11b), 16 m (Figure 4.11c) and 32 m (Figure 4.11d) simulations. In this case, the coarser mesh resolution transmitted the effects of water level fluctuations in the channel (Figure 3.19) too rapidly across the floodplain (see Figure 4.10). Accompanied by the rapid propagation of wetted extent, there was also a rapid propagation of deeper water at the wetting front, and the result was extension of the inundated area well beyond the laterally confined floodplain. In this case, aerial observations of wrack lines (Lane *et al.*, 2003) suggested that the peak inundation extent did extend beyond the zone of lateral confinement, but only marginally. This observation is important as it suggests a strong sensitivity of maximum predicted inundation extent to model resolution in relation to the size of the event being simulated and the local floodplain configuration. The interaction between event size and local floodplain configuration will be specific to individual river reaches and implies that, unless the timing of inundation extent through time is correct, local evaluation of whether or not the flood remains laterally confined will be required. Most previous applications of diffusion wave models seek to predict inundation extent associated with a given peak flow (e.g. Bates and De Roo, 2000). In such situations, the model is a basic improvement over one-dimensional models as rather than interpolating water levels laterally and intersecting them with the ground level, the diffusion wave model allows the explicit representation of topographic forcing associated with floodplain structure, albeit with a weak physical representation of the momentum transfer process. If the floodplain is laterally confined, and the concern is with inundation by a flood peak that is sufficient to fill the floodplain, the exact timing of the inundation process ought not to matter too much. However, in situations where the floodplain is not laterally confined, and given that the maximum inundation is strongly sensitive to mesh resolution, getting the timing of inundation right might be the only means of getting the peak inundation extent right. This is why calibration of timing using Manning's  $n$  might be viewed as important.

The high sensitivity to mesh resolution appears to be associated with three connected effects. First, the effect of re-sampling a dense mesh onto a coarse one will result in a smoother floodplain. This has implications for the flow, as a smoother floodplain will allow water to

inundate more easily. It has been found that, using finite-element methods, the two-stage filtering of raw data into a digital elevation model and then into a numerical mesh coarsens the data used in the model (Bates and Anderson, 1996) and this reduces the detail and accuracy of the resultant land surface (Marks and Bates, 2000). This also holds for the re-sampling process using different interpolation methods for data of the same resolution. The three commonly used re-sampling methods: nearest-neighbour interpolation; bilinear interpolation; and cubic convolution interpolation; will each have some degree of smoothing effect on the input data. Bilinear interpolation determines the value of a cell based upon the weighed distance average of the four nearest input cell centres. Cubic convolution interpolation tends to smooth the data more than the bilinear interpolation due to the smooth curve used and the large number of cells involved. The smoothing effects of nearest-neighbour interpolation are the least among these three methods. These methods are compared for the first 50 hours of simulation in Figure 4.18, using the conditional Kappa statistic for wet cells, with the 4 m data as reference data. The results suggest that whilst different interpolation methods do have some impact upon the conditional Kappa statistic, these impacts are much reduced as compared with mesh resolution effects and are restricted to the period of most rapid wetting. Using different interpolation methods doesn't seem to impact upon the double filtering problem.

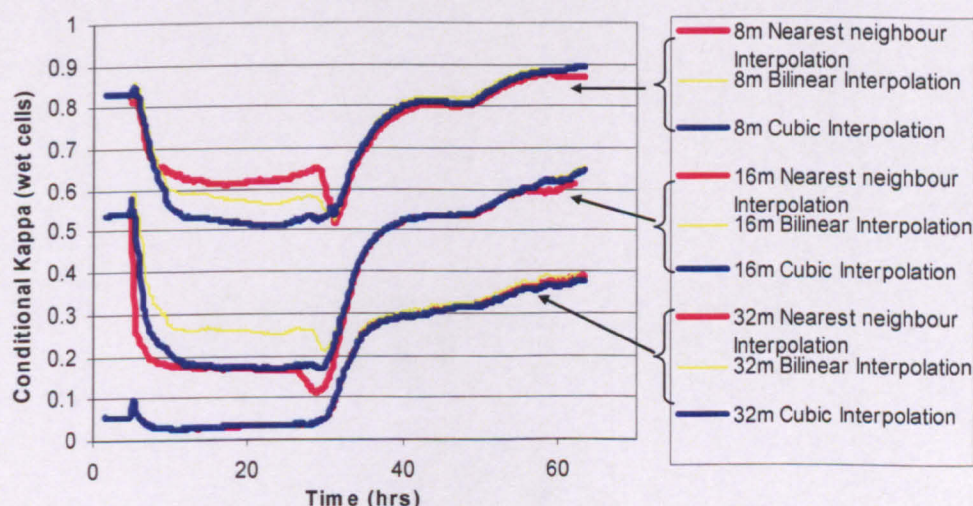


Figure 4.18: Comparison of time series of conditional Kappa values for wet cells for model predications with different interpolation methods at each time step, with the inundation extents from 4 m resolution simulation used as the reference verification data (first 60 hours).

Second, as the mesh is coarsened, the effects of cell blockage upon the timing and direction of flow will be reduced. Third, the representation of small-scale wetting processes will be simplified when the mesh is coarsened. The effect of the wetting treatment in the model is to slow down flow transfer. The velocity controls the timing of the wetting process for a grid cell (Equation 4.11) and the evaluation of the velocity will be resolution dependent. As the mesh is coarsened, the variance in velocity decreases and the timing of the wetting front

migration tends to have a greater possibility of error due to the simplified description of the timing of the flow routing. This would otherwise be much more complex in a finer mesh and it explains the high model sensitivity to mesh resolution in relation to flood wave travel time. Likewise, the difference between water surface elevations of two grid cells determines the direction of flow routing (Equation 4.7) and the variance in water surface elevations tends to decrease as the mesh is coarsened. The heterogeneity of water surface elevations in the cells will decrease and this may increase errors in the direction of flow. This is especially true for flow routing in urban areas where structural features on the floodplain can have considerable effect on flow direction and timing. It is expected that the higher the resolution of data, the more adequate representation of small-scale routing processes and thus the more accurate the predictions with respect to both flood wave travel time and inundation pattern. The use of a wetting parameter might to some extent reduce model sensitivity to mesh resolution, but not fundamentally as it primarily accounts for the timing of the floodwave, but not the direction. Thus, in this respect, there is a need to represent the small-scale sub-grid wetting processes more accurately in order to improve model performance. This will be addressed in Chapter 5 where a sub-grid scale wetting approach is developed and tested in Site 1 and Site 2.

Given the strong sensitivity to mesh resolution, it is necessary to consider the extent to which  $n$  can be used to counter this effect. In both 1D and 2D models,  $n$  explicitly controls the magnitude of the friction slope and hence is a major momentum sink. As such,  $n$  is strictly an effective roughness parameter, whose values should not only depend upon the system being modelled but also the mesh (e.g. cross-section spacing in a 1D model, node density in a 2D finite-element model) that is being used to discretize the model equations. Thus, the sensitivity to  $n$  in relation to mesh resolution (e.g. Figures 4.14 and 4.15) is expected, and may be used to calibrate the model to predict inundated extent through time as mesh resolution is increased. Very high values of  $n$  ( $> 1.0$ ) were required to have a significant effect on inundated area (Figures 4.14 and 4.15) and these clearly extend beyond the range of  $n$  values for which the Manning's relationship was originally formulated. However, if it is recognised that  $n$  is being used as an effective roughness parameter, and if  $n$  can be shown to result in acceptable recovery of the correct inundation-time relationship, then this may not be a problem. In this case, tests showed that for the 16 m and 32 m meshes, it was not possible to use uniform values of  $n$  to achieve such recovery. This leads us to question the extent to which  $n$  is a reliable calibration parameter, in this type of model, at least without some form of spatial distribution. It also demonstrates the danger in diffusion-based routing models of assuming that a field-estimated value of  $n$ , set independent of mesh considerations, will give the correct inundation behaviour. The simulations presented here make no attempt to distribute  $n$ , which may improve the inundation-time relationship.

In a more general sense, the simulations emphasise the danger of relying upon model assessment using single at-a-point in time data to judge model performance. If the 50 hour simulation had been the time when validation data were available, and under the assumption that the 4 m mesh resolution best approximated actual inundation at that time period, the best calibration would involve a 16 m resolution with  $n = 10.0$  (Figure 4.15) in terms of the inundation area predicted, even though, at the point when validation data were actually available, this calibration may not be as effective as other simulations. This is important as most validation data are at-a-point in time (e.g. obtained from a single satellite overpass, or a single airborne campaign). This finding is no different to the findings of other models in the hydrological sciences where choosing a particular value of a model parameter may result in some time periods providing reasonable predictions, but not all of them. If a model calibrated through optimisation of  $n$  on a single validation point in time does not produce the correct time variation in inundation area, then there is a high probability that the spatial pattern of inundation is not correct, even at maximum inundation extent: because the model is explicitly based upon mass conservation, incorrect inundation areas will be associated with incorrect water depths. With a structurally complex floodplain, this may have a very major effect upon where water goes. Both: (i) steady state treatments; and (ii) treatments that use a mesh resolution and  $n$  combination that do not give the correct inundation-time pattern; may not give the correct maximum inundation extent.

#### **4.6 Model application 2: simplified analysis at Site 2 (A64 Trunk Road) and Site 3 (City Centre of York)**

To test the repeatability of the model performance, the model was applied to two other sites on the River Ouse (Figure 3.2): (i) a reach near the A64 Trunk Road; and (ii) a reach cross the city centre of York. Both applications carried out are simplified as compared with the Site 1 application. The primary aim of the Site 2 application is to evaluate the effects of spatial resolution upon model performance as compared with Site 1 application. This is carried out using an 8 m, 16 m and 32 m DEM. The 4 m simulation was not carried out due to the computational demands of the simulation in this site. The Site 3 application aims to look at the performance of the model in a strictly urban location in a more general sense using a single 8 m mesh resolution. Both applications were validated using the at-a-point in time aerial imagery as reference data and the validation data have been presented in Section 3.5.3. The LiDAR-derived DEM was used to derive the floodplain topography using the same procedure outlined in Section 3.6 for sites 2 and 3. DEMs of different resolution (8 m to 32 m) were created for Site 2. An 8 m mesh was created for Site 3. Due to computational constrains, higher resolution topographical data are not used in Site 3. These computational constrains

arise from the very long duration of the flood. Boundary condition data at the river-floodplain boundary have been described in Section 3.7. Compared with the extensive analysis carried out at Site 1, roughness parameterization was not investigated in these two applications and the value of the roughness coefficient was fixed at 0.06.

#### 4.6.1 Results 1: Site 2

Figure 4.19, Figure 4.20 and Figure 4.21 show the time series of inundation extent from the 8 m, 16 m and 32 m simulations respectively for Site 2. These show the changes in the estimated inundation patterns during the first 100 hours of the flood event, of which wetting is predicted to be the dominant process.

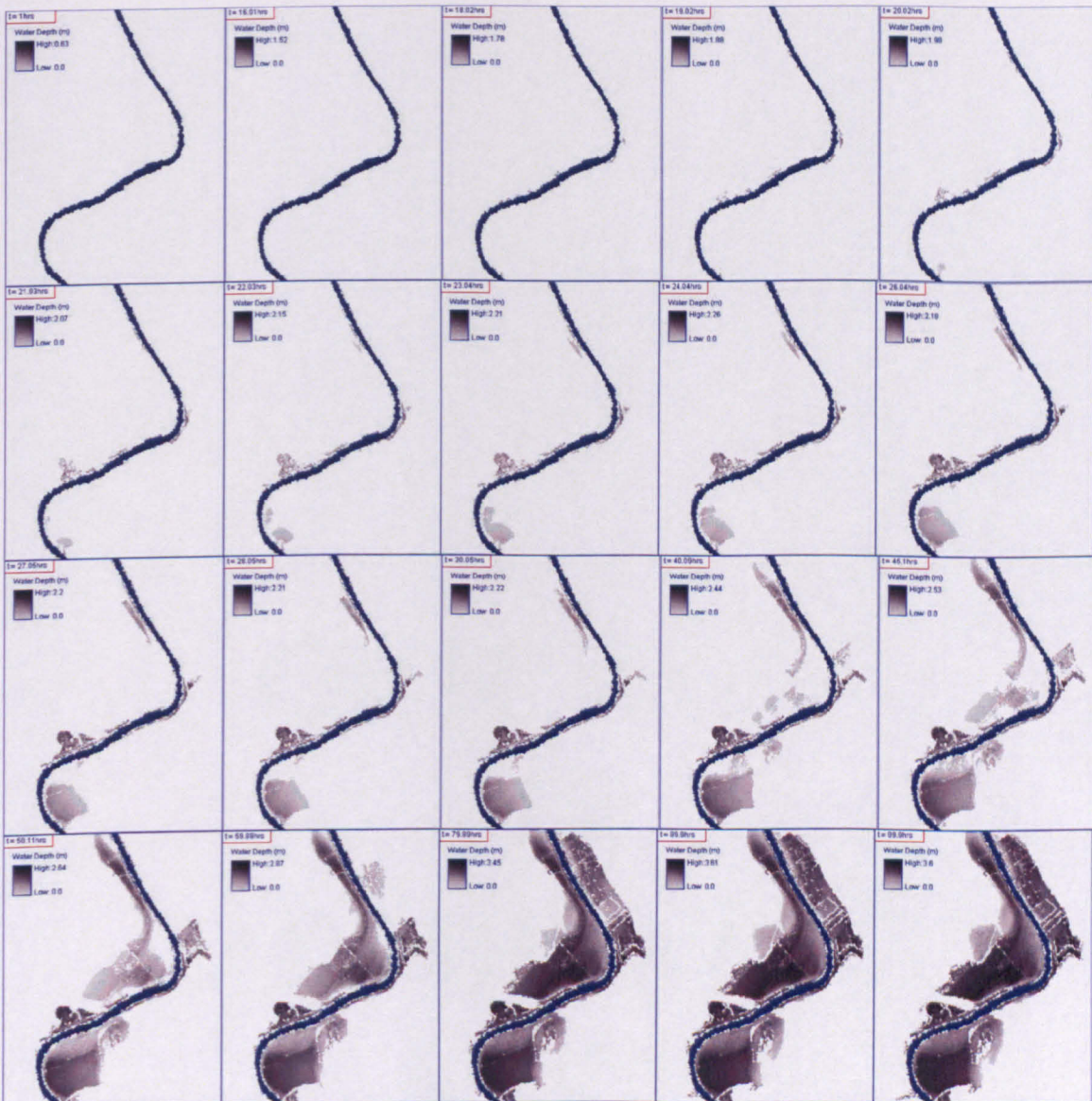


Figure 4.19: Time series of estimated inundation extent (for the first 100 hours) obtained using an 8 m DEM.

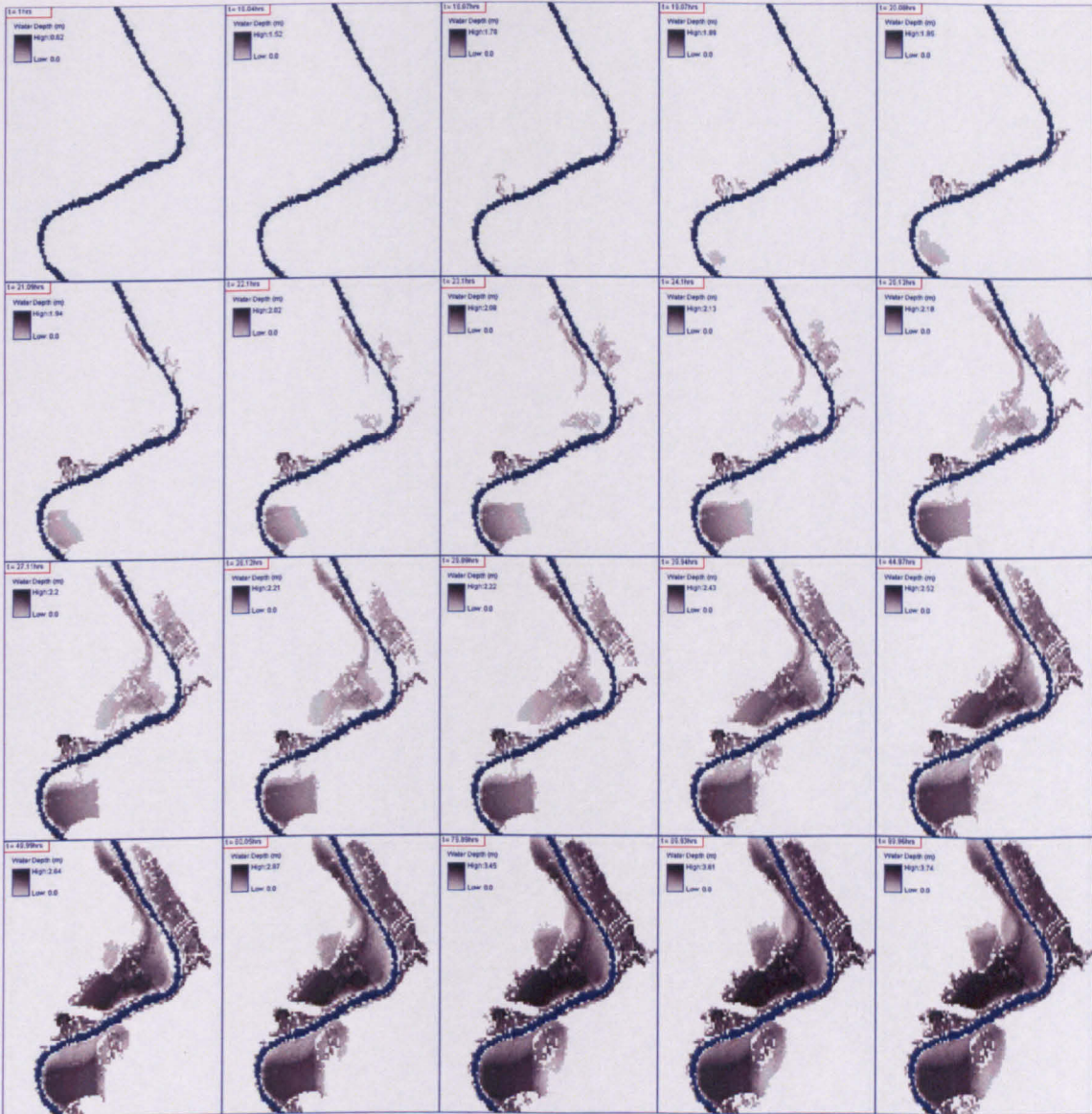


Figure 4.20: Time series of estimated inundation extent (for the first 100 hours) obtained using a 16 m DEM.

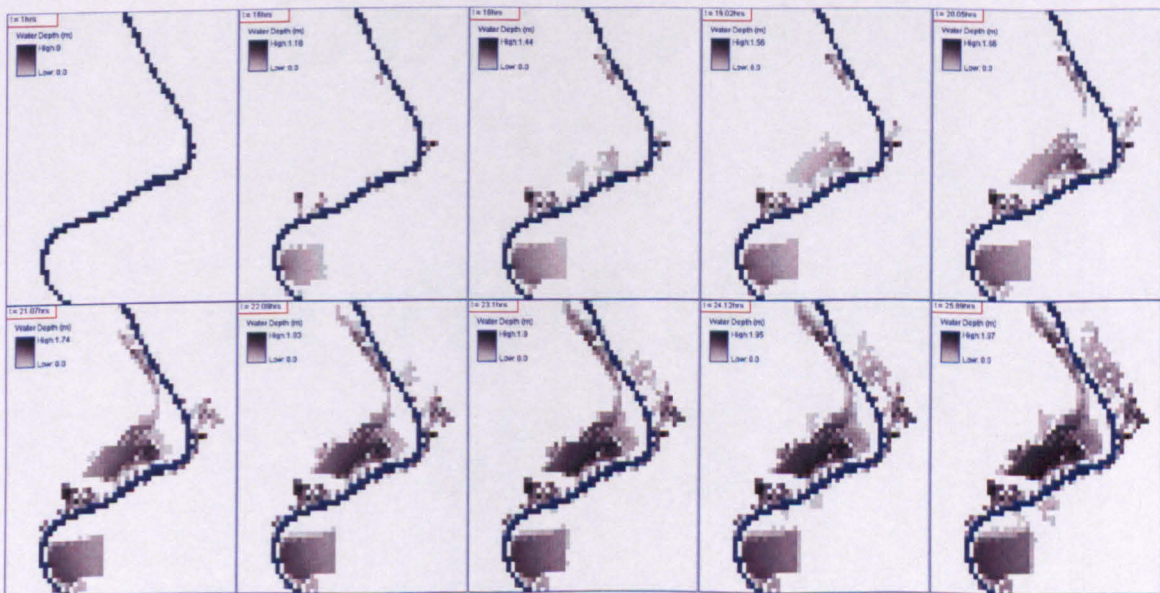
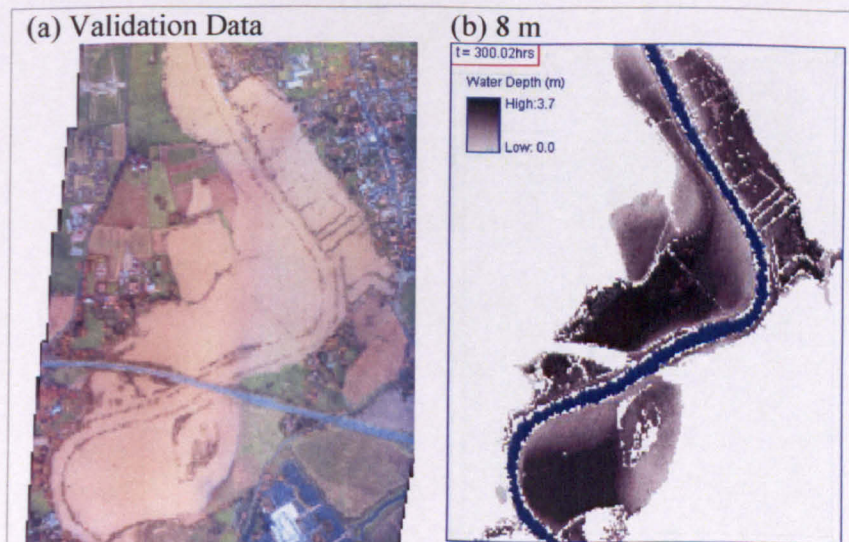




Figure 4.21: Time series of estimated inundation extent (for the first 100 hours) obtained using a 32 m DEM.

Comparison of the results with those obtained for Site 1 (§4.5) confirms the Site 1 findings. The model shows quite strong sensitivity to mesh resolution during the initial wetting process and the general trend is that inundation is faster in a coarser DEM. Indeed, the 8 m simulation gives a much slower flood inundation rate than the 32 m simulation, and the 16 m simulation gives a moderate rate of flood inundation compared with the 32 m simulations. However, the level of sensitivity to mesh resolution shown at Site 2 application is not as pronounced as that shown in the Site 1 application. The main reasons for the observed sensitivity in the Site 2 application have been discussed in Section 4.5.4 with reference to the Site 1 application, but the reduced sensitivity is discussed below. The estimated inundation extents obtained from different mesh simulations at the validation point are shown in Figures 4.21b-4.21d, compared with the validation data (Figure 4.22a). Figure 4.22 suggests that all simulations appear to perform reasonably well. This was assessed quantitatively, using the approach described in Section 3.5.2 (Table 4.3).



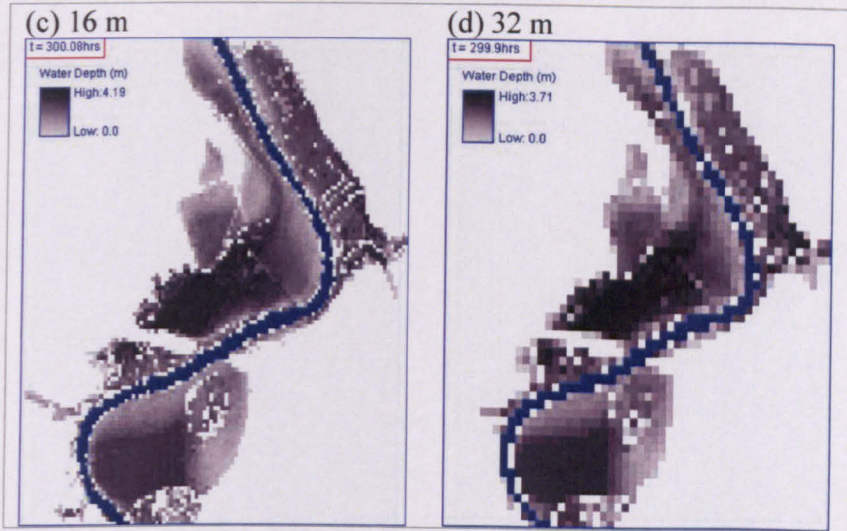


Figure 4.22: Predicted inundation extents obtained using different model resolutions at the time when the validation data was acquired (around 300 hrs into the flood event): 4.22a, validation data; 4.22b; 8 m; 4.22c; 16 m; and 4.22d; 32 m.

Table 4.3: Accuracy statistics for model validation at a single point when the aerial imagery is used as the reference data (Site 2).

	8 m	16 m	32 m
Overall accuracy	0.93	0.91	0.88
$F$	0.85	0.83	0.80
Kappa	0.85	0.82	0.78
Conditional Kappa (Wet Cells)	0.91	0.85	0.78

The accuracy statistics (Table 4.3) confirm the visual assessments of Figure 4.22, particularly with respect to the  $F$  statistic and overall accuracy: there is less sensitivity to mesh resolution in terms of quantitative agreements. In line with the results from the Site 1 application, finer resolution gives higher accuracy statistics in all categories. However, the difference between the accuracy statistics obtained from different mesh simulations is not as pronounced as that shown in the Site 1 application. For example, in terms of the overall accuracy,  $F$  statistic and Kappa, the difference between the adjacent mesh simulations is within  $\pm 2$ -4%. Conditional Kappa, which was shown to be the most sensitive accuracy statistic in the Site 1 application, shows a bigger difference. However, compared with the results for Site 1, the difference is still minor. When the absolute values of the accuracy statistics are compared with those for Site 1, for all statistics, the model performs better than the application to Site 1. Of particular interest are the accuracy statistics associated with the 32 m simulation. At Site 1, it was found that the performance of the 32 m simulation deteriorates significantly compared with the finer resolution simulations. However, this is not found in the simulations carried out for Site 2. The accuracy statistics associated with the 32 m simulations are only slightly degraded as compared with the 16 m simulation and are much better than those obtained from the Site 1 application in all categories. The observed model sensitivity to mesh resolution during the first 100 hours of the flood event was further investigated by looking at the full time scale

inundation area plot. The estimated inundation areas through time obtained from simulations with different mesh resolutions are illustrated in Figure 4.23.

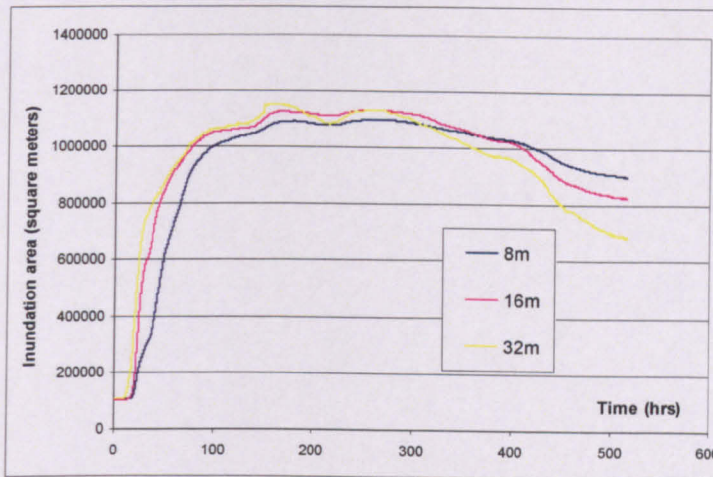


Figure 4.23: Estimated inundation areas through time obtained from simulations with different mesh resolutions.

The percentage overestimation in inundation areas predicted by the 32 m simulation through time as compared with the 16 m simulation is shown in Figure 4.24 for both Site 1 (Figure 4.24a) and Site 2 (Figure 4.24b) applications.

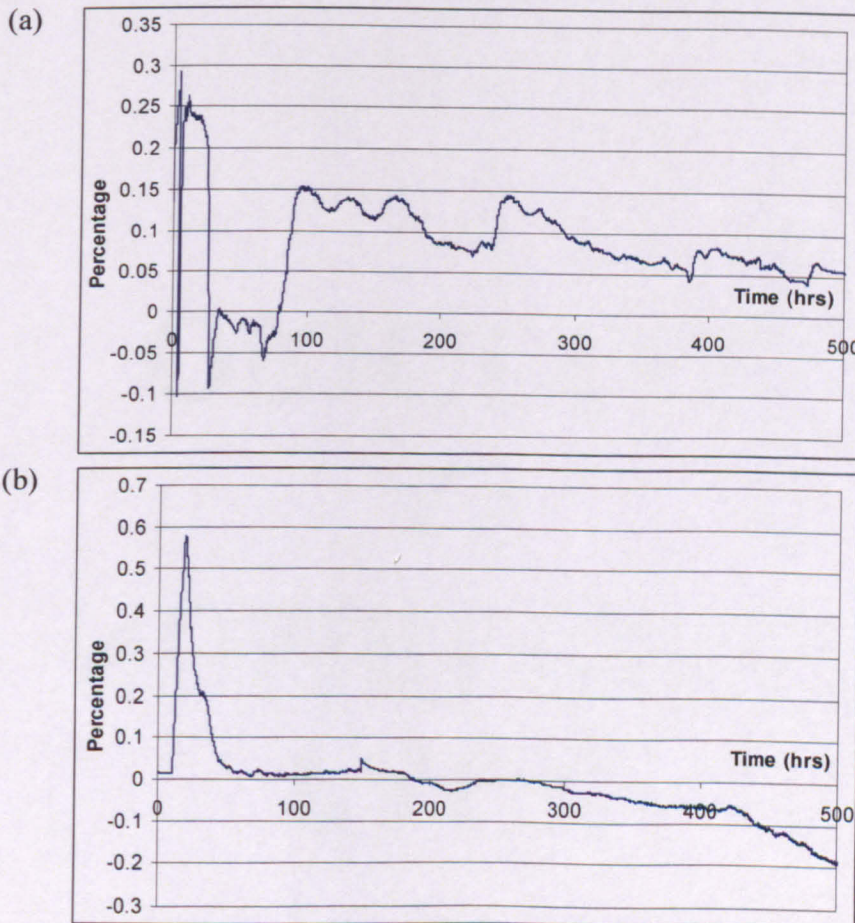


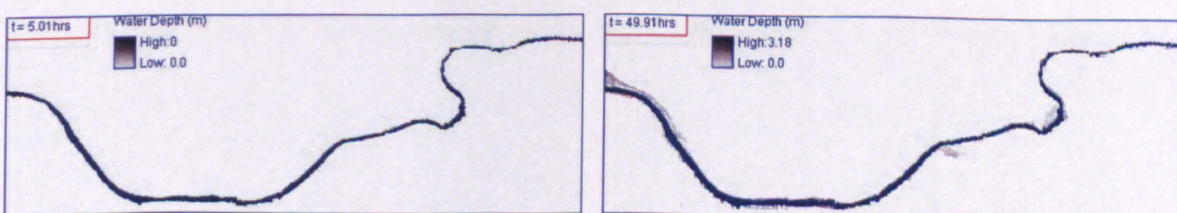
Figure 4.24: Overestimation of the inundation area using the 32 m simulation compared with the 16 m simulation: (a) Site 1 application; and (b) Site 2 application. (A negative value is equivalent to underestimation).

Quantisation noise exists in Figure 4.24. However, the output of the model is at a 15 minute interval, and so the quantisation noise is expected to be small. This, combined with the time series of inundation extents shown in Figure 4.19 to Figure 4.21, suggests that the strong sensitivity of predicted inundation area observed at Site 1 (Figure 4.10) is also captured in this site, but at a reduced level and only for the wetting phase (the first 100 hours). The sensitivity gradually decreases after around 100 hours. Indeed, at the validation point (300hrs into the hydrograph), the inundation area predicted by the 16 m simulation has become slightly larger than that obtained with the 32 m simulation. Moreover, the degree of sensitivity shown in this application is not as high as that shown in the Site 1 application, particularly after the initial wetting phase (around 38 hours at Site 1 and 100 hours at Site 2).

#### 4.6.2 Results 2: Site 3

A third application was conducted in the city centre of York. The aim of this application is to look at the general performance of the model in a strictly urban site. Mesh resolution effects and roughness parameterization were not investigated in this application. A single 8 m simulation was carried out. The model performance was evaluated using the same approach as for sites 1 and 2. Topographic data processing including tree removal, correction of overlapping areas of river channels with bridges, and correction of lake elevations was carried out using the approaches described in Section 3.6.2. The inflow hydrograph used in this application is shown in Figure 3.19. A uniform roughness value of 0.06 was used in this application.

Figure 4.25 shows the estimated time series of inundation extent during the first 185 hours of the flood event. This is the point at which the estimated maximum inundation extent was reached (around 185 hours). Figure 4.27 shows the validation imagery used for model validation. Visual comparison suggests that the model performs reasonably well in most parts of the floodplain. Most of the small-scale wetting patterns have been predicted correctly. However, notably, the model underestimates the observed wet areas in the upstream of this reach (red circle in Figure 4.27) which, in the validation imagery, are indicated as wet. This is reflected in the accuracy statistics summarised in Table 4.4. The relatively poor accuracy statistics compared with those obtained from the applications to Site 1 and Site 2 are largely due to the areas wrongly predicted as dry at the upstream end of the reach.



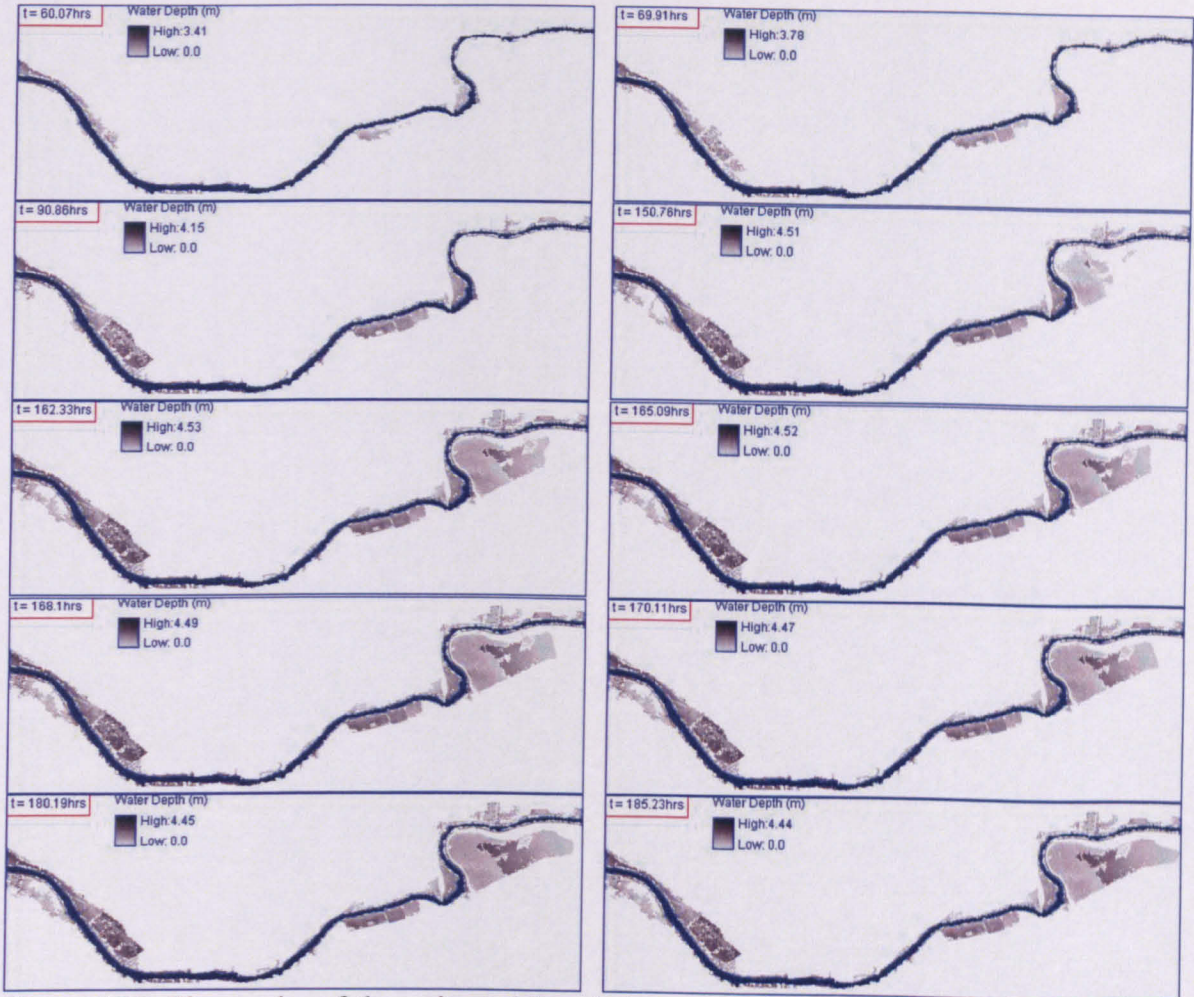


Figure 4.25: Time series of the estimated inundation extent during the first 185 hours of the flood event, obtained from an 8 m simulation in the city centre of York.

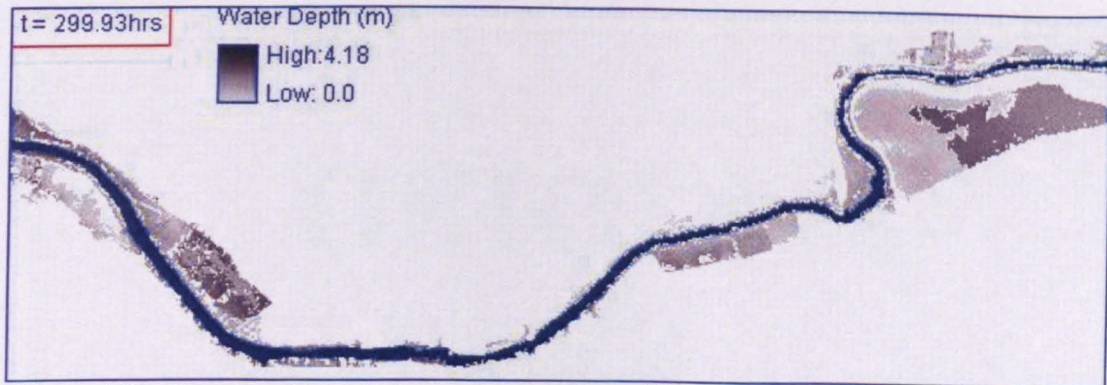


Figure 4.26: Estimated inundation extent at the validation point (around 300 hours into the flood event).

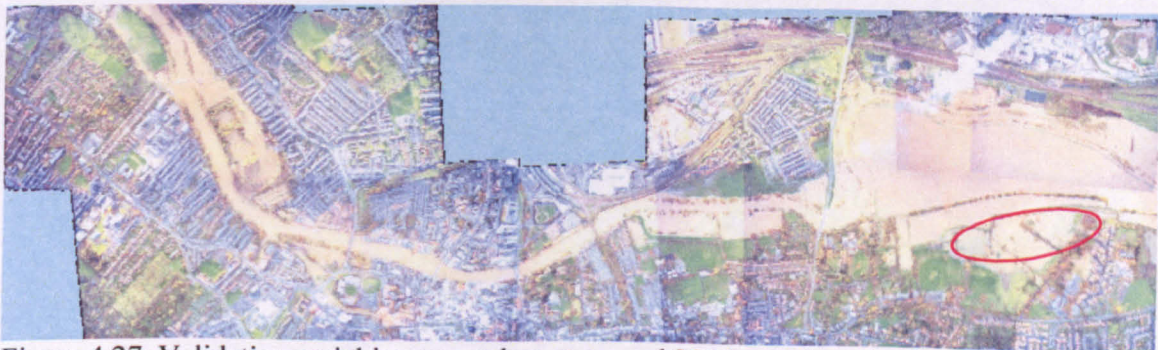


Figure 4.27: Validation aerial imagery taken at around 300 hours into the flood event.

Table 4.4: Accuracy statistics for model validation at a single point when the aerial imagery is used as the reference data (Site 3)

	8 m
<i>F</i>	0.65
Overall accuracy	0.86
Kappa	0.66
Conditional Kappa (Wet Cells)	0.92

The imagery suggests that, at the river side of the wrongly predicted area, this area is separated from the rest of the floodplain by a footpath. Image analysis shows that, without overtopping of the footpath, water at the river side of this area will not be able to enter this field. It suggests that there is no water entering this field from the river side of the floodplain throughout the simulation. Thus, the underestimation in model prediction is probably not due to the timing of the flood, at least within the simulation length (around 500 hours). The imagery shows that the footpath was completely dry at the validation point. Whether or not the footpath was overtopped during the 2000 flood event is unknown without field knowledge. One or a combination of the following hypotheses might contribute: (i) water overtopped the footpath and entered this field during the 2000 flood; (ii) water accumulated from the other side of the floodplain (residential sites) due to local runoff; (iii) water enters through underground pipes from the river side of the footpath; or (iv) this field is a lake and is wet all the time. It is difficult to tell whether (ii), (iii) and (iv) are true without field knowledge. Thus, here the investigation is centred on (i). If (i) is true, it suggests the model seriously underestimated the water levels at this point. There can be a number of reasons attributed to this. Two possible causes are considered here. First, as the inflow hydrograph used in the river channel is the same as that used at Site 2 which is around 2 km downstream of the downstream boundary of this site, the water depth might be too low for this site (§3.7.1). Stage records are available at the Skelton Gauging Station (4 km upstream of Site 3) (Figure 4.12). This is compared with the stage hydrograph used at Site 3 and shown in Figure 4.28. This shows quite big difference between the stages at these two locations during the 2000 flood. It was reported that a peak stage of 10.7 m was observed in the city centre of York during the 2000 flood (Environment Agency, 2004). However, the peak stage in the stage hydrograph used at Site 3 is only 9.5 m. This suggests the inflow stage hydrograph used for Site 3 might be too low to represent the stage during the flood event. As a result, there might not be enough water routed from the river channel to the floodplain. This is most likely to be the reason, or at least to be one of the reasons if there is more. To test whether using stage data at the Skelton Gauging Station (Figure 3.11) can give better predictions, another simulation was carried out where the stage hydrograph (Figure 4.28) at the Skelton Gauging Station was used to calculate inflow from the river. The inundation extent predicted at the validation point is shown in Figure 4.29. As expected and in qualitative terms, using stage

data at the Skelton Gauging Station severely overestimates the inundation extent for most of the site though it performs better for the upstream end of the site.

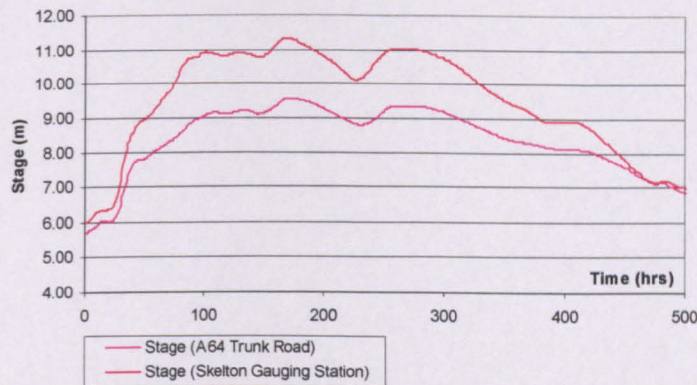


Figure 4.28: Comparison of the stages at A64 Trunk Road and Skelton Gauging Station (stage at A64 Trunk Road is used at Site 3).

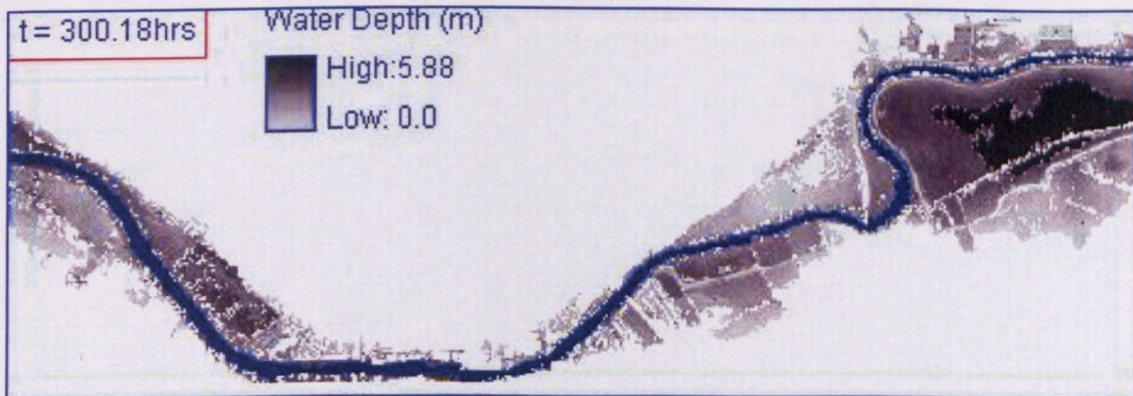


Figure 4.29: Inundation extent predicted using the stage hydrograph (Figure 4.28) at Skelton Gauging Station as inflow data at the validation point (300 hrs into the flood event).

Second, the model only takes into account the channel inflow within the domain and routes the flow accordingly on the floodplain. However, at the upstream of the river, water may enter from the upstream boundary as well. This will increase the water depth of the flow on the river side of the footpath to a point that may allow the flow to overtop the footpath and enter this field. However, as no upstream inflow data is available, this can not be confirmed at this stage. This issue is explored in Chapter 6 through the application using the tightly-coupled model over a longer reach covering Site 3 where, the tightly-coupled approach breaks down for long reaches.

#### 4.6.3 Discussion of Site 2 and 3 applications

The results for Site 2 suggest a better overall performance of the model as compared with the Site 1 application, in particular for the 32 m simulation. There was decreased sensitivity to mesh resolution after the initial wetting process in terms of inundation area. This is thought to be caused by the complex relationship between local floodplain configuration, size of the flood and the validation data used for model assessment.

In a confined floodplain, the effects of mesh resolution upon flood inundation may need to be interpreted by looking at three consecutive stages of the flood inundation process: (i) before the flood reaches the lateral confinement boundary; (ii) after the lateral confinement boundary is reached and before the boundary is overtopped by the outflow; and (iii) after the flow passes the lateral confinement boundary. In both applications, strong sensitivity to mesh resolution was observed during the initial wetting process (around the first 38 hours for Site 1 and 100 hours for Site 2), but only before lateral confinement of the floodplain is reached (Figure 4.23 and Figure 4.24b). If the floodplain is not laterally confined, we would expect this sensitivity to continue during the whole simulation. However, in both applications, the floodplain is confined laterally, though the size of the confinement zone and the level of confinement are different. Before the lateral confinement is overtopped and after the confinement boundary is reached, if no significant drying occurs, there won't be much change in inundation areas. Once this confinement region is filled and the confinement boundary is reached, there might be flows out of the confinement zone. If this happens, the strong sensitivity to mesh resolution in terms of the inundation areas might still exist, depending on the size of the out of confinement flow. This has been observed in the Site 1 application where the 8 m, 16 m and 32 m simulations all have predicted some levels of flows in the non-confinement regions (Figure 4.9b-d). However, for Site 2, the flow is restricted to the lateral confinement zone of the floodplain and for simulations with all mesh resolutions and significant outflow due to the breakthrough of the confinement zone is not observed. Thus, for this application, the strong sensitivity to mesh resolution in terms of the inundated area is not observed after the lateral confinement region is reached (Figure 4.23 and Figure 4.24b). This, also, to some extent, explains the significantly deteriorated performance of the 32 m simulation at Site 1 application and its relatively good performance in the Site 2 application.

Whether this lateral confinement can be reached depends on the relative size of the flood and the level of confinement in terms of both the size and the storage capacity of the confinement. The confinement zone of Site 1 is approximately  $8 * 10^6$  square meters and that of Site 2 is approximately  $1.1 * 10^7$  square meters. The flux at Site 1 (Figure 3.14) is large enough to fill the lateral confinement region and, eventually in some parts, extends beyond the confinement zone. This is not the case for Site 2. It should be noted that it will be the volume of water associated with the flux and not the peak water level that will determine whether or not the lateral confinement is exceeded.

Model applications at sites 1 and 2 show some difference in the sensitivity to flow peaks in the hydrograph in terms of the inundation areas predicted with different mesh resolutions, particularly after the initial wetting phase. The inflow hydrograph at Site 1 application is

associated with several marked flow peaks and lows while the inflow hydrograph used in the Site 2 application is relatively smooth. For both applications, the inflow hydrograph can be plotted against the time series of inundated area obtained from different mesh resolutions (Figure 4.30).

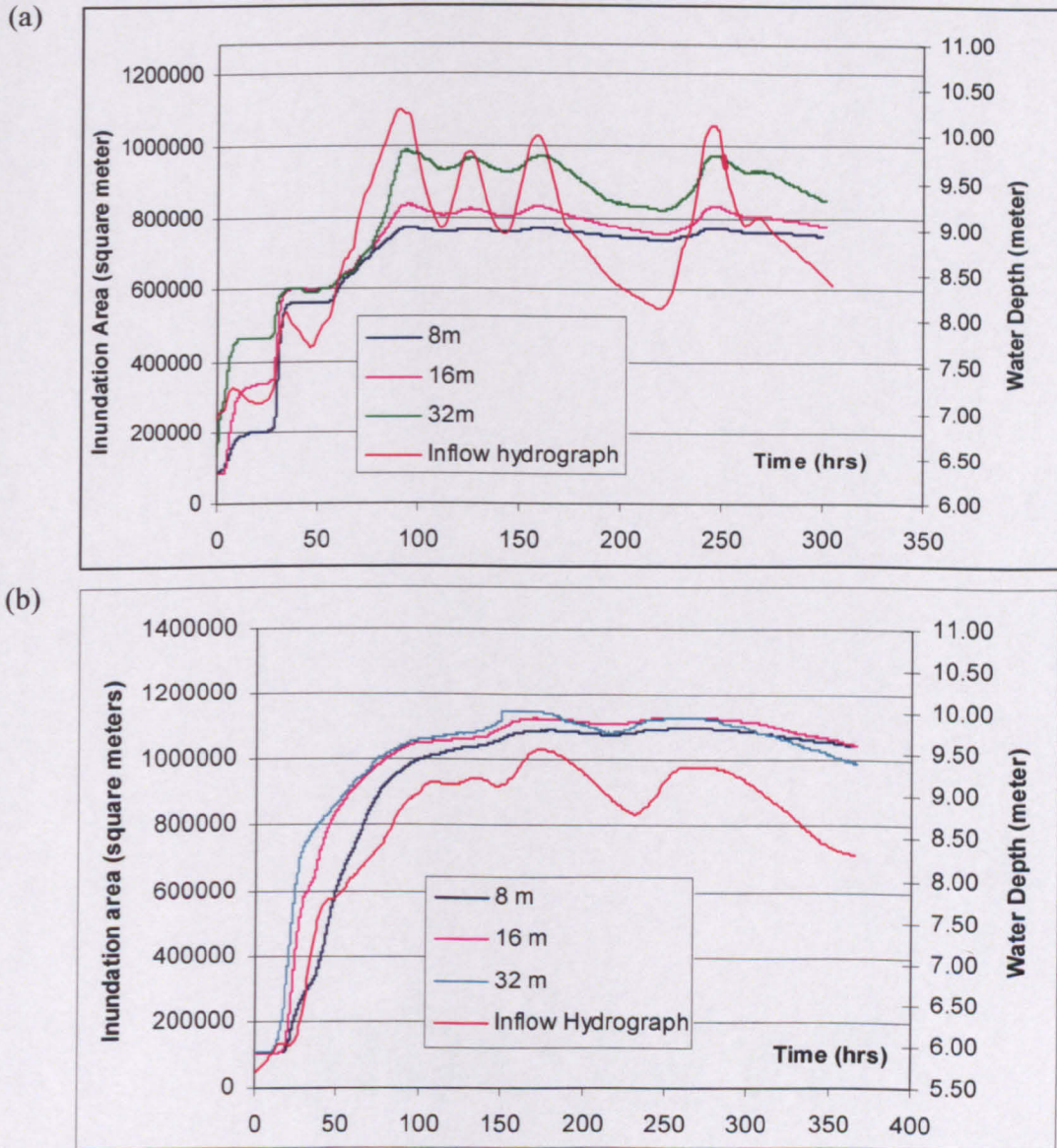


Figure 4.30: Inflow hydrograph plotted against predicted time series of inundated areas obtained from different mesh resolutions: (a) application at Site 1; and (b) application at Site 2.

Both applications show some sensitivity to flow peaks in terms of the predicted inundated areas. Of particular interest is the strong model sensitivity to changes in inflow hydrographs with the 32 m simulations, as compared with the finer mesh resolutions. The time series of inundated area obtained from the 32 m simulation in the Site 1 application shows a similar pattern to that found in the inflow hydrograph. Every flow peak is immediately followed by an increase in the inundation area (Figure 4.30a) and, similarly, every fall in the inflow water depth is followed by a notable decrease in inundation area. However, this sensitivity gradually

decreases with the finer mesh resolutions. This is not that obvious for the Site 2 application. The main reason for this has been discussed in Section 4.5.2: a coarser mesh tends to transfer water depth fluctuations in the river too quickly across the floodplain, which may result in a deeper water depth at the wetting front line, leading flow to places which would be otherwise too high for the flow to reach in a finer mesh.

Application to the city centre suggests that the model performs relatively poorly as compared with the Site 1 and 2 applications. This is most likely due to input stage data at the river-floodplain boundary. The model used the same stage hydrograph as that used at Site 2. This is expected to have underestimated the stage of the river reach at Site 3 which is around 2 km upstream of the A64 Trunk Road. Furthermore, inflow from upstream is not considered in the simulation and outflow from this boundary is allowed. It is expected that if the upstream inflow from the outside of the domain boundary could be taken into account, the model might be able to perform better in this part of the floodplain, thus improving the overall accuracy statistics. The fact that the model allows outflow in all 4 domain boundaries may also contribute to the underestimation of water depth and inundation extents at the upstream of the boundary. Thus, the model was modified to prevent outflow from the upstream of the river and another simulation was carried out. However, this simulation failed to improve model performance (Table 4.5) in terms of the predicted inundation extent. It is concluded that the use of the downstream stage hydrograph might be the dominant factor that caused the underestimation of flood extents at the upstream of the river. The possibility of inflow from upstream might also contribute. However, without field knowledge, this can not be confirmed as other processes such as local runoff and underground pipes, may also contribute.

## **4.7 Conclusion**

This chapter presented the development of a two-dimensional raster-based diffusion wave flood inundation model and demonstrated the effects of model spatial resolution and roughness parameterization upon the estimated inundation extent in a 2D diffusion wave model. The model was applied to three separate sites on a reach of the River Ouse in Yorkshire, U.K, to simulate a major flood event in the year 2000. Model response shows that the model is quite sensitive to spatial resolution in terms of both flood wave travel time and inundation extent. This is thought to be caused by three interrelated effects: (i) the smoothing effect of mesh coarsening in relation to topographical and topological effects; (ii) the poorer representation of small-scale flow routing processes and mass blockage effects associated with the reduced topological complexity resultant from (i); and (iii) the effect of (ii) upon

water depth, velocity, which in turn determine those parts of the floodplain that the flow can actually reach and when.

The local topographical complexity, linked to the presence of small-scale structural features on the floodplain in urban areas, makes this even more complex for urban flood modelling, as many of these features have topological properties that may have a major effect upon both the timing and direction of the flow routing. Two points emerge. First, the details of structural features may be reduced as the mesh is coarsened, resulting in a poorer representation of these features in the model. Second, current methods of representing small-scale flow routing processes associated with structural features in flood models have their limitations. Traditional methods of representing structural features usually involve up-scaling of the roughness parameter that, in previous research, has been used as a key calibration parameter to compensate for the poorly represented momentum transfer process found in raster-based modelling. This may reduce the flux through these features, but this will not necessarily recognize topological aspects of the structure. In this application, the wetting treatment approach that is used has the effect of reducing model dependence upon the roughness parameter. Roughness parameters can compensate in part for a coarser mesh resolution. However, the coarser the resolution, the lower the ability to control the inundation process, as these parameters only partly control the speed and not the direction of wetting. Thus, coupling of high-resolution data, which can capture small scale variation in topography, to more sophisticated representation of the inundation process, will be required in order to obtain effective predictions of flood inundation extent for urban fluvial flood modelling. In Chapter Five, the sub grid-scale representation of flow routing in urban areas using a porosity-based treatment is presented and tested.

Comparison of the results obtained from the three applications shows the complex relationship between local floodplain configuration, the size of the flood being modelled, and the validation data used. Good accuracy statistics using single at-a-point in time validation data might be obtained even though the actual inundation process and even the peak inundation extent are poorly predicted. Thus, given the strong model sensitivity to mesh resolution in terms of inundation extent, accuracy statistics obtained from diffusion wave flood inundation models need to be analyzed with caution. This is particularly important for an unconfined floodplain and the initial wetting phase of a confined floodplain, as inundation extents in such situations are very sensitive to water depth and getting the timing of the inundation right might be the only way to get the peak inundation extent right. Thus, validation data in the form of inundation extent might not be the optimum validation option for high-resolution flood modelling. Distributed hydrometric data such as surface velocity

might be the data that can distinguish between different higher order model predictions (Bates and Anderson, 2001).

# Chapter 5

## Model Developments and Testing 2: development and testing of a sub grid-scale treatment for urban fluvial flooding

### 5.1 Introduction

Chapter 4 investigated the complex interaction between mesh resolution and roughness parameterization in relation to flow routing and highlighted the need to couple high-resolution topographic data to a more sophisticated small-scale flow routing representation for improved flood inundation prediction over topographically complex floodplains. Based upon these findings, this chapter develops and tests a sub grid-scale wetting and drying correction for use with 2D diffusion wave models of urban flood inundation.

The method recognises explicitly that treatments of sub grid-scale topography using roughness parameters will provide an inadequate representation of the effects of structural elements on the floodplain (e.g. buildings, walls) as such elements not only act as momentum sinks, but also have mass blockage effects. The latter may dominate, especially in structurally-complex urban areas. The approach developed herein uses high-resolution topographic data to develop explicit parameterization of sub grid-scale topographic variability to represent both: (i) the volume of a grid cell that can be occupied by the flow; and (ii) the effect of sub grid topography upon the timing and direction of fluxes (§5.3). This approach was tested at Site 1 (Naburn Weir) and Site 2 (A64 Trunk Road) on the River Ouse, with extensive analysis carried out at Site 1 (§5.4) and the repeatability of the model performance checked at Site 2 through a restricted assessments of roughness effects (§5.5). This approach is found to give significantly better prediction of fluvial flood inundation over topographically complex floodplains as compared with traditional calibration of sub grid-scale effects using Manning's  $n$ . In particular, it simultaneously reduces the need to use exceptionally high

values of  $n$  to represent the effects of using coarser meshes process representation whilst increasing the sensitivity of model predictions to variation in  $n$ .

## 5.2 Chapter aims and objectives

Fluvial flood modelling in urban areas requires explicit representation of small-scale topographic variation in order to capture the correct patterns of flux associated with structural elements (e.g. walls, buildings and railroads, etc). The last chapter demonstrated the potential effectiveness of combining high-resolution topographic data with a two-dimensional diffusion wave model in order to predict inundation over topographically complex floodplains. However, it also demonstrated the severe sensitivity of this type of model to mesh resolution and the poor performance of spatially uniform parameterization using an effective roughness parameter (Manning's  $n$ ). Even using a wetting parameter (following Bradbrook et al., 2004) to reduce the effects of artificial numerical diffusion across the floodplain, strong model sensitivity to mesh resolution was found. Much of this is related to the effects of changing mesh resolution upon topographic information content.

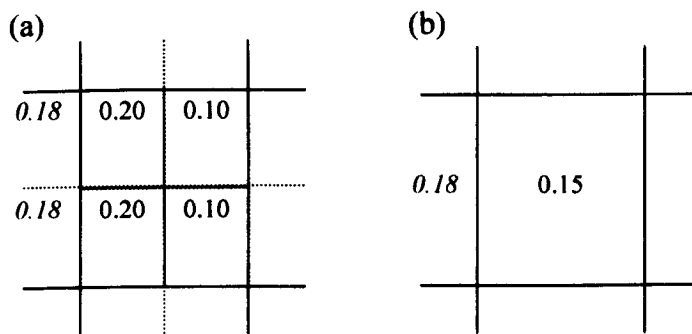


Figure 5.1: A schematic illustration of the effects of averaging a high-resolution topographic dataset (a) to a lower resolution (b) in relation to a wave of water moving from the left (elevation shown in italic). Topographic data in (a) (non-italic) is averaged to (b) (non-italic) on a coarsening ratio of 2:1. Solid lines are the coarsened mesh cell boundaries. Dotted lines are the sub grid cell boundaries.

Figure 5.1 shows a hypothetical 2\*2 set of grid cells (5.1a) and an associated coarsened set (5.1b). The average blockage of the cell in each of 5.1a and 5.1b is the same. However, the distribution of sub grid blockages is different. If we consider a cell with water in it, to the left of the coarsened cell (shown in italic) then, in 5.1a, there should be no inundation. However, averaging as per 5.1b will lead to inundation when it shouldn't do when water levels to the left of the cells are between 0.15 m and 0.20 m. Thus, with the coarser resolution, and even with the standard wetting treatment used by Bradbrook *et al.* (2004) and Chapter 4, water will diffuse more readily across the coarser mesh, leading to a more rapid diffusion of flood inundation extent. It may be argued that if the model is only being used to determine inundation extent, the timing is not important. However, Chapter 4 showed that, for an

unconfined floodplain or a large flood on a confined floodplain, the maximum inundation extent was significantly greater for coarser mesh resolutions. This arises because deeper water diffuses too quickly. This may be the case particularly in urban areas, where the structural complexity of the surface will be affected quite significantly by averaging from fine to coarser mesh resolutions. Roughness parameterization will not deal with this effect fully: even with very high values of the roughness parameter, diffusion will occur across a grid cell in the scenario shown in Figure 5.1b when it is meant not to.

Given the above, this chapter seeks to develop and test a method for sub grid-scale topographic representation with an explicit treatment of the effects of structural elements over the floodplain upon both blockage and flux. This is considered to be a major contribution to the improved representation of urban flooding noted as needed by Wheater (2002).

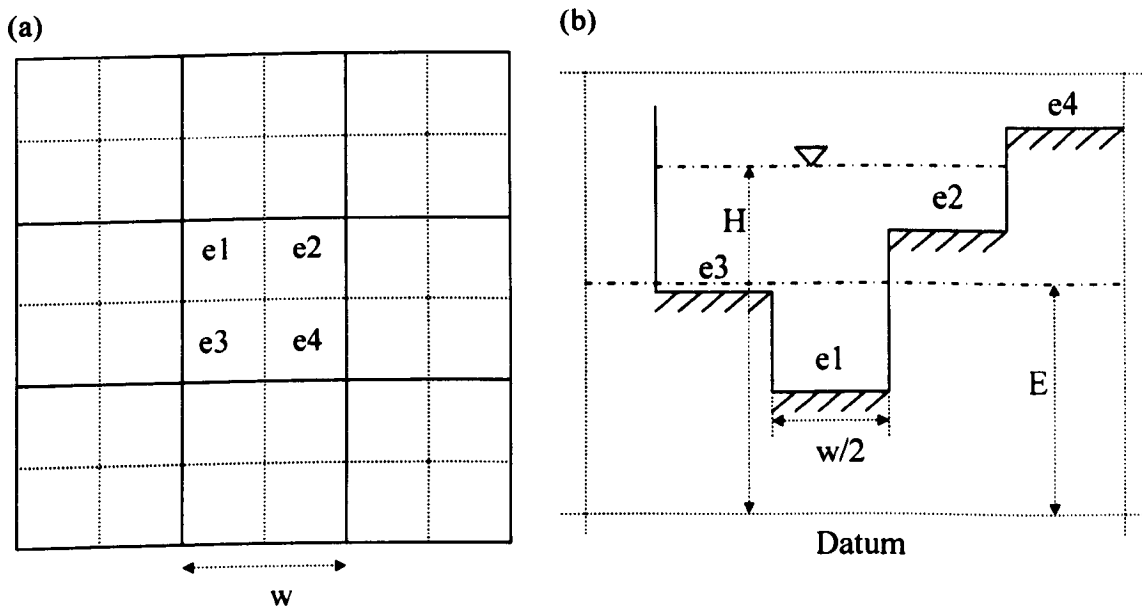


Figure 5.2: Schematic view of the sub grid topography. (a) shows the model with its sub grid cells; e1, e2, e3 and e4 are sub grid cell bed elevations; w is the resolution of the model grid. (b) shows the four elevations unwrapped onto a 1D plain; H is the sub grid water surface elevation; E is the bed elevation of the model cell which is equal to the average of its sub grid cell elevations.

### 5.3 Theoretical derivation of a sub grid-scale topographic treatment

#### 5.3.1 Cell blockage effects

Consider a cell and its sub grid cells in the configuration shown in Figure 5.2. The cell is composed of four sub grid cells with bed elevation e1, e2, e3 and e4 (Figure 5.2a). These are shown schematically in 1D in Figure 5.2b.

Without a sub grid-scale topographic representation, the elevation of the coarsened cell ( $E$ ) can be calculated simply as the average of the four sub grid cells. The relationship between water surface elevation and the volume of water that can be stored within the cell without considering the sub grid topography (i.e. Figure 5.2a) is a simple linear one, taking the form:

$$V_{ij} = w^2 \left( H_{ij} - \frac{1}{N_{ij}} \sum_{k=1}^{N_{ij}} e_k \right) \quad (5.1)$$

where  $w$  is the grid resolution,  $H_{ij}$  is the water surface elevation in cell  $ij$ ,  $N_{ij}$  is the number of sub grid cells in grid cell  $ij$  and  $e_k$  is the bed elevation of each sub grid cell.

(5.1) needs to be modified to represent the actual volume storage effect (Figure 5.2b), as (5.1) will under-estimate the true volume of storage for  $\min(e_k) < H_{ij} < \max(e_k)$ . Under-estimation of storage volumes will lead to over-estimation of water levels, and this partly explains why the effects of mesh coarsening will be amplified in a diffusion type model. In the case of a 2 x 2 set of cells being averaged to a single cell, the peak under-estimation of volume (or over-estimation of water level) is at  $H_{ij} = E$  and this diminishes to zero for  $H_{ij} = \max(e_k)$ . This allows us to develop a first approximation of the relationship between water volume ( $V_{ij}$ ) and water surface elevation ( $H_{ij}$ ) taking into account sub grid-scale topography:

$$V_{ij} = \frac{w^2}{N_{ij}} \left( N_{ij}^k H_{ij} - \sum_{k=1}^{N_{ij}^k} e_k \right) \quad (5.2)$$

where  $e_k$  is the bed elevation of the sub grid cell  $k$ ,  $w$  is the width of the grid cell which contains  $N_{ij}$  sub grid cells and  $N_{ij}^k$  is the number of sub grid cells within the grid cell that are wet. When the cell is fully wet,  $N_{ij}^k = N_{ij}$  and (5.2) reduces to (5.1).

In a forward differencing scheme, fluxes into and out of cell  $ij$  would be determined to give  $V_{ij}$ . However, this still leaves two unknowns in (5.2),  $H_{ij}$  and  $N_{ij}^k$ . Thus,  $N_{ij}^k$  from the previous time step is used to determine  $H_{ij}$ . If  $H_{ij}$  exceeds  $e_{k+1}$  then  $N_{ij}^k$  is increased by one

and (5.2) is re-evaluated. This continues until  $H_{ij}$  no longer exceeds  $e_{k+1}$ . A final check is then undertaken to make sure that  $H_{ij}$  also exceeds  $e_k$ . If not,  $N_{ij}^k$  is reduced by one and (5.2) is re-evaluated. With the water surface elevation as the dependent variable, the difference between these two scenarios is calculated as:

$$\frac{V_{ij}}{w^2} \left( \frac{N_{ij}}{N_{ij}^k} - 1 \right) + \frac{1}{N_{ij} N_{ij}^k} \left( N_{ij} \sum_{k=1}^{N_{ij}^k} e_k - N_{ij}^k \sum_{k=1}^{N_{ij}} e_k \right) \quad (5.3)$$

(5.3) is the general result illustrated above for the case of 2 x 2 cells: as the water volume increases, the difference in water surface elevation for the two cases decreases, resulting in no difference once all the sub grid cells are wet, i.e., the number of wet sub grid cells is equal to the total number of grid cells ( $N_{ij} = N_{ij}^k$ ). Figure 5.3 superimposes (5.1) and (5.2) to illustrate the difference between the two treatments (Figure 5.3).

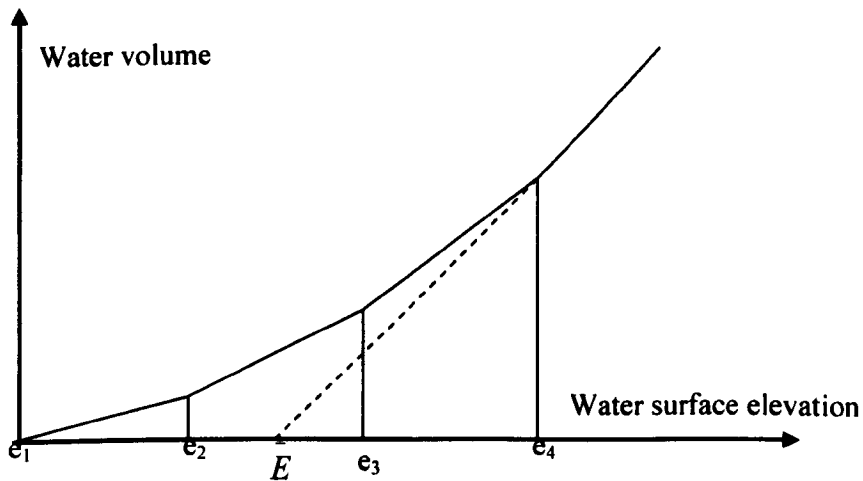


Figure 5.3: Super-position of elevation-flux relationship (Equation 5.1) (dashed line) on sub grid elevation-flux relationship (Equation 5.2).

First, when the water surface elevation is less than the average value of the sub grid-scale elevations, but higher than the minimum sub grid-scale elevation, (5.2) allows inundation, whereas (5.1) does not. Once the water surface is higher than the average sub grid-scale elevation, (5.1) will allow inundation. Thus, the peak error with (5.1) is when the water surface elevation equals the average sub grid-scale elevation. The error reduces as the water surface continues to rise until the cell is fully wet when the error is zero. The reverse will occur during the falling limb. Thus, the error due to (5.1) is associated with the wetting and drying process in which cells wet up more quickly and dry more slowly than would be the case if (5.1) alone were adopted. Second, the sub grid-scale topography has implications for the rate of rise of the water surface within a grid cell. When the cell is wet under (5.1), but

still partially wet under (5.2) (i.e. when the water surface elevation is greater than the average value of the sub grid-scale elevations but less than the maximum value), then the water surface rise within the cell will be more rapid than predicted under (5.1).

Third, given that both of these effects determine the rate at which water levels rise, and that diffusion models are based upon the evaluation of water level differences between adjacent cells, the representation in (5.2) may affect the way in which water diffuses across the floodplain. With a coarser mesh, when wetting starts, there should already have been flow into (and storage within) the cell. This will have implications for outflow fluxes, with potentially more rapid diffusion of a flood wave than under (5.1). However, if the cell is partially wet, then flux cannot occur across all grid cell faces. Thus, it is also necessary to look at a sub grid-scale treatment for cell fluxes (§ 5.3.2).

Finally, more complex sub grid features may produce non-linear relationships. Examples are provided in Figure 5.4. As higher-resolution DEMs, which are able to describe the shapes of those features, become available, these relationships could be implemented in the model developed here.

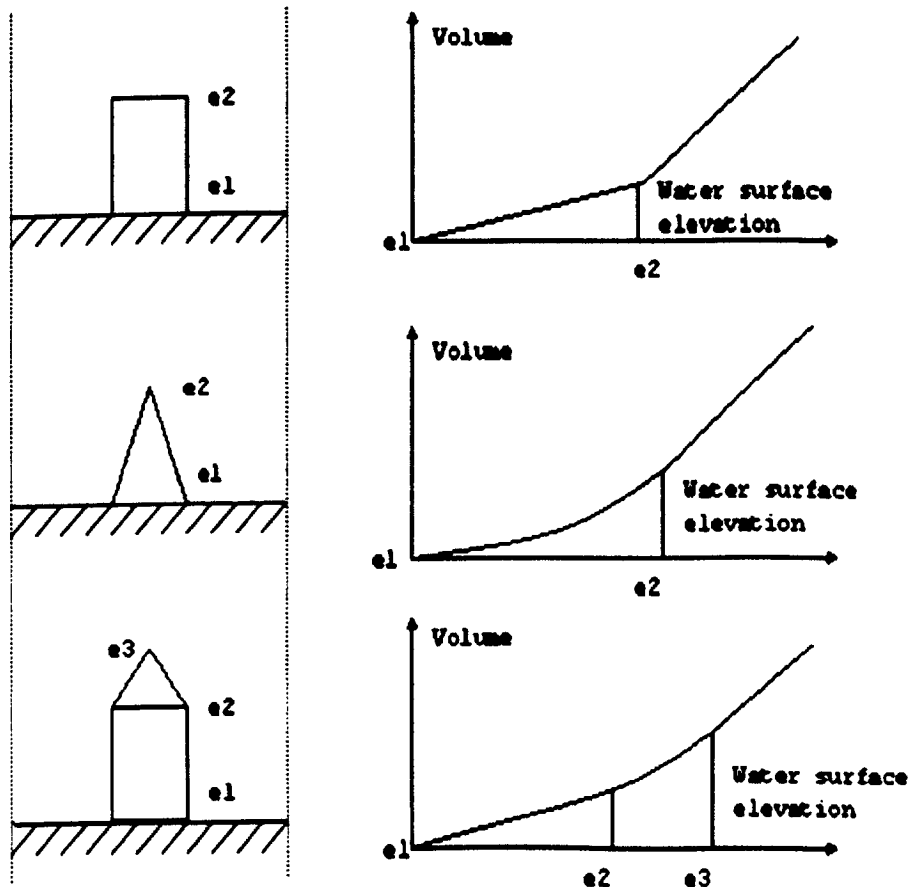


Figure 5.4: Complex sub grid features and their volume-water surface elevation relationship.

### 5.3.2 Cell flux effects

The cell flux effects were represented using a porosity type treatment which has proved to be a powerful means of representing sub grid-scale topographic effects in river flows (e.g. Olsen and Stokseth, 1995; Lane and Hardy, 2002; Lane *et al.*, 2002; Lane *et al.*, 2004) and for representation of wetting and drying processes in depth-averaged hydrodynamic models of floodplain inundation (e.g. Bates, 2000). Consider two adjacent grid cells labelled 1 and 2. The assumption made here is that flux should only occur across the face between two cells when a sub grid-scale cell in cell 1 is wet and the water surface in that sub grid-scale cell is higher than that the adjacent sub grid cell in cell 2. Thus, the first step is to establish a set of rules that determine when flux can occur across the common face of cell 1 and 2, and this has to be done in both directions (i.e. for flux from cell 1 to 2 and from cell 2 to 1). The method retains computational efficiency by establishing porosity values as a DEM pre-processing step, such that the porosity values do not have to be re-evaluated during model solution. A porosity term is set based upon the percentage of cells that will be able to flux from cell 1 to 2, which varies as a function of water surface elevation. If the number of sub grid-scale cells along a common face is  $l$ , there will always be  $l-1$  values of porosity between zero (no flux across that face) and one (flux across all of the face), and the values of porosity will be multiples of  $1/l$ . For the case of flux from cell 1 to 2, the porosity values are set by evaluating two conditions: (i) the water surface elevation values that must be reached in cell 1 for there to be water in a given sub grid cell in cell 1; and (ii) the elevation of the adjacent grid cell in cell 2, which must be exceeded by the water surface elevation value in cell 1 for there to be a sub grid-scale flux. The porosity values are used to scale the flux explicitly.

One additional correction is introduced. As the flux is a non-linear function of water depth (from the discretized form of the simplified shallow water equations), then we need to make sure that the correct water depth is used in the evaluation of flux. This is done by determining an effective depth for the flux, based upon:

$$d_e = \sqrt[3/5]{\frac{\sum_{i=1}^n d_i^{5/3}}{n}} \quad (5.4)$$

where  $n$  is the number of sub grid cells that are wet along the outflow side of the modelling cell and  $d_i$  is the effective depth of the individual sub grid wetted cells along the outflow wall of the modelling cell. If flux occurs across one sub grid cell face, then the flux evaluated using (5.4) with the porosity scaling gives the same flux as if a mesh set at the sub grid-scale

resolution was being adopted. This is not the case when more than one sub grid-scale flux occurs because of the non-linear form of the depth-flux relationship in the Manning equation. In this case, there will be a difference between the effective depth calculated from (5.4) and that by averaging. However, provided the topographic variability within fluxing sub grid-scale cells is small, then the difference is small. The weighting used in (5.4) gives more weight to higher sub-grid effective depths. This is based on the understanding that in the Manning equation (4.4), effective depth has a weighting ratio of a 5/3 power in the calculation of discharge. For example, if we considered a sub-grid cell with 6 sub-grid cells of sub-grid effective depths of {0.1, 0.12, 0.15, 0.1, 0.2, 0.4}, if all sub-grid effective depths are used in the calculation, cell effective depth calculated from (5.4) will be 0.149, compared with that calculated from simple averaging of 0.145. Table 5.1 shows a simple analysis on the effect of the power function used in (5.4). It shows that in all cases, except when only one sub-grid cell is used, the effective depth calculated from (5.4) is higher than that calculated from a simple averaging. Thus, (5.4) gives more weight to higher sub-grid effective depths. The difference increases as the topographical variability within the sub-grid cells increase. For example, if the effective depth of the sub-grid cell with an effective depth of 0.4 in Table 5.1 becomes 0.12, with all 6 sub-grid effective depths used in (5.4), the difference between the power weighting approach and simple averaging approach will be 0.023 as the standard derivation of the sub-grid effective depth decreases from 0.115 to 0.038.

Table 5.1: Illustration of the sub-grid effective calculation.

Number of sub-grid cells and sub-grid effective depth	Weighting approach	Simple averaging	Percentage of difference
{0.1} - 1	0.100	0.100	0.000
{0.1, 0.12} - 2	0.110	0.110	0.003
{0.1, 0.12, 0.15} - 3	0.124	0.123	0.009
{0.1, 0.12, 0.15, 0.1} - 4	0.119	0.118	0.010
{0.1, 0.12, 0.15, 0.1, 0.2} - 5	0.137	0.134	0.026
{0.1, 0.12, 0.15, 0.1, 0.2, 0.4} - 6	0.197	0.178	0.105

In the context of flood inundation modelling, one factor that may affect the rate of flux routing on the floodplain is the amount of inflow from the river through bank cells to the floodplain. In order to allow the same amount of water to the floodplain for the sub grid-scale treatment as the normal treatment, the evaluation of the water depth of the bank cells does not use the sub grid-scale treatment. This is to ensure that the water depths at the bank cells are evaluated in the same way as in the normal treatment for comparison purposes.

In summary, this sub grid cell treatment should represent a simple method for improving the representation of structurally complex topography within two-dimensional diffusion wave modelling. In particular, it should reduce the dependence upon mesh resolution noted in

Chapter 4, especially in dynamic rather than steady state solutions. It differs from the wetting and drying parameter developed by Bradbrook *et al.* (2004) and used in Chapter 4 in that their wetting and drying parameter represents an empirical means for dealing with mesh resolution effects. The approach used here is explicitly grounded in rules that are locally evaluated in relation to information on the sub grid-scale topography in a particular grid cell. The next sections evaluate the effects of this development upon sensitivity to mesh resolution within a flood inundation model in two different locations.

### **5.3.3 Model validation using the sub grid-scale treatment**

Model validation using the sub grid-scale treatment is different to that used in the normal treatment. For the normal treatment, the wetness of a grid cell is simply based upon water depth in the cell. In the sub grid-scale treatment, the wetting status of a grid cell is based upon the number of grid cells in the sub grid topography that are wet. If all the sub grid cells are wet, the cell is treated as wet. If none of the sub grid cells are wet, it is treated as a dry cell. Otherwise, it is a wetting front cell. The validation data are also subject to re-sampling onto the model resolution. In this study, the validation data have a resolution of 2 m. Thus, this needs to be coarsened onto the model resolution and the wetting status of the validation data re-evaluated using the same approach as described in Section 3.6.2. Again, it should be recognized that this will introduce some bias into the evaluation of the coarser mesh simulation in which the percentage of wetting front cells in the reference data is higher than the finer mesh. The magnitude of bias will depend on the percentage of wetting front cells in the reference data.

### **5.4 Model testing 1: extensive analysis in Site 1 – Naburn Weir**

The sub grid-scale wetting treatment approach described above was assessed using the same flood event (§3.8) as used in Chapter 4 at Site 1 (§3.4) on the River Ouse. The model was set up in the same way as in the previous chapter and the loosely coupled version of the model (§3.7) was used. Topographic data are the same as those used in Chapter 4 and these were presented in Section 3.7. The model was run using three different spatial resolutions: 8 m, 16 m; and 32 m; and this study restricted consideration of sub grid treatments to a coarsening ratio of 2:1 (i.e. the sub grid-scale treatment was used to represent the effects of coarsening: a 4 m mesh to 8 m; an 8 m mesh to 16 m; and a 16 m mesh to 32 m). 2 m DEM is not used as sub-grid mesh due to computational constraints. At this point,  $n$  was set at 0.06 throughout. Chapter 4 showed that careful attention has to be given to how the main river is represented as a mesh is progressively coarsened. The same also applies to the sub grid case. It is

particularly important when one or more coarse model cells contain no river features but where there are river cells in the sub grid topographic data. This can arise as a result of interpolation of the original topographic data from a fine resolution grid to a coarser one. If this is not resolved, due to the low elevation of the sub grid river cell(s), too much water will flow into certain sub grid cell(s) and other sub grid cell(s) in the model cell may never get inundated. In such cases, the sub grid cell elevation is set as equal to the nearest floodplain cells.

As with the Chapter 4, the focus of model testing at this site combines both validation and verification. For validation purposes, the at-a-point in time data at c. 300 hours in the November 2000 flood (§3.6) were used. As with Chapter 4, methods adopted from remote sensing (Congalton and Green, 1999) were used to assess model predictions. This sets up model output as a contingency table and calculates the overall accuracy,  $F$  (following Bates and Horritt, 2002), Kappa and conditional Kappa from these data. As shown in Chapter 4, reliance upon data from single time periods can give a misleading assessment of model performance, especially where, as in this case, the primary interest is in reproducing the correct diffusion of inundation through time. Thus, verification was undertaken, and the original 8 m, 16 m and 32 m simulations were compared with the 8m, 16 m and 32 m sub grid model simulations as well as the default 4 m simulation. The determination of the wetting status of a model cell during model validation is different from that of the original model as there is no wetting parameter in the sub grid treatment approach. Instead, the sub grid-scale wetting treatment determines the wetting status of a model cell based solely on the number of sub grid cells that are wet. If there are no wet sub grid cells in the model cell, this cell is considered to be predicted as dry. If all of the sub grid cells are wet, this cell is considered to be wet. Otherwise, the cell is considered to be a wetting front cell. The validation data used in all cases was of a 2 m resolution ( § 3.6.2). For the comparison of the validation data with the model output on a cell-by-cell basis as required by the quantitative assessment approach ( § 3.6.3) used in this study, the validation data were projected to the same resolution as the mesh used in the model. This was described in Section 3.6.2.

The original and sub grid models with different values of  $n$  were also considered for comparing the effectiveness of using  $n$  to represent sub grid-scale topographic effects, with the explicit sub grid treatment. As the focus is the sub grid treatment, this is expected to reduce model dependence upon high values of  $n$ . Thus, in the first instance, lower values of Manning's  $n$  (0.04, 0.06, 0.08 and 0.1) were used; but also simulations with much higher values of  $n$  (1.0 and 10.0) were undertaken; following the findings of Chapter 4.

### **5.4.1 Results 1: Inundation patterns through time**

Figures 5.5, 5.6 and 5.7 show the first 40 hours of model simulation, with and without the sub grid-scale treatment. It is clear that, in all cases, there is a significant reduction in the rate of inundation diffusion with the sub grid-scale treatment. Figure 5.5a shows inundation of the confined floodplain by 30.5 hours with the original treatment. With the sub grid treatment, this increases to 40 hours (Figure 5.5b), and it is clear that the sub grid treatment has a major impact upon the timing of inundation. The conclusions made regarding the effects of the 8 m sub grid-scale treatment (Figure 5.5) are mirrored in the 16 m and 32 m treatments. Flow diffuses much more rapidly in the 16 m (original) case than in the 16 m (sub grid-scale) case (Figure 5.6), with almost complete inundation at 32 hours (original case) compared with 36 hours (sub grid-scale). The 32 m (original) case results in extensive inundation within the first 10 hours of simulation whereas the 32 m (sub grid-scale) case does not have inundation until c. 31 hours. It seems that, for the first part of the hydrograph, the sub grid-scale treatments slow the inundation process. Figure 5.8 shows the effects of the sub grid-scale treatment upon inundated area with  $n = 0.06$ .

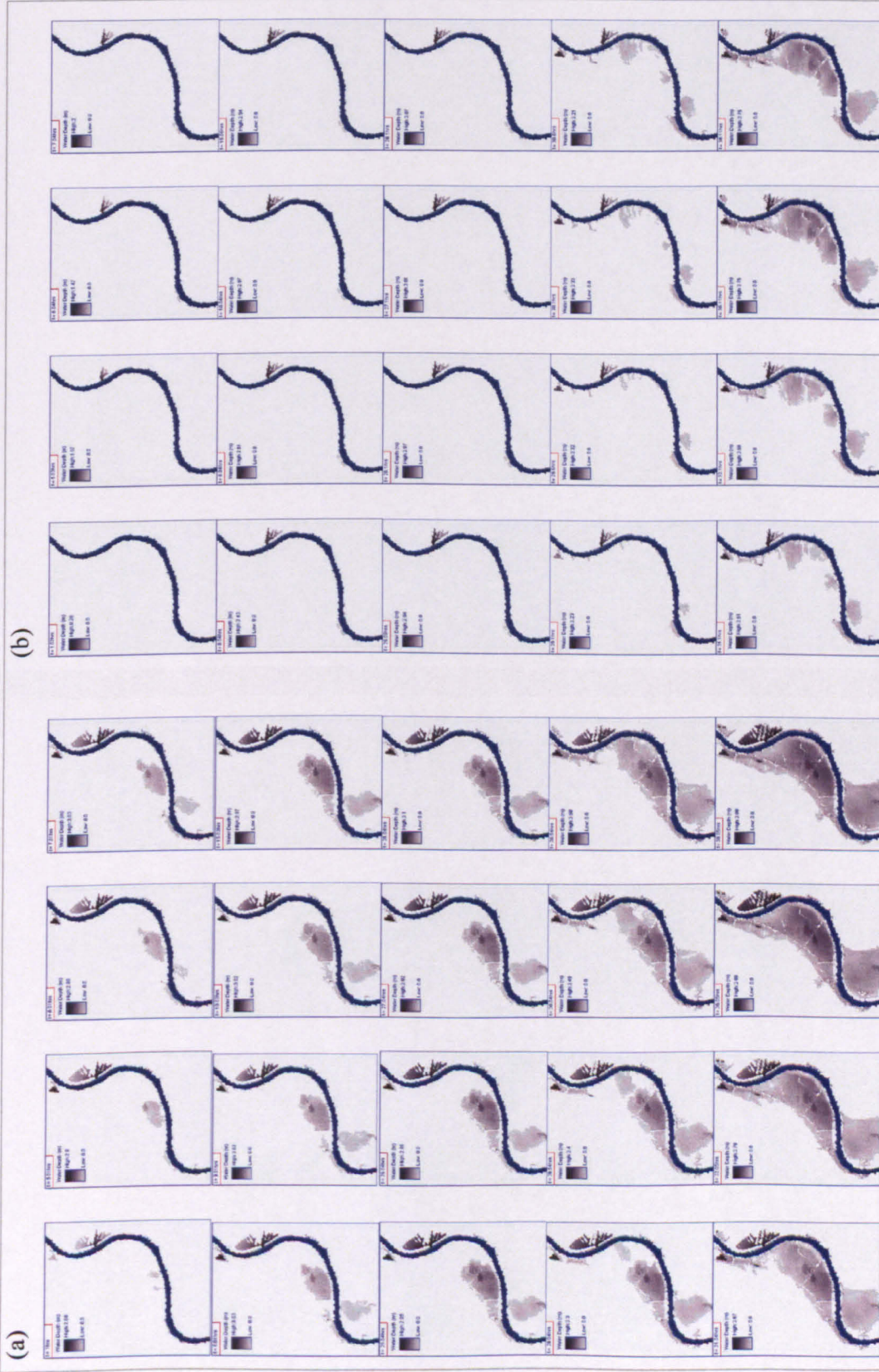


Figure 5.5: Comparison of the time series inundation extents in the first 40 hours for: (a) the original diffusion model; and (b) the sub grid treatment model; using an 8 m resolution DEM.

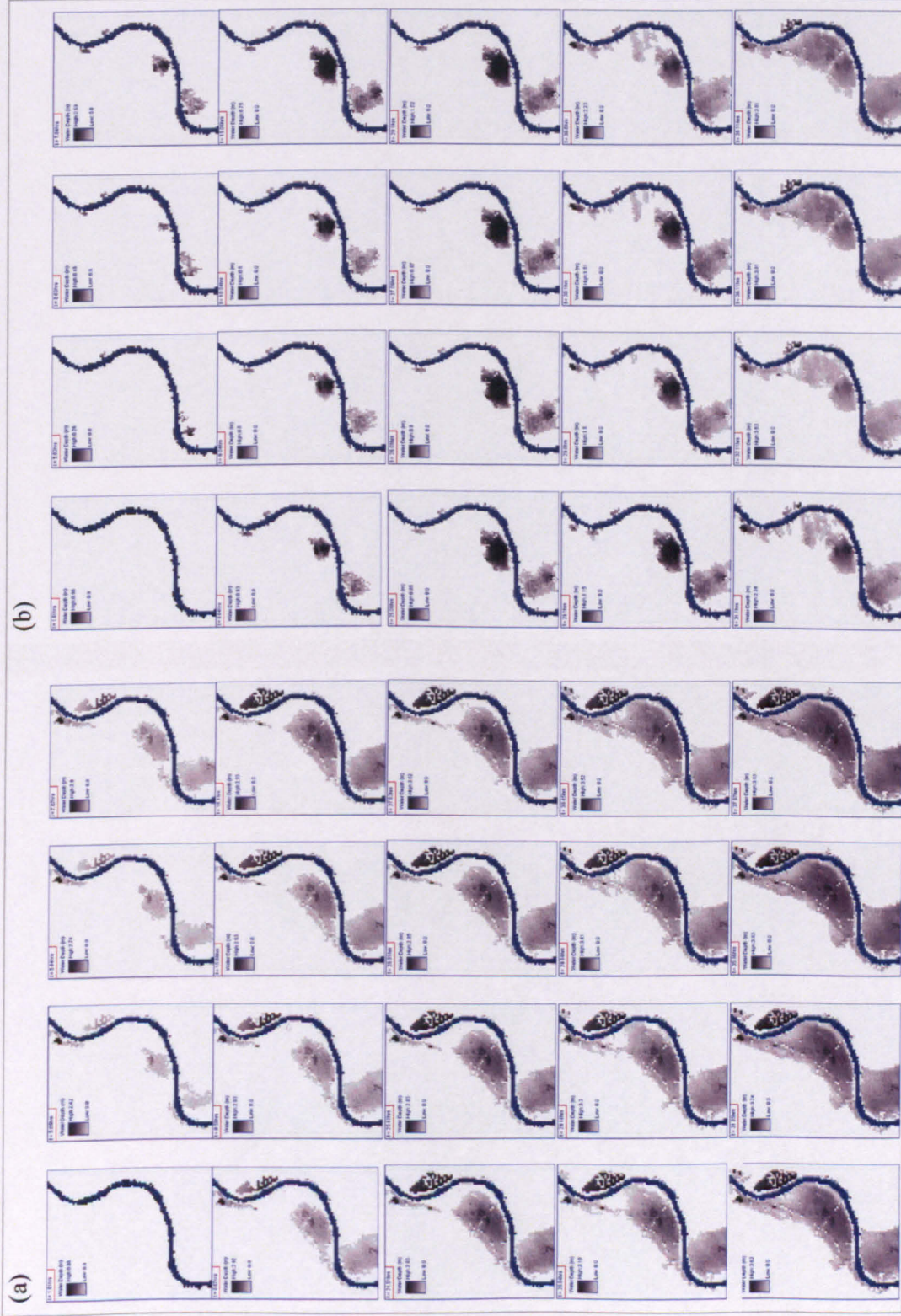


Figure 5.6: Comparison of the time series inundation extents in the first 40 hours for: (a) the original diffusion model; and (b) the sub grid treatment model; using a 16 m resolution DEM.

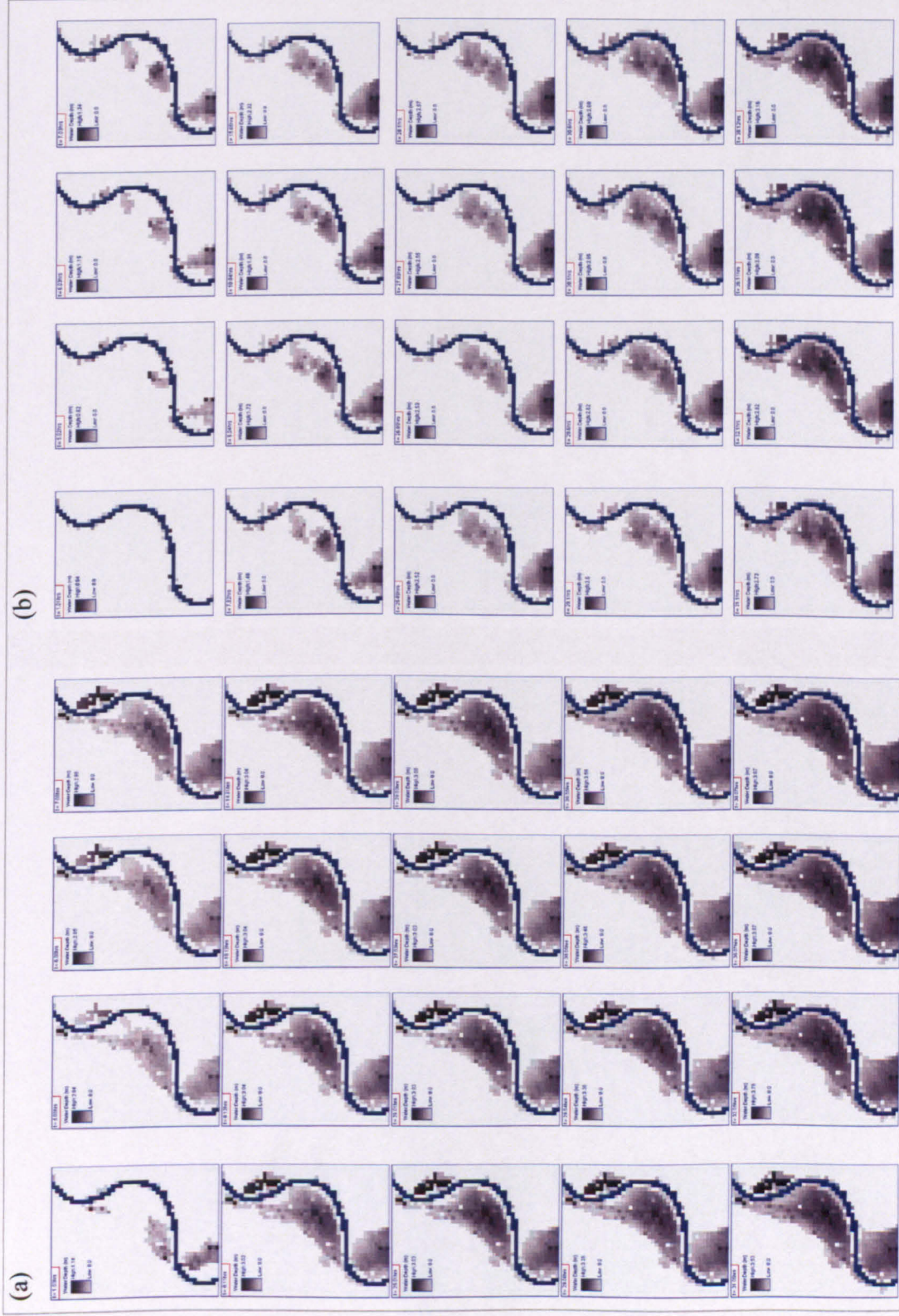


Figure 5.7: Comparison of the time series inundation extents in the first 40 hours for: (a) the original diffusion model; and (b) the sub grid treatment model; using a 32 m resolution DEM.

This shows that not only do the sub grid-scale treatments reduce the speed of inundation (Figures 5.5-5.7) but also the maximum inundation area for all mesh resolutions at all time periods. The original hydrograph had multiple water level peaks. With the 32 m resolution mesh, the inundated area responded rapidly to fluctuations in water level, with multiple flood peaks evident in the inundated area. In the absence of a sub grid-scale treatment, these fluctuations are present in both the 16 m and the 8 m inundated area records. With the sub grid treatments, the inundated area is much less responsive, with response only evident between the third and the fourth water level peak in all sub grid treatments. The sub grid treatments also reduce the total inundation area at all time periods. The differences are quite substantial, especially for the coarsest mesh resolution.

The obvious question that emerges from the above simulations is whether or not the reduced speed of flood wave inundation and the reduced flood inundation extent that are obtained with the sub grid-scale treatment are improvements over the original diffusion wave formulation. This is addressed with respect to the remotely-sensed validation data and the original 4 m simulation in the next two sections.

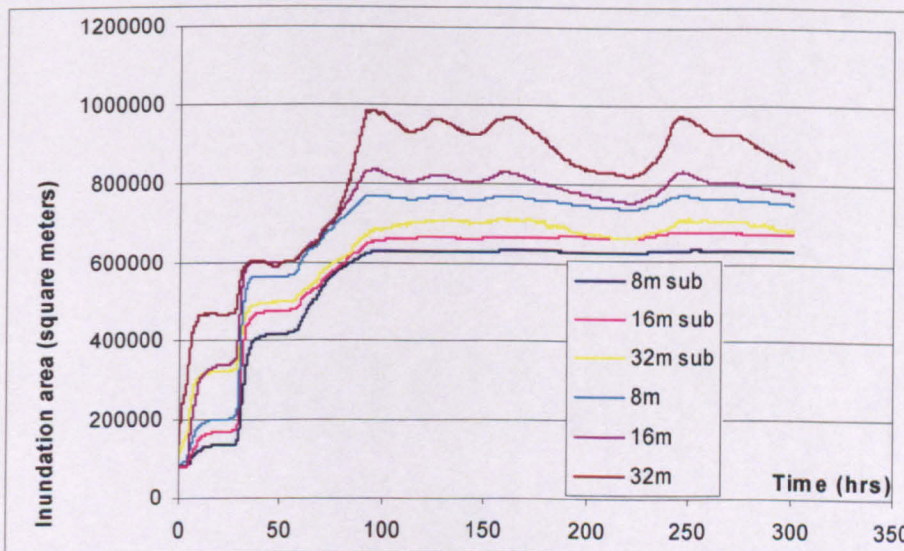


Figure 5.8: Predictions of inundated area against time for the first 300 hours of model simulation for three mesh resolutions with both default treatments and sub grid-scale treatments.

#### 5.4.2 Results 2: Model validation and verification

Table 5.2 shows the results of the accuracy assessment with the four simplified mesh resolutions and with the three sub grid-scale treatments applied to the three coarser mesh resolutions. Table 5.2 shows the results from Chapter 4: that as the mesh is coarsened from 8 m to 32 m, all of the accuracy statistics suggest progressively poorer model performance. It

should be remembered that there is an anomaly in that the 4 m resolution only gives the best results for overall accuracy, and performs significantly less well in term of the Conditional Kappa statistic. In all cases, Table 5.2 shows that the sub grid-scale treatment improves the level of agreement over the original case. For the 8 m mesh resolution, the improvements in overall accuracy, Kappa and  $F$  are small. However, the conditional Kappa improves substantially. The sub grid-scale treatment has a progressively greater effect at coarser mesh resolutions with large improvements in  $F$  and conditional Kappa at 16 m and in all accuracy statistics at 32 m. Given the discussion in Chapter 4 of the problems of these types of accuracy measures, reliance on absolute values from at-a-point in time data must be treated with caution. What matters here is that, in every case, the sub grid-scale treatment improves the level of agreement as compared with the original diffusion model.

Table 5.2: Accuracy assessment based upon model predictions with different mesh resolutions and with and without the sub grid treatment. The validation data are based upon remotely-sensed imagery obtained at 300 hours into the flood event (Site 1).

	4 m	8 m	16 m	32 m	8 m sub grid-scale treatment	16 m sub grid-scale treatment	32 m sub grid- scale treatment
Overall accuracy	90.7	87.5	83.7	71.4	88.8	83.8	80.6
Kappa	82.0	75.8	70.1	51.0	78.3	70.2	66.0
$F$	81.3	78.9	75.5	60.9	81.0	78.0	76.0
Conditional Kappa for wet areas	89.5	80.3	64.8	40.3	92.6	82.7	71.0

In order to extend assessment of model performance to a larger number of time steps, accuracy statistics (overall accuracy, Kappa and conditional Kappa) were determined for the first 50 hours by comparing a range of mesh resolutions, with and without sub grid-scale treatments, to the 4 m case (Figure 5.9). In all cases,  $n$  was held constant at 0.04. The overall accuracy statistic reduces through time (Figure 5.9a), reflecting the fact that this statistic is strongly dependent upon the initial number of dry cells used in the comparison and that, at the start of a flood event, both the 4 m and the coarsened mesh and sub grid-scale treatments will both have a larger number of dry cells. However, Figure 5.9a shows that use of the sub grid-scale treatment improves agreement with the 4 m case, as judged by overall accuracy.

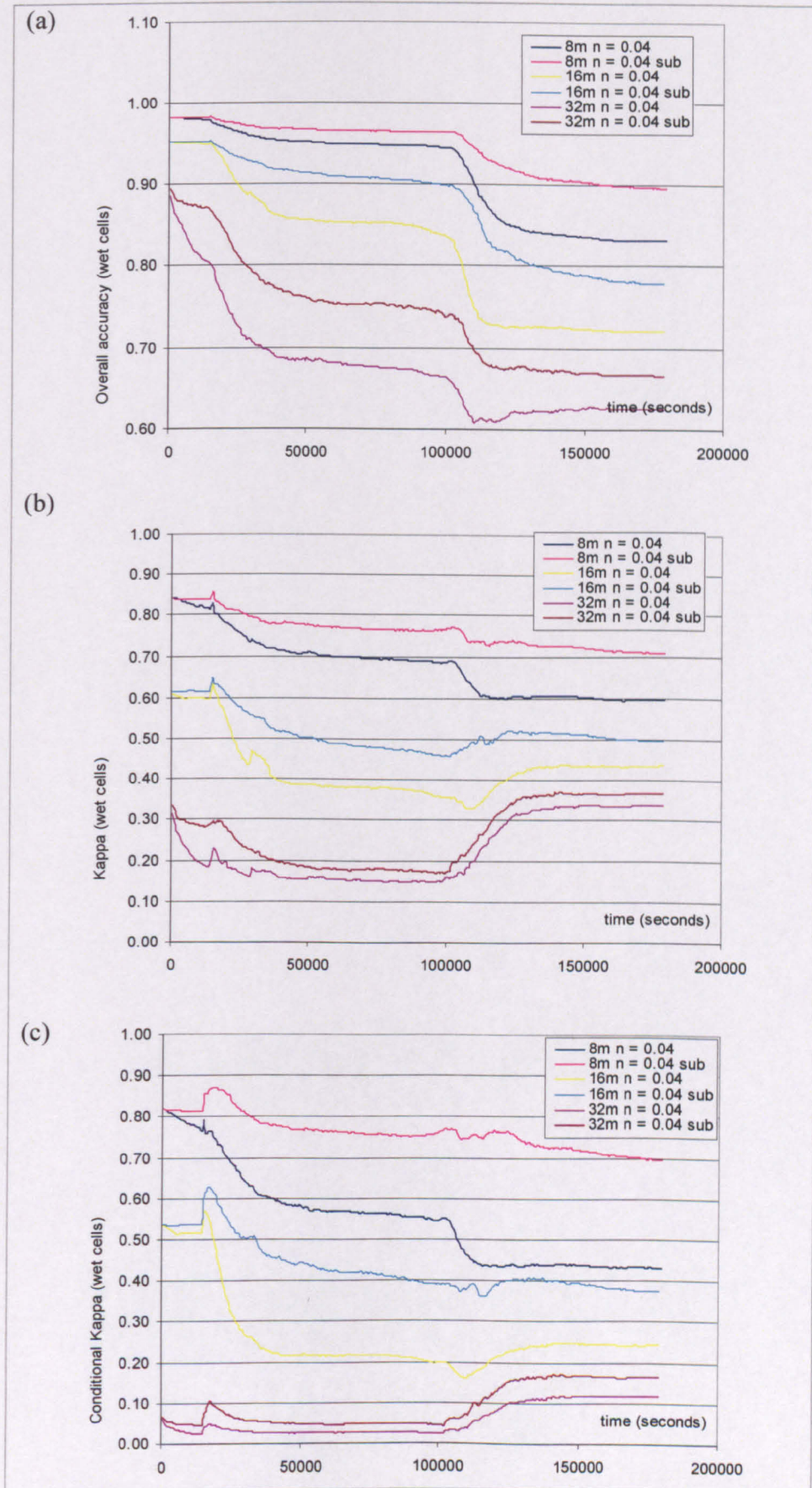


Figure 5.9: Accuracy statistics (overall accuracy, Kappa and conditional Kappa for wet cells only) determined for model simulations at 32 m, 16 m and 8m, with and without a sub grid treatment. These are determined as a function of time, taking the 4 m solution without a sub grid treatment as ‘true’ for verification purposes.

For Kappa, Figure 5.9b confirms that the 32 m and 16 m simulations are more degraded as compared with the 4 m predictions than the 8 m degradation as compared with the 4 m predictions. The sub grid-scale treatments are then most effective in the 8 m case and least effective in the 32 m case. Figure 5.9c shows the conditional kappa for wet cells and demonstrates that the sub grid-scale treatment results in a substantial improvement in model accuracy in the 8 m case as compared with the 4 m simulation. It appears that, in all cases, using the sub grid-scale treatment with the 8 m resolution mesh results in a significant improvement in model accuracy, however judged, but that this improvement is reduced at coarser mesh resolutions. Although Table 5.2 shows that the best improvement is with the 32 m simulation. However, this is evaluated at the time when the validation data are available. The improvement of the 32 m simulation is largely not due to the effect of sub-grid, rather, it is because of the poor performance of the original wetting treatment. Floodplain configuration contributes to much of the improvement. The first 50 hours simulation gives a 'true' picture of the relative effects of sub-grid treatment on different mesh resolutions. This is not surprising as only the sub grid-scale topographic data from the 2 x 2 cells at the next finer resolution (e.g. the 32 m simulations make use of a 16 m DEM) is used. It should be noted that, for the conditional Kappa results (Figure 5.9c), accuracy of the 32 m sub grid treatment with respect to the 4 m simulation approaches that of the 16 m no sub grid treatment towards the latter half of the simulation and the 16 m sub grid treatment approaches that of the 8 m no sub grid treatment. Higher order sub-grid scale treatment will be a further model development.

### **5.4.3 Results 3: Comparison of calibration using Manning's $n$ with sub grid-scale treatment**

The above two sections showed a significant improvement in model predictions, through adopting the sub grid-scale treatment, in terms of reproducing time-dependent changes in flood inundation, particularly for Site 1. This section compares a more traditional approach to representing sub grid-scale topographic variability based upon calibration using Manning's  $n$  with the sub grid-scale treatment. This is undertaken in terms of both: (i) the inundated area versus time plots; and (ii) accuracy statistics, as compared with the 4 m data reported in the above section. The results in terms of the area-time plot using a  $n = 0.4$  are presented in Figure 5.10. As shown in Chapter 4, Figure 5.10a shows that, for the 8 m case, there is relatively low sensitivity to Manning's  $n$  until  $n \gg 0.1$ . However, the 8 m sub grid-scale treatment almost exactly recovers the inundation area versus time plot with  $n = 0.04$ . The default treatment with  $n = 1.0$ , is closest to the 4 m curve at first, but deviates significantly after c. 140000 s. The area-time plot is not recovered as well with the 16 m (Figure 5.10b) and 32 m (Figure 5.10c) sub grid-scale treatments, although they are still a significant

improvement on all values of  $n$  without a sub grid-scale treatment. In particular, whilst the area may be correctly estimated with calibration through  $n$  alone at certain times during the simulation (e.g. with  $n = 10.0$  and a 32 m mesh resolution at c. 120000 s), even with high values of  $n$  ( $>1.0$ ), the inundated extent exceeds the 4 m inundated extent by the end of the time period. Clearly,  $n$  cannot compensate for lack of topographical data. There remains much emphasis in practical flood risk modelling upon determining the correct values of  $n$  to describe flows routed on floodplains. If the floodplain is considered as the higher stage component of a two-stage channel, then this makes some sense. If floodplain routing is more complex than this, there are logical limits to parameterisation using  $n$ .

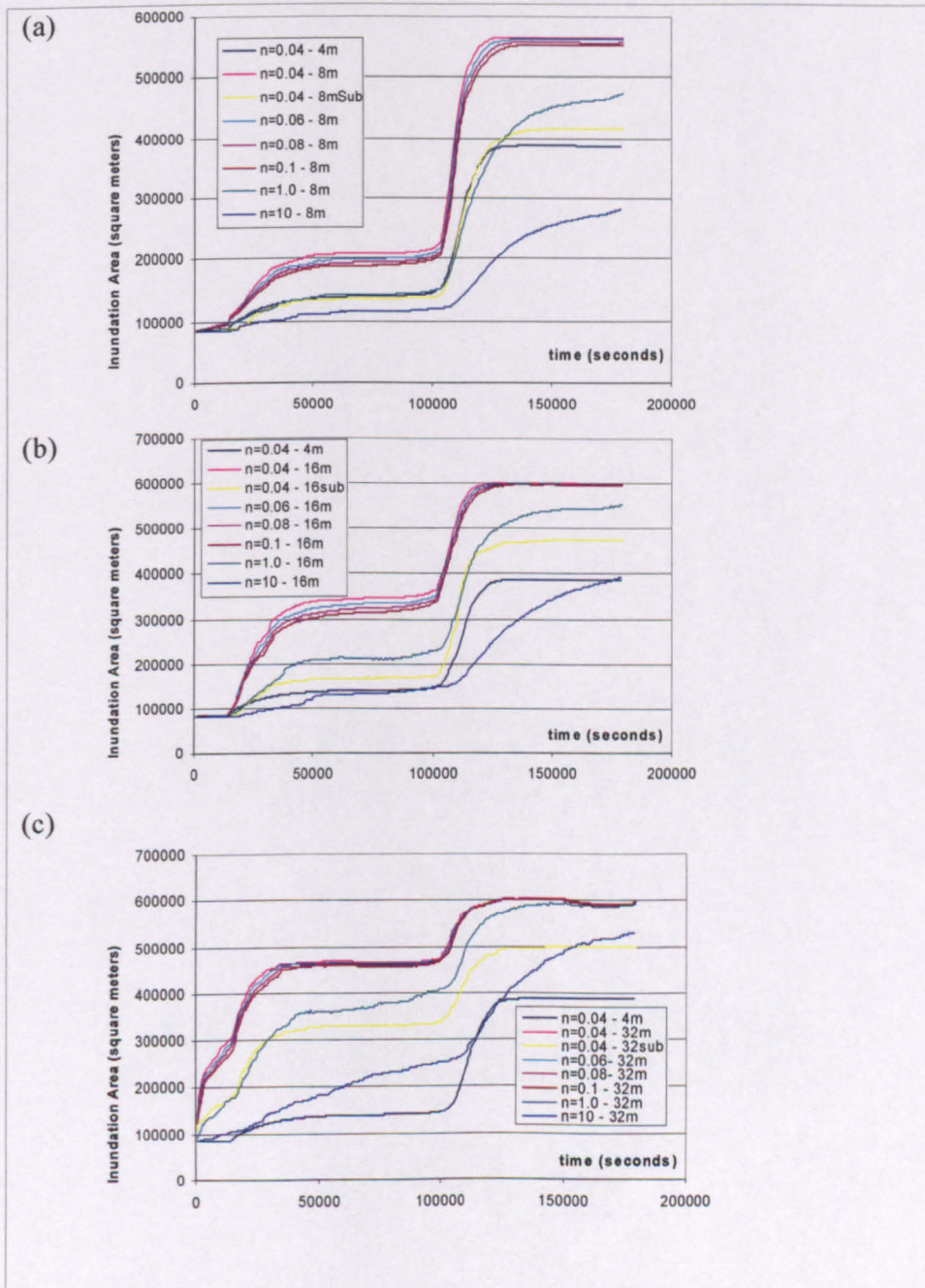


Figure 5.10: Plots of inundation area versus time for the first 50 hours of simulation, with different mesh resolutions and values of  $n$ .

These findings are mirrored when the analysis is extended to include accuracy assessment statistics (Figure 5.11), showing that the combination of sub grid-scale treatment with  $n$  calibration gives the most effective reproduction of the 4 m inundation-time patterns. Here, higher values of  $n$  are used (from 0.4 upwards). For the 32 m mesh, the sub grid-scale treatments all result in better overall accuracy (Figure 5.11a), Kappa (Figure 5.11d) and conditional Kappa (Figure 5.11g) results than all calibrations with  $n$  and no sub grid-scale treatments, except for  $n = 10$ . With the latter, the overall accuracy is better, but both Kappa and conditional Kappa are degraded by the end of the simulation. However, it is also notable that the best results (e.g. Figure 5.11g) are obtained with the combination of  $n$  calibration and a sub grid-scale treatment, even though the final results (e.g. the conditional Kappa values) are not that good. Of particular importance is the greater sensitivity to  $n$  perturbation when using the sub grid-scale treatment (all three accuracy measures are more responsive to  $n$  at this scale) which is important for effective model calibration. The results are somewhat more complex for both 16 m and 8 m. At 16 m, the original treatment with  $n = 10$  performs better than all of the sub grid treatments in terms of overall accuracy (Figure 5.11b, except the combination of  $n = 10$  and a sub grid treatment) and Kappa (Figure 5.11e), but not conditional Kappa (Figure 5.11h). Bearing in mind that the conditional Kappa will be a more reliable accuracy statistic as it is less sensitive to the number of dry cells originally used in the comparison, the conditional Kappa (Figure 5.11h) has the best results with  $n = 10$  and a sub grid treatment. All of the original treatments for simulations with  $n < 10$  have very poor accuracies. The sub grid treatments for  $n < 10$  produce results that are similar to the original treatment,  $n = 10$  case. Again, there is greater sensitivity of conditional Kappa to  $n$  with the sub grid treatment. At 8m, the overall accuracies (Figure 5.11c) are generally best with the sub grid treatment, except for simulation  $n = 10$ . Indeed, both the original and sub grid treatment with  $n = 10$  produce poor results, especially compared with the 32 m (Figure 5.11a) and 16 m (Figure 5.11b) cases. Finally, as the mesh being considered approaches the resolution of the reference mesh, the sub grid treatment results in a notable improvement in accuracy statistics. At coarser mesh resolutions, the improvement is less noticeable. This may reflect the fact that in this form of the sub grid treatment, only the topographic data in the mesh immediately finer is being used to in the sub grid treatment.

Ongoing research is seeking to use finer resolution data than that contained in the finer mesh. This is not straightforward as assumptions have to be made about flow behaviour within the cells that do not have to be made with a single resolution reduction.

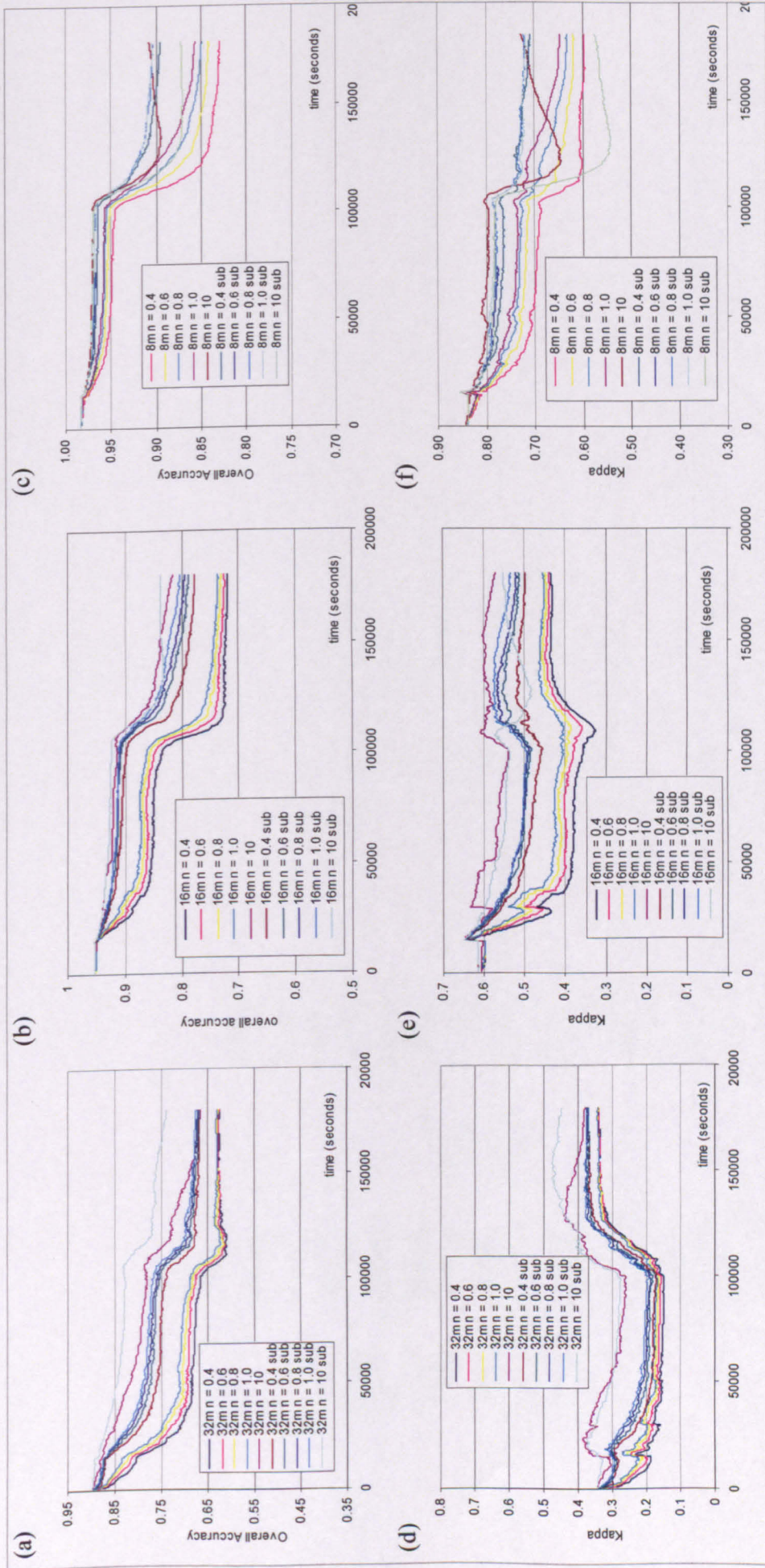


Figure 5.1.1: Overall accuracy (a, b, c), Kappa (d, e, f) and conditional Kappa (for wet cells only) (g, h, i) for the 8 m (a, d, g), 16 m (b, e, h) and 32 m (c, f, i) original (heavy weighted lines) and sub grid (light weighted lines) treatments, with varying values of  $n$ . To aid plotting, the different  $n$  simulations are not highlighted. In almost all cases, higher values of  $n$  are given by the upper lines and lower values of  $n$  by the lower lines. Where this is not the case, it is highlighted on the relevant plot. (continued on next page)

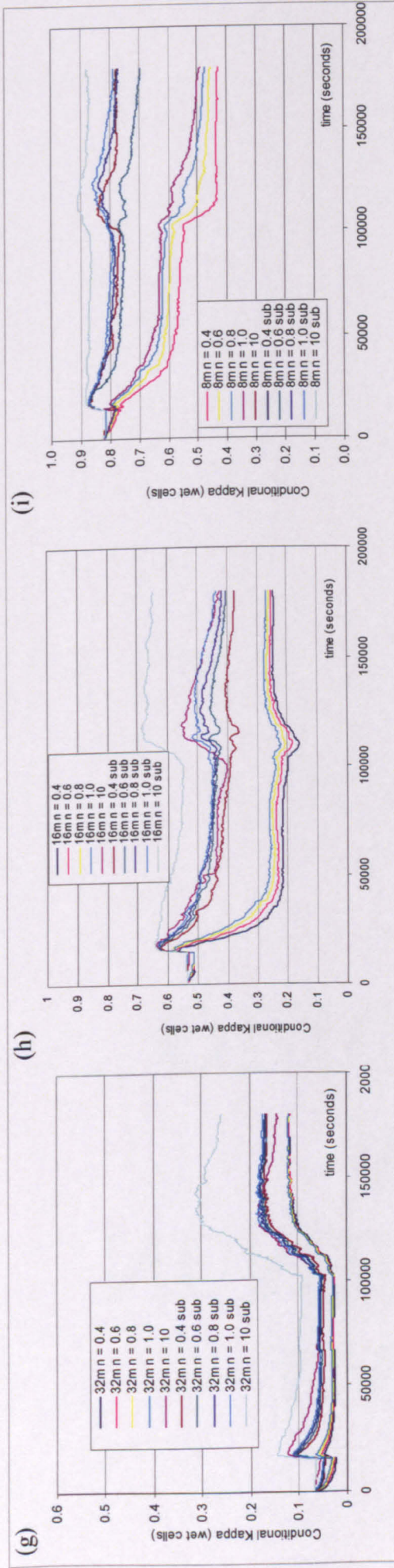


Figure 5.11: Overall accuracy (a, b, c), Kappa (d, e, f) and conditional Kappa (for wet cells only) (g, h, i) for the 8 m (a, d, g), 16 m (b, e, h) and 32 m (c, f, i) original (heavy weighted lines) and sub grid (light weighted lines) treatments, with varying values of  $n$ . To aid plotting, the different  $n$  simulations are not highlighted. In almost all cases, higher values of  $n$  are given by the upper lines and lower values of  $n$  by the lower lines. Where this is not the case, it is highlighted on the relevant plot. (continued from last page)

#### 5.4.4 Discussion of Site 1 application

A number of key points emerge from the above results. First, and most importantly, the results show that the sub grid treatment is effective in reducing simulation dependence upon mesh resolution. The sub grid treatment reduced the speed of inundation in the early part of the flood wave (Figures 5.5-5.7) and also the maximum inundated area for all mesh resolutions at all time periods (Figure 5.8) with a markedly reduced sensitivity of inundated area to water level fluctuations in the main channel. The 8 m sub grid treatment was effective in recovering the 4 m inundation-time plot (Figure 5.10a). For the coarser mesh resolutions, the improvements were in the right direction but not as effective (Figures 5.10b and 5.10c). This was reflected in the at-a-point validation data, and notably the  $F$  and conditional Kappa statistics, which are taken to be the most reliable validation statistics. When extended to comparison with the 4 m resolution simulation, which allowed consideration of many more time periods, the sub grid treatments resulted in reduced sensitivity to mesh coarsening. Second, the model used only the immediately finer DEM in parameterizing the sub grid treatment (i.e. the 2 x 2 DEM cells in the finer DEM). This was reflected in the comparisons with the 4 m simulations, where degradation to 8 m, with a sub grid treatment, produced the best accuracy statistics through time. It was also reflected in the inundation-time plots, where the 16 m and 32 m sub grid treatments were progressively less effective in reducing inundated area through time back to the 4 m plots. Using a 16 m DEM (i.e. with 8 m sub grid data) and a 32 m DEM (i.e. with 16 m sub grid data) progressively degraded the accuracy statistics derived with respect to the 4 m data. This is not surprising and confirms that model performance will be conditioned by the quality of the sub grid data used to parameterize the sub grid treatment. Further research should explore whether using sub grid topographic data with 4 x 4 cells (in this case with 32 m and 16 m meshes) and 8 x 8 (in this case with a 32 m mesh) cells results in accuracy assessments that approach the 8 m sub grid treatment.

Third, and as expected, the effective value of  $n$  required to reproduce the 4 m data reduces as mesh resolution is fined. This is reflected in the inundation area versus time plots (Figure 5.10), where higher values of  $n$  were required with coarser meshes in order to reduce the inundated area to closer to that at 50 hours than with finer meshes. It should be emphasised that this questions the extent to which field estimated values of  $n$  can be used to parameterize a model such as this. It reinforces the point that  $n$  is an effective parameter, not only in relation to the sub grid-scale topographic variability but also in relation to decisions being made about how to discretize a model. Any guidance that is provided to assist with roughness specification for floodplain flow should be oriented towards the interaction between

roughness and mesh resolution in the calibration process as well as towards how it should relate to the surface of the floodplain under consideration.

However, these simulations (Figure 5.10) also showed that  $n$  alone was not effective in reproducing the 4 m inundation-time plot and, although there were some time periods when using very high values of  $n$  gave a reasonable estimation of the predicted 4 m inundation for a short period of time, the shape of the area-time plots with high values of  $n$  with coarser mesh resolutions was often very different to that found with finer mesh resolutions. Introduction of the sub grid treatments was more effective than  $n$  perturbation in recovering the 4 m inundated area-time plot, especially for the 8 m sub grid treatment, and this was reflected in the accuracy assessments (Figure 5.11). However, use of the sub grid treatment in turn changed the interaction between model predictions and  $n$ . In general terms, the model became more sensitive to  $n$ . This is not surprising as implicit in the sub grid treatment developed here is incorporation of the effects of sub grid-scale depth variability, which given the form of the Manning equation will result in greater sensitivity to  $n$ . The value of  $n$  required to reproduce the 4 m results is generally reduced for a given mesh when the sub grid treatment is used as compared to the original treatment. Figure 5.10 showed that the sub grid treatment with the 8 m mesh resolution reproduced the inundated area-time plot with a very low value of  $n$  ( $=0.04$ ) and none of the values of  $n$  without a sub grid treatment were able to reproduce the inundated area except with very high values of  $n$  and then for only limited periods of the first 50 hours of simulation (Figure 5.10). When compared through to the validation point, the combination of  $n$  calibration with the sub grid treatment resulted in the best accuracy statistics, aided by a generally increased sensitivity to  $n$ . This suggests that combining the sub grid treatment with optimisation of  $n$  may produce optimal model predictions on a coarse mesh but, and more importantly, coarser mesh predictions with the sub grid treatment are more reliable at reproducing the 4 m patterns than those without. This is regardless of whether or not any optimisation using  $n$  is undertaken. It should be emphasised that changing mesh resolution also changes topographic data content. Thus, it may be the case that the sub-grid scale model is effective because it retains high resolution topographic information within coarser meshes. As it is emphasised in Section 4.5.3, this validation approach assumes the 4 m data to be 'true data' when it is not. However, model predictions are mesh independent. Therefore, which mesh is used as reference should not matter: all meshes should give the same conclusions (§4.5.3).

The obvious question is whether or not all this matters in terms of applying diffusion wave models to floodplains that are complex, such as those found in urban areas. Figure 5.12 shows

the peak inundated area estimated with the original (8 m, 16 m and 32 m) and the sub grid (8 m, 16 m and 32 m) treatments.

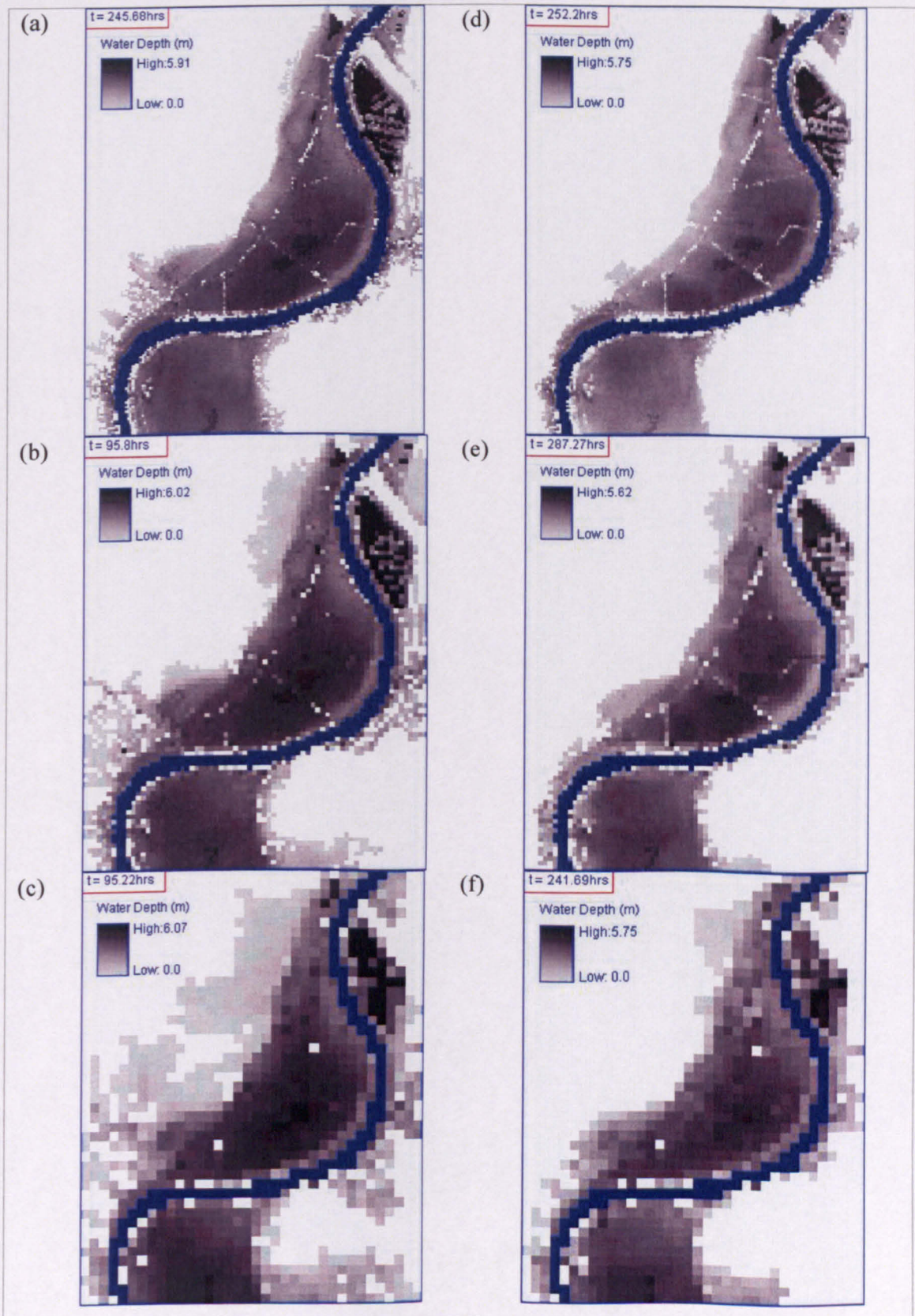


Figure 5.12: The peak inundated area estimated with the original and the sub grid treatments and  $n = 0.06$ . (a) shows the 8 m default simulation; (b) shows the 16 m default simulation; (c) shows the 32 m default simulation; (d) shows the 8 m sub grid simulation; (e) shows the 16 m sub grid simulation; and (f) shows the 32 m sub grid simulation.

It is clear that the original treatments have different peak inundation areas to the sub grid treatments, by an amount that increases with the level of mesh coarsening. As Chapter 4 and Figure 5.10 both show, the inundation-time relationship varies strongly with mesh resolution, and very high values of  $n$  are required in order to achieve a reasonable level of fit. Thus, the prime effect of changing mesh resolution is to change the timing of flood inundation. The sub grid treatments result in better model validation (Table 5.2) and reduce mesh dependence as compared with the 4 m case (Figure 5.11). When taken in combination, this suggests that if the timing of inundation is not right, then it may be difficult to get the inundated area right, whether at the peak flow, or some other point on the hydrograph. This is an important point for any situation where the floodplain is not laterally-confined in relation to the water level associated with the peak inundation extent. In the floodplain system reported here, the floodplain is not laterally confined for the flood event being simulated which had in excess of a 1:100 year return period on the basis of current records. The associated water levels appear to be sufficient to extend beyond the area of lateral confinement, the latter being restricted to flows with return periods of greater than 1:100 years (see Figure 4.12 in Chapter 4). Thus, for more extreme flow events in situations with weak lateral floodplain confinement, sub grid treatments may be required in coarser meshes. Further, important questions emerge over the predictions made for complex floodplains using low quality or low resolution topographic data, where optimization using Manning's  $n$  is relied upon.

## **5.5 Model testing 2: simplified analysis at Site 2 – A64 Trunk Road**

The repeatability of the sub grid-scale wetting treatment is now tested for Site 2 on the River Ouse, with a simplified analysis focusing upon model validation using at-a-point in time validation data. The model was set up the same way as in Section 5.4. Input data are the same as these used in the Site 2 application described in Section 4.6. Validation data and approach are also set up in the same way as in Section 4.6. The roughness value of the floodplain was fixed at 0.06 and roughness parameterization was not undertaken. The model was run using the normal wetting treatment as developed by Bradbrook *et al.* (2004) (as described and used in Chapter 4) and the sub grid-scale wetting treatment described in Section 5.2, with different mesh resolutions of 8 m, 16 m and 32 m, with their immediate finer meshes (a coarsening ratio of 2:1) as the sub grid meshes.

### **5.5.1 Result 1: Inundation patterns through time**

Figures 5.13 to 5.15 show the time series of inundation pattern for the results obtained with the sub grid-scale wetting treatment based upon sub grid topography (§5.3), as compared with the results obtained with the normal wetting treatment controlled by the wetting parameter (§4.3). These give the initial wetting process of the flood event during approximately the first 100 hours. Visual comparisons suggest that the observations obtained from Site 1 were found in this application. It shows that, with the sub grid-scale wetting treatment, the speed of flood inundation was significantly reduced in all three simulations, particularly with the 32 m mesh.

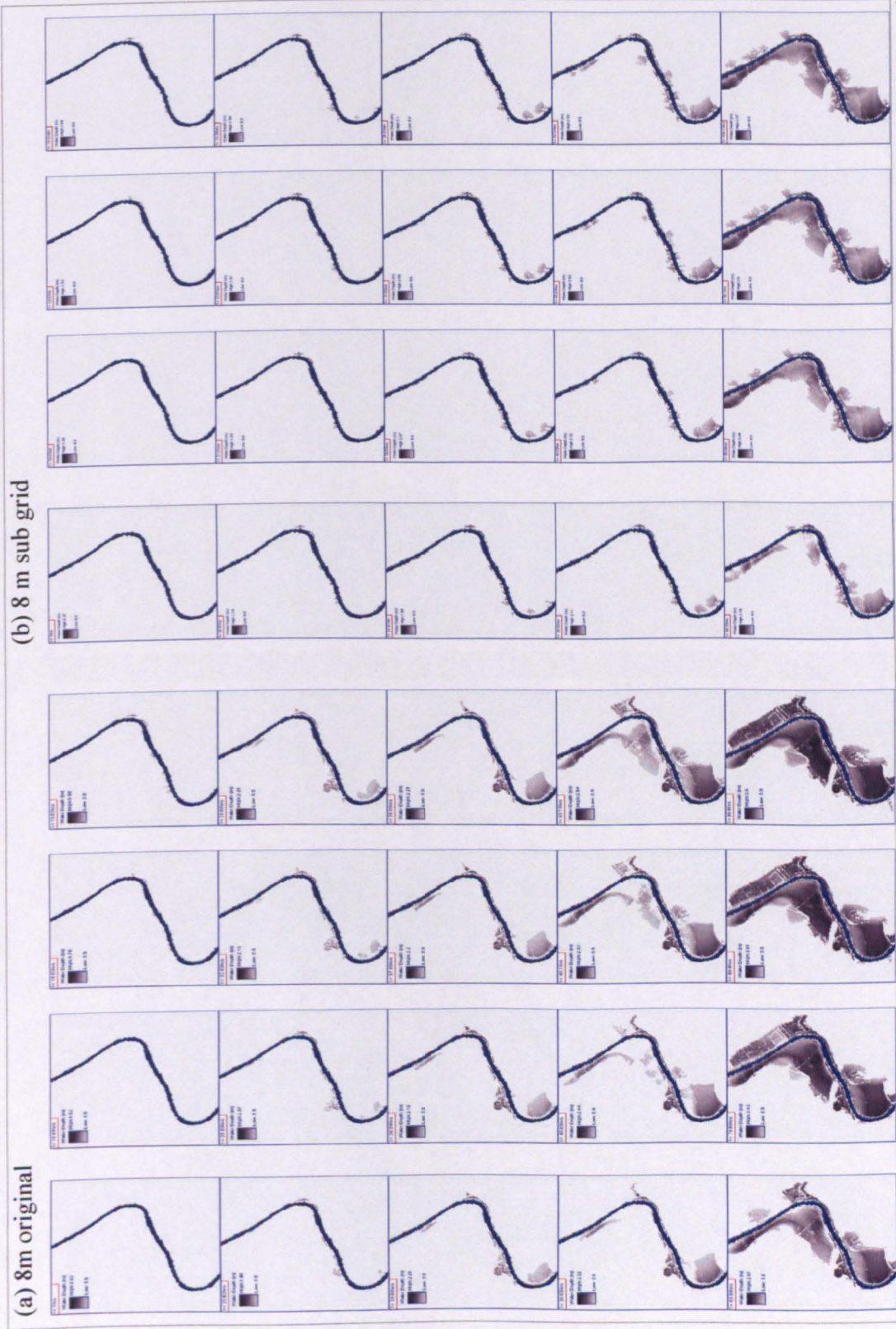


Figure 5.13: Comparison of the time series inundation extents in the first 100 hours for: (a) the original diffusion model; and (b) the sub grid treatment model; using an 8 m resolution DEM.

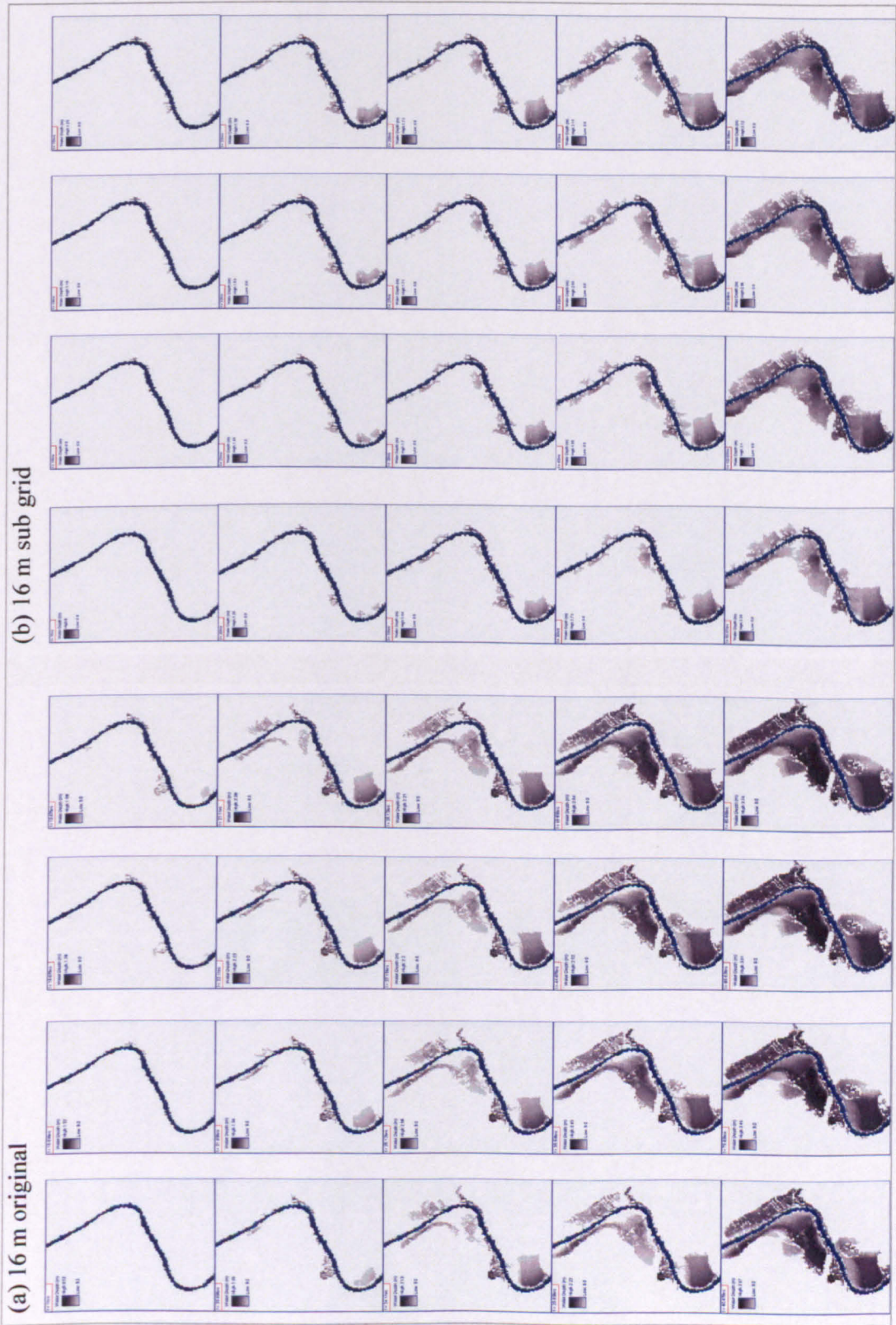


Figure 5.14: Comparison of the time series inundation extents in the first 100 hours for: (a) the original diffusion model; and (b) the sub grid treatment model; using a 16 m resolution DEM.

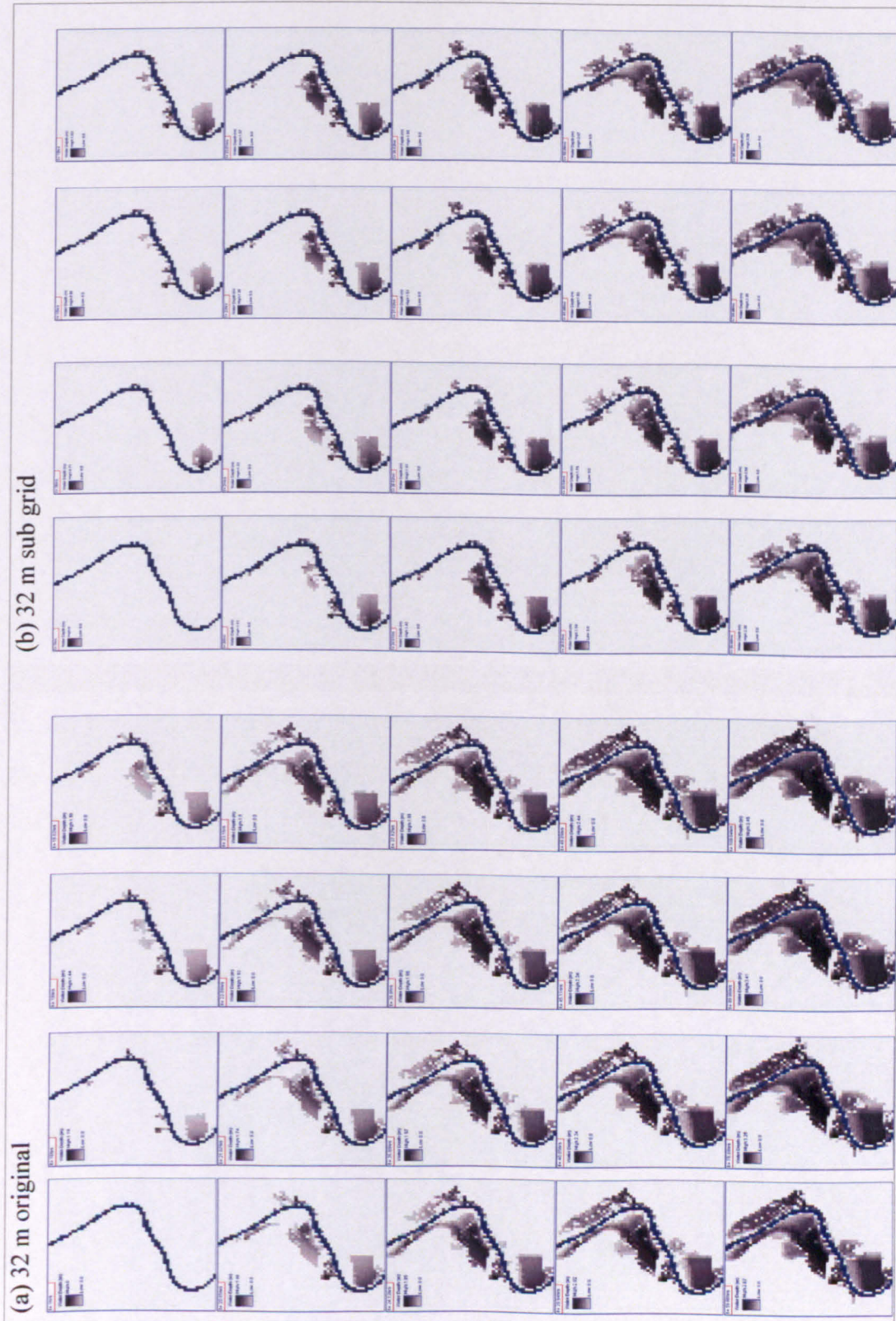


Figure 5.15: Comparison of the time series inundation extents in the first 100 hours for: (a) the original diffusion model; and (b) the sub grid treatment model; using a 32 m resolution DEM.

### 5.5.2 Result 2: Model validation

The inundation extents obtained using different mesh resolutions at the validation point are shown in Figure 5.17. This is compared with the results obtained from the normal treatment (reproduced from Figure 4.22) and with the aerial imagery shown in Figure 5.16. The validation aerial imagery is obtained from the same source as the one used in the Site 1 application and processed using the same procedures described in Section 3.6.1.



Figure 5.16: Aerial imagery used to validate the model performance of the Site 2 application (reproduced from Figure 4.22a).

Visual comparison of the inundation extents shown in Figure 5.17 suggests that, in terms of the inundation extent, there is not much difference between the normal and the sub grid-scale wetting treatment for the same mesh simulation at the validation point. Quantitative evaluation of the model performance was undertaken for the sub grid-scale treatment and the results are shown in Table 5.3, compared with the accuracy statistics obtained using the normal wetting treatment approach. This is obtained using the accuracy assessment approach presented in Section 3.6.

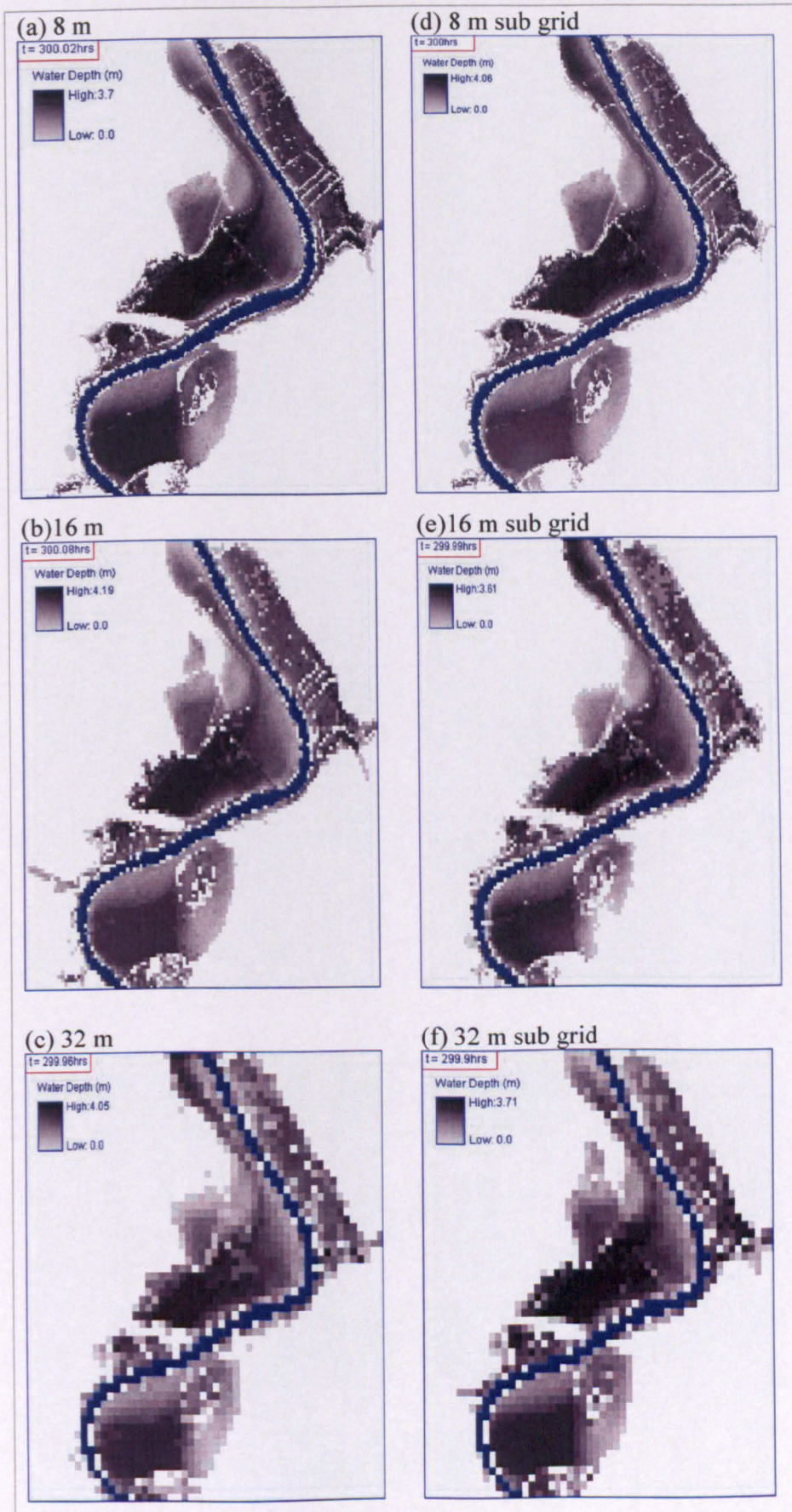


Figure 5.17: Predicted inundation extents obtained with the sub grid-scale treatment using different model resolutions at the time when the validation data was acquired (around 300 hrs into the flood event): (a) validation data; (b) 8 m; (c) 16 m; and (d) 32 m.

Table 5.3: Accuracy assessment based upon model predictions with different mesh resolutions and with and without the sub grid treatment. The validation data are based upon remotely-sensed imagery obtained at 300 hours into the flood event (Site 2).

	8 m	16 m	32 m	8 m sub grid-scale treatment	16 m sub grid-scale treatment	32 m sub grid-scale treatment
Overall accuracy	0.93	0.91	0.89	0.92	0.92	0.88
Kappa	0.85	0.83	0.80	0.88	0.83	0.79
<i>F</i>	0.85	0.82	0.78	0.86	0.85	0.81
Conditional Kappa for wet areas	0.91	0.85	0.74	0.90	0.88	0.78

Accuracy statistics confirms the visual comparison in Figure 5.16. The improvement of the sub grid-scale wetting treatment is not as obvious as shown in the Site 1 application. The *F* statistics and overall accuracy show some improvement for all the sub grid treatments. However, a sub grid-scale mesh simulation does not perform better than its immediate finer mesh simulation in terms of the overall accuracy and the *F* statistics, though the difference is only 2%. In terms of the other accuracy statistics, the sub grid-scale treatment also underperforms its immediate finer mesh simulations. This should be interpreted with caution and probably is due to the bias that is inherent in the way the model evaluates the wetting status of a grid cell (§3.6.2 and §5.3.3).

### 5.5.3 Computational performance of the sub grid wetting treatment

One major concern of flood inundation modelling with high-resolution DEMs is computational constraints. Memory usage is normally a function of the number of grid cells used to represent the topography. Thus, a simulation with a finer mesh takes longer than that with a coarser mesh. For the sub grid-scale wetting treatment, the number of cells that need to be evaluated at each time step is the same as that of the normal wetting treatment with the same cell size. The only difference is that the sub grid-scale wetting treatment approach needs to iterate through the sub grid cells in a model cell. It is necessary to look at the computational performance of the sub grid treatment by comparing it with the normal wetting treatment using the same mesh as well as using an immediate finer or coarser mesh. For this purpose, the simulations carried out in Section 5.5.1 were used for comparison. These include simulations with different mesh resolutions (8 m, 16 m and 32 m), with a normal wetting treatment and a sub grid-scale wetting treatment respectively. All the simulations were carried out on computers with the same specification (Pentium IV running at 3.0GHz). The average time (millisecond) used to simulate one second of the flood event for each simulation is plotted in Figure 5.18. This shows the performance statistics throughout the first 300 hours.

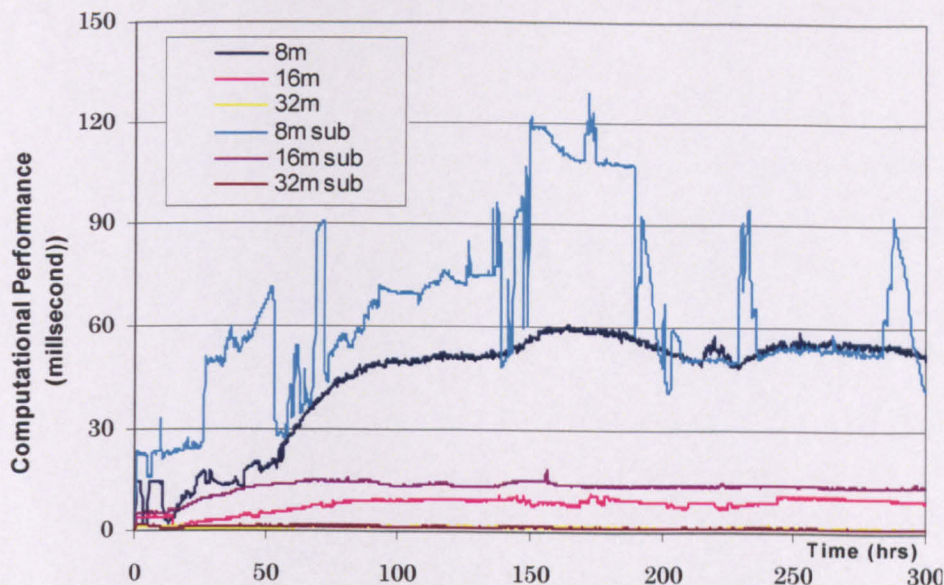


Figure 5.18: Computational performance of the simulations using different mesh resolutions for both the sub grid-scale and normal wetting treatments.

The total time used to simulate the 300-hour flood event used in the model for each simulation is shown in Table 5.4. Figure 5.18 suggests that, with the normal wetting treatment, the computational performance of the 8 m simulation is significantly slower than that of the 32 m simulation. The time that is needed to simulate one second of the flood event increases dramatically from below 2.5 milliseconds in the 32 simulation to around 60 milliseconds for the 8 m simulation during the peak computational period. This is due to the large numbers of grid cells involved in the 8 m simulations. The performance of the 16 m simulation lies in between the 8 m and 32 m simulations. In terms of the sub grid-scale treatment, the graph shows that the computational performance of the sub grid-scale treatment is more computationally efficient than its immediate finer mesh simulation (on a 2:1 coarsening ratio), particular for the finer mesh simulation. The computational performance curve for most simulations shows a smooth pattern, except for the 8 m sub grid-scale treatment which has abrupt changes in computational performance during certain periods of the simulation.

Table 5.4: The total computational time used to simulate the flood event for simulations with different mesh resolution and wetting treatment.

	8 m	16 m	32 m	8 m sub	16 m sub	32 m sub
Length of simulation (hours)	14.7	2.67	0.46	21.21	4.34	0.48

Given the run time in Table 5.3, the kind of uncertainty analysis reported by Aronica *et al.* (2002) ought to be possible. However, as the focus of thesis was coding the diffusion wave model, the sub-grid scale model and the coupled model from scratch (see Chapter 6), time did not permit this to be undertaken.

#### **5.5.4 Discussion of the Site 2 application**

In terms of flood inundation, results obtained from Site 2 using the sub grid-scale wetting treatment approach show a similar flood inundation response to those obtained from the Site 1 application (§5.4.1). With the sub grid-scale treatment, the rate of flood inundation is reduced for all mesh simulations. It appears that the effect of sub grid-scale wetting treatment is more effective for a coarser mesh simulation.

Model validation suggests that the sub grid-scale wetting treatment also improves the accuracy statistics in the majority of accuracy categories. However, the level of improvement in terms of the accuracy statistics is not as high as that found for Site 1. This is expected as the floodplain is laterally confined and even the normal treatment gives quite high accuracy statistics (§4.6). It suggests that the relative performance of the sub grid-scale approach as compared with the normal treatment is dependent upon the relationship between the floodplain configuration and the size of the flood event being considered (see §4.6.3). With the 2000 flood event, the flow remains laterally confined (Figure 5.16) such that the sub grid-scale treatment the sub grid-scale treatment did not lead to a major improvement as compared with the default treatment, at least at the validation point. However, the at-a-point in time data may not be effective at distinguishing between different model realisations as noted in Chapter 4 (§4.5.4 and §4.6.3).

The performance of the sub grid-scale wetting treatment shows that, compared with its immediate finer mesh simulation on a 2:1 coarsening ratio (e.g. 32 m sub grid-scale simulation compared with a 16 m normal simulation), the sub grid-scale wetting treatment is more computationally efficient.

One reason for the reduced flow propagation rate on the floodplain might be due to the reduced amount of flux from the river to the floodplain. In other words, if the amount of water routing from the river to the floodplain is less in the sub grid-scale treatment than with the normal treatment, the flow routing rate might be slower and the inundation extent might be smaller than its counterpart. This is not a concern in the sub grid-scale treatment used in this study as the bank cells which receive flux from the river use the sub grid-scale treatment use the normal treatment to calculate the water depth in the cell. In this way, the effective water depth, and thus the flux from a river cell to a bank cell, is roughly the same if the effect of back flow from the floodplain is considered. With the effect of floodplain routing, there might be differences in the water surface elevation of the bank cells. This might cause the amount of flux that can enter from the river to vary between the sub grid-scale and the normal treatment,

and also for simulations with different mesh sizes. This was investigated in this application and the amount of total flux received from the river to the floodplain is found to be minor when the sub grid-scale and the normal treatment are compared.

The computational performance of the 8 m simulations with and without sub grid-scale treatment is significantly worse than the other simulations. The difference between the 32 m normal and sub grid-scale treatment is minor compared with the 8 and 16 m simulations.

## **5.6 Conclusion**

This chapter has described and tested a treatment for representation of the effects of topographic variability at the sub mesh scale at two application sites on the River Ouse. This approach is based upon explicit representation of sub grid-scale topographic effects through treatment of both sub grid blockage and flux effects. The method is developed for situations where topographic data are available for 2 x 2 sub grid cells within each coarser mesh cell. Future developments of these methods will involve dealing with situations where the number of sub grid cells is greater. Results from Site 1 application suggest that, when using a coarser mesh, this treatment is much more effective than optimization using Manning's  $n$ , in terms of both: (i) validation data derived from aerial imagery at a single point on the falling limb of the hydrograph; and (ii) recovering the inundated area-time plot obtained with a finer resolution mesh. Further testing of this approach in Site 2 confirms the finding from Site 1, although lateral confinement at Site 2 significantly reduced the effects of the sub-grid treatment. As the ease with which topographic data are measured and processed is progressively increased, this type of approach should allow diffusion wave models to be applied over very long river reaches whilst making use of the high-resolution of topographic data that can now be acquired.

# Chapter 6

## Coupling of a 1D solution of the St. Venant equations to the 2D diffusion wave model

### 6.1 Introduction

The applications described in Chapter 4 and 5 were carried out using the loosely coupled version of the model (§3.3) where an existing 1D river flow model was used to calculate the stage hydrograph in the river channel as boundary condition along the river for the floodplain model (§3.8.1).

Though the loosely coupled model allows water from the floodplain to leave the domain through comparison of the water surface elevations between the river bank cells and river cells, this approach does not account for the effects of return floodplain on flow in the 1D river flow model. Thus, there is an effective mass balance error as floodplain leaving water is explicitly removed from the solution. Floodplain flow may change the way waters flow back into the river. This is concerned with both the direction and the timing of the floodplain flow back into the river. Furthermore, in a more general sense, the return water does not affect river flow explicitly. To address these issues, this chapter couples a river flow model with a 1D solution of the full form of the St. Venant equations and the 2D floodplain flow model described in Chapter 4 and Chapter 5.

This chapter describes the 1D river flow model in terms of its process representation, discretization, and numerical solution. The approach to the coupling of the 1D river flow model to the 2D floodplain model is then described. The tightly-coupled model was tested on a 10 km long river reach across the city centre of York on the River Ouse. Stage predictions at the upstream of the river were validated against the recorded stage and inundation extents were validated against the aerial imagery at Site 3.

## 6.2 Chapter aims and objectives

Based on the understanding obtained from the applications carried out in Chapter 4 and Chapter 5, the aim of this chapter is to develop and to test an approach that couples a 1D river flow model to the 2D floodplain model used in the last few chapters. This involves, in the first place, the development of the 1D river flow model. The discretization and solution of the 1D model in a 2D environment for coupling purposes is then addressed. This requires calculation of the exchange of flow at the common boundary of the river-floodplain system. The effect of this exchange of water upon floodplain flow has been investigated in the last few Chapters in the loosely-coupled version of the model. The objectives of this chapter include: (i) to use the tightly-coupled model to investigate the effect that return flow from the floodplain has upon river flow; and (ii) to compare the predicted inundation extent with that obtained using the loosely-coupled model.

## 6.3 Model description

The tightly-coupled model consists of two sub models: a 1D river flow model; and a 2D floodplain flow model. The 2D floodplain flow model was described and tested in Chapters 3, 4 and 5. This section describes the 1D river flow model in terms of its process representation, discretization and solution (§6.3.1), the approach to coupling the 1D river flow model to the 2D floodplain flow model (§6.3.2) and the model Graphic User Interface (GUI) (§6.3.3).

### 6.3.1 1D model process representation, discretization and solution

The 1D river flow model presented here is based upon the fixed bed model of Abbott and Basco (1989). The model solves the one-dimensional St. Venant equations for unsteady flow using the Preissmann Scheme. The Preissmann Scheme is also known as an implicit box scheme because of the way it approximates the hydraulic variables. This model involves a number of assumptions. These include that: (i) the flow is one-dimensional so that variation of water depth and velocity within the cross-section can be ignored; (ii) the flow is hydrostatic (i.e. vertical acceleration is negligible and streamline curvature is small); and (iii) boundary friction and turbulence can be represented by channel conveyance rules derived from steady state flow using uniform flow equations such as the Manning equation or Chézy equation. The respective mass and momentum conservation forms of the equations are:

$$\frac{\partial h}{\partial t} + h \frac{\partial u}{\partial x} + u \frac{\partial h}{\partial x} = 0 \quad (6.1)$$

$$\frac{\partial u}{\partial t} + u \frac{\partial u}{\partial x} + g \frac{\partial h}{\partial x} = 0 \quad (6.2)$$

where  $h$  is water depth,  $u$  is velocity,  $x$  is the increment over space,  $t$  is the increment over time, and  $g$  is acceleration due to gravity. The Preissmann Scheme approximates  $u$  and  $h$  as:

$$\frac{\partial h}{\partial t} = (1 - \psi) \frac{h_j^{n+1} - h_j^n}{\Delta t} + \psi \frac{h_{j+1}^{n+1} - h_{j+1}^n}{\Delta t} \quad (6.3a)$$

$$\frac{\partial u}{\partial t} = (1 - \psi) \frac{u_j^{n+1} - u_j^n}{\Delta t} + \psi \frac{u_{j+1}^{n+1} - u_{j+1}^n}{\Delta t} \quad (6.3b)$$

$$\frac{\partial u}{\partial x} = (1 - \theta) \frac{u_{j+1}^n - u_j^n}{\Delta x} + \theta \frac{u_{j+1}^{n+1} - u_j^{n+1}}{\Delta x} \quad (6.3c)$$

$$\frac{\partial h}{\partial x} = (1 - \theta) \frac{h_{j+1}^n - h_j^n}{\Delta x} + \theta \frac{h_{j+1}^{n+1} - h_j^{n+1}}{\Delta x} \quad (6.3d)$$

$$h = \frac{h_j^{n+1} + h_{j+1}^{n+1} + h_j^n + h_{j+1}^n}{4} \quad (6.3e)$$

$$u = \frac{u_j^{n+1} + u_{j+1}^{n+1} + u_j^n + u_{j+1}^n}{4} \quad (6.3f)$$

where  $\psi$  (for  $0 \leq \psi \leq 1$ ) and  $\theta$  (for  $0 \leq \theta \leq 1$ ) are weighting coefficients in time and space respectively, and  $n$  and  $j$  are the time and space indices respectively. The weighting coefficients ( $\psi$  and  $\theta$ ) are used to provide model flexibility with respect to numerical stability and solution convergence. For example, taking  $\psi = 1/2$  gives an averaged time derivative at the space address  $j+1/2$  and, similarly, when  $\theta = 1/2$ , the space derivative is centred at the time address  $n+1/2$ . These equations are formed without considering the influence of the boundary. When the boundary shear stresses are incorporated, the local bed slope ( $S_0$ , as an energy source) and the slope of the energy grade line ( $S_f$  as essentially an energy sink) are introduced into the momentum conservation equation (6.2). (6.2) is rewritten as:

$$\frac{\partial u}{\partial t} + u \frac{\partial u}{\partial x} + g \frac{\partial h}{\partial x} = gS_0 - gS_f \quad (6.4)$$

where:

$$S_0 = -\frac{\partial z}{\partial x} = -\frac{1}{2\Delta x} (z_{j+1}^{n+1} + z_{j+1}^n - z_j^{n+1} - z_j^n) \quad (6.5a)$$

If there is no change in bed slope throughout time (i.e.  $n = n+1$ ) then (6.5a) is simplified to (6.5b)

$$S_0 = -\frac{\partial z}{\partial x} = -\frac{1}{\Delta x}(z_{j+1} - z_j) \quad (6.5b)$$

In this case,  $S_0$  is evaluated using a forward difference method. It can also be evaluated as a central difference:

$$S_0 = -\frac{\partial z}{\partial x} = -\frac{1}{2\Delta x}(z_{j+1} - z_{j-1}) \quad (6.6c)$$

For the evaluation of the boundary shear stress, the de Chézy resistance law is taken, giving the following approximation:

$$gS_f = g \frac{u|u|}{C_c^2 h} \quad (6.6d)$$

where:

$C_c^2$  = Chézy resistance coefficient

$$S_f = \frac{u|u|}{C_c^2 h} = \frac{4}{C_c^2 h} \left| \frac{u_j^n + u_{j+1}^n}{2} \right| \left( \frac{u_j^{n+1} + u_{j+1}^{n+1}}{2} \right) = \frac{|u_j^n + u_{j+1}^n| (u_j^{n+1} + u_{j+1}^{n+1})}{C_c^2 (h_j^{n+1} + h_{j+1}^{n+1} + h_j^n + h_{j+1}^n)} \quad (6.7)$$

This is the discretization derived from the Preissmann scheme for the approximation of  $S_f$ . Strict approximation from the Preissmann scheme should also include discretization of the Chézy resistance coefficient, which yields:

$$S_f = \frac{4|u_j^n + u_{j+1}^n| (u_j^{n+1} + u_{j+1}^{n+1})}{((C_c^2)_j^n + (C_c^2)_{j+1}^{n+1} + (C_c^2)_{j+1}^n + (C_c^2)_j^{n+1}) (h_j^{n+1} + h_{j+1}^{n+1} + h_j^n + h_{j+1}^n)} \quad (6.8)$$

Substituting all the above approximations into equation (6.1) and (6.4) yields:

$$\begin{aligned}
 & (1-\psi) \frac{u_j^{n+1} - u_j^n}{\Delta t} + \psi \frac{u_{j+1}^{n+1} - u_{j+1}^n}{\Delta t} \\
 & + \frac{u_j^{n+1} + u_{j+1}^{n+1} + u_j^n + u_{j+1}^n}{4} \left( (1-\theta) \frac{u_{j+1}^n - u_j^n}{\Delta x} + \theta \frac{u_{j+1}^{n+1} - u_j^{n+1}}{\Delta x} \right) \\
 & + g \left( (1-\theta) \frac{h_{j+1}^n - h_j^n}{\Delta x} + \theta \frac{h_{j+1}^{n+1} - h_j^{n+1}}{\Delta x} \right) \\
 & = \frac{g}{2\Delta x} (z_{j+1}^{n+1} + z_{j+1}^n - z_j^{n+1} - z_j^n) \\
 & - \frac{4g|u_j^n + u_{j+1}^n|(u_j^{n+1} + u_{j+1}^{n+1})}{((C_c^2)_j^n + (C_c^2)_j^{n+1} + (C_c^2)_{j+1}^n + (C_c^2)_{j+1}^{n+1})(h_j^{n+1} + h_{j+1}^{n+1} + h_j^n + h_{j+1}^n)}
 \end{aligned} \tag{6.9a}$$

$$\begin{aligned}
 & (1-\psi) \frac{h_j^{n+1} - h_j^n}{\Delta t} + \psi \frac{h_{j+1}^{n+1} - h_{j+1}^n}{\Delta t} \\
 & + \frac{h_j^{n+1} + h_{j+1}^{n+1} + h_j^n + h_{j+1}^n}{4} \left( (1-\theta) \frac{u_{j+1}^n - u_j^n}{\Delta x} + \theta \frac{u_{j+1}^{n+1} - u_j^{n+1}}{\Delta x} \right) \\
 & + \frac{u_j^{n+1} + u_{j+1}^{n+1} + u_j^n + u_{j+1}^n}{4} \left( (1-\theta) \frac{h_{j+1}^n - h_j^n}{\Delta x} + \theta \frac{h_{j+1}^{n+1} - h_j^{n+1}}{\Delta x} \right) = 0
 \end{aligned} \tag{6.9b}$$

Rearranging and collecting all the high time level terms on the left side of the equations gives

$$A1u_j^{n+1} + B1h_j^{n+1} + C1u_{j+1}^{n+1} + Dh_{j+1}^{n+1} = E1 \tag{6.10a}$$

$$A2u_j^{n+1} + B2h_j^{n+1} + C2u_{j+1}^{n+1} + D2h_{j+1}^{n+1} = E2 \tag{6.10b}$$

where:

$$A1 = \left[ \frac{1-\psi}{\Delta t} - \frac{\theta(u_{j+1}^{n+1} + u_{j+1}^n + u_j^{n+1} + u_j^n)}{4\Delta x} \right] + \frac{4g|u_j^n + u_{j+1}^n|}{((C_c^2)_j^n + (C_c^2)_j^{n+1} + (C_c^2)_{j+1}^n + (C_c^2)_{j+1}^{n+1})(h_j^{n+1} + h_{j+1}^{n+1} + h_j^n + h_{j+1}^n)} \tag{6.11a}$$

$$A2 = -\frac{\theta(h_{j+1}^{n+1} + h_{j+1}^n + h_j^{n+1} + h_j^n)}{4\Delta x} \quad (6.11b)$$

$$B1 = -\frac{\theta g}{\Delta x} \quad (6.11c)$$

$$B2 = \frac{1-\psi}{\Delta t} - \frac{\theta(u_{j+1}^{n+1} + u_{j+1}^n + u_j^{n+1} + u_j^n)}{4\Delta x} \quad (6.11d)$$

$$C1 = \left[ \begin{array}{c} \frac{\psi}{\Delta t} + \frac{\theta(u_{j+1}^{n+1} + u_{j+1}^n + u_j^{n+1} + u_j^n)}{4\Delta x} \\ + \frac{4g|u_j^n + u_{j+1}^n|}{((C_c^2)_j^n + (C_c^2)_j^{n+1} + (C_c^2)_{j+1}^n + (C_c^2)_{j+1}^{n+1})(h_j^{n+1} + h_{j+1}^{n+1} + h_j^n + h_{j+1}^n)} \end{array} \right] \quad (6.11e)$$

$$C2 = \frac{\theta(h_{j+1}^{n+1} + h_{j+1}^n + h_j^{n+1} + h_j^n)}{4\Delta x} \quad (6.11f)$$

$$D1 = \frac{\theta g}{\Delta x} \quad (6.11g)$$

$$D2 = \frac{\psi}{\Delta t} + \frac{\theta(u_{j+1}^{n+1} + u_{j+1}^n + u_j^{n+1} + u_j^n)}{4\Delta x} \quad (6.11h)$$

$$\begin{aligned} E1 = & \left[ \frac{1-\psi}{\Delta t} + \frac{(1-\theta)(u_{j+1}^{n+1} + u_{j+1}^n + u_j^{n+1} + u_j^n)}{4\Delta x} \right] u_j^n \\ & + \left[ \frac{(1-\theta)g}{\Delta x} \right] h_j^n + \left[ \frac{\psi}{\Delta t} - \frac{(1-\theta)(u_{j+1}^{n+1} + u_{j+1}^n + u_j^{n+1} + u_j^n)}{4\Delta x} \right] u_{j+1}^n \\ & - \left[ \frac{(1-\theta)g}{\Delta x} \right] h_{j+1}^n + \left[ \frac{(1-\theta)g}{\Delta x} (z_{j+1}^{n+1} + z_{j+1}^n - z_j^{n+1} - z_j^n) \right] \end{aligned} \quad (6.11i)$$

$$\begin{aligned} E2 = & \left[ \frac{(1-\theta)(h_{j+1}^{n+1} + h_{j+1}^n + h_j^{n+1} + h_j^n)}{4\Delta x} \right] u_j^n \\ & + \left[ \frac{(1-\psi)}{\Delta t} + \frac{(1-\theta)(u_{j+1}^{n+1} + u_{j+1}^n + u_j^{n+1} + u_j^n)}{4\Delta x} \right] h_j^n - \left[ \frac{(1-\theta)(h_{j+1}^{n+1} + h_{j+1}^n + h_j^{n+1} + h_j^n)}{4\Delta x} \right] u_{j+1}^n \\ & + \left[ \frac{\psi}{\Delta t} - \frac{(1-\theta)(u_{j+1}^{n+1} + u_{j+1}^n + u_j^{n+1} + u_j^n)}{4\Delta x} \right] h_{j+1}^n \end{aligned} \quad (6.11j)$$

Application of the momentum and mass conservation expression (6.11a), (6.11b) at every spatial grid point leads to a system of non-linear algebraic equations, the linearity of which is embedded in coefficients  $A1, A2, B1, B2$ , etc.

With  $jj$  nodes, equation (6.11) can be represented using the pentadiagonal matrix below

$$\begin{bmatrix}
 A1_1 & B1_1 & C1_1 & D1_1 & 0 & 0 & 0 & 0 & 0 & 0 & 0 & 0 \\
 A2_1 & B2_1 & C2_1 & D2_1 & 0 & 0 & 0 & 0 & 0 & 0 & 0 & 0 \\
 0 & 0 & A1_2 & B1_2 & C1_2 & D1_2 & 0 & 0 & 0 & 0 & 0 & 0 \\
 0 & 0 & A2_2 & B2_2 & C2_2 & D2_2 & 0 & 0 & 0 & 0 & 0 & 0 \\
 0 & 0 & 0 & 0 & . & . & . & . & 0 & 0 & 0 & 0 \\
 0 & 0 & 0 & 0 & . & . & . & . & 0 & 0 & 0 & 0 \\
 0 & 0 & 0 & 0 & 0 & 0 & A1_{j-1} & B1_{j-1} & C1_{j-1} & D1_{j-1} & 0 & 0 \\
 0 & 0 & 0 & 0 & 0 & 0 & A1_{j-1} & B1_{j-1} & C1_{j-1} & D1_{j-1} & 0 & 0 \\
 0 & 0 & 0 & 0 & 0 & 0 & 0 & 0 & A1_j & B1_j & C1_j & D1_j \\
 0 & 0 & 0 & 0 & 0 & 0 & 0 & 0 & A1_j & B1_j & C1_j & D1_j
 \end{bmatrix}
 \begin{bmatrix}
 u_1 \\
 h_1 \\
 u_2 \\
 h_2 \\
 . \\
 . \\
 u_{j-1} \\
 h_{j-1} \\
 u_j \\
 h_j
 \end{bmatrix}^{n+1}
 =
 \begin{bmatrix}
 E1_1 \\
 E2_1 \\
 E1_2 \\
 E2_2 \\
 . \\
 . \\
 E2_{j-1} \\
 E2_{j-1} \\
 E1_j \\
 E2_j
 \end{bmatrix}
 \tag{6.12}$$

With the provision of an upstream and downstream boundary condition, an algebraic solution is possible for the above equations. Three principle solutions are available to solve the system of linearized equations: (i) matrix inversion; (ii) relaxation method and (iii) double sweep method. The first category of approaches is matrix inversion, which provides a direct solution of these equations. However the number of operations is then equal to  $N^3$ , or at best  $N^2$ , where  $N$  is the number of spatial grid points. Models with a fine resolution running over a large spatial scale using such methods can be unfeasible in terms of computational requirements. The second category of method is composed of iterative techniques that have come to be called 'relaxation methods' such as 'successive-over-relaxation' (SOR). The computational efforts required by these approaches remain considerable. However, they are usually of a lower order than necessitated by the use of direct selection methods. The third method is the double sweep method, which has been widely accepted as the most efficient way of solving both non-linear and linear equations (Abbott and Basco 1989). The number of operations is nearly proportional to the number of grid points.

The double sweep solution requires the formulation of an auxiliary relation. The solution depends on which boundary condition is known. Here, this method is illustrated assuming that the upstream boundary condition is known. When the velocity  $u$  is known as the upstream boundary condition with  $j=1$ , then the auxiliary relation can be formed as:

$$u_1^{n+1} = F1_1 h_1^{n+1} + G1_1 \quad (6.13)$$

where  $F1_j$  and  $G1_j$  are auxiliary variables that linearly relate  $h_j^{n+1}$  and  $u_j^{n+1}$ . Substituting equation (6.13) into equation (6.11) leads to

$$(A1F1_j + B1)h_j^{n+1} + C1u_{j+1}^{n+1} + D1h_{j+1}^{n+1} = E1 - A1G1_j \quad (6.14a)$$

and

$$(A2F1_j + B2)h_j^{n+1} + C2u_{j+1}^{n+1} + D2h_{j+1}^{n+1} = E2 - A2G1_j \quad (6.14b)$$

Eliminating  $h_j^{n+1}$  gives

$$\begin{aligned} & [(A2F1_j + B2)C1 - (A1F1_j + B1)C2]u_{j+1}^{n+1} \\ & + [(A2F1_j + B2)D1 - (A1F1_j + B1)D2]h_{j+1}^{n+1} \\ & = [(A2F1_j + B2)(E1 - A1G1_j) - (A1F1_j + B1)(E2 - A2G1_j)] \end{aligned} \quad (6.15)$$

where:

$$F1_{j+1} = - \frac{[(A2F1_j + B2)D1 - (A1F1_j + B1)D2]}{[(A2F1_j + B2)C1 - (A1F1_j + B1)C2]} \quad (6.16a)$$

and

$$G1_{j+1} = \frac{[(A2F1_j + B2)(E1 - A1G1_j) - (A1F1_j + B1)(E2 - A2G1_j)]}{[(A2F1_j + B2)C1 - (A1F1_j + B1)C2]} \quad (6.16b)$$

Equations (6.16a) and (6.16b) define a set of recurrence relations to calculate the initial sweep coefficients.  $F1_2, G1_2, F1_3, G1_3, \dots, F1_{jy}, G1_{jy}$ . Each successive pair only depends on the value of the previous pair. Thus, once the initial values  $F1_1, G1_1$  are defined, the double sweep method can proceed. This is achieved by taking  $F1_1$  to be zero, thus

$$G1_1 = u_1^{n+1} \quad (6.17)$$

by which time  $F1$  and  $G1$  can be evaluated at all subsequent points. We can begin the reverse sweep by picking up the end boundary data, in this case the downstream boundary data. We can use the following equation to initialize the return sweep

$$u_{jy}^{n+1} = F1_{jy} h_{jy}^{n+1} + G1_{jy} \quad (6.18)$$

To get the value of  $h_j^{n+1}$ , we need to use either equation (6.13a) or (6.13b). By convention, equation (6.13a) is used for the calculation. Rearranging equation (6.13a) we get

$$h_j^{n+1} = P1_j u_{j+1}^{n+1} + Q1_j h_{j+1}^{n+1} + R1_j \quad (6.19)$$

where:

$$P1_j = \frac{-C1}{(A1F1_j + B1)} \quad (6.20)$$

$$Q1_j = \frac{-D1}{(A1F1_j + B1)} \quad (6.21)$$

$$R1_j = \frac{E1 - A1G1_j}{(A1F1_j + B1)} \quad (6.22)$$

Equations (6.18) and (6.19) are then implemented sequentially, moving upstream, finishing the return sweep when the upstream boundary is reached. Thus, all unknowns have been evaluated.

One more issue that needs to be addressed is the convergence of the model. Convergence is a mathematical concept in the case of a sequence of numbers. In the case of modelling, convergence refers to how the sequences of solutions of discrete, finite-difference equations approach the true solution of the continuum, differential equations. Convergence criteria need to be specified in a model to end the iterative simulation. In this model, the convergence criteria are set using equation (6.23):

$$\omega = \frac{Q_i \Delta t - Q_j \Delta t}{Q_i \Delta t} < 0.1\% \quad (6.23)$$

where  $Q_i$  and  $Q_j$  refer to mass going inside and outside of a control volume respectively.

$\Delta t$  refers to the time step defined in the equation. In summary, a sample solution to the Preissmann Scheme using Java is shown in Figure 6.1.

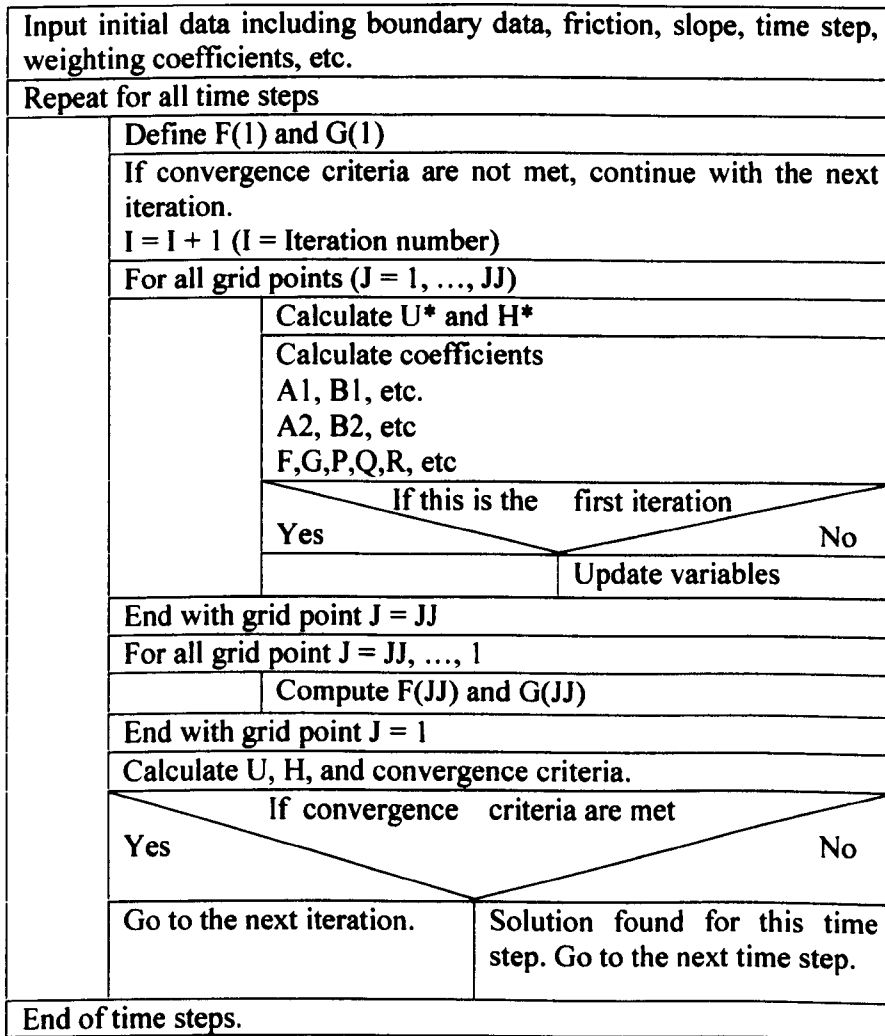


Figure 6.1: A sample solution to the Preissman Scheme using Java.

### 6.3.2 Model coupling

Both the loosely coupled and the tightly-coupled models assume that the floodplain is protected by an embankment that essentially acts as a continuous, broad-crested weir. These two models differ in the way the exchange of flux between the river channel and the floodplain is treated. As described in Chapter 3, in the loosely coupled model, flux from the river channel to the floodplain is calculated using a weir equation (§4.14), while flux from the floodplain to the river channel is calculated using the Manning equation. However, return water from the floodplain to the river channel has no effect upon the 1D river flow. In the loosely coupled model, the inflow at the river-floodplain boundary is calculated before the initialization of the floodplain flow model using an existing 1D river flow model. Return flow from the floodplain to the river channel is simply calculated as mass loss from the 2D model at the river-floodplain boundary (§3.2).

There are a number of limitations in the way the loosely coupled model is formulated. First, the use of uniform flow in the river channel is likely to introduce errors to the model. Though

options exist for non-uniform inflow for the 2D floodplain model, the applications carried out in the last three chapters have been using a uniform stage hydrograph for the whole river reach. This approximation may not be appropriate in situations where abrupt changes in water depth occur e.g. curved channels as in Site 1 and 2 applications. However, the major limitation of the loosely coupled model is that it fails to recognize that floodplain flow routing may change the way the water returns to the river channel and, hence, change flow behaviour in the river channel.

The tightly-coupled model seeks to couple floodplain and river flows by establishing this connection. This is carried out by solving the 1D river flow model in the raster-based environment where the 2D floodplain model is discretized and solved. The river channel in the 1D river model is represented by continuous cells in the grid environment that represents the floodplain where the 2D floodplain model is discretized and solved. The location of the river in the 1D model is the same as that of the river channel represented in the 2D floodplain model. Thus, river width will always be the multiples of cell size. Cells on the floodplain that represent the river channel are assigned different reaches according to the locations of the cross-section. The geometry of the reach is assumed to be uniform for each individual reach. The cross-section, which describes the geometry of the individual reach is located at the upstream of the reach. The tightly-coupled model starts its computation from the 1D model which calculates water level for each reach based on its boundary condition. In the next time step, the 2D floodplain model evaluates the water surface slopes of the river-floodplain boundary cells in the river channel in the simulation domain. If a positive slope exists between a river cell and its adjacent floodplain cell(s), the flow is calculated using the weir equation (equation 4.14). At this time step, there is no return water from the floodplain to the river channel and thus there is no floodplain routing calculation. The model continues with the 1D river flow calculation where the water level for each reach is re-evaluated. Inflow from the river channel to the floodplain is calculated in the same way as in the last time step. Floodplain routing calculations start once there are wet floodplain cells on the floodplain. If return water from the floodplain to the river channel occurs for a particular river reach at one time step, the water level of that reach is recalculated. The calculation of the water level is based upon mass conservation. The total volume of return water from the floodplain to the river channel is calculated for each reach at each time step. Positive return water value causes a change in the water depth for the river reach. The change in water depth for a particular river reach is calculated using:

$$\Delta d = \frac{V}{A} \tag{6.24}$$

where  $V$  is the volume of return water from the floodplain to the river channel and  $A$  is the horizontal area of the river reach. The area of river reach can be calculated either from the river cross-section geometry or simply by calculating the number of the grid cells in this reach. This recalculated water level, instead of the one calculated solely from the 1D model in this time step, is used as the boundary data in the 1D river flow model for the calculation of the water level at the next time step. This is summarized in Figure 6.2.

The control on time step is an import factor for the stability of the coupled model. In the 2D model, time step is calculated based upon the Courant condition (§4.3.1). As the Preissmann Scheme that is used to solve the 1D river flow model is weakly stable for  $0.5 < \theta < 0.6$  and strongly stable for  $0.6 < \theta < 1.0$  (Abbott and Basco, 1989), the time step cannot generally provide a constraint for the 1D river flow model on its own. Simulations using the 1D river model alone confirm this. However, as the coupled model has a common boundary for the 1D and 2D sub models and there are flux exchanges at this boundary, time step becomes crucial for the stability of the coupled model. This matters in two aspects: (i) if, given a time step, too much flux was routed from the river channel to the floodplain for a reach, the water depth at this reach might decrease too much.; and (ii) if too much flux is routed from the floodplain to a reach, the water depth at this reach might increase too much. Both of these affect the stability of the river flow model. Thus, in the coupled model, the calculated time step based upon the Courant number is scaled by 0.8 at each time step. This guarantees the stability of the model but at the expense of lowered computational performance.

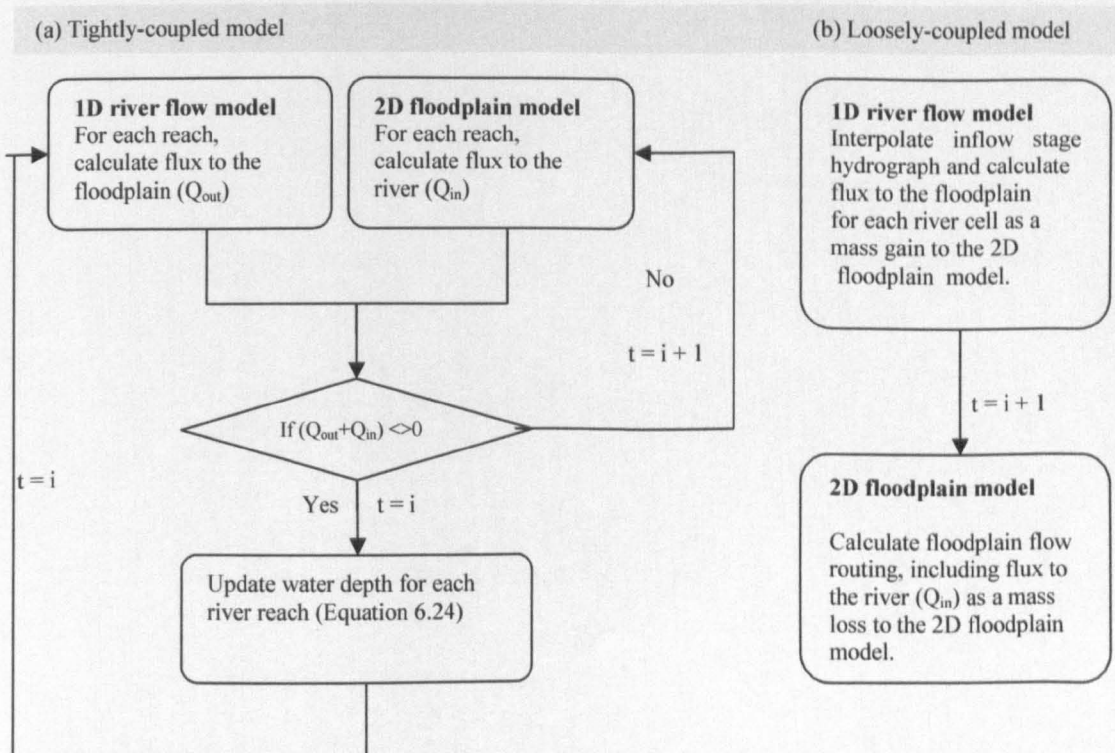


Figure 6.2: Comparison of the solution sequence for the loosely- and tightly-coupled models.

### 6.3.3 Model Graphic User Interface (GUI)

The tightly-coupled model can be activated from the main user interface (Figure 4.2) of the model. This opens another dialogue (Figure 6.3) through which the 1D river flow model and the 2D floodplain model are configured. The configuration of the 2D model in the tightly-coupled model is similar to that shown in the loosely coupled version of the model (§4.4) except that there is no need to define the input hydrograph in the river channel as it is coupled tightly with the 1D river flow model which provides the inflow data.

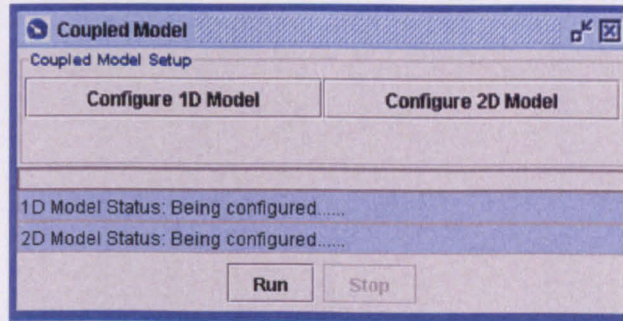


Figure 6.3: Tightly coupled model main configuration frame

Configuration of the 1D model is carried out using the panel shown in Figure 6.4. The 1D river flow model described above requires that either the depth at the upstream and velocity at the downstream or depth at the downstream and velocity at the upstream be specified as boundary conditions. This can be specified from the “Boundary conditions” panel. The Preissmann’s scheme requires that the boundary condition data be either (i) velocity upstream and stage downstream; or (ii) velocity downstream and stage upstream. This panel also provides options for calculating water depth and velocity using discharge hydrograph and other necessary input data. For example, if upstream stage and downstream discharge instead of velocity are available, the model provides an option to calculate downstream velocity using the available flow data and cross-section geometry. The “Basic input/output” panel defines the sources of these boundary input data, the location of the model output and the geometry of cross-sections. Boundary input data are of ASCII format. Cross-sections geometry is defined in the dialogue (Figure 6.5) activated from the “cross-sections” button.

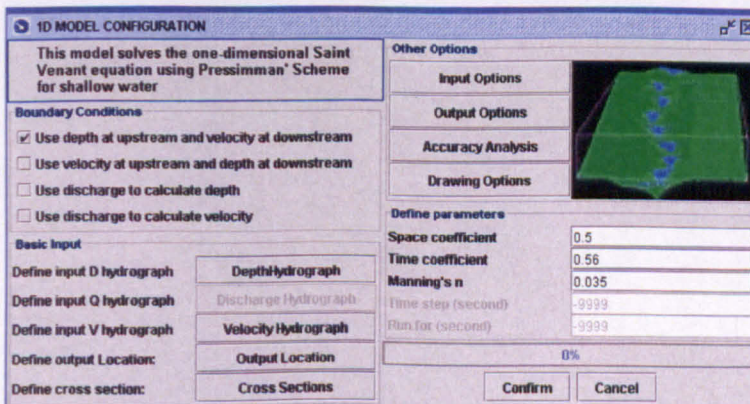


Figure 6.4: 1D river flow model main configuration frame.

The location of the river and cross-sections are defined from the “location” button and this is displayed in the canvas on the right of the dialogue box. The number of cross-sections is calculated from this input. The length of each river reach and the associated roughness coefficient are entered accordingly. The geometry of each cross-section is defined using a series of points according to the shape of the cross-section specified in this dialogue box.

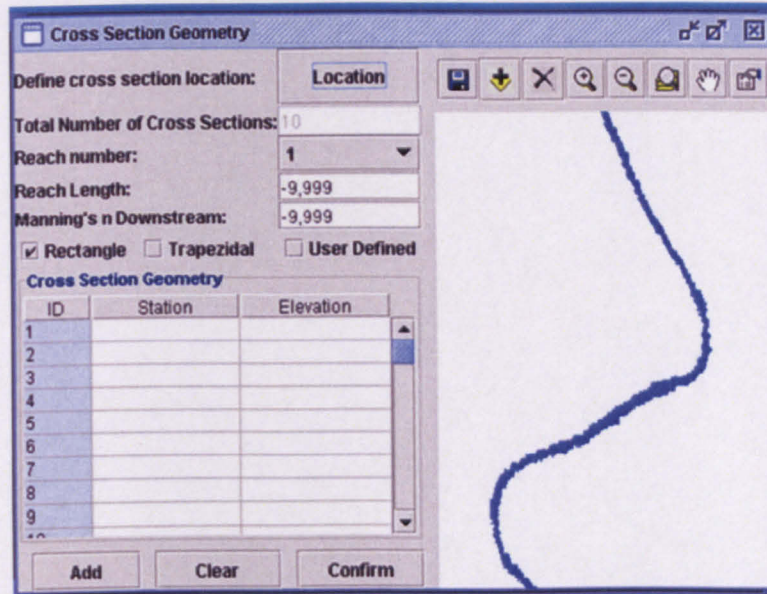


Figure 6.5: Frame for defining cross-section geometry.

After the 1D and 2D models are configured, the coupled model can be run and the visualization of the flood inundation process is shown in the main interface (Figure 4.2).

#### 6.4 Model application: data processing

The tightly-coupled model was tested in a longer reach on the River Ouse (Figure 6.6) extended across the city centre of York. It extends from the upstream boundary of the Site 3 (Figure 3.2) further upstream to Skelton Gauging Station and from the downstream boundary of Site 3 further downstream until the A64 Road Bridge at Site 2 (Figure 3.2). Thus, this Site covers the whole reach of Site 3 and the upstream part of Site 2. The reach commences in a rural setting upstream of the city of York. Downstream, the river runs through the city of York, which is highly urbanized, with dense commercial and residential properties within a short distance of the river bank. Further downstream, the river setting becomes more rural. This provides a chance to check the model predictions at Site 3 again where the model performance was found to be relatively poor, particularly in the upstream reach (§4.6.2). The river is around 10 km long and this Site is shown in Figure 6.6 using LiDAR data. The flood event simulated in this application has been described in Chapter 3 (§4.5).

Data requirements, availability and processing for the loosely coupled model were described in Chapter 3. This section describes the relevant issues for the tightly-coupled model. The data requirements and availability for the tightly-coupled model are summarised in Table 6.1.

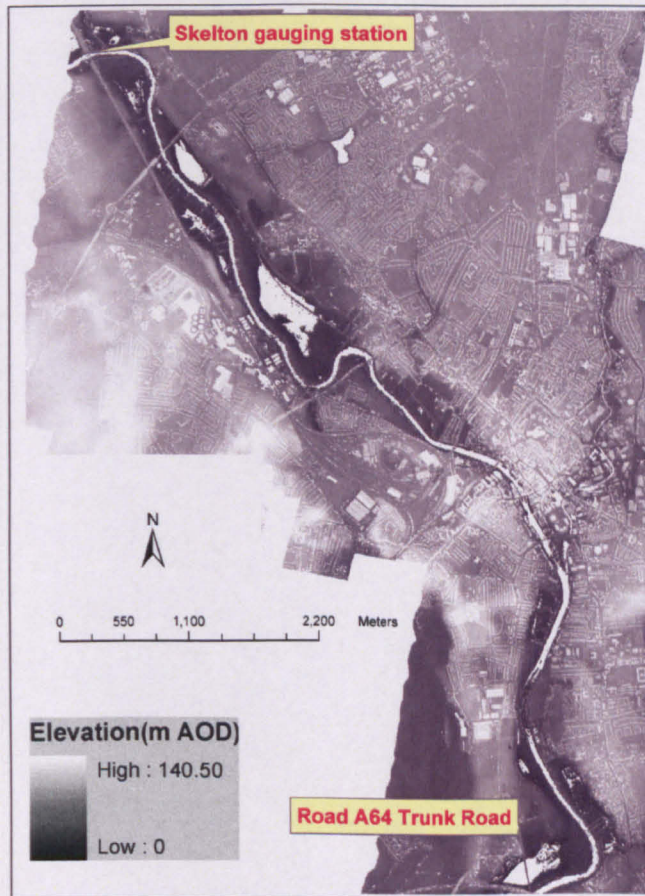


Figure 6.6: Location of the application of the tightly-coupled model on the river Ouse.

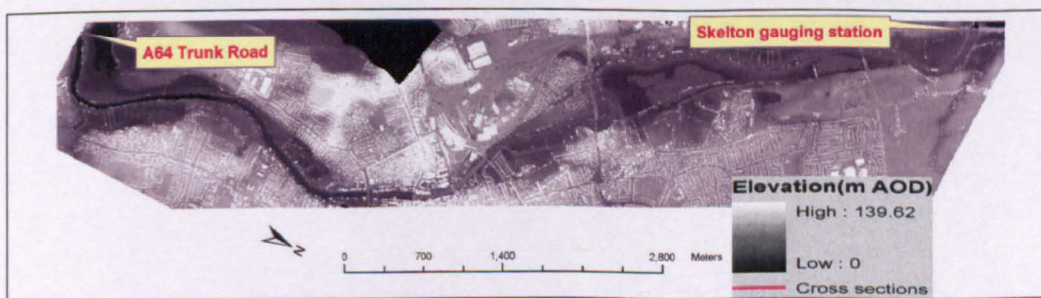


Figure 6.7: DEM derived from LiDAR data for the long reach simulation using the tightly-coupled model.

The data required by the 2D floodplain sub model in the tightly-coupled model include floodplain topography, stage hydrograph along the river-floodplain boundary and floodplain roughness. In terms of the floodplain topography, the application presented here used the same topographic data source as that used in the loosely coupled model, i.e. LiDAR data. Topographic data processing followed the same procedures as these described in Chapter 3 (§3.7). The 8 m DEM derived from the LiDAR data is shown in Figure 6.7, with the location

of the river channel shown in blue. For computational efficiency, this has been processed to a different orientation.

Table 6.1: Summary of the data needs and availability for the tightly-coupled model

Data Types		Data Requirements		Data Availability
		1D river	2D floodplain	
Model	Cross-section data	Required	Not required	Available (survey Data)
Geometry (MG)	Floodplain topography with vegetation and trees removed	Not required	Required	Available (Lidar data)
Boundary Condition (BC)	Stage hydrographs along river-floodplain boundaries	Not required	Required	Available (calculated from the 1D river model)
	Flow data	Optional	Not required	Available (recorded data at upstream)
	Stage data	Required at downstream	Not required	Available (ISIS model results)
	Velocity data	Required at upstream	Not required	Available (calculated based on discharge, stage and CS geometry)
	Floodplain roughness	Not required	Required	Estimated
	River channel roughness	Required	Not required	Estimated
Validation (V)	Inundation area	Not required	Optional	Available (aerial imagery)
	Hydrometric data	Optional	Optional	Available (recorded stage at upstream)

The 2D floodplain sub model requires the stage hydrograph at the river-floodplain boundary as the inflow data. In the tightly-coupled model, instead of using the inflow data obtained from an existing 1D river flow model, the flow data at the river-floodplain boundary are provided by the 1D river flow sub model directly at each time step. Roughness coefficients of the floodplain are required for the 2D floodplain sub model. In this application, spatially and temporally varied roughness values were not addressed. Thus, uniform roughness values of 0.06 were used throughout for the floodplain surface. The following sections focus on describing the data requirements, availability and processing for the 1D model. These include the topographic data, flow boundary condition and validation data.

### Cross-section geometry

The topographic data required by the river flow sub model are cross-section geometries. Cross-section surveys were carried out by British Waterways in 2001 (Environment Agency, 2004). Cross-section geometries are available in the form of drawing schemes. The channel is non-prismatic throughout the river length. However, in this study, the actual geometry of the river cross-section is not used. While the model can accept detailed field survey data to specify channel form, the data available for this study was not digitised. The time required to digitise the Ouse data was considered to be too long given the time available for the analysis, and therefore a uniform channel section approach was employed. Instead, a simplified cross-section geometry scheme is used based upon a prismatic channel with a uniform rectangular cross-section shape. The locations of the cross-sections at the study site are shown in Figure

6.8. In general, cross-sections were taken every 200 meters along the river channel (Environment Agency, 2004). More cross-sections were taken at meander bends and a cross-section is taken immediately upstream and downstream of each bridge. In total, 80 cross-sections are used in the model for this application site.

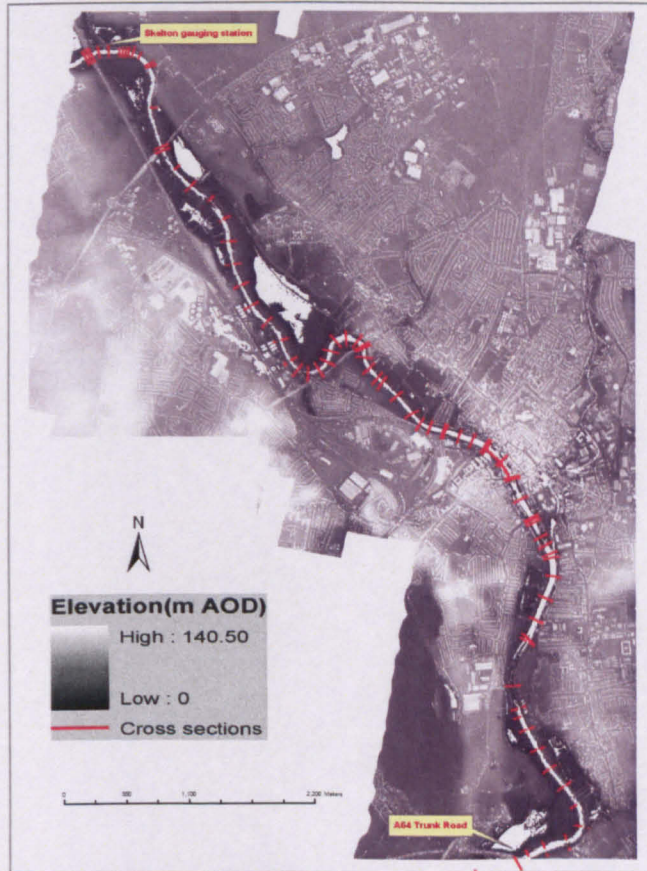


Figure 6.8: Cross-section locations at application Site on the River Ouse.

The simplified cross-section geometry scheme assumes that all the cross-sections are rectangular. It is recognized that such an assumption inevitably introduces some errors into the model with respect to the cross-section areas calculated. However, the disadvantages of this simplified approach might be reconciled by the use of roughness parameterization and the coupling of the 1D river flow model to the 2D floodplain model. If, through the adjustment of the roughness in the river channel, acceptable solution can be found, such simplified cross-section schemes may be enough for the modelling. Cross-sections are numbered from upstream, starting with a number 1. This is shown in Figure 6.9 with the orientation of the data changed for computational purpose.

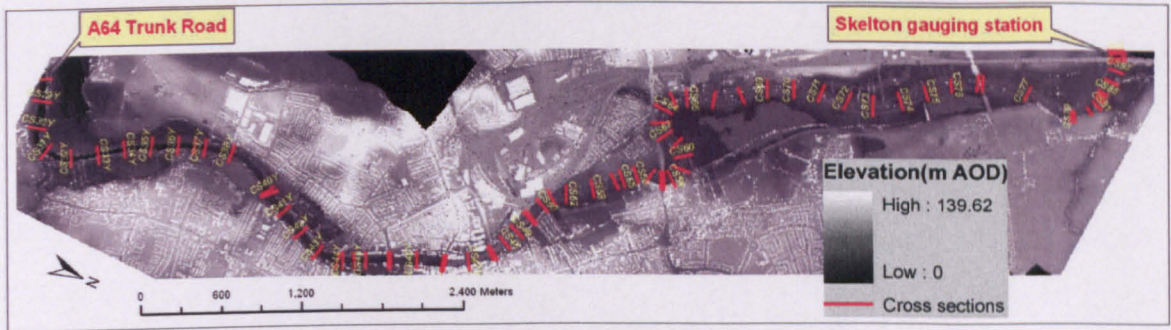


Figure 6.9: Location and naming of the cross-sections.

The width of the cross-section was calculated using the schematic drawings of the cross-sections. The distances between cross-sections, i.e., the length of the individual reach can be readily measured from the LiDAR data. The ground elevations of the cross-sections were taken from the schematic drawing as the average elevation of the lowest and highest elevations of the cross-section and these are shown in Figure 6.10. The slope profiles were calculated based on these ground elevations (Figure 6.10).

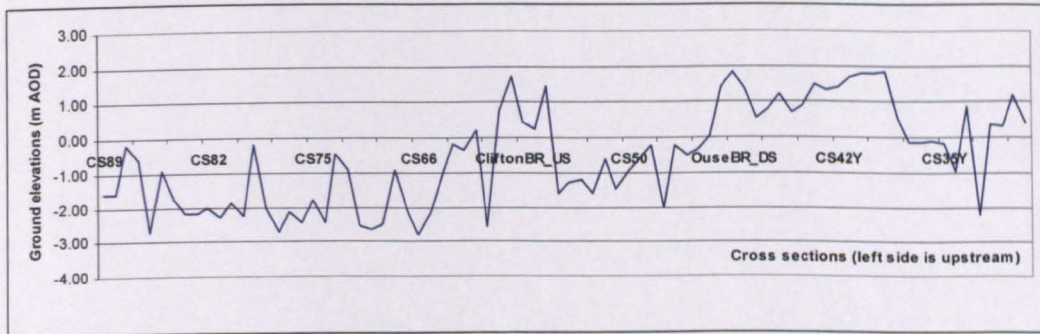


Figure 6.10: Ground elevation profiles of the river according to cross-section geometries.

To establish the connection between the river flow model and the floodplain model, the river channel in the 2D floodplain model needs to be discretized into different reaches according to the locations of the cross-sections (Figure 6.8). This was carried out in the grid environment of the 2D floodplain flow model. The river channel in the 2D floodplain flow model was assigned different codes to represent the different reaches of the river channel in the 1D model. The results are shown in Figure 6.11 along with the rectified 8 m LiDAR data.

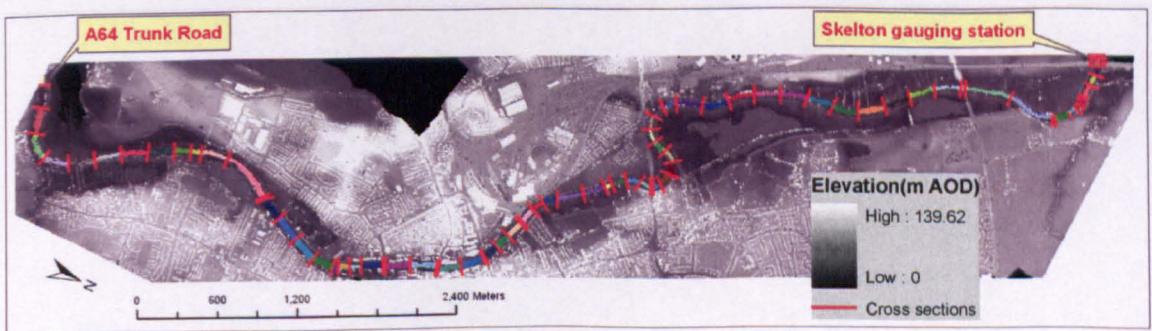


Figure 6.11: Representation of the 1D river channel (coloured polygon) in the raster environment of the 2D floodplain model according to the cross-sections (red lines across the river).

## Flow Data

The boundary condition data required by the 1D river flow model can be either: (i) velocity upstream and stage downstream; or (ii) velocity downstream and stage upstream. In addition: (i) requires the velocity at each cross-section at the start point of simulation; and (ii) requires the water depth at each cross-section at the start of simulation, as initialisation data. This is summarized in Table 6.2.

Table 6.2: Boundary condition requirements for the 1D river model (Option 2 is used in this application).

	Upstream depth	Downstream depth	Upstream velocity	Downstream velocity	Depth at each cross-section	Velocity at each cross-section
Option 1	✓			✓	✓	
Option 2		✓	✓			✓

In this study, the hydrometric data available include upstream flow and stage data recorded at the Skelton Gauging Station and downstream stage data at the A64 Road Bridge. The flow and stage data at the Skelton gauging station are recorded data. The stage data at A64 Road Bridge were obtained from an existing hydraulic model (ISIS). These are shown in Figure 6.12, 6.13 and 6.14.

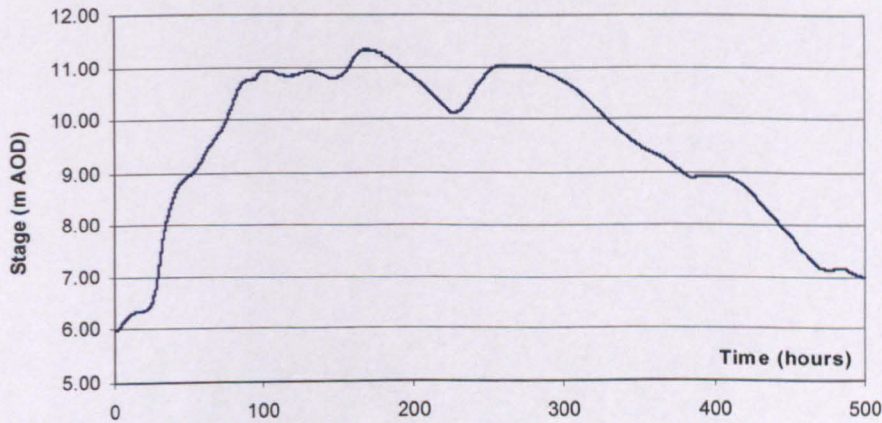


Figure 6.12: Stage hydrograph recorded at Skelton Gauging Station.

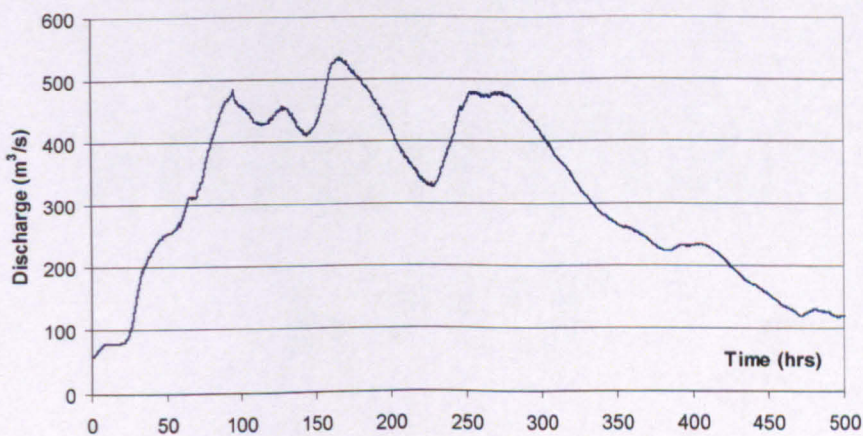


Figure 6.13: Discharge hydrograph recorded at the Skelton Gauging Station.

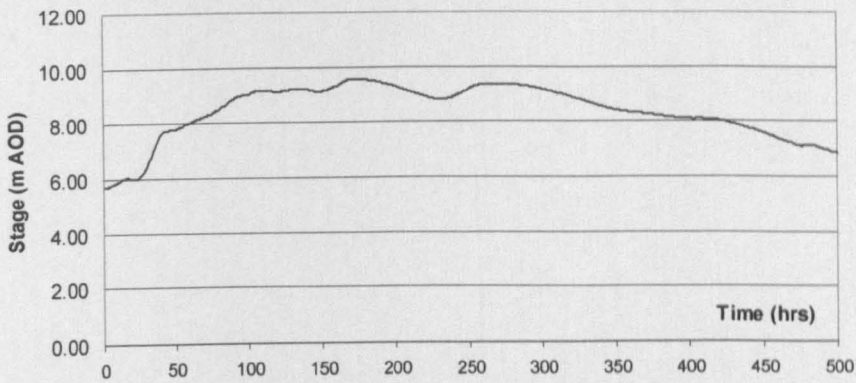


Figure 6.14: Stage hydrograph calculated at the A64 Road Bridge (from the ISIS model).

Water depth hydrographs at both the Skelton Gauging Station and the A64 Road Bridge can then be calculated using the stage data and the ground elevation information identified from the schematic drawing of the corresponding cross-sections (Figure 6.10). The water depth hydrograph at the A64 Road Bridge was used as the boundary condition for the 1D model. The stage record at Skelton Gauging Station was used for the validation of the 1D river model. As the 1D river model developed in this study requires flow velocity at the upstream as boundary condition, the flow data and stage data at the Skelton Gauging Station were used to calculate flow velocity using the cross-section geometry at the Skelton Gauging Station. The generalized cross-section geometry at the Skelton Gauging Station is shown in Figure 6.15.

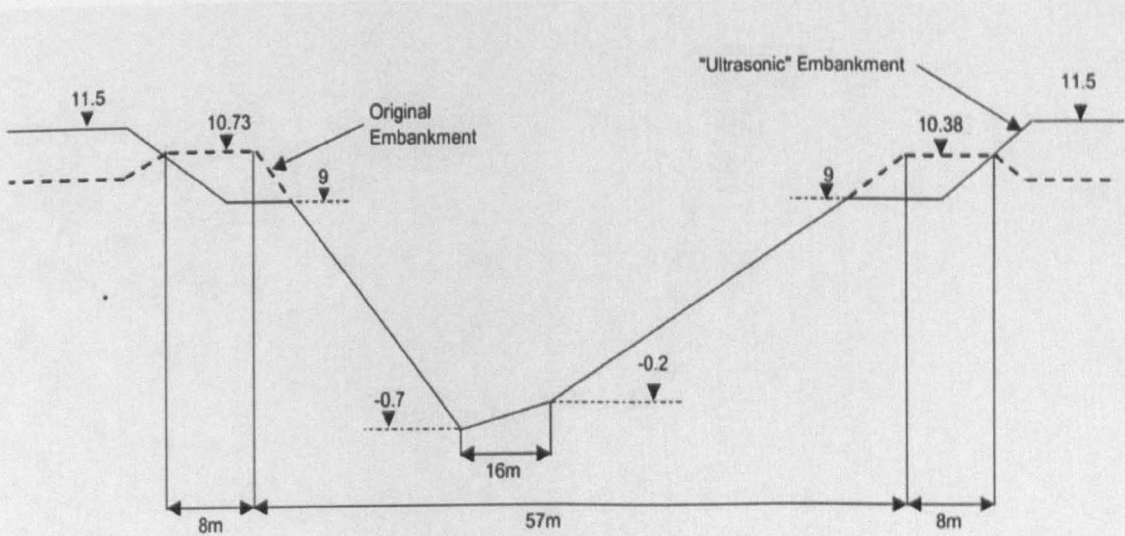


Figure 6.15: Cross-section geometry of the Skelton Gauging Station (after Environment Agency, 2004).

Velocity was calculated based on the flow data and cross-section geometry. The cross-section area at certain water depths is calculated based on known information about the cross-section. Basically, if water depth is lower than 0.5 m, the water surface area is calculated as:

$$A_0 = 17D^2 \tag{6.25}$$

If water depth is higher than 0.5 m and lower than 9.7 m, cross-section area is calculated from:

$$A_1 = A_0 + (D - 0.5) * (2.18D + 15.91) \quad (6.26)$$

If water depth exceeds 9.7 m and is lower than 11.5 m, cross-section area is calculated using

$$A_2 = A_1 + (3D + 46.1) * (D - 9.7) \quad (6.27)$$

where  $D$  is the water depth at the cross-section. Cross-sectional averaged flow velocity can be determined from:

$$V = Q / A_i \quad (6.28)$$

The resultant velocity hydrograph is shown in Figure 6.16.

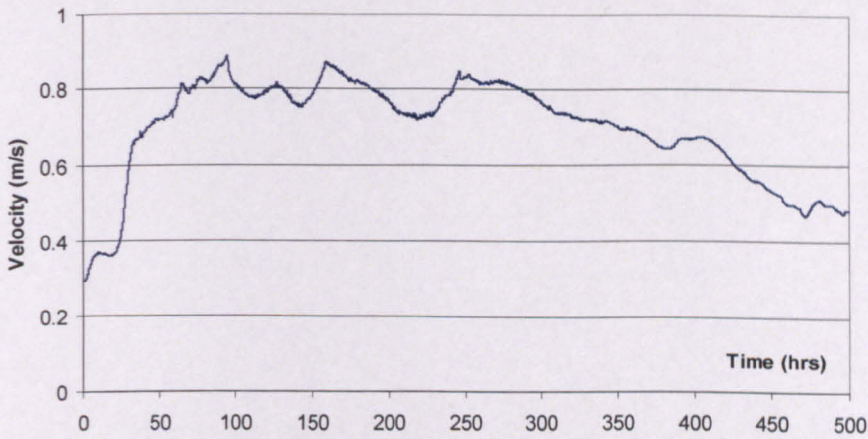


Figure 6.16: Velocity hydrograph calculated for the Skelton Gauging Station

The peak flow recorded by the Skelton Gauging Station is  $534 \text{ m}^3/\text{s}$  (Figure 6.13). However, for the ISIS model simulation, it was found impossible to calibrate the model using the recorded flow data. Investigation found that the ultrasonic flowmeter at the Skelton Gauging Station might have underestimated the peak flow in the year 2000 flood event due to the fact that: (i) flows behind the transducers were not recorded; and (ii) the bed level programmed into the flowmeter is incorrectly set at  $+0.5 \text{ m AOD}$  as opposed to  $-0.7 \text{ m AOD}$ . Both of these could have caused some underestimation of flow (Environment Agency, 2004). If (i) is taken into account, the peak flow would be higher by around  $23 \text{ m}^3/\text{s}$  for the peak flow. If (ii) is taken into account, the flow would have been  $26 \text{ m}^3/\text{s}$  higher than the recorded flow. In total, it was calculated that if these factors are taken into account, the peak flow was probably around  $583 \text{ m}^3/\text{s}$ . This recalibration also provides a better reconciliation with the historical record. The previous maximum measured flow for Skelton was in January 1982 at  $542 \text{ m}^3/\text{s}$ . However, this resulted in substantially less inundation than in the 2000 event, where water levels were the highest recorded since the seventeenth century. Although there are other explanations of stage change (e.g. changes in conveyance), research by Lane (2003b)

confirms that conveyance through the City of York has not changed significantly since the 1982 record. Thus, the recorded flow hydrograph was modified. This was carried out based on the known geometry of the cross-section (Figure 6.15) when the stage is lower than the ground elevation of the transducer, and a linear interpolation of the increase according to the water depth if the stage is higher than the transducer. If the stage is lower than the ground elevation of the transducers (9.00 m), the flow is increased by 26 m<sup>3</sup>/s uniformly. This accounts for the wrongly programmed bed level in the flowmeter. If the stage is higher than the ground elevation of the transducers, the flow is further increased by:

$$\Delta Q = \frac{(D - 9)}{(D_{Max} - 9)} * 23 \quad (6.29)$$

where  $D$  is the water stage and  $D_{max}$  is the maximum value in the stage hydrograph. This accounts for the flow at the back of the transducers. This gives a peak flow of 583 m<sup>3</sup>/s. The modified flow hydrograph and the corresponding velocity hydrograph are shown in Figure 6.17 and 6.18 compared with the recorded flow and velocity data.

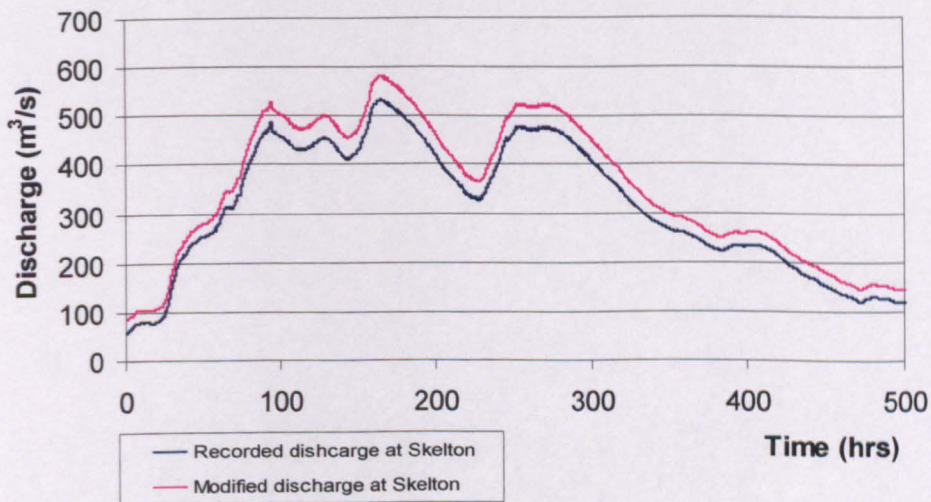


Figure 6.17: Discharge hydrograph corrected at Skelton Gauging Station compared with that recorded.

### Validation data

The results of the coupled model need to be validated for its 1D and 2D components. The 1D river flow sub model was validated against the recorded stage hydrograph (Figure 6.12) at the Skelton Gauging Station. Validation of the predicted inundation extents was not carried out for the whole reach. Rather, this was carried out for Site 3 (Figure 3.2). This is due to the incomplete coverage of the full reach.

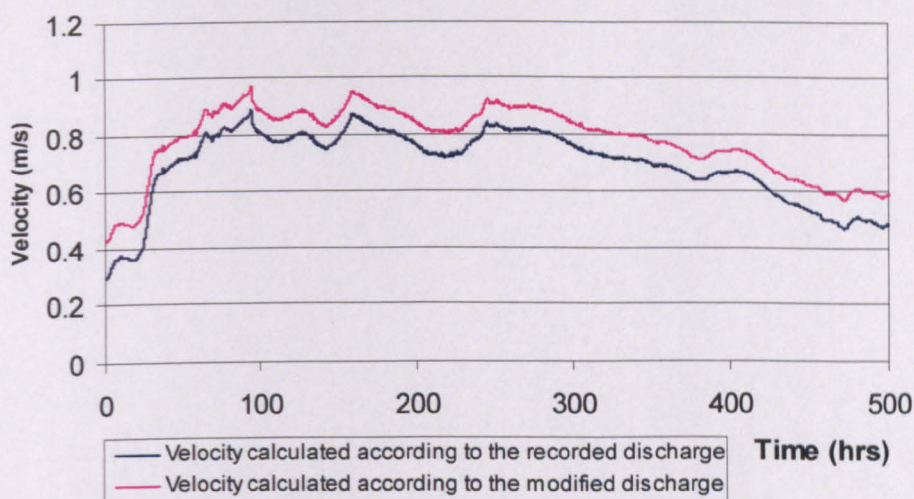


Figure 6.18: Velocity hydrograph corrected at Skelton Gauging Station compared with the original velocity estimates.

## 6.5 Model applications: results and discussion

The tightly-coupled model described in section 6.3 was applied to the river reach described in section 6.4. This section compares the model results with the recorded data in terms of hydrometric predictions in the river channel. It also compares model performance with that obtained with the loosely coupled version of the model (§4.6.2) and the inundation extents obtained from aerial imageries.

The comparison with other model results such as ISIS (storage cell approach) could be very valuable, but at this point, this has not been undertaken although Tayefi *et al.* (in review) do undertake such a comparison for a complex rural floodplain.

### 6.5.1 Model calibration and validation

Model calibration using the ISIS model for the 2000 flood event in the River Ouse has been shown to be very complex (Environment Agency, 2004). Without considering errors inherent in the recorded flow data at the Skelton Gauging Station, the ISIS model could not achieve a satisfactory level of calibration. Satisfactory calibration was based upon the Environment Agency (2004) finding, that the flow input had to be increased by 9% based on the errors found in the recorded flow data at the Skelton Gauging Station (Environment Agency, 2004). Other hydraulic parameters used in the EA calibration included, among others: (i) removal of city centre reservoirs; (ii) removal of a number of cross-sections; (iii) adjusting flow data at some cross-sections; (iv) adjusting bed elevation for some reaches; and (v) adjusting the Manning's  $n$ . Thus, calibration efforts for the 2000 flood event in the River Ouse using ISIS model were paramount. One might question the physical basis of these calibration procedures.

The ISIS model for York is still being used for flood risk mapping. It reflects best practice in flood inundation modelling using a one-dimensional approach. Hence, this was the focus of the model calibration and validation. In this study, model calibration was carried out simply by adjusting Manning's  $n$ . The modified inflow hydrograph (Figures 6.17 and 6.18) was used. No other hydraulic parameters were altered. This is due to the high computational requirements of the application using the tightly-coupled model over this long reach.

In terms of the spatial derivative, previous studies found that the Preissmann Scheme was weakly stable for  $0.5 < \theta < 0.6$  and strongly stable for  $0.6 < \theta < 1.0$  (Moore and Foster, 1990). Linear analysis without considering friction slope and boundary shear reveals that, when  $\theta < 0.5$ , the Preissmann scheme is always unstable (Abbott and Basco, 1989). With a  $\theta$  value of 1.0, the model is most stable and fully implicit, but with the highest distortion in that no information from the last time step is used to approximate the partial derivatives (Brakensiek, 1967). Numerical stability associated with the value of  $\theta$  depends on the Froude number, Courant number and the wave number in a very complicated way (Ponce and Simons, 1977). Thus, in the model calibration, the spatial derivative ( $\theta$ ) was kept at 0.52, which is within the weakly stable range of the scheme, whilst with controlled distortion. The time derivatives ( $\psi$ ) are normally computed with  $\psi = 0.5$  and appeared in the original publication (Preissmann, 1961, cited by Abbott and Basco, 1989). In this study, the time derivative was kept at 0.5 and the space derivative was set at 0.52.

In the final calibration of the ISIS model, the roughness values for the main Ouse channel were set at 0.049 at the Skelton Gauging Station and gradually decreased downstream to 0.025 (Environment Agency, 2004). This is spatially distributed and based on the channel characteristics. A uniform Manning's  $n$  was used for the whole river channel during roughness parameterisation in this study. Floodplain roughness values are fixed at 0.06 throughout (§6.4). Manning's  $n$  values were adjusted in the range from 0.03 to 0.08 with an interval of 0.005. Manning's  $n$  on the floodplain is set to be a uniform value of 0.06, given the earlier finding that the model was relatively insensitive to  $n$  validation within a realistic range.

Figure 6.19 shows that the tightly coupled model is quite sensitive to roughness coefficients in terms of the predicted water levels. For example, a 0.05 increase of Manning's  $n$  from 0.035 to 0.040 results in an increase of 13 mm in peak stage. This increased to 25 mm if Manning's  $n$  is adjusted from 0.065 to 0.07. Thus, the sensitivity is more pronounced for higher roughness values. Best calibrations with Manning's  $n$  were found to be in the range of 0.05 and 0.055 (Figure 6.19). This high sensitivity to roughness in the 1D model is in marked

contrast to the results in Chapter for the 2D inundation model where sensitivity was found to be much lower. This is not surprising because of the dominant effect that the friction law has on the friction slope in equation 6.4.

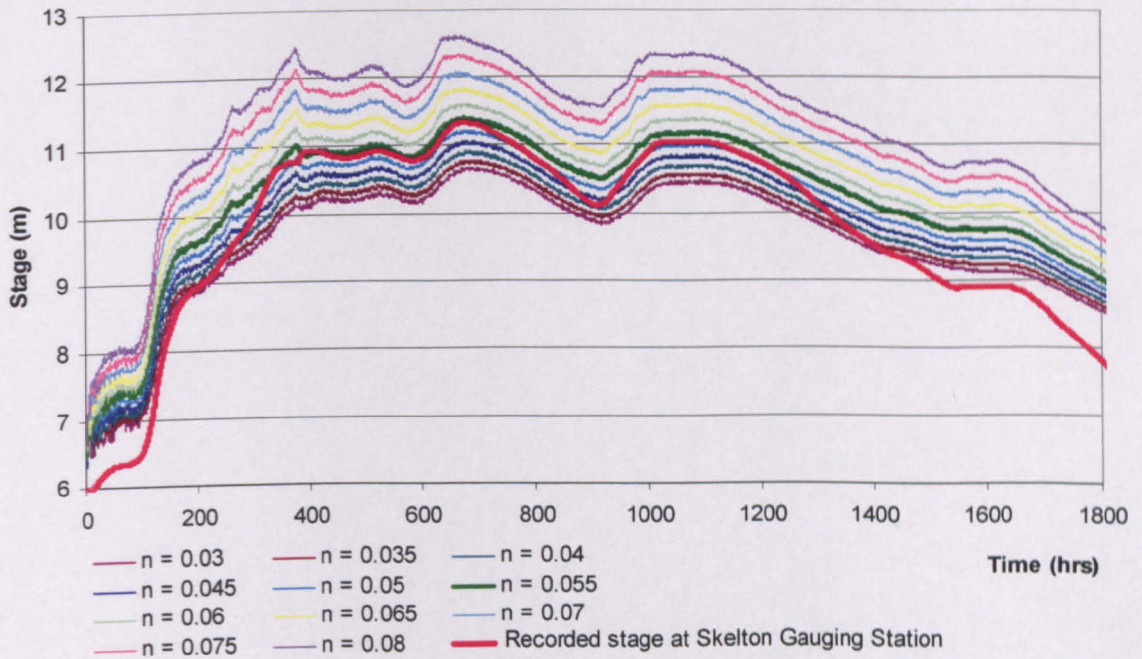


Figure 6.19: Calibration using Manning's  $n$ , with space derivative fixed at 0.52.

The optimum calibration was found to be associated with the modified flow data (Figure 6.17 and 6.18), a Manning's  $n$  value of 0.053 and a space derivative value of 0.52 (Figure 6.20). There might be other combinations of different parameters that can also give equivalent levels of calibration as the one found in this study. This issue is not explored further in this study.

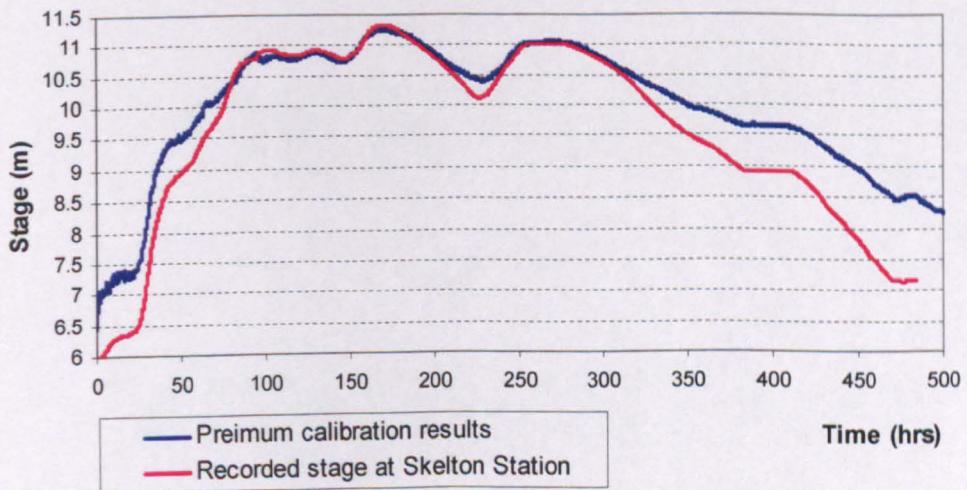


Figure 6.20: Optimum calibration results at the Skelton Gauging Station.

In terms of the performance, the best calibration results obtained are not satisfactory, particularly when the performance of the model during the rising and the falling limbs of the flood event is considered. In terms of peak water levels predicted (between 100 hrs and 200 hrs), the model performs extremely well, with an average of 8 mm between the predicted and

the recorded peak levels (4 flow peaks during the 100 hrs and 300 hrs were considered). This compares with what the Environment Agency commonly deems adequate ( $\pm 25$  mm) and good ( $\pm 15$  mm) for peak flow predictions in model studies of this kind. The model does not perform well during the rising and falling limbs. This was compared with the results obtained from the ISIS model (Environment Agency, 2004) (Figure 6.21). It was found that the ISIS model was also not able to give satisfactory stage predictions for the rising and falling limbs. However, the discrepancy seems to be more obvious in the results obtained in this study. On the rising limb, right from the beginning of the simulation, the model overestimates water level substantially. This was corrected when peak levels were reached (between 100 hrs and 300 hrs). Thereafter, the model performs reasonably well until around 320 hours, when the flood level starts to fall. During the falling limb, the model overestimates water levels substantially again. There were potentially many causes of these errors. For instance, errors in boundary conditions may be linked to flow magnitude. Similarly, the approach assumes that  $n$  is constant for all flows. This is unlikely as  $n$  is stage-dependent. The over-estimation of stage is associated with flows that predominantly in bank of Skelton: the channel becomes (weakly) two stage for flows above 9.0 m. It may be the case that roughness values are too high for in bank flows. This is not what would be expected, as Manning's  $n$  should be lower at higher flows as roughness effects are drowned out. However, it is possible that the onset of flow in the second stage channel results in significant increases in flow interaction between the low stage and second stage channel, since that for stage hydrograph values greater than 9.0 m, higher values of roughness are required to reproduce observed shape. There are other explanations of this possible discrepancy as well as limitations with this one (e.g. over-estimation of stage at flows higher than 9.0 m above datum). However, the key point is that the over-estimation of stage is predominantly for in bank flows which are not of significance for flood inundation.

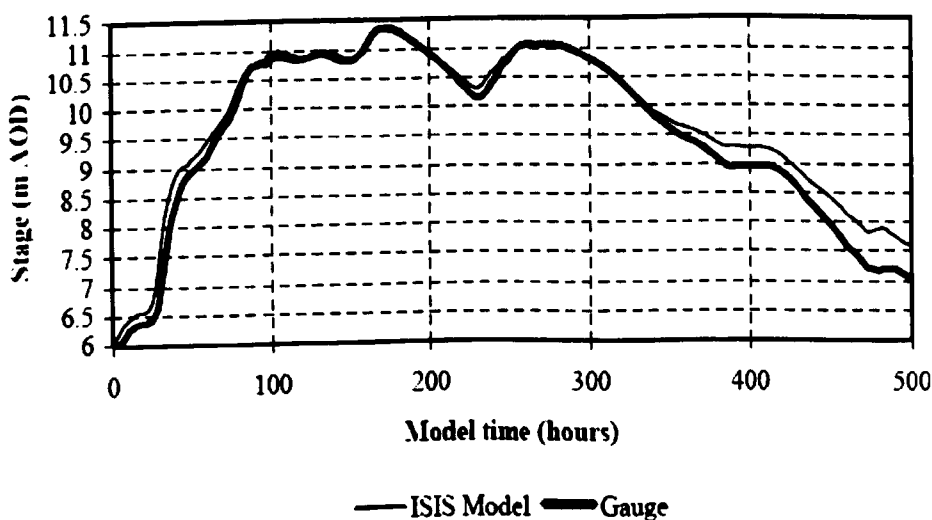
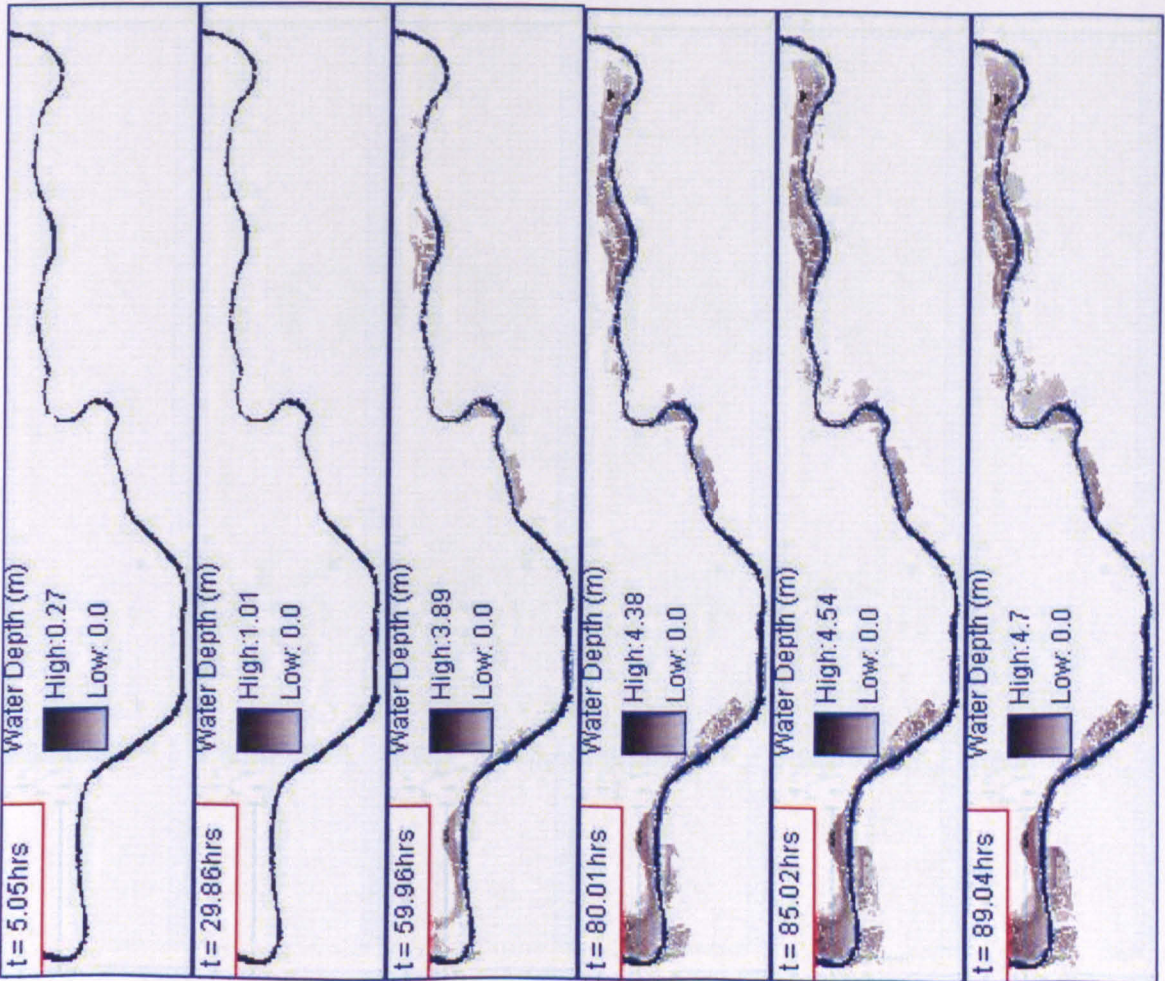


Figure 6.21: Optimum calibration results at the Skelton Gauging Station, obtained from the ISIS model.

The model performance in terms of the inundation extent was validated using at-a-point in time flood inundation extents obtained from aerial imageries (§6.4). The imagery was obtained at around 300 hours into the flood event. The validation was carried out only for the model predictions at Site 3. For the wetting phase of the flood event, the predicted time series of inundation extent at Site 3 were compared with the observed inundation extents using the approach presented in Section 3.5.2 and used in the applications at Sites 1, 2 and 3. The time series of inundation extents predicted using the tightly-coupled model for the wetting phase (first 182 hours) and those (first 185 hours) obtained from Site 3 using the loosely coupled model are shown in Figure 6.22 and Figure 6.23.



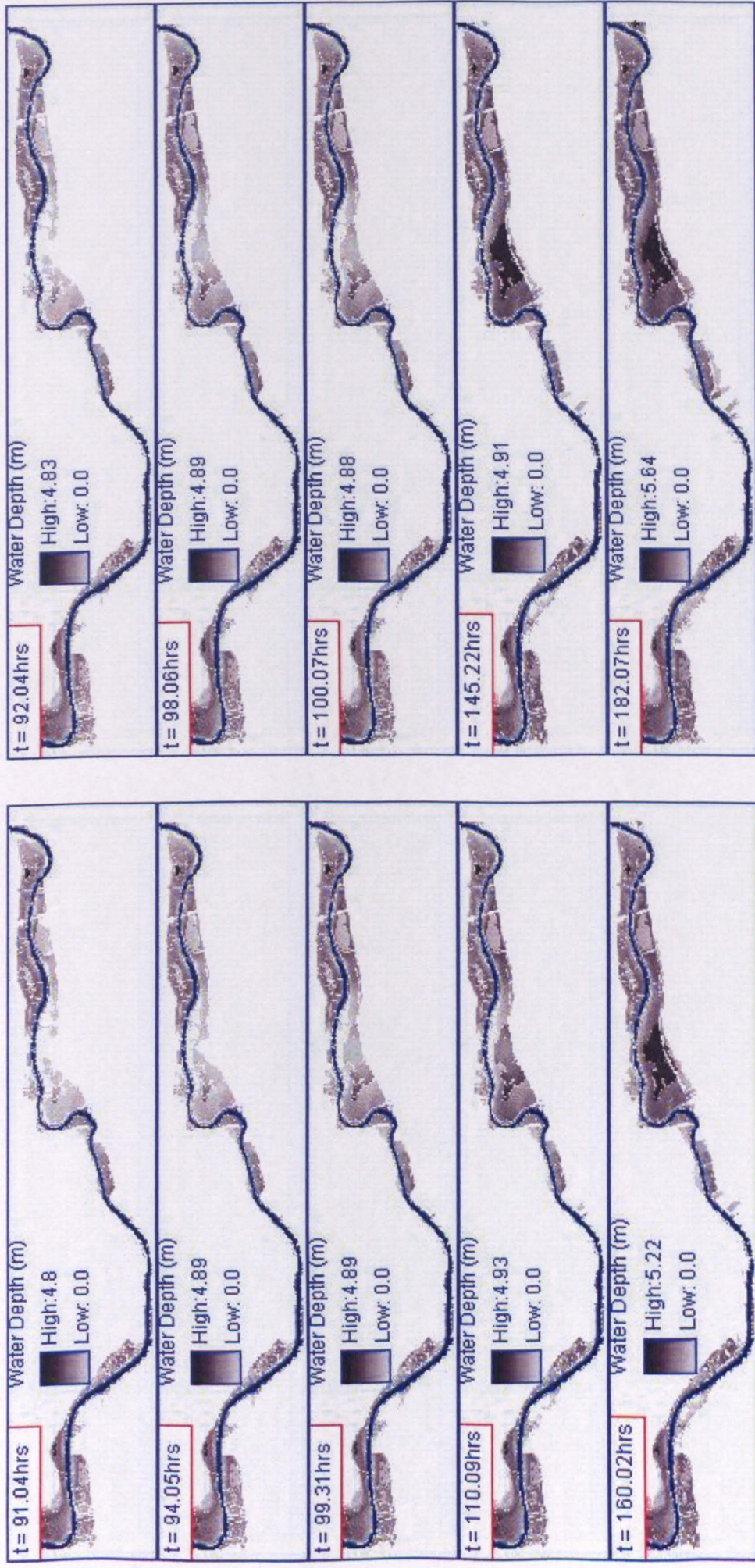


Figure 6.22: Time series of inundation extents obtained from the tightly-coupled model at the long reach for the wetting phase (first 182 hours).

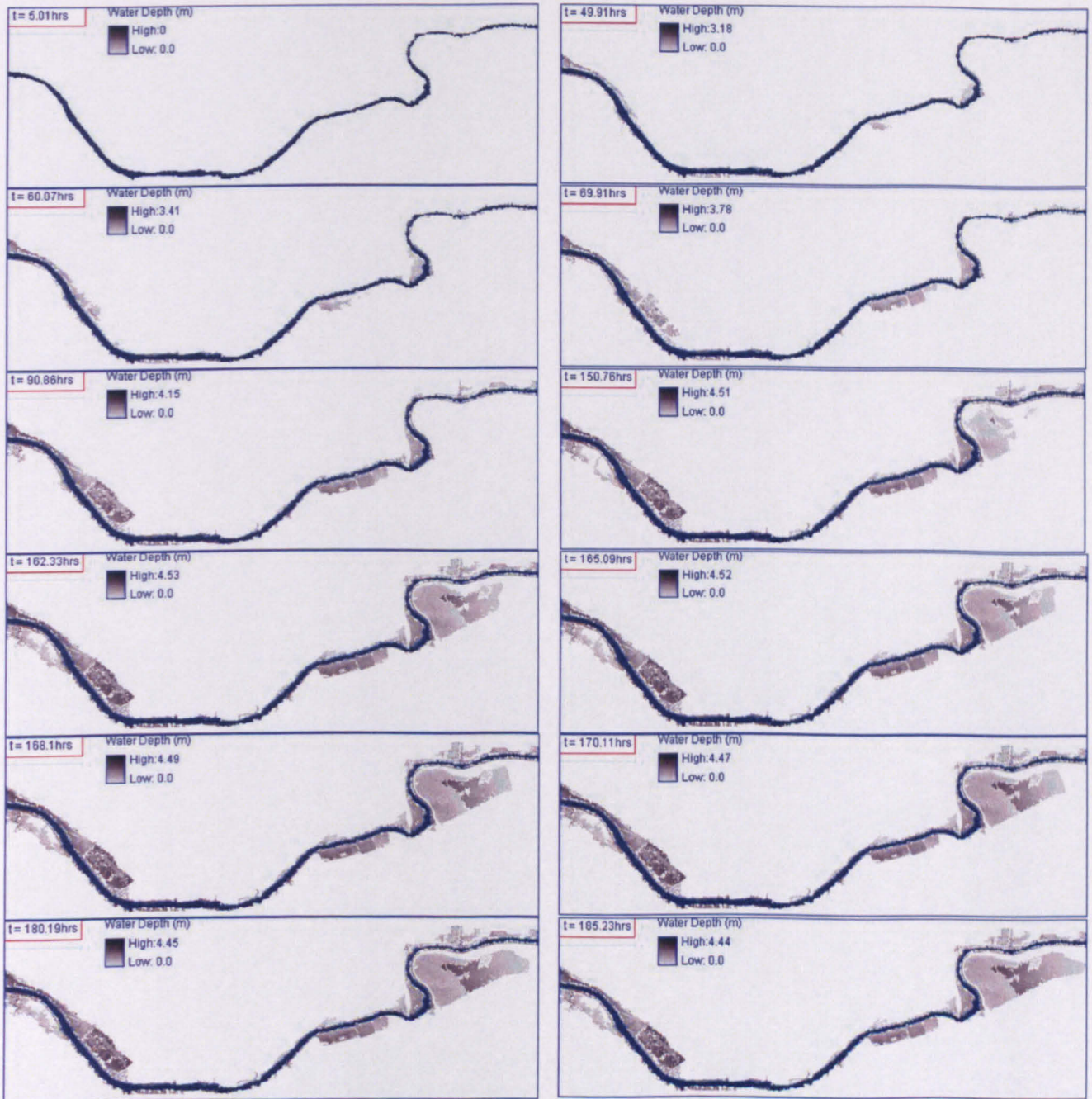


Figure 6.23: Time series of estimated inundation extents obtained from the loosely coupled model at Site 3 for the wetting phase (first 185 hours) (reproduced from Figure 4.25).

The estimated inundation extent obtained using the tightly-coupled model at the validation point is shown in Figure 6.24, as compared with the results from the loosely coupled model. Comparison of the two time series of inundation extents at Site 3 during the initial wetting phase shows some differences between the predictions of these two simulations. First, flood inundation appears to be slower for the loosely coupled model than that for the tightly-coupled model. Second, water enters from the upstream boundary of Site 3 into the upstream storage area at Site 3 where the loosely coupled model was found to underestimate inundation extents in this area (§4.6.2). The upstream inflow is expected to affect the inundation extent at the upstream of Site 3. The predicted inundation extent at the validation point confirms these

observations: inundation patterns are different from those obtained using the loosely coupled model at Site 3, particularly upstream. These are compared in Figure 6.24, with the aerial imagery obtained at the validation time period (Figure 6.24c). Accuracy assessment was carried out using the approach described in Section 3.5.3 and the accuracy statistics are shown in Table 6.3.

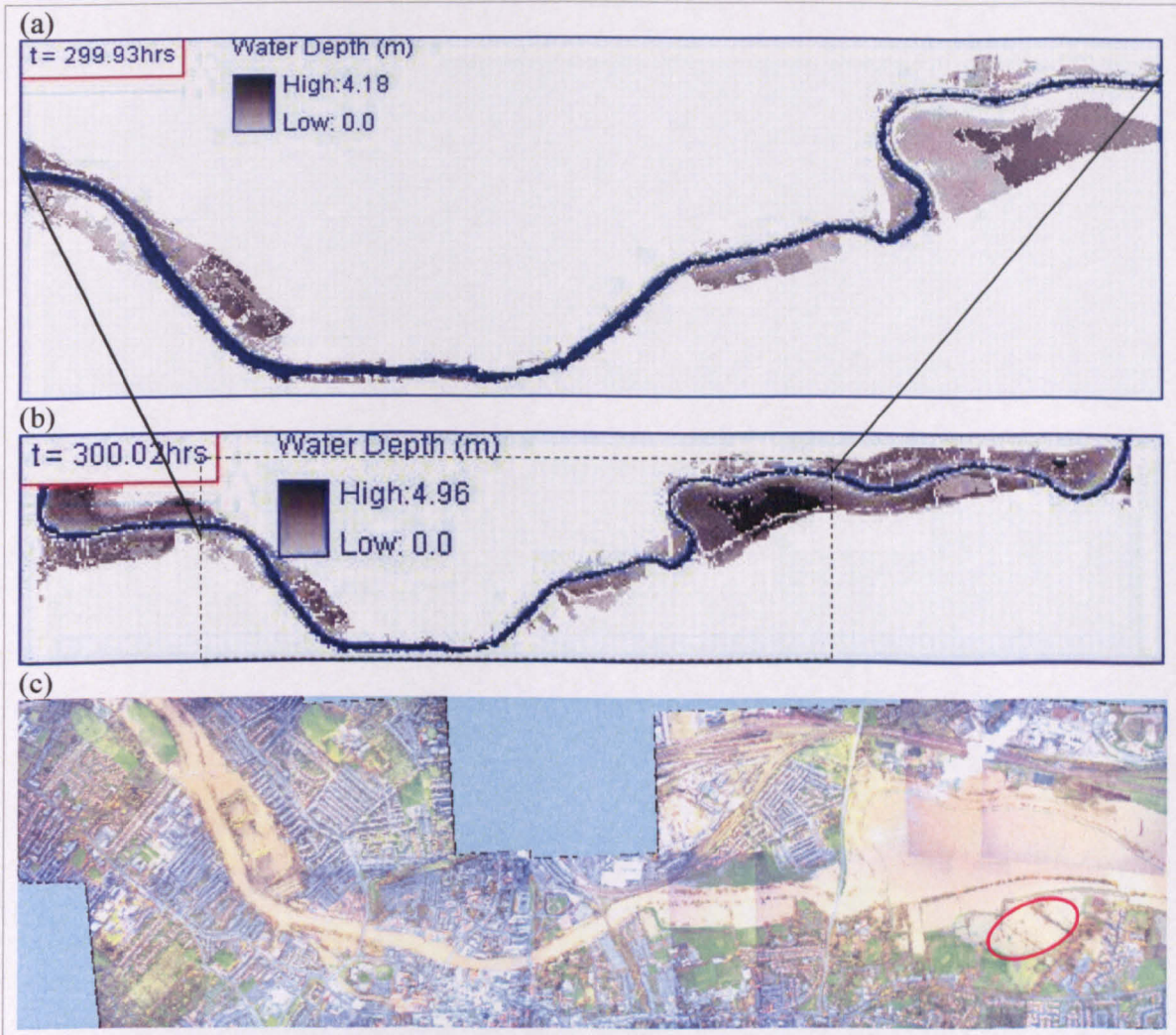


Figure 6.24: Estimated inundation extent at the validation point (around 300 hours into the flood event): (a) using the loosely coupled model (reproduced from Figure 4.26); (b) using the tightly-coupled model; and (c) aerial imagery at the validation point (reproduced from Figure 4.26).

Table 6.3: Accuracy statistics obtained using the loosely coupled model and the tightly-coupled model.

	Loosely coupled model	Tightly coupled model
Overall accuracy	0.65	0.76
$F$	0.86	0.88
Kappa	0.66	0.75
Conditional Kappa (Wet Cells)	0.92	0.94

The wetting and drying processes associated with the flooding were investigated in terms of the velocity vectors in  $x$  (horizontal) and  $y$  (vertical) directions. Figure 6.25 shows the velocity vectors at  $x$  and  $y$  direction at around 94 hours when inflow from the river fills in the

upstream storage area quickly (Figure 6.22). After the peak inundation extent was reached at around 182 hours, the drying phase began. The magnitudes of flow velocity in the x and y directions during the drying phases are shown in Figure 6.26 (at around 200 hours) for the tightly-coupled model. Figure 6.25 and Figure 6.26 show that, during both wetting and drying phases, in both directions, flow velocities are higher near the bank regions. Flow velocities at both the wetting and drying phases exhibit complex patterns. This shows the complex interaction between the river flow and floodplain flow at the river-floodplain boundary.

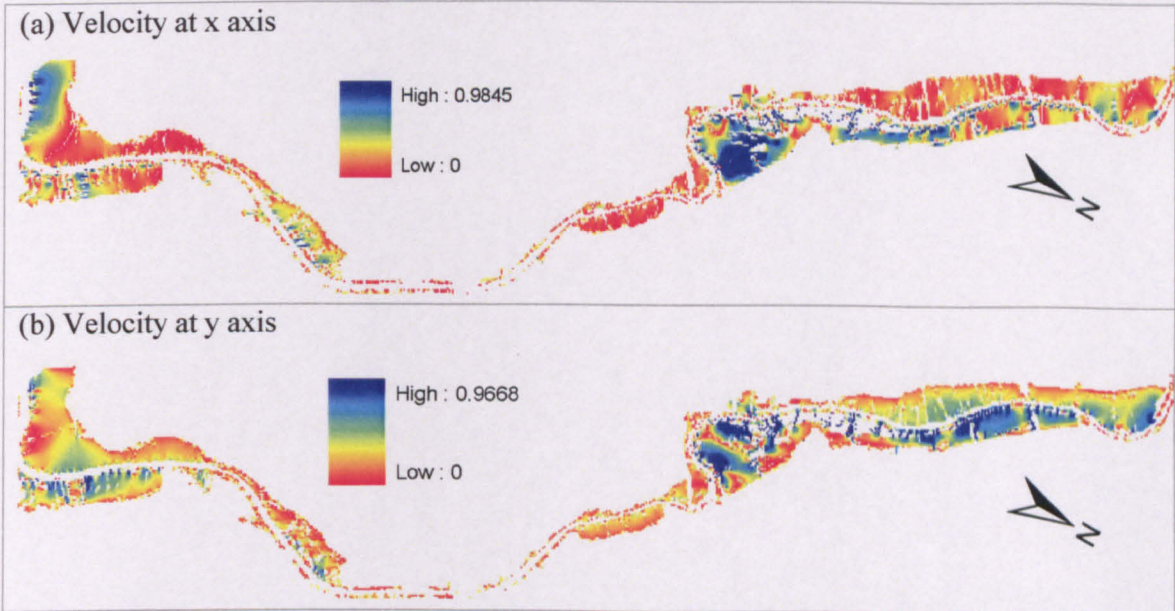


Figure 6.25: Velocity vectors in x and y directions: (a) flow velocity in x (horizontal) direction; and (b) flow velocity in y (vertical) direction; during the wetting phase (around 94 hours).

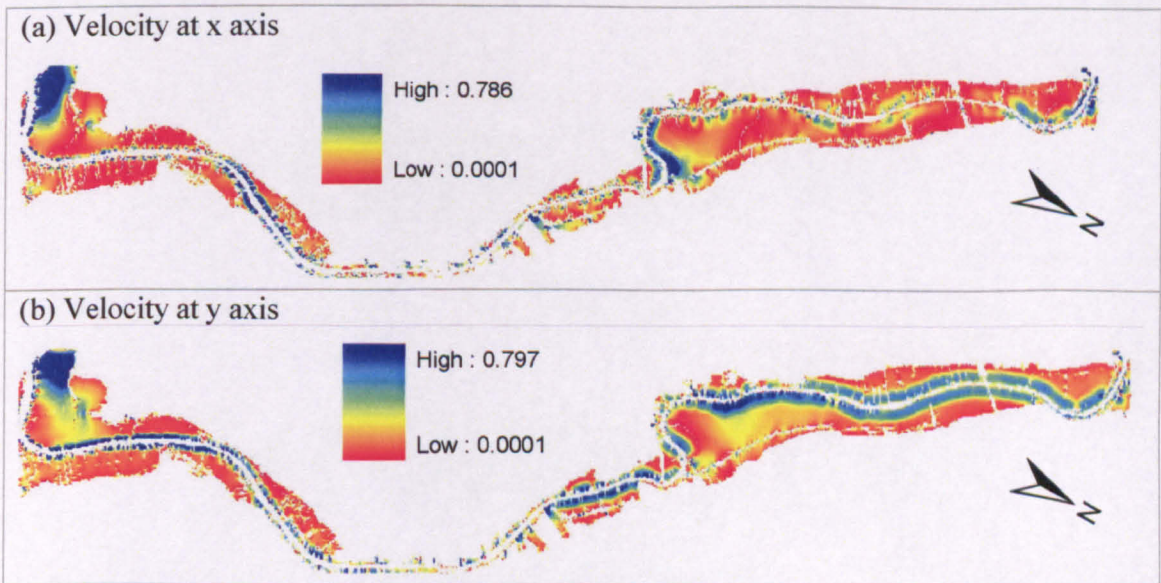


Figure 6.26: Velocity vectors in x and y directions: (a) flow velocity in x (horizontal) direction; and (b) flow velocity in y (vertical) direction; during the drying phase (around 200 hours).

This is caused by the discontinuity in the stage-discharge relationship. As the connection between the river channel and floodplain is represented using a weir equation for both the

loosely- and tightly-coupled models, the flow processes are very likely to be inadequately represented at this boundary. More sophisticated approaches are required to represent the complex interaction between the river flow and floodplain flow. This will be discussed further in Chapter 7.

### **6.5.2 Discussion**

In terms of stage predictions in the river channel, optimum calibration was found when the modified flow boundary data with a peak flow of 582 m<sup>3</sup>/s (Figure 6.17), and a Manning's *n* value of 0.053 were used. Peak water levels predicted with these parameters are accurate to within 8 mm at the Skelton Gauging Station. However, model predictions during the rising and falling limbs of the flood event are poor, particularly for the falling limb. This was compared with the results obtained from the ISIS model (Figure 6.21), which was also found to give poor predictions for the rising and falling stages of the flood event. Three reasons might contribute to this: (i) the simplified represented cross-section geometry; (ii) errors in the input data at the downstream boundary used in the model; and (iii) issues associated with model calibration. The downstream boundary condition data were obtained from the ISIS model. As the ISIS model overestimated the water levels for the rising and the falling limbs of the flood event, it might also overestimate water levels at the downstream boundary. Given the simplified cross-section geometry used in the model and the performance of the ISIS model, the model is considered to perform relatively well in terms of stage predictions, as compared with the ISIS model.

Validation of model predictions in terms of inundation extents at Site 3 shows that the tightly-coupled model performed better than the loosely coupled model. However, this is only improved marginally (Table 6.3) for the *F* and conditional Kappa statistics. The relatively small improvement with the tightly-coupled model compared with the loose-coupled one at site 3 is probably due to the over-simplification of river geometries used in the model. The fact that the tightly-coupled model resulted in only a modest improvement in model performance implies that the return flow treatment assumed in Section 3.2 is probably acceptable. Reaching this conclusion needs some caution as the error in the tightly-coupled model may be dominated by hydrograph uncertainty so making the return flow assessment difficult. The loosely coupled model was found to underestimate inundation extents upstream of Site 3 (§4.6.2). Various reasons were explored (§4.6.2). The use of a downstream stage hydrograph from the river-floodplain boundary and the influence of inflow from the upstream boundary were thought to be the two main causes. The loosely coupled model used a uniform stage hydrograph as input at the river-floodplain boundary. This might be inappropriate given

the length of the river as variations in the river stage are expected in the reach modelled. To evaluate whether the stage hydrograph used in the loosely coupled model was too low, stage profiles along the river channel for the loosely coupled and tightly-coupled models are compared at two time points (1 hr and 147 hrs). This is shown in Figure 6.27. The stage at the upstream of Site 3 (CS70) predicted by the tightly-coupled model is compared with the stage used in the loosely coupled model (Figure 6.28).

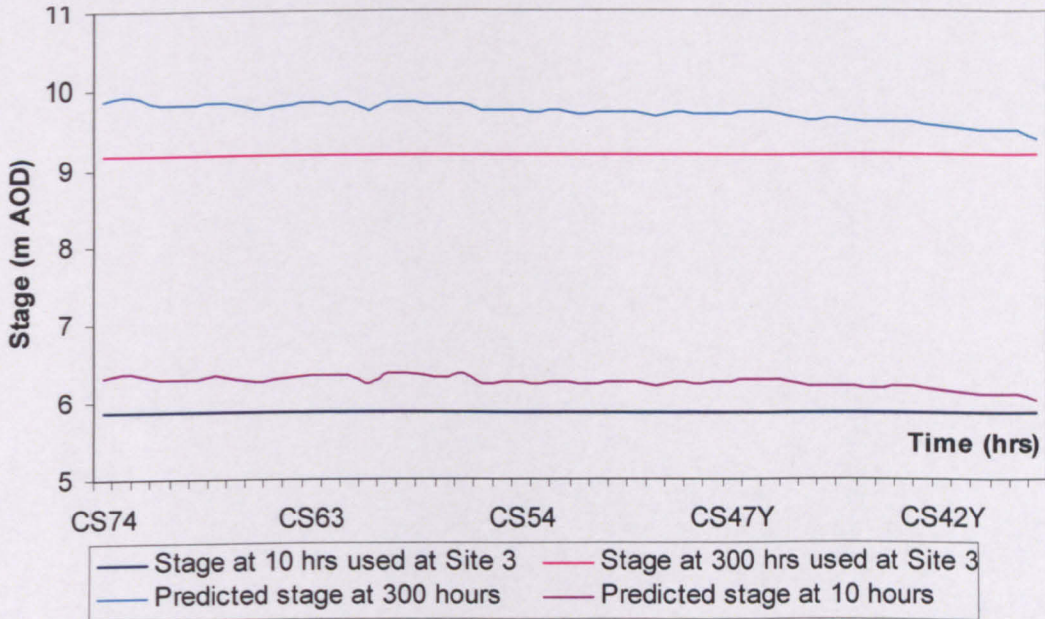


Figure 6.27: Comparison of stage profiles along the river used in the loosely coupled and tightly-coupled models at 10 hrs and 300 hrs (Site 3 starts with cross-section code CS72 (upstream) and ends with cross-section code CS38 (downstream)).

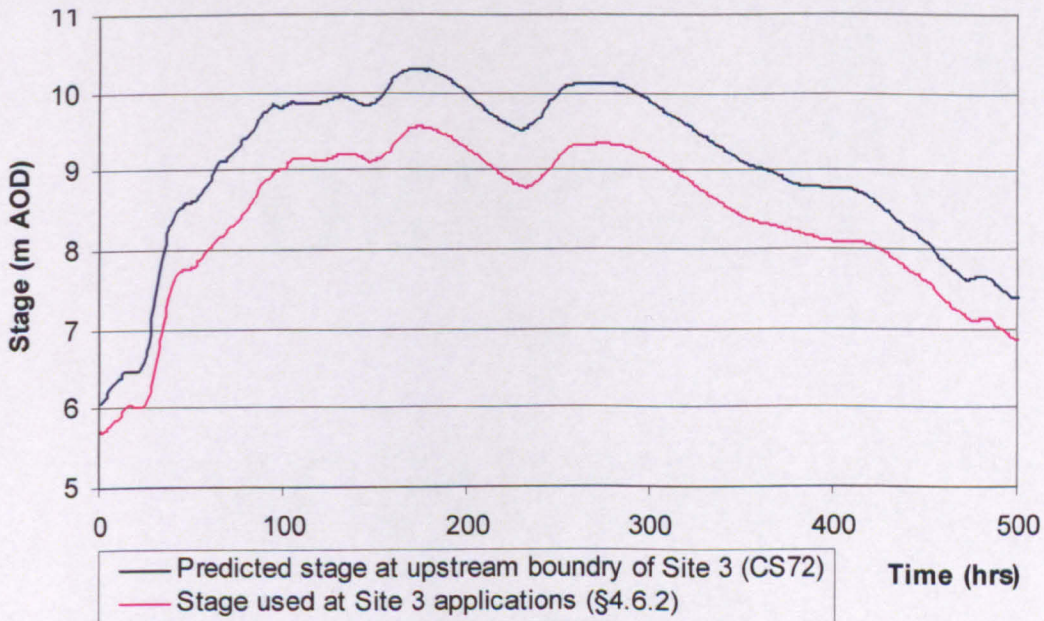


Figure 6.28: Comparison of the stage hydrograph at the upstream cross-section of Site 3 (CS70) obtained using the tightly-coupled model with that used in the loosely coupled model.

Figure 6.27 shows that, as expected, the stage along the channel predicted in the tightly-coupled model is higher than the stage used for the Site 3 application with the loosely coupled model. Single point comparison through time (Figure 6.28) shows that water level predicted at the upstream in the tightly-coupled model is higher than the stage used at Site 3 application throughout the simulation. These comparisons suggest that the use of the downstream stage hydrograph at the A64 Trunk Road, for the whole river and during the whole simulation, underestimated the river stage, and thus, underestimated the amount of inflow from the river to the floodplain. This, to a large extent, caused the underestimated inundation extents upstream of Site 3.

However, both the tightly coupled and the loosely coupled models failed to produce the inundation pattern (red circle in Figure 6.24c) found at the upstream of the reach as shown the aerial imagery. For both simulations, the inundation time series show that the footpath that separates the two wet zones in the aerial imagery was not overtopped. The time series of inundation extents obtained using the tightly-coupled model shows that water entered from the upstream boundary of Site 3, but only at the river side of the footpath that separates the two wet zones in the upstream. This is shown in Figure 6.29.

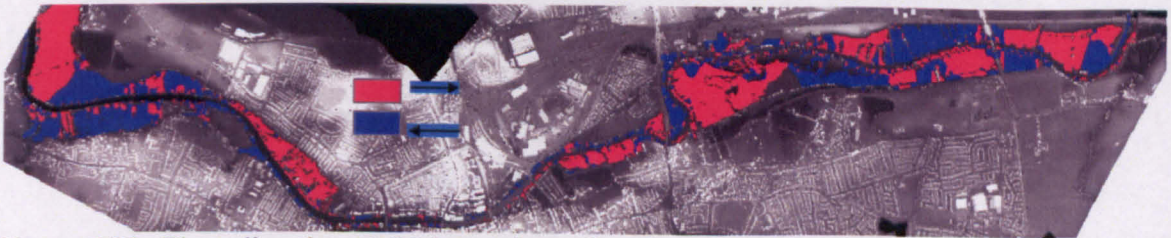


Figure 6.29: Flow direction at 94 hours in x direction: flow directions of the red areas are pointing to the right and blue to the left.

However, this did not exert a significant influence on inundation patterns upstream. As the stage in the river channel is validated in the 1D river flow model, it is likely that, in the 2000 flood event, the footpath was not overtopped. The wetted areas the other side of the footpath might be caused by other factors such as local runoff or underground pipes.

The comparison of the results obtained from the tightly coupled and loosely coupled models presents several important issues with respect to flood inundation modelling over topographically complex floodplains. First, the accuracy of flow data is important in that this eventually determines the amount of water that is available on the floodplain. If the amount of flow exchange between the river and the floodplain is not calculated correctly, it may result in underestimation or overestimation of inundation extents. Two simulations (Figure 6.22 and Figure 6.23) carried out at Site 3 show significantly different wetting phases. In terms of the

inundation rate, simulation using the tightly-coupled model suggests that during the initial wetting phase, the inundation rate is significantly lower in the loosely coupled model using the downstream stage hydrograph than that in the tightly-coupled model in which the stages along the river is varied according to the calculation in the 1D river flow sub model (Figure 6.22 and Figure 6.23). This is expected as the stage used in the tightly-coupled model is much higher than that used in the loosely coupled model (Figure 6.26 and Figure 6.27). Thus, for coupled modelling of flood inundation, the validation of inflow data is important for accurate prediction of inundation extents.

Second, it emphasises again the danger of using at-a-point in time data for validation in relation to the data errors (§3.5, §4.5.4 and §4.7) Using aerial imagery obtained after the initial wetting process and before the mis-predicted zone is wetted might give good validation results, even if an inaccurate stage hydrograph is used.

Third, it demonstrates the needs for field survey in situations where complex topography occurs. Upstream of Site 3, near the residential side of the river, there is complex topography associated with structural features such as roads, hedges and buildings. The underestimated inundation extent at the residential side of the footpath might be caused by many factors (§4.6.2). However, as no field knowledge is available with respect to the flow pattern at upstream of Site 3 at the validation point, it is impossible to ascertain the cause of this underestimation.

## **6.6 Chapter summary**

This chapter described the tightly-coupled model and its application to a 10 km reach across the city centre of York on the River Ouse. The tightly-coupled model is composed of a 1D river flow model that solves the full Saint-Venant equations and the raster-based 2D diffusion wave floodplain flow model described in Section 4.3. The 1D river flow sub model was described in Section 6.3.1 in terms of its process representation, discretization and solution. In contrast to the loosely-coupled model, where the inflow data from the river channel are obtained prior to the initialisation of the 2D floodplain flow, the tightly-coupled model calculates the river flow and floodplain flow simultaneously by treating the flux exchange at the river-floodplain boundary explicitly through mass control at each time step (§6.3.2). The data requirements of the tightly-coupled model and the associated data processing were described in Section 6.4.

The model was applied to simulate the November 2000 flood event that occurred on the River Ouse for a longer reach than that used at Site 3, covering Site 3. The 1D component of the model was validated against the recorded stage hydrograph at the Skelton Gauging Station. The peak stage was found to be well predicted, with the accuracy of the peak prediction within 8 mm for the 4 flow peaks. However, the predictions of stage on the rising and falling limb were found to be poor. Predicted water levels upstream of Site 3 were compared with those used in the Site 3 application (§4.6.2). Results suggest that the stage hydrograph used in the Site 3 application was much lower than the predicted stage at upstream of the river using the tightly-coupled model.

The predicted inundation extents were validated for Site 3. This was compared with the results obtained from the application to Site 3 (§4.6.2). The accuracy statistics show that the tightly-coupled model performs better at Site 3 than the simulation using the loose-coupled model, although only marginally. Results suggest that use of the downstream stage hydrograph at Site 3 with the loosely-coupled model significantly underestimated the inundation extent. Though the tightly-coupled model also failed to give correct inundation prediction at upstream of Site 3, other factors such as local runoff and flux through underground pipes need to be investigated before this can be confirmed.

# Chapter 7

## Conclusions and future development

The proceeding chapters have described the development of a two-dimensional raster-based diffusion wave flood inundation model and its applications to four sites on the River Ouse, using two different coupling approaches to the treatment of river flow and floodplain flow; and two wetting treatment approaches to the small-scale flow routing over topographically complex floodplains. This chapter aims: (i) to summarize the research achievements by reference back to the research aims and objectives identified in Chapter 1 (§7.1); (ii) to assess the methods used in and the results obtained from the research critically (§7.2); and (iii) to discuss future research issues related to the work carried out in this thesis (§7.3).

### 7.1 Research achievements with respect to aims and objectives

This research originated from the observation that there has been a lack of development of tools for and approaches to the determination of flood inundation over topographically complex floodplains, particularly in urban areas where flood risk is potentially greater than rural areas and has a higher political profile. This is due partially to the lack of high-resolution topographic data and partially to the constraints of computational resources required by modelling approaches. Recent developments in modelling approaches, data capture techniques and computational resources are gradually making more sophisticated modelling mode feasible. Thus, the developments of a two-dimensional raster-based diffusion wave inundation model which can take advantages of these developments were identified as the main research aim (§1.2.1). Research objectives were identified in relation to model developments and applications in terms of the coupling approach between the river flow and floodplain flow, the approaches to small-scale wetting treatment and the test of the model through application to simulate a real flood event. In order to achieve the aims and objectives identified, previous work was reviewed (§2), including river flow and floodplain inundation modelling, applications of remotely-sensed data, and the data representation in a GIS environment.

### **7.1.1 Achievements with respect to the development of the flood inundation model**

In terms of model development, a 2D raster-based diffusive wave flood inundation model was developed. This model solves the 2D Saint-Venant by ignoring the inertial terms in the momentum equations. The governing equations of the model were solved in a raster-based environment. The topographic domain was discretized into a mesh consisting of regular-sized cells and flux between cells is calculated based on topographic properties using a diffusive wave approach (§4.3.1). The model was coded in Java and visualisation tool was developed to facilitate analysis.

Compared with more complex flood inundation models such as finite-element models, the advantages of the raster-based diffusion wave model developed in this study are its ease of formulation, computational efficiency and its ability to use higher resolution topographic data. This allowed the model to be applied to larger areas with relatively higher resolution mesh, and over longer periods. As analysis of the interactions between mesh resolution, roughness parameterization and small-scale flow processes has generally involved a large number of simulations. These properties were fully utilized in this study.

### **7.1.2 Achievements with respect to coupled modelling of river flow and floodplain flow**

In terms of the coupling between the river flow and floodplain flow, the model can be classified as either loosely-coupled or tightly-coupled. Both the loosely-coupled and tightly-coupled approaches establish the connectivity between the river flow and floodplain flow through the common river-floodplain boundary. The loosely-coupled model treats the river flow and floodplain inundation as two separate processes (§3.2). River flow can be provided by an existing river flow model in the form of either stage or flow hydrographs (either uniform or non-uniform). If flow hydrographs are provided, flux from the river onto the floodplain is interpolated for each cell. If stage hydrographs are provided, flux from the river onto the floodplain is approximated by assuming the riverbank to be encompassed by a continuous, broad-crested weir where a weir equation can be applied. Regardless of the river flow data type, return flow from the floodplain to the river channel is calculated using the same approach as used in the floodplain flow routing. However, as the river flow is calculated before the initialisation of the 2D floodplain flow model, this return flow has no effect upon the river flow. Flux into a river from the floodplain is simply calculated as a mass loss.

Considering the complexity of floodplain flow observed when the loosely-coupled model was applied, particularly over structurally complex topographies and the effects this complexity might have upon river flow in terms of both the timing and direction of the return flow from the floodplain to the river channel, a tightly-coupled approach was developed. Return flow is used in the calculation of river flow instead of being treated merely as a mass loss from the 2D floodplain model (§6.3.2). In order to achieve this, a one-dimensional river flow model was developed. This model solves the full 1D Saint-Venant equations using a Preissmann Scheme in the raster-based environment of the 2D floodplain model (§6.3.1).

To establish the connectivity between the 1D river model and the 2D floodplain, the river channel in the 1D river flow model is represented by continuous sets of cells which represent the river channel in the 2D floodplain model. Individual river reaches are represented by different sets of continuous cells in the 2D environment of the floodplain model. Cross-sectional geometries are used to represent the geometries of individual reaches. Given appropriate boundary conditions, the 1D river flow model can be initialised and the stage and velocity profiles can be obtained for each river reach. Similar to the loosely-coupled model, the tightly-coupled model calculates the flux from the river to the floodplain by assuming a broad-crested weir along the river bank where a uniform flow equation can be applied. The flux from the floodplain into the river channel is calculated the same way as the floodplain flow routing. Unlike the loosely-coupled model, this return flow is used in the 1D river flow model as a boundary condition at each time step. This causes a change in water depth for each reach based on the volume of the inflow from the floodplain, the outflow onto the floodplain and the geometry of the reach. Thus, the 1D river flow and the 2D floodplain flow are calculated simultaneously.

In this way the effect of floodplain routing on the river flow is accounted for. This is novel as existing flood inundation models are either loosely coupled to a full 1D river flow model or tightly-coupled to a simplified 1D river flow model. Bates and De Roo (2000) coupled a kinematic wave river flow model to the 2D diffusive wave floodplain flow model and Horritt and Bates (2001a, b) coupled the 1D diffusive wave form of the full dynamic wave equations to the 2D diffusive wave floodplain model. The flow from the river channel to the floodplain is calculated the same way as the floodplain flow routing these two cases. Flux from the floodplain to the river channel is treated as lateral inflow in the 1D river flow model and this is incorporated into the mass equation. The tightly-coupled approach used here differs from these two cases in that: (i) the full dynamic wave routing scheme is used for the river flow; (ii) the flux from the river to the floodplain is calculated using a weir equation; and (iii) the flow from the floodplain to the river channel is treated explicitly through mass control instead of

being incorporated implicitly in the solution. The use of a river flow model that solves the full Saint-Venant equations was noted by Bates and De Roo (2000) as a refinement of the coupled model. In terms of the calculation of flux exchanges between the river channel and floodplain ((ii) and (iii)), the tightly-coupled approach used here is subtly different to those used in Bates and De Roo (2000) and Horritt and Bates (2001a, b).

### **7.1.3 Achievements with respect to the development of sub grid wetting treatment**

In terms of wetting treatment, the model used either a normal wetting treatment (§4.3.1) developed by Bradbrook *et al.* (2004), or a sub grid wetting treatment, developed in this study (§5.3). The normal wetting treatment controls the wetting process using a wetting parameter the value of which ranges from 0 to 1, with a value of 0 for wet cells, a value of 1 for fully wet cells, and values in between for the wetting front cells. The wetting parameter for a given cell is calculated as the accumulated value of the percentage of wetted areas of the cell over time. The percentage of the wetted area for a given cell at each time step is defined by inflow velocity, time step and cell size (Equation 4.11). Thus, the direction of the wetting of a cell is not accounted for in this approach.

In the sub grid wetting treatment, the wetting process within a grid cell is determined by the sub grid topography. Based on the investigation of the interaction between roughness parameterization and mesh resolution using the original wetting treatment, the sub grid approach recognises that treatments of sub grid-scale flow routing using roughness parameterization might not be able to represent the effects of structural elements on the floodplain (e.g. buildings, walls) adequately as such elements not only act as momentum sinks, but also have mass blockage effects. The latter may dominate, especially in structurally-complex urban areas. The sub grid approach developed here uses high-resolution topographic data to develop explicit parameterization of sub grid-scale topographic variability to represent both: (i) the volume of a given cell that can be occupied by the flow; and (ii) the effect of sub grid topography upon the timing and direction of fluxes (§5.3). Cell blockage effects are represented by establishing the relationship between water surface elevations of individual sub grid cells and the total volumes of water in a model cell. The sub grid water surface elevations can then be used to derive the direction and magnitude of flux from and into a grid cell based on a boundary porosity treatment approach. This approach differs from the original wetting treatment (adopted from Bradbrook *et al.*, 2004) in that, instead of using an empirical means for dealing with mesh resolution effects, it evaluates the wetting and

drying through sub grid topography explicitly, thus, reducing model dependence on mesh resolution.

#### **7.1.4 Achievements with respect to model applications**

Model applications were carried out using the two different coupling approaches and two different wetting treatment approaches developed in this study. These approaches allow a series of analysis central to the research objectives to be conducted. These have mainly involved: (i) the development of validation and verification approaches; (ii) the data processing related to model requirements; (iii) the investigation of interaction between roughness parameterization and mesh resolution, (iv) the investigation of relationship between validation data, floodplain configuration and flood size; (v) the effect of sub grid treatment upon flow routing; and (vi) comparison of the loosely- and tightly-coupled models.

#### **Development of the validation and verification approaches**

This study used both a validation and verification approach to evaluate model performance. The validation approach was adopted from an accuracy assessment approach used in remote sensing (Congalton and Green, 1999). As the model divides floodplain into three different wetting states (wet cells, wetting front cells and dry cells), this allows a number of accuracy statistics to be derived in terms of both the overall performance of the model and the performance in relation to individual wetting state. Accuracy assessment in previous studies normally considers two wetting states of the floodplain: wet and dry cells (e.g. Bates and De Roo, 2000; Horritt and Bates, 2001a, b). This study also considered the wetting front cells based on the understanding that: (i) wetting front cells do exist during flood inundation, particularly for a coarser mesh simulation; and (ii) the means of determining a wetting front cell is available in both the normal wetting treatment and the sub grid wetting treatment approaches.

The verification approach used in this study allows time series of comparison of model performance between model simulations. This is novel as traditional validation of inundation studies typically use single at-a-point in time validation data. As shown in the study, such data may be inappropriate to judge model performance because there are situations where good model performance might be obtained for some periods, but not all of them, due to the complex relationships between validation data, floodplain configuration and flood size, as well as the use of calibration parameters. The use of a time series verification approach allows a series of accuracy statistics to be derived using the quantitative assessment approach adopted from remote sensing. More importantly, this verification approach allows cross

comparison between model simulations to determine whether simulations with different calibration parameters are significantly different. This study used the model results obtained from the finest resolution simulation (4 m) as the reference data in the verification.

### **Data processing**

Most data available to this study are raw data. These need to be processed before they can be used in the model. The processing was mainly concerned with the topographic data. For both the loosely-coupled and tightly-coupled models, river location and floodplain topography are required. This study outlined a number of procedures that may be required in the extraction of river channel: (i) the removal of cells related to water bodies (except river channel) on the floodplain; (ii) the correction of elevations associated with overlapping areas of river channel with bridges; and (iii) the removal of the connection between the river channel and other water bodies on the floodplain. This study also outlined a number of procedures related to the processing of floodplain topography. These include: (i) the removal of ground elevations associated with tree canopies; (ii) the correction of bank elevation; and in places where lakes exist, (iii) the determination of the initial water surface elevations associated with lakes.

Validation data used for the 2D floodplain model were exclusively inundation extents. These were obtained from the aerial imagery available during recession period of the flood event. The processing of aerial imagery is required for obtaining inundation extent both for model validation and for the removal of elevations associated with tree canopies from the topographic data. This involved image classification during which the water bodies and trees were identified. This study used a supervised classification approach.

The tightly-coupled model also requires cross-section geometry to determine flow conveyance at different parts of the river. Raw drawings of cross-section geometry are available. However, due to the time involved in the processing of such data, these were not used to their full extent. Only the cross-section widths and ground elevations were taken from the drawings. A simple rectangular shape of the cross-section was assumed.

### **Findings in relation to roughness parameterization and mesh resolution**

In terms of roughness parameterization and mesh resolution, a large number of simulations were undertaken to investigate the interaction between model resolution and roughness specification. These were compared to each other using single point validation and time series verification approaches. This study found that the model is strongly sensitive to mesh resolution and less sensitive to roughness coefficients on the floodplain. The strong sensitivity to mesh resolution is related to three reasons: (i) the smoothing effect of mesh coarsening; (ii)

the cell blockage effect; and (iii) the effect of local topography upon small-scale flow wetting and drying. The smoothing effect associated with mesh coarsening is similar to the double-filtering problem encountered in finite-element models (Bates and Anderson, 1996). This study also investigated the smoothing effect of different interpolation approaches (nearest-neighbour, bilinear, and cubic convolution) and no significant differences were found between these three approaches. The effect of topographic variation at the model resolution scale is thought to be another important factor that causes the strong sensitivity to mesh resolution. This is associated particularly with complex floodplains where structural elements on the floodplain exert strong influence upon flow routing. First, these features tend to be smoothed out in a coarser mesh. Second, the timing and directions of the flow will be simplified with a coarser mesh. This might result in error as to where the flow can reach and the timing of the flow. Using roughness parameterization may reduce flux over certain features. But in some situations, some features on the floodplain act as complete barriers to the flow and this property might not be fully recognized using roughness parameterization. Moreover, as shown in this and other studies (e.g. Bates and De Roo, 2000), 2D raster-based models are relatively insensitive to roughness coefficients on the floodplain. Applications carried out in this study showed that in order for the roughness coefficient to reduce flow rate effectively, very high values of  $n$  are required. These values are well beyond the range of  $n$  values for which the Manning equation was originally formulated. This leads us to question the meanings of roughness in the calibration of such models in relation to mesh size and model structure. At the same time, this calls for the development of alternative calibration and parameterization approaches for 2D raster-based models. As noted by Bates (2000), there has been a lack of developments of small-scale wetting and drying treatment for practical applications of such numerical schemes. This is addressed in this study in the sub grid-scale wetting treatment approach.

### **Development of the sub grid wetting treatment**

In relation to the above findings, the sub grid wetting treatment approach developed in this study addressed this problem through explicit use of high-resolution topographic data. The sub grid wetting treatment approach developed in this study represents the cell blockage and cell flux effects explicitly through the use of higher resolution sub grid topography, reducing the computation costs associated with models using the sub grid mesh alone. Applications of this approach using the first order approximation with a 2:1 ratio of sub grid topography found that this approach was able to reduce model sensitivity to mesh resolution effectively and to improve model performance in terms of inundation extent prediction. This approach was found to be more effective for a finer mesh simulation. This is probably because the model uses the immediate finer mesh to represent the sub grid topography. If higher orders of

sub grid topography (on a 4:1, 8:1 or higher ratio) are used, a model with a coarser mesh is expected to perform better. It was also found that use of the sub grid treatment increased model sensitivity to roughness coefficient. During model verification, models with lower values of  $n$  combined with a sub grid treatment were found to produce much better results than models with higher values of  $n$  and a normal treatment. In terms of computational costs, this study showed that the sub grid approach was more computationally effective than its immediate finer mesh model with the normal treatment, while with improved predictive performance. Thus, the sub grid wetting treatment approach changes the way mesh resolution and roughness coefficients interact in positive way. The development of the sub grid wetting treatment approach is believed to be a major contribution to the improved representation of urban flooding as noted by Wheater (2002).

### **Findings in relation to floodplain configuration, flood size and validation**

In terms of model validation and verification, this study showed the danger of using at-a-point in time inundation extent data for model validation due to the complex relationship between model validation, floodplain configuration and flood size. Although it is recognized that inundation extent data can provide distributed validation data for inundation studies and it is sensitive to errors in predicted water depths for relatively flat floodplains, they are normally zero-dimensional in time. Thus, using such data to evaluate model performance over time might be problematic, particularly for laterally confined floodplains when confinement is reached and changes in water depth do not make much difference to inundation extents. Validation using at-a-point in time data may suggest good model performance for certain periods of the flood, but poor results for the rest. This is related to timing of inundation and the floodplain configuration. For example, for a laterally confined floodplain, validation data obtained long after the lateral confinement areas are filled are not able to assist in model developments as, in terms of the timing of the flood as, after this point, the inundation extent might stay the same unless significant drying occurs or the lateral confinement zone is broken. In such cases, if inundation extents were to be used, validation data obtained before the point when the lateral confinement of the floodplain is filled might be the only way to discriminate between the wetting and drying treatments of different models. For this reason, Bates and Anderson (2001) suggested that surface velocity measurements might be the only way to evaluate high order flood inundation models. However, such data are generally unavailable during a flood event.

### **Findings in relation to inflow data accuracy**

Applications carried out in this study noted the importance of using accurate inflow in flood inundation studies. The applications using the loosely-coupled model have used uniform stage

hydrographs in the river regardless of the configuration of the river channel. This might be an inappropriate approximation for long channels or for channels with significant variation in stage along the channel. If inaccurate amount of flux are routed from the river to the floodplain, the inundation pattern over time is likely to be wrong. Moreover, the amounts and timings of the return flow to the river are also likely to be wrong. Indeed, the application at Site 3 showed the danger of using inaccurate inflow data for the 2D inundation model due to the approximation of the river flow using a uniform hydrograph. Thus, the tightly-coupled model was developed and applied to a longer reach on the River Ouse. However, this also failed to produce satisfactory results in places where the loosely-coupled underperformed, though with improved overall performance. This was thought to be caused by other reasons.

## **7.2 Critical assessment of methods and results**

This study involves a number of assumptions and simplifications with respect to model developments and applications. These are reviewed in the next few sections.

### **7.2.1 Limitations in model development**

#### **Diffusion wave approach**

In terms of model developments, the diffusion wave model developed here uses a highly simplified treatment of momentum transfer on the floodplain by ignoring the local and convective acceleration terms in the governing equations. This is a limitation in the model structure as known hydraulics are not fully represented in the model. However, the process representation required to simulate flood characteristics is a subject of current research and debate (Horritt and Bates, 2001a). Studies (e.g. Horritt and Bates, 2001b) have found that despite the simplified representation of hydraulic processes, raster-based models can produce good results when compared with the more complex modelling approaches such as finite-element approaches. However, these comparisons were only carried out to investigate the relative performance of the model in terms of inundation extent predictions. Model performance in terms of depth and velocity predictions has not been explored explicitly. Compared with complex flood inundation models such as those based on finite-element approaches, the calibration and parameterization efforts required by raster-based diffusion wave models are much less. This is an advantage given the poorly understood calibration efforts involved in complex models. Furthermore, given the simplicity in model formulation and the possibility of simulating flood inundation using higher resolution topographic data over larger areas and for longer periods, the advantages of using such models outweigh limitations in model structure.

### **Coupling between the river flow and floodplain flow**

In terms of river flow modelling, in this study, the river channel geometry was highly simplified to rectangular shapes in the tightly-coupled model. This approach was found to underestimate discharge capacity significantly at low overbank flow depths due to the uniform velocity assumption (Myers and Brennen, 1990). In terms of the coupling between river and floodplain flows, Bates and De Roo (2000) noted that there is a need for the representation of momentum exchange across the shear layers between the river channel and floodplain. However, in this study, both the loosely- and tightly-coupled models assumed continuous broad-crest weirs along the river channel and a weir equation was used to calculate flow exchange between the river channel and floodplain. The connection between the river flow and floodplain flow only accounts for the mass transfer. Momentum transfer and the effects of advection and secondary circulation on mass transfer are not represented.

Given the complex cross-sectional geometries found for the river, it is expected that flow behaviour at the main river channel-floodplain boundary will be much more complex than assumed in this study. This is an important issue and needs to be addressed in future model development.

### **Sub grid wetting treatment**

Another limitation in model development is related to the sub grid wetting treatment approach. The sub grid wetting treatment approach developed in this study has used the immediate finer mesh on a 2:1 ratio as the sub grid topography regardless of the original mesh resolution. Applications suggested that this approach was more effective for a finer mesh. This is due to the fact that only the immediate finer sub grid topography was used for a given mesh. Thus, higher orders of sub grid topography are required to represent cell block and cell flux effects at the sub grid-scale in order for this approach to have better results for the coarser mesh.

### **7.2.2 Limitations in model applications**

A number of simplifications exist in model applications and these need to be refined in future model applications where necessary. These generally include: (i) the selection of application sites in relation to the approximation of river stage; (ii) data processing in relation to topographic parameterization and model validation; (iii) approximation of river geometry for the tightly-coupled model; (iv) the roughness parameterization using high values of Manning's  $n$  and (v) the validation of the 1D river flow model.

First, for the loosely-coupled model, uniform flow was assumed for the applications, regardless of river configuration. All application sites have strongly curved reaches and are over 5 km long. Thus, the use of uniform flow is likely to be inappropriate, particularly for longer reaches such as Site 3. For Site 3, the use of downstream stage hydrographs outside of the simulation domain has been shown to underestimate inflow from the river to the floodplain. Although for the other 2 sites, stage hydrographs within the simulation domain were used, errors in the amount of flux from the river to the floodplain were also expected. This might have important effects upon the timing of flow routing and, thus, inundation pattern for some parts of the floodplain. If the amount of water entering from the river channel is not right, it is likely that inundation patterns are not right either, as the model is mass conservative and incorrect amounts of water lead to incorrect water depths which eventually determine where flow can reach. This can be investigated if inundation extents during the wetting process are available. However, given that, in this study, the validation aerial imagery were obtained long after the confined parts of the floodplain were filled, it was impossible to determine whether using a uniform hydrograph has caused significant errors in the estimation of influx. This, again, underlines the danger of using single at-a-time inundation extent data to evaluate model performance. In relation to this, if inundation extent data, or surface velocity and water depth during the wetting process are available, a number of questions unanswered in this study including those associated with the accuracy of inflow stage, can be investigated. This might not be a problem for the investigation of interaction between roughness parameterization and mesh resolution, as well as for the comparison between normal and sub grid wetting treatments as, in addition to the single-point validation, time series verification approach allows model performance to be compared with each other in a relative sense. The effect of inflow data on different simulations should be the same. Indeed, the current generation of distributed models have been limited by the availability of distributed time series of internal state variables for model evaluation (Beven, 2002).

Second, in terms of data processing, image classification and topographic data processing involve a number of simplifications. These may have some effects upon model predictions and validation. Image classification used a simple supervised classification approach. The results of image classification were not satisfactory in terms of the accuracy of the classified water bodies and trees (§3.5.3). This is probably due to the large degrees of overlapping areas in the spectral signatures of the image, as a result of the degradation in image quality during the rectification and combination of individual image tiles. The resultant water body and tree layers were further processed using mask layers based on known knowledge. This is expected to have improved the accuracy of the classifications. The accuracy of the classification is closely related to the reliability of model validation and the processing of floodplain

topography regarding the removal of ground elevations associated with tree canopies. The accuracy statistics of image classification for the water bodies are theoretically the best possible accuracy statistics the applications can obtain. However, some of the model applications carried out in this study obtained better accuracy statistics than those obtained from image classification. This is due to the post-processing of the resultant classification.

The tree layer was used to remove elevations associated with tree canopies from the DEM (§3.6.1) derived from first-return LiDAR data. Two sorts of errors are likely to exist during this process: (i) the errors in the tree locations; and (ii) the errors associated with determination of tree heights. Although the accuracy for the classification of trees was not high, post-processing using the mask layer was believed to have improved the classification. Most errors are considered to be associated with the assumption that tree heights are uniform throughout the domain. Visual comparison of the vegetation in the aerial imagery shows that vegetation heights vary for different types and even for the same type. This assumption might in some cases lead to overestimates, while, in other cases, to underestimates in relation to the storage effects associated with vegetations. Although, there are methods for determining tree heights, including field survey and comparing ground elevations of tree cells with surrounding ground cells (e.g. Mason *et al.*, 2003), these were not adopted in this study. It is expected that tree removal has a similar effect for all simulations. This should not invalidate analysis where verification approaches were used.

Third, the drag effects of floodplain vegetations upon flood inundation were not explored in this study. This study assumed that storage effects of vegetations dominate over flow resistance associated with these features. Although it is recognized that the drag effects associated with the presence of vegetation are likely to form the bulk of resistance term (Kouwen, 1988, cited by Lane, 2003a), this is not addressed due to the complexity involved in determining the drag coefficient of vegetation (Bates, 2004) and the lack of required data.

Fourth, the tightly-coupled model used highly simplified cross-section geometries to represent river channel topography (§6.4). Hydraulic structures such as bridges and culverts were not represented in the model structure. These features normally act as flow restrictions and flow might back up behind these features as storage volumes. Thus, the actual flow through these restrictions and the corresponding energy grade line may be considerably less, resulting in significant differences in water surface elevations. Others (e.g. Bates and De Roo, 2000; Bradbrook *et al.*, 2004) have used similar approaches and acceptable predictions were found. However, in these studies, predictions for the river flow were not validated strictly. In this study, validation of stage predictions was only carried out at the upstream boundary of the

river. The peak stages at the upstream were predicted reasonably well. However, the predictions on the rising and falling limb were poor. This may be caused by a number of reasons. First, the simplified cross-section geometry might be an inappropriate assumption for such a complex river. Second, as the reach simulated is over 10 km long and several bridges are located along the river, the effects of these bridges need to be accounted for in the model. For a given bridge, the difference between upstream and downstream of the bridge can be quite high during a flood event. However, this is not considered in the boundary condition specification during model initialisation. Third, uniform roughness coefficients for the whole river channel were used and downstream of the river was found to be smoother than the upstream. Thus, varied roughness values might be able to improve model predictions. Moreover, in relation to cross-section geometry, flow resistance may vary for a given cross-section. These need to be addressed in future model development.

Fifth, the use of high values of Manning's  $n$  is theoretically questionable. The high values of Manning's  $n$  used at Site 1 and Site 2 clearly extend beyond the range of  $n$  values obtained based on the original formulation of Manning's law. However, given our current understanding of the physical meaning of Manning's  $n$  in diffusion wave models and the fact that high values of Manning's  $n$  improved model performance, this might not be a problem. Roughness coefficients in diffusion wave models represent not only boundary resistance related to flow and channel properties but also those processes that are not represented explicitly in the model such as advection and secondary circulation. Thus, calibration using roughness coefficients is in fact also used to compensate for these processes that are not represented in the model. Thus, the actual meaning of roughness coefficients needs to be interpreted with caution in such situations.

Lastly, in terms of the validation of the 1D river flow model, comparison with other models such as HEC-RAS and ISIS (storage cell approach) could be very valuable, but at this point, this has not been undertaken.

### **7.3 Future research developments**

The development of the 2D flood inundation model, either loosely-coupled to an existing 1D river flow model or tightly-coupled to the 1D river flow model developed in this study requires further refinements. These include, among others: (i) the development of the 1D river flow model to incorporate important hydraulic structures such as bridges/culverts, lateral structures and pumping stations; (ii) the development of approaches to represent the

momentum exchange between river channel and floodplain; and (iii) the development of the sub grid wetting treatment for better representation of small-scale routing process.

### **7.3.1 Development of the 1D river flow model**

The development of the 1D river flow model in relation to the hydraulic structures such as bridges and culvers, along the river channel is straight forward. The model can be readily modified to represent these structures in the raster environment as internal properties of individual cross-sections, to adjust conveyance capacity of cross-sections. These developments are expected to improve the prediction of river flow, particularly in a complex river channel like the one simulated in this study.

### **7.3.2 Representation of momentum transfer at the river-floodplain boundary**

The development of approaches that account for the momentum exchange between the river channel and floodplain requires much effort. Cross-section data available in this study suggested that the shapes of cross-sections on the River Ouse vary significantly. Many of the cross-sections are characterised by compound river channels where a deep main channel is bounded by a relatively shallow floodplain on one or both sides. Particularly, cross-sectional geometries upstream and downstream of a bridge are very likely to be different to the others. Thus, the conveyance capacity of cross-sections is likely to be significantly different. The simulations carried out in this study assumed a uniform rectangular shape and a single uniform Manning's  $n$  for all cross-sections. Thus, cross-sectional geometries and the associated conveyance capacity might have been oversimplified. Modelling the momentum transfer in the river channel and at the river-floodplain boundary generally involves the specification of friction factors for different part of the cross-sections. Since the 1960s, a number of approaches to conveyance estimation of compound channels have been developed. These include: (i) the single channel (SCM) method (Nuding, 1991, cited by Helmiö, 2004), (ii) the divided channel method (DCM); and (iii) the apparent shear stress (ASS) method (see the review of Helmiö, 2004). In the divided channel method, the interface between the main river channel and floodplain is used in the calculation of the wetted perimeter (Posey, 1967, cited by Helmiö, 2004; Myers, 1987). The ASS method assumes that the shear stress at the interface between the main river channel and floodplain is significantly higher than the boundary shear stress at the channel boundary or the floodplain (Wormleaton et al., 1982; Knight and Demetrious, 1983; Pasche, 1984, cited by Helmiö, 2004; Mertens, 1989; Nuding, 1991, cited by Helmiö, 2004). These approaches were developed for different cross-sectional

geometries and can be readily used for natural river applications. The next step for model development will involve the application of these approaches to the coupled modelling of river flow and floodplain inundation. Given the available approaches, the main challenge is to represent the cross-sectional geometry of the river in relation to the floodplain topography near the bank region in the 2D raster-based environment where the 1D river flow and 2D floodplain model are solved.

### 7.3.3 Coupling the flood inundation model with other hydrological processes

As a natural extension of the coupling between the river flow and floodplain flow, this model can be readily modified to incorporate other hydrological processes such as precipitation, evaporation and interception of soil water and groundwater, and runoff processes (including hillslope hydrology). Thus, this is an area of future model development which will allow the investigation of the interaction between fluvial flood and related hydrological processes over the floodplain and on the hillslopes. Particularly, the coupling between hillslope and channel has been addressed in several studies since the early 1980s (e.g. Brunsden and Thornes, 1979; Nortcliff and Thornes, 1984, Brunsden, 1993, cited by Michaelides and Wainwright, 2002). These studies mainly involved the investigation of connectivity between the hillslopes and channel in terms of the runoff- and sediment-delivery rates from the hillslopes to the channel and in terms of the fluvial activity imposed by the channel on the hillslope base (Michaelides and Wainwright, 2002). An example of the discretization of domain topography for coupled modelling of river flow and hillslope runoff was described in Michaelides and Wainwright (2002). This is shown in Figure 7.1.

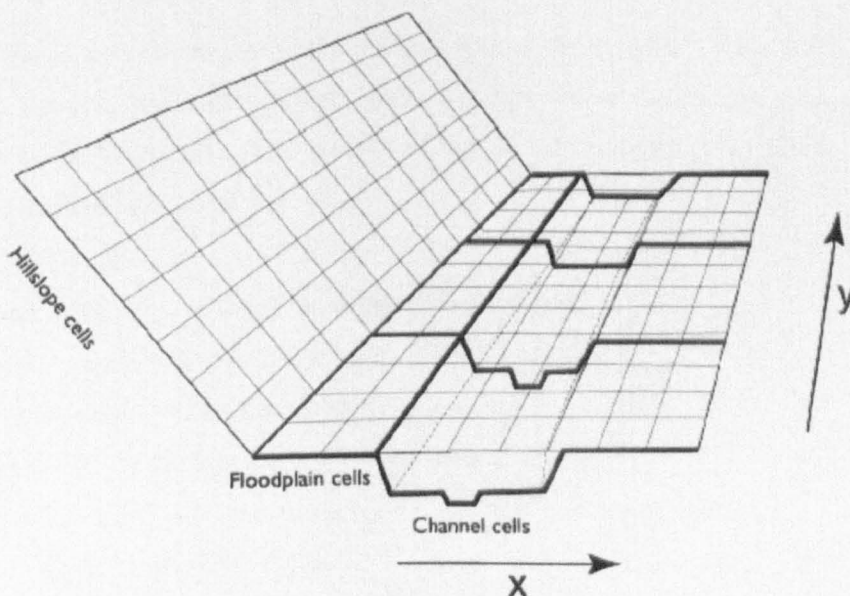


Figure 7.1: Discretization of the domain topography for the coupled modelling of river flow and hillslope runoff in a 2D environment. (after Michaelides and Wainwright, 2002)

Much of the research has been at the conceptual level and focusing on the impact of hillslope runoff upon river flow. The future development of the model will allow a number of issues to be investigated, including: (i) the effects of hillslope runoff on flood inundation and, implicitly, on river flow; (ii) the effects of rainfall on flood inundation; (iii) the effects of mesh resolution on flood inundation, with reference to hillslope runoff; and (iv) model sensitivity to calibration parameters including rainfall rate, infiltration rate, and roughness coefficient, etc.

### **7.3.4 Representation of small-scale wetting treatments**

Basically, the research carried out in this thesis showed the complex relationship between mesh resolution and small-scale flow processes. These two aspects are interrelated with both the methodological and data provision aspects of flood inundation studies. Although the increasing availability of high-resolution topographic data is gradually relieving the uncertainties in topographic data representation, the use of such data over large scales (in space and time) is still constrained by computational resources. There remains a need for the development of approaches to small-scale flow routing representation. Thus, future model development with respect to wetting and drying treatments at the local scale is also required. This can be based on the sub grid wetting treatment approach developed in this study. Given the relatively low effects of the sub grid wetting treatment upon coarser meshes as compared with finer meshes, the next step in this is to develop higher orders of sub grid topography treatments.

# Appendix A

The CD attached to this thesis includes visualizations of several flooding processes simulated using the model developed in this thesis. The flood events modelled occurred on the River Ouse and River Wharfe in 2000. The visualizations were produced as Java applets embedded in web pages. A web browser which supports Java applet is required for the visualization. Depending on PC performance, time to load the Java applet varies.

The visualizations are shown as time series of inundation extents for the 2000 flood event on the River Ouse and River Wharfe. These include:

- 1) Applications to Naburn Weir (Site 1) on the River Ouse using the loosely-coupled model;
- 2) Applications to the city centre of York on the River Ouse using the loosely-coupled model;
- 3) Applications to the a long reach on the River Ouse using the tightly-coupled model; and
- 4) Applications to the River Wharfe using the loosely-coupled model.

Simulations on the River Ouse were presented in this thesis. Simulations on the River Wharfe were presented in Tayefi (2005). Simulations on both rivers were carried out using the model developed in this thesis. The difference between the applications on the River Ouse and River Wharfe is the types of inflow data used. Simulations on the River Ouse used uniform stage hydrograph for the whole river. Simulations on the River Wharfe used flow hydrographs for different parts of the river as inflow data.

The index file in the root directory of the CD is named "Index.html". This file contains links to different visualizations. Alternatively, the visualizations can be accessed through separate html pages in the "Appendix A" directory of the CD. In summary, the file names and the associated visualizations are as follow:

- OuseFlood2000\_NaburnWeir.html (loosely coupled)  
A reach near the Naburn Weir on the River Ouse (Site 1)
- OuseFlood2000\_CityOfYork.html (loosely coupled)  
A reach across the city centre of York (Site 3)
- OuseFlood2000\_LongerReachCityOfYork.html (tightly coupled)  
Long reach on the River Ouse
- WharfeFlood2000\_Walls.html (loosely coupled)

- With walls built into the topography on the River Wharfe  
WharfeFlood2000\_NoWalls.html (loosely coupled)
- Without walls built into the topography on the River Wharfe  
WharfeFlood2000\_Comparison.html (loosely coupled)
- Comparison of the effects of walls upon flow routing

# Bibliography

- Abbott, M.B. and Basco, D.R. (1989). *Computational Fluid Dynamics: an Introduction for Engineers*. London, Longman Scientific and Technical Ltd.
- AIAA (1998). *Guide for the verification and validation of computational fluid dynamics simulations (G-077-1998e)*, American Institute of Aeronautics and Astronautics.
- Akanbi, A. and Katopodes, N.D. (1988). "Model for flood propagation on initially dry land." *ASCE Journal of Hydraulic Engineering* **114**: 689-719.
- Al-Sabhan, W., Mulligan, M. and Blackburn, G.A. (2003). "A real-time hydrological model for flood prediction using GIS and the WWW." *Computers, Environment and Urban Systems* **27**(1): 9-32.
- Baltsavias, E. (1999a). "Airborne laser scanning: existing systems and firms and other resources." *Photogrammetric Engineering and Remote Sensing* **54**(2-3): 164-198.
- Baltsavias, E. (1999b). "A comparison between photogrammetry and laser scanning." *Photogrammetric Engineering and Remote Sensing* **54**(2-3): 83-94.
- Bates, P.D. and Anderson, M.G. (1993). *A two-dimensional finite element model for river flow inundation*. *Proceedings of the Royal Society of London Series A*, 400.
- Bates, P.D. (2000). "Development and testing of a sub grid-scale model for moving-boundary hydrodynamic problems in shallow water." *Hydrological Processes* **14**(2073-2088).
- Bates, P.D. (2004). "Remote sensing and flood inundation modelling." *Hydrological Processes* **18**: 2593-2597.
- Bates, P.D. and Anderson, M.G. (1996). "A preliminary investigation into the impact of initial conditions on flood inundation predictions using a time/space distributed sensitivity analysis." *Catena* **26**(1-2): 115-134.
- Bates, P.D. and Anderson, M.G. (2001). Validation of hydraulic models. *Model Validation: Perspectives in Hydrological Science*. Anderson, M.G. and Bates, P.D. Chichester, John Wiley and Sons.
- Bates, P.D., Anderson, M.G., Baird, L., Walling, D.E. and Simm, D. (1992). "Modelling floodplain flows using a two-dimensional finite element model." *Earth Surface Processes and Landforms* **17**: 575-588.
- Bates, P.D., Anderson, M.G. and Hervouet, J.M., Eds. (1994). *Computation of a flood event using a two-dimensional finite element model*. *Modelling Flood Propagation over Initially Dry Areas*. New York, American Society of Civil Engineers.
- Bates, P.D., Anderson, M.G. and Hervouet, J.M. (1995). *Initial comparison of two two-dimensional finite-element codes for river flood simulation*. *Proceedings of the Institute of Civil Engineers, Water, Maritime and Energy*.
- Bates, P.D., Anderson, M.G., Hervouet, J.-M. and Hawkes, J.C. (1997). "Investigating the behaviour of two-dimensional finite element models of compound channel flow." *Earth Surface Processes and Landforms* **22**(1): 3-17.
- Bates, P.D., Anderson, M.G., Price, D.A., Hardy, R.J. and Smith, C.N. (1996). *Analysis and development of hydraulic models for floodplain flows*. *Floodplain Processes*. Bates, P.D. and Anderson, M.G. Chichester, John Wiley and Sons, 215-254.
- Bates, P.D., Horritt, M.S. and Hervouet, J.-M. (1998). "Investigating two-dimensional, finite element predictions of floodplain inundation using fractal generated topography." *Hydrological Processes* **12**(8): 1257-1277.
- Bates, P.D., Marks, K.J. and Horritt, M.S. (2003). "Optimal use of high-resolution topographic data in flood inundation models." *Hydrological Processes* **17**: 537-557.
- Bates, P.D. and De Roo. (2000). "A simple raster-based model for flood inundation simulation." *Hydrological Processes* **236**: 54-77.
- Bates, P.D., Stewart, M.D., Siggers, G.B., Smith, C.N., Hervouet, J.-M. and Sellin, R.H.J. (1998). *Internal and external validation of a two-dimensional finite element code for river flood simulations*. *The Institution of Civil Engineers - Water and Maritime*

*Engineering.*

- Becheteler, W., Hartmann, S. and Otto, A.J. (1994). Coupling of 2D and 1D models and integration into Geographic Information Systems (GIS). *Proceedings of the 2nd International Conference on River Flood Hydraulics*, Chichester: John Wiley and Sons.
- Beffa, C. (1996). Application of a shallow water model to braided flows. *HydroInformatics 96'*, Zurich.
- Beffa, C. and Connell, R.J. (2001). "Two-dimensional floodplain flow - part 1: model description." *Journal of Hydrological Engineering* **6**: 397-405.
- Benkhaldoun, F. and Monthe, L. (1994). An adaptive nine-point finite volume Roe scheme for two dimensional Saint Venant equations. *Modelling Flood Propagation over Initially Dry Areas*. Molinaro, P. and Natale, L. New York, American Society of Civil Engineers: 30-44.
- Beven, K.J. (1989). "Changing ideas in hydrology - the case of physically-based models." *Journal of Hydrology* **105**: 157-172.
- Beven, K.J. (1996). Equifinality and uncertainty in geomorphological modelling. *The Scientific Nature of Geomorphology*. Rhoads, B. L. and Thorn, C. E. Chichester, John Wiley and Sons.
- Beven, K.J. (2000). *Rainfall-Runoff Modelling: the Premier*. Chichester, John Wiley and Sons.
- Beven, K.J. (2001). Calibration, validation and equifinality in hydrological modelling. *Model Validation: Perspectives in Hydrological Science*. Anderson, M.G. and Bates, P.D. Chichester, John Wiley and Sons.
- Beven, K.J. (2002). "Towards an alternative blueprint for a physically based digitally simulated hydrologic response modelling system." *Hydrological Processes* **16**(2): 189-206.
- Biggin, D.S. and Blyth, K. (1996). "A comparison of ERS-1 satellite radar and aerial photography for river flood mapping." *Journal of Chartered Institute of Water and Environmental Management* **10**: 59-64.
- Bishop, Y., Fienberg, S. and Holland, P. (1975). *Discrete Multivariate Analysis: Theory and Practice*. Cambridge, MIT Press, MA.
- Brackett, R.A., Arvidson, R.E., Izenberg, N.R. and Saatchi, S.S. (1995). Use of polarimetric and interferometric radar data for flood routing models: first results for the Missouri River, section 36 - Planetary Geology: Radar Remote Sensing of Floodplains, Mountain Belts, and Volcanoes. *Annual Meeting of the Geological Society of America*, New Orleans.
- Bradbrook, K.F., Lane, S.N., Waller, S.G. and Bates, P.D. (2004). "Two dimensional diffusion wave modelling of flood inundation using a simplified channel representation." *International Journal of River Basin Management* **2**(3).
- Brakensiek, D. L. (1967). A simulated watershed flow system for hydrograph prediction: A kinematic application. Paper no. 3, Proc. of the International Hydrology Symp., Fort Collins, Colorado.
- Burrough, P.A. and McDonnell, R.A. (1998). *Principles of Geographical Information Systems*. Oxford, Clarendon Press.
- Charlton, M.E., Large, A.R.G. and Fuller, I.C. (2003). "Application of airborne laser in river environments: the River Coquet, northumberland, UK." *Earth Surface Processes and Landforms* **28**: 299-306.
- Chow, V.T. 1959. Open-channel hydraulics. McGraw-Hill book company, New York.
- Chow, V.T., Maidment, D.R. and Mays, L.W. (1988). *Applied Hydrology*. New York, McGraw-Hill.
- Cioffi, F. and Gallerano, F. (2003). "A two-dimensional self-adaptive hydrodynamic scheme for the assessment of the effects of structures on flooding phenomena in river basins." *River Research and Applications* **19**(1).
- Cobby, D.M., Mason, D.C., Horritt, M.S. and Bates, P.D. (2003). "Two-dimensional hydraulic flood modelling using a finite-element mesh decomposed according to vegetation and topographic features derived from airborne scanning laser altimetry."

- Hydrological Processes* 17(10): 1979-2000.
- Cohen, J. (1960). "A coefficient of agreement for nominal scales." *Educational and Psychological Measurement* 20: 37-40.
- Cohen, L.D. (1991). "On active contour models and balloons." *CVGIP: Image Understanding* 53: 211-218.
- Congalton, R.G. and Green, K. (1999). *Assessing the Accuracy of Remotely Sensed Data: Principles and Practice*. Boca Raton, Lewis Publishers.
- Connell, R.J., Painter, D.J. and Beffa, C. (2001). "Two-dimensional floodplain flow - part 2: model validation." *Journal of Hydrological Engineering* 6: 406-415.
- Courant, R. and Friedrichs, K.O. (1948). *Supersonic Flow and Shock Waves*. New York, InterScience Publishers.
- Cunge, J.A. (1969). "On the subject of a flood propagation computation method (Muskingum Method)." *Journal of Hydraulic Research* 7(205-230).
- Cunge, J.A., Holly, J.F.M. and Verwey, A. (1976). *Practical Aspects of Computational River Hydraulics*. London, Pirman.
- Darby, S.E. (1998). "Modelling width adjustment in straight alluvial channels." *Hydrological Processes* 12(8): 1299-1321.
- Defina, A., D'Alpaos and Matticchio, B. (1994). A new set of equations for very shallow water and partially dry areas suitable to 2D numerical models. *Modelling Flood Propagation over Initially Dry Areas*. Molinaro, P. and Natale, L. New York, American Society of Civil Engineer, 72-81.
- Downs, P.W. and Priestnall, G. (1999). "System design for catchment-scale approaches to studying river channel adjustments using a GIS." *International Journal of Geographical Information Science* 13(3): 247-266.
- El-Hames, A.S. and Richards, K.S. (1998). "An integrated, physically based model for arid region flash flood prediction capable of simulating dynamic transmission loss." *Hydrological Processes* 12(8): 1219-1232.
- Environment Agency (1997). *Evaluation of the LiDAR Technique to Produce Elevation Data for Use within the Agency*, Environment Agency National Centre for Environmental Data and Surveillance, Bath.
- Environment Agency (2004). *Hydraulic Model of the River Ouse*, York, Environment Agency.
- Estrela, T. and Quintas, L., Eds. (1994). Use of GIS in the modelling of flows on floodplains. *Proceedings of the 2nd International Conference on River Flood Hydraulics*. Chichester, John Wiley and Sons.
- Evans, E., Ashley, R., Hall, J., Penning-Rowsell, E., Sayers, P., Thorne, C. and Watkinson, A. (2004). *Foresight: Future Flooding: Scientific Summary: Volume II: Managing Future Risks*. London, Office of Science and Technology.
- Eveitt, B.S. (1998). *The Cambridge Dictionary of Statistics*. Cambridge, Cambridge University Press.
- Falconer, R.A. and Chen, Y. (1991). An improved representation of flooding and drying and wind stress effects in a two-dimensional tidal numerical model. *Proceedings of the Institution of Civil Engineers, Part 2*.
- Feldhaus, R., Höttages, R., Brockhaus, T. and Rouvé, G., Eds. (1992). Finite element simulation of flow and pollution transport applied to part of the River Rhine. *Hydraulic and Environmental Modelling: Estuarine and River Waters*. Ashgate, Aldershot.
- Flood, M. and Gutelius, B. (1997). "Commercial implications of topographic terrain mapping using scanning airborne laser radar." *Photogrammetric Engineering and Remote Sensing*(63): 327.
- France, P.W. (1981). "A simple technique for the analysis of free surface flow problem." *Advances in Water Resources* 4: 20-22.
- Fread, D. L. (1984). *The NWS DAM-BREAK Flood Forecasting Model*. Silver Spring, Maryland, Office of Hydrology, National Weather Service.
- Fread, D.L., Ed. (1993). *Handbook of Applied Hydrology (Chapter 10)*. New York, McGraw-

Hill.

- French, L.R. (2003). "Airborne Lidar in support of geomorphologic and hydraulic modelling." *Earth Surface Processes and Landforms* **28**: 321-335.
- Fryer, J.G., Chandler, J.H. and Cooper, M.A.R. (1994). "On the accuracy of heighting from aerial photographs and maps - implications to process modellers." *Earth Surface Processes and Landforms* **19**(6): 577-583.
- Galland, J.C., Goutal, N. and J-m., H. (1991). "TELEMAC-a new numerical model for solving shallow-water equations." *Advances in Water Resources* **14**(3): 138-148.
- Gee, D.M., Anderson, M.G. and Baird, L. (1990). "Large scale floodplain modelling." *Earth Surface Processes and Landforms* **15**: 512-523.
- Giammarco, P.D., Todini, E. and Lamberti, P. (1996). "A conservation finite elements approach to overland flow: the control volume finite element formulation." *Journal of Hydrology* **175**: 267-291.
- Gopalakrishnan, T.C. and Tung, C.C. (1983). "Numerical analysis of a moving boundary problem in coastal hydrodynamics." *International Journal of Numerical Methods in Fluids* **3**: 179-200.
- Helmiö, T. (2004). "Flow resistance due to lateral momentum transfer in partially vegetated rivers." *Water Resources Research* **40**(W05206).
- Holmgren, P. (1994). "Multiple flow direction algorithms for runoff modelling in grid based elevation models: an empirical evaluation." *Hydrological Processes* **8**: 327-334.
- Holster, H. (1978). Mathematical modelling of tidal flats: a few remarks. In Sundermann J, Holz KP (eds) *Mathematical Modelling of Estuarial Flows*, Springer: 172-177.
- Holz, K.P. and Leister, K. (1988). *Accurate waterline calculation in the Wadden Sea*. Berlin, Springer.
- Holz, K.P. and Nitsche, G. (1982). "Tidal wave analysis for estuaries with inter-tidal mud flats." *Advances in Water Resources* **5**: 142-148.
- Hord, R.M. (1982). *Digital Image Processing and Remotely Sensed Data*. New York, Academic Press.
- Horritt, M.S. (2000). "Calibration of a two-dimensional flood flow model using satellite radar imagery." *Water Resources Research* **36**(11): 3279-3291.
- Horritt, M.S. (2002). "Evaluating wetting and drying algorithms for finite element models of shallow water flow." *International Journal for Numerical Methods in Engineering* **55**: 835-851.
- Horritt, M.S. and Bates, P.D. (2001a). "Effects of spatial resolution on a raster based model of flood flow." *Journal of Hydrology* **253**: 239-249.
- Horritt, M.S. and Bates, P.D. (2001b). "Predicting floodplain inundation: raster-based modelling versus the finite-element approach." *Hydrological Processes* **15**: 825-842.
- Horritt, M.S. and Bates, P.D. (2002). "Evaluation of a 1D and 2D models for predicting river floodplain inundation." *Journal of Hydrology* **268**: 87-99.
- Horritt, M.S., Mason, D.C. and Luckman, A.J. (2001). "Flood boundary delineation from Synthetic Aperture Radar imagery using statistical active contour model." *International Journal of Remote Sensing* **22**(13): 2489-2507.
- Hyypä, J., Pyysalo, U., Hyypä, H. and Samberg, A. (2000). *Elevation accuracy of laser scanning-derived digital terrain and target models in forest environment*. *Proceedings of the 4th EARSeL Workshop LiDAR Remote Sensing of Land and Sea*. 20th EARSeL Symposium, Dresden, Germany.
- Imhoff, M.L., Vermillion, C., Story, M.H., Choudbury, A.M., Gafoor, A. and Pokyn, F. (1987). "Monsoon flood boundary delineation and damage assessment using spaceborne imaging radar and landsat data." *Photogrammetric Engineering and Remote Sensing* **54**(405-413).
- Katopodes, N. and Strelkoff, T. (1978). "Computing two-dimensional dam-break flood waves", *ASCE J. Hydraul. Div.*, 104, 1269-1288.
- Kawahara, M. and Umetsu, T. (1986). "Finite element method for moving boundary problems in river flows." *International Journal of Numerical Methods in Fluid* **6**: 365-386.

- King, I.P. and Roig, L. (1988). Two dimensional finite element models for floodplains and tidal flats. *Proceedings of an International Conference on Computational Methods in Flow Analysis*.
- Kloer (1994). "ERDAS IMAGINE Field Guide." ERDAS online documentation.
- Kloer, B.R. (1994). Hybrid parametric/non-parametric image classification. *ACSM-ASPRS Annual Convention*, Reno, Nevada.
- Knight, D.W. (1989). Hydraulics of flood channels. *Floods: Hydrological, Sedimentological and Geomorphological Implications*. Beven, K., Chichester, John Wiley and Sons. 83-105.
- Knight, D.W. and Brown, F.A. (2001). "Resistance studies of overbank flow in rivers with sediment using the flood channel facility." *Journal of Hydraulic Research* 39(3): 283-301.
- Knight, D.W. and Shiono, K., Eds. (1996). River channel and floodplain hydraulics. *Floodplain Processes*. Bates, P.D. and Anderson, M.G. Chichester, John Wiley and Sons.
- Kouwen, N. (1988). "Field estimation of the biomechanical properties of grass." *Journal of Hydraulics Engineering, American Society of Civil Engineers* 26(5): 559-568.
- Kouwen, N. and R. Li (1980). "Nonrigid, nonsubmerged, vegetative roughness on floodplains." *Journal of Hydraulic Engineering* 106(HY6): 1085-1103.
- Kouwen, N. and Fathi-Moghadam, M. (2000). "Friction factors for coniferous trees along rivers." *Journal of Hydraulic division, American Society of Civil Engineers* 126(10): 732-740.
- Kouwen, N. and Unny, T.E. (1973). "Flexible roughness in open channels." *Journal of Hydraulic Division, American Society of Civil Engineers* 99(5): 1085-1103.
- Krabill, W.B., Collins, J.G., Link, L.E., Swift, R.N. and Butler, M.L. (1984). "Airborne laser topographic mapping results." *Photogrammetric Engineering and Remote Sensing* 50: 685-694.
- Kraus, K. and N. Pfeifer (1998). "Determination of terrain models in wooded areas with airborne laser scanner data." *Journal of photogrammetry and remote sensing*. 53.
- Lane, S.N. (1998). "Hydraulic modelling in hydrology and geomorphology: A review of high resolution approaches." *Hydrological Processes* 12 (8) 1131-1150.
- Lane, S.N. (2000). "The measurement of river channel morphology." *Photogrammetric Record* 16: 937-961.
- Lane, S.N. (2003a). Lecture notes for GEOG 5730. University of Leeds, UK.
- Lane, S.N. (2003b). "Geomorphological Audit: Non-Tidal River Ouse (Yorkshire): Volume 1: Non-Technical Summary and Detailed Account of Evidence." Geocat, University of Leeds. EA/NE/338.
- Lane, S.N., Bradbrook, K.F., Richard, K.S., Biron, P.A. and Roy, A.G. (1999). "The application of computational fluid dynamics to natural river channels: three-dimensional versus two-dimensional approaches." *Geomorphology* 29(1-2): 1-20.
- Lane, S.N., Brookes, C.J., Kirkby, A.J. and Holden, J. (2004a). "A network-index based version of TOPMODEL for use with high-resolution digital topographic data." *Hydrological Processes* 18(1): 191-201.
- Lane, S.N. and Chandler, J.H. (2003). "The generation of high quality topographic data for hydrology and geomorphology: new data sources, new applications and new problems." *Earth Surface Processes and Landforms* 28: 229-230.
- Lane, S.N. and Hardy, R.J. (2002). Porous rivers: a new way of conceptualising and modelling river and floodplain flows. *Transport Phenomena in Porous Media II*. Ingham, D. B. and Pop, I. Oxford, Pergamon: 425-449.
- Lane, S.N., Hardy, R.J., Elliott, L. and Ingham, D.B. (2002). "High-resolution numerical modelling of three-dimensional flows over complex river bed topography." *Hydrological Processes* 16(11): 2261-2272.
- Lane, S.N., Hardy, R.J., Elliott, L. and Ingham, D.B. (2004b). "Numerical modelling of flow processes over gravely surfaces using structured grids and a numerical porosity treatment." *Water Resources Research* 40(1): art. no. W01302.

- Lane, S.N., James, T., Pritchard, H. and Saunders, M. (2003). "Photogrammetric and laser altimetric reconstruction of water levels for extreme flood event analysis." *Photogrammetric Record* **18**: 293-307.
- Lane, S.N. and Richards, K.S. (1998). "Two-dimensional spatial modelling of flow processes in a multi-thread channel." *Hydrological Processes* **12**(8): 1279-1298.
- Lane, S.N. and Richards, K.S. (2001). The 'validation' of hydrodynamic models: some critical perspectives. *Model Validation for Hydrological and Hydraulic Research*. Bates, P.D. and Anderson, M.G. Chichester, John Wiley and Sons: 413-438.
- Lane, S.N., Richard, K.S. and Chandler, J.H. (1994). "Developments in monitoring and terrain modelling small-scale river-bed topography." *Earth Surface Processes and Landforms* **19**: 349-368.
- Lane, S.N., Timothy, D.J., Hamish, P. and Marks, S. (2003). "Photogrammetric and laser altimetric reconstruction of water levels for extreme flood event analysis." *Photogrammetric Record* **18**(104): 293.
- Laura, R.A. and Wang, J.D. (1984). "Two dimensional routing on steep flows." *ASCE Journal of Hydraulic Engineering* **110**: 1121-1135.
- Leclerc, M., Bellemare, J.-F., Dumas, G. and Dhatt, G. (1990). "A finite element models of estuarine and river flows with moving boundaries." *Advances in Water Resources* **13**: 158-168.
- Lewin, J. and Hughes, D. (1980). "Welsh floodplain studies II. Application of a qualitative inundation model." *Journal of Hydrology* **25**: 37-50.
- Lim, Y.H. and Lye, L.M. (2003). "Regional flood estimation for ungauged basins in Sarawak, Malaysia." *Hydrological Sciences Journal* **48**(1): 79-94.
- Lynch, D.R. and Gray, W.G. (1980). "Finite element simulation of flow deforming regions." *Journal of Computational Physics* **36**: 135-153.
- Mason, D.C., Cobby, D.M., Horritt, M.S. and Bates, P.D. (2003). "Floodplain friction parameterization in two-dimensional river flood models using vegetation heights derived from airborne scanning laser altimetry." *Hydrological Processes* **17**: 1711-1732.
- Marks, S. and Bates, P.D. (2000). "Integration of high-resolution topographic data with floodplain flow models." *Hydrological Processes* **14**: 2109-2122.
- Michel, C., Perrin, C. and Andreassian, V. (2003). "The exponential store: a correct formulation for rainfall runoff modelling." *Hydrological Sciences Journal* **48**(2): 109-124.
- Moore, I.D., Grayson, R.B. and Ladson, A.R. (1991). "Digital terrain modelling: a review of hydrological, geomorphological, and biological applications." *Hydrological Processes* **5**: 3-30.
- Myers, W.R.C. (1987). "Velocity and discharge in compound channels." *Journal of Hydraulic Engineering* **113**(6): 753-765.
- Myers, W.R.C. and Brennen, E.K. (1990). "Flow resistance in a compound channel." *Journal of Hydraulic Research* **28**: 141-146.
- Nicholas, A.P. and McLelland, S.J., Eds. (1999). *Hydrodynamics of a floodplain recirculation zone investigated by field monitoring and numerical simulation. Floodplains: Interdisciplinary Approaches, Special Publication 163*. London, Geological Society.
- Nicholas, A.P. and Mitchell, C.A. (2003). "Numerical simulation of overbank processes in topographically complex floodplain environments." *Hydrological Processes* **17**: 727-746.
- Nicholas, A.P. and Walling, D.E. (1997). "Modelling flood hydraulic and overbank deposition on river floodplains." *Earth Surface Processes and Landforms* **22**: 59-77.
- O'Loughlin, E.M. (1990). "Modelling soil water status in complex terrain." *Agriculture and Forestry Metrology* **50**: 23-38.
- Olsen, N.R.B. and Stokseth, S. (1995). "Three-Dimensional numerical modelling of water-flow in a river with large bed roughness." *Journal of Hydraulic Research* **33**(4): 571-581.
- Pearson, D., Horritt, M.S., Gurney, R.J. and Mason, D.C. (2001). The use of remote sensing

- to validate hydrological models. *Model Validation: Perspectives in Hydrological Science*. Anderson, M.G. and Bates, P.D. Chichester, John Wiley and Sons.: 512.
- Pfeifer, K.a. (1998). "Determination of terrain models in wooded areas with airborne laser scanner data." *Photogrammetric Engineering and Remote Sensing* 54(4): 193-203.
- Ponce, V.M. and Simons, D.B. (1977). "Shallow water propagation in open channel flow." *Journal of Hydraulic Research* 103(HY12): 1461-1476.
- Pietroniro, A. and Prowse, T.D. (2002). "Preface: Applications of remote sensing in hydrology." *Hydrological Processes* 16(8): 1537-1541.
- Priestnall, G., Jaafar, J. and Duncan, A. (2000). "Extracting urban features from LiDAR digital surface models." *Computers, Environment and Urban Systems* 24(2): 65-78.
- Profeti, G. and MacIntosh, H. (1997). "Flood management through Landsat TM and ERS SAR data: a case study." *Hydrological Processes* 11(10): 1397-1408.
- Quinn, P., Beven, K., Chevallier, P. and Planchon, O. (1991). "The prediction of hillslope flow paths for distributed hydrological modelling using digital terrain models." *Hydrological Processes* 5: 59-79.
- Rajar, R. (1978). "Mathematical simulation of dam-break flow." *Journal of Hydraulic Division, ASCE* 104: 1011-1026.
- Refsgaard, J.C. (1997). "Parameterization, calibration and validation of distributed hydrological models." *Journal of Hydrology* 198: 69-97.
- Ritchie, J.C., Grissinger, E.H., Murphey, J.B. and Garbrecht, J.D. (1994). "Measuring channel and gully cross-sections with an airborne laser altimeter." *Hydrological Processes* 8: 237-243.
- Roache, P.J. (1998). *Verification and Validation in Computational Science and Engineering*. Albuquerque, New Mexico, Hermosa Press.
- Rodi, W., Pavlovic, R.N. and Srivatsa, S.K., Eds. (1981). *Prediction of flow and pollutant spreading in rivers. Transport Models for Inland and Coastal Waters*. New York, Academic Press.
- Salomonson, V.V. (1983). Water Resources Assessment: Falls Church. *Manual of Remote Sensing: Second Edition*. Colwell, J., Photogrammetry and Remote Sensing: 1497-1570.
- Samuels, P.G., Ed. (1990). *Cross-section location in one-dimensional models. International Conference on River Flood Hydraulics*. Chichester, John Wiley and Sons.
- Sargent, R.G. (1982). Verification and validation of simulation models. *Progress in Modelling and Simulations*. Cellier, F. E. London, Academic Press.
- Shiono, K. and Knight, D.W. (1991). "Turbulent open channel flows with variable depth across channels." *Journal of Fluid Mechanics* 222: 617-646 (and 231, 693).
- Simm, D. (1993). *The deposition and storage of suspended sediment in contemporary floodplain system: a case study of the River Culm, Devon.*, University of Exeter.
- Singh, V.P. (1994). "Accuracy of kinematic wave and diffusion wave approximations for space-independent flows with lateral inflow neglected in the momentum equations." *Hydrological Processes* 8: 311-326.
- Singh, V.P. (1996). *Kinematic Wave Modelling in Water Resources: Surface Water Hydrology*. New York, John Wiley and Sons.
- Smith, L.C. (1997). "Satellite remote sensing of river inundation area, stage and discharge: a review." *Hydrological Processes* 11(10): 1427-1439.
- Tayefi, V. (2005) *One- and two-dimensional modelling of upland floodplain flows in response to different channel configuration*. PhD Thesis. School of Geography, University of Leeds.
- Tayefi, V., Lane S.N., Hardy, R.J., and Yu, D. in review. Submitted to *Hydrological Processes*. A comparison of 1D and 2D approaches to modelling flood inundation over complex upland floodplains.
- Tchamen, G.W. and Kahawita, R.A. (1998). "Modelling wetting and drying effects over complex topography." *Hydrological Processes* 12(8): 1151-1182.
- Tholey, N. (1995). *Monitoring flood events with remote sensing data: an example of ERS-1's contribution to flood events in Northern and Southern France regions*. *Proceedings of*

- the 1st ERS Thematic Working Group Meeting on Flood Monitoring*, ESA-ESRIN, Frascati.
- Tholey, N., Clandillon, S. and DeFraipont, P. (1997). "The contribution of spaceborne SAR and optical data in monitoring flood events: examples in northern and southern France." *Hydrological Processes* **11**(10): 1409-1413.
- Townsend, P.A. (2002). "Relationships between forest structure and the detection of flood inundation in forested wetland using C-band SAR." *International Journal of Remote Sensing* **23**(3): 443-460.
- Weinmann, P.E. and Laurenson, E.M. (1979). "Approximate flood routing methods: a review." *Journal of Hydraulic Division, ASCE*, **105**.
- Wesseling, C.G., Karssenbergh, D., Deursen, V. and Burrough, P.A. (1996). "Integrating dynamic environmental models in GIS: the development of a dynamic modelling language." *Transactions in GIS* **1**: 40-48.
- Westaway, R.M., Lane, S.N. and Hicks, D.M. (2000). "The development of an automated correction procedure for digital photogrammetry for the study of wide, shallow, gravel-bed rivers." *Earth Surface Processes and Landforms* **25**(2): 209-226.
- Westaway, R.M., Lane, S.N. and Hicks, D.M. (2001). "Airborne remote sensing of clear water, shallow, gravel-bed rivers using digital photogrammetry and image analysis." *Photogrammetric Engineering and Remote Sensing* **67**: 1271-1281.
- Westaway, R.M., Lane, S.N. and Hicks, D.M. (2003). "Remote survey of large-scale braided rivers using digital photogrammetry and image analysis." *International Journal of Remote Sensing* **24**: 795-816.
- Wheater, H.S. (2002). "Progress in and prospects for fluvial flood modelling." *Philosophical Transactions of the Royal Society of London: Mathematical, Physical and Engineering Sciences* **360**(1796): 1409-1431.
- Williams, D.J. and Shah, M. (1992). "A fast algorithm for active contours and curvature estimation." *CVGIP: Image Understanding* **55**: 14-26.
- Wilson, C., Stoesser, T., Olsen, N. and Bates, P.D. (2003). Application and validation of numerical codes in the prediction of compound channel flows. *Proceedings of the Institution of Civil Engineers - Water and Maritime Engineering*.
- Wimmer, C., Siegmund, R., Schwabisch, M. and Moreira, J. (2000). "Generation of high precision DEMs of the Wadden Sea with airborne interferometric SAR." *IEEE Transactions on Geoscience and Remote Sensing* **38**(5): 2234-2245.
- Wu, F., Shen, H. and Chou, Y. (1999). "Variation of roughness coefficients for unsubmerged and submerged vegetation." *Journal of Hydraulic Engineering* **125**: 934-942.
- Zeilke, W. and Urban, W. (1981). *Two Dimensional Modelling of Rivers with Floodplains*. Delft, The Netherlands., IAHR.

**THESIS CONTAINS  
CD/DVD**